The kinetics and mechanisms of the oxidation and precipitation of iron: The High Density Sludge (HDS) process

Thesis presented for the Degree of

DOCTOR OF PHILOSOPHY

in the Department of Chemical Engineering

UNIVERSITY OF CAPE TOWN

by

Mfandaidza Hove

April 2008

Dedication

To my late father, my mother and Ropafadzo and the whole family of Stephan Mthoboli Hove

ACKNOWLEDGEMENTS

To students and staff members of the Department of Chemical Engineering at the University of Cape Town, I express my sincere thanks for your generous assistance. In particular, I would like to thank Professor A. E. Lewis for her supervision and Dr R.P. van Hille for co-supervising this project.

To all members of the Crystallisation and Precipitation Unit in the Department of Chemical Engineering, thank you all for your friendship and support.

To Mrs Frances Pocock, thank you for your encouragement and helping me settle in at the University of Cape Town.

To Miranda Waldron of the Electron Microscope Unit (University of Cape Town), Mrs Divey (Department of Chemical Engineering) and Sabine Verryn of the University of Pretoria for their assistance with the scanning electron microscope, particle size analysis and X-ray powder diffraction respectively.

The financial support from the National Research Fund and the PROTEA/CNRS is gratefully appreciated. The use of the CNRS-ENSIC (Nancy, France) facilities for some of the experiments is also greatly appreciated as well as the discussions with Dr Herve Muhr, Research Fellow and Director of the GRC research group at CNRS-ENSIC, Nancy, France.

Thank you to the National University of Science and Technology (Zimbabwe) for offering me study leave to come to South Africa to undertake this project.

To Richard and Darlington for proof reading this thesis.

Most importantly, a special thank-you to my wife, Sihle and daughter Ropafadzo for their patience, understanding, encouragement and loving support throughout the course of the project.

Publications list

Publications

M. Hove, R. P., van Hille, A. E., Lewis, (2007). Iron solids formed from oxidation precipitation of ferrous sulphate solutions, *AIChE Journal, Vol 53. pp 2569-2577.*

M. Hove, R. P. van Hille, A. E. Lewis, (2008). Mechanisms of formation of iron precipitates from ferrous solutions at high and low pH, *Chemical Engineering Science, Vol 63. pp 1626 – 1635*

M. Hove, R. P. van Hille, A. E. Lewis, The effect of different types of seeds on the oxidation and precipitation of iron from ferrous sulphate solutions, *Manuscript under review, Applied Geochemistry*

Presentations

M. Hove, R. P. van Hille, A. E. Lewis**,** Rate processes in the removal of iron from acid mine drainage by hydroxide precipitation, *South African Institute of Mining and Metallurgy (SAIMM***)** *Proceedings, 4-5 August 2005, OR32, pp54, Somerset West, South Africa*

M. Hove, R. P. van Hille, A. E. Lewis**,** Characterisation of iron sludge formed during hydroxide precipitation of iron from ferrous sulphate solutions, *South Africa Institute of Mining and Metallurgy (SAIMM) Proceedings, 3-4 August 2006, Newlands, South Africa*

M. Hove, R. P. van Hille, A. E. Lewis, The effect of different types of seeds on the oxidation and precipitation of iron from homogeneous solutions. *14th International Workshop on Industrial Crystallisation, BIWIC 2007, 9-11 September 2007, University of Cape Town, South Africa, pp 108-118*

Abstract

The oxidation and precipitation of iron are key reactions in the treatment of hydrometallurgical waste water and acid mine drainage (AMD) by the high density sludge process (HDS). The removal of other pollutants by adsorption and co-precipitation using this technique depends on the nature and the process by which iron is removed. Although this technique is cheap and easy to operate and therefore the most common method by which hydrometallurgical waste water is treated, there are some problems inherent in this technique. Such problems include; the formation of gelatinous sludge which is difficult to dewater, the low solids density resulting in considerable water losses and a large land area for sludge disposal, the instability of the sludge thus requiring post neutralisation stabilisation and the formation of the solids as mixed sludge, thus diminishing chances for waste material recovery, reuse or recycle.

In view of the above problems, the objectives of the present study were; to gain more understanding of the oxidation and precipitation reactions of iron through investigating the effect of pH on the oxidation rate and on the chemical and physical characteristics of the iron precipitates, to make an inference on the mechanisms by which iron precipitates are formed and finally to investigate the effect of seeding on the oxidation and precipitation of iron.

To achieve the set objectives, experiments were carried out in a 4 L perspex batch reactor. The reactor was fitted with four equally spaced buffles and a draft tube to maximise mixing. Ferrous iron (Fe^{2+}) was added as $FeSO_4.7H_2O$ at initial concentrations of 200 mg/L and oxidised using air. pH control was achieved by titration with either 0.1 M NaOH or 0.1 M H_2SO_4 through a custom made Hitech Micro Systems controller. The reactions were carried out at pH levels 6.0, 8.0, 9.0 and 10.0. Three types of materials (recycled solids, natural haematite and natural goethite) at three concentration levels (C_s = 1.0, 0.5 and 0.1) were used as seed material in the seeded experiments.

Initial studies revealed that the oxidation of iron was second order with respect to pH at pH levels around 6.0. At higher pH levels, the order was found to decrease reaching ≈ 0.7 at pH 10.0. In all cases, the oxidation rate was found to be first order with respect to the concentration of Fe^{2+}. Prediction of the hydrolysis of both Fe^{2+} and Fe^{3+} could be achieved using OLI Stream Analyser software. It was difficult, however, to predict the hydrolysis of both Fe^{2+} and Fe^{3+} in the presence of oxidation reactions.

The average rates of oxidation were found to increase with pH from 2.1 mg/L/min at pH 6.0 reaching 24.7 mg/L/min at pH 10.0. The average size of the particles, the zeta potential, BET specific surface area, stability and crystallinity were all found to depend on the pH. The largest particles of ≈ 3 μm average size, were obtained at pH 10.0, the smallest particles of just over 1 μm were obtained at pH 9.0. Particles of intermediate size were obtained at pH 6.0 and 8.0. Particles with the largest surface area of ≈ 250 m^2/g were obtained at pH 6.0, smallest was pH 10.0 at ≈ 100 m^2/g while pH 8.0 and 9.0 produced particles of intermediate surface area (≈ 200 m^2/g). As the pH increased, the crystallinity of the precipitates was found to decrease. This was due to the decrease in the proportion of ferrihydrite formed. The stability of the precipitates was also found to increase with increase in the pH. At pH 10.0, the most stable precipitate was formed, consisting of mainly goethite. The process mechanisms were also found to depend on the operating pH. At pH 6.0 and 10.0, it was found that oxidation proceeded through dissolved state oxidation (DSO) while at pH 8.0 and 9.0, the reaction proceeded via solid state oxidation (SSO). This was because the solubility of ferrous hydroxide is minimum at pH around 8.0. In all cases, (although to varying degrees) the precipitation process involved the formation of intermediate green rusts which later transformed into mainly lepidocrocite. The particle formation processes were found to be dominated by nucleation (which increased with increase in pH), aggregation (which also increased with increase in pH) and finally ageing of the precipitates. In all cases growth was not a significant particle enlargement mechanism.

Seeding, regardless of the seed type used, was found to increase the rate of oxidation by about two times. At seed concentration levels considered here, the catalytic effect of seeding did not depend on the seed concentration. Recycled solids seeding produced the biggest increase in the particle size (about two fold). Haematite and goethite seeding did not result in appreciable increases in average particle sizes except for reactions carried out at pH 9.0. In all cases the biggest increase in particle sizes were obtained when seed concentration was minimum at 0.1. The evolution of the average size of the particles was found to increase up to a plateau and then decrease. The decrease was attributed to removal of aggregates as they coated on the seed surface and final ageing of the precipitates. It was also found that regardless of the seed type and seed concentration, primary nucleation was reduced but not totally prevented. In all cases the final precipitation products were found to be simpler and more stable when compared to single pass systems. In recycled solids seeded systems, lepidocrocite was formed in highest proportions, with its proportion increasing with increase in the seed concentration. Goethite seeding promoted the formation of goethite and suppressed the precipitation of lepidocrocite. The proportion of goethite in the precipitate mixture also increased with increase in seed concentration. Haematite seeding, on the other hand promoted the precipitation of goethite, while suppressing the formation of lepidocrocite. The proportion of goethite precipitated also increased with increase in the haematite seed concentration. However, at pH 10.0, the composition of the precipitate was found to dependent on the pH only and not on seeding. Thus for all seed types and concentrations, the major product (minimum 94% and maximum 99%) at pH 10.0 was always goethite. For all cases, the particle formation mechanisms were found to be made up of nucleation in the bulk solution, nucleation on seed surface, coating of fine particles on seeds, aggregation of the fine particles and aggregation of the seeds among themselves. The final stage was the ageing of the precipitate which was usually accompanied by the ejection of some bound water molecules.

The information presented in this work on iron oxidation kinetics, origin of chemical instability in the precipitates and the effects of seeding of the oxidation and precipitation process all have important implications for hydrometallurgical and acid mine drainage treatment. Seeding with natural iron oxides exhibited was demonstrated to be attractive because this ensures high iron conversions, high throughputs, the formation of simple, denser and stable precipitates. The formation of such precipitates opens potential opportunities for material reuse and/or recycle and water savings.

TABLE OF CONTENTS

Chapter 2 : Experimental methods and materials………………………………. 42

Chapter 3 : Oxidation of Fe^{2+} ………………………………………………… 48

Chapter 4: Hydrolysis of iron in solution 53

List of Figures

List of Tables

Chapter 1 : Introduction

1.1 Generation of acid mine drainage

Acid mine drainage results when sulphide minerals that are exposed to air and water undergo oxidation. Exposure to these oxidising conditions is usually caused by mining activities. Pyrite is the main mineral responsible for the generation of acid mine drainage and as result iron is the major metal contained in a typical South African acid mine drainage stream (Pulles et al., 1996). Formation of acid mine drainage from pyrite (FeS_2) is illustrated by the following chemical reaction steps.

Initiator reaction:

$$2FeS_{2(s)} + 7O_{2(g)} + 2H_2O_{(l)} \leftrightarrow 2Fe^{2+}_{(aq)} + 4SO_4^{2-}{}_{(aq)} + 4H^+_{(aq)} \qquad (1.1)$$

Propagation reaction:

$$4Fe^{2+}_{(aq)} + O_{2(g)} + 4H^+_{(aq)} \leftrightarrow 4Fe^{3+}_{(aq)} + 2H_2O_{(l)} \qquad (1.2)$$

Reaction (1.2) is catalysed by different types of naturally occurring bacteria. The ferric iron formed through reaction (1.2) can either undergo hydrolysis or further oxidise the pyrite.

Hydrolysis:

$$Fe^{3+}_{(aq)} + 3H_2O_{(l)} \leftrightarrow Fe(OH)_{3(s)} + 3H^+_{(aq)} \qquad (1.3)$$

Further oxidation of pyrite:

$$FeS_{2(s)} + 14Fe^{3+}_{(aq)} + 8H_2O_{(l)} \leftrightarrow 15Fe^{3+}_{(aq)} + 2SO_4^{2-}{}_{(aq)} + 16H^+_{(aq)} \qquad (1.4)$$

The net effect of reactions (1.1) to (1.4) is the generation of four moles of hydrogen ion acidity for every mole of pyrite oxidized and the precipitation of ferric hydroxide.

Net Reaction:

$$4FeS_{2(s)} + 15O_{2(g)} + 14H_2O_{(l)} \leftrightarrow 4Fe(OH)_{3(s)} + 8SO_4^{2-}{}_{(aq)} + 16H^+{}_{(aq)} \qquad (1.5)$$

The acid formed from these reactions causes the dissolution and mobilization of other heavy metals. The result is a wastewater stream with high concentrations of metals as shown in Table 1.1.

Table 1.1 *Typical composition of an acid mine drainage stream from South Africa.*

Parameter	**Grootvlei Mine***	**Vaal Barrage Site 2****	**Vaal Barrage site 3****	**Discharge standard**
Ca	422	474.0	649.0	200
Mg	197	1639.0	2023.0	200
K	-	14.3	4.6	-
Fe	135	12438.0	5999.0	-
Mn	4.1	133.3	42.3	10
Al	0.3	1795.0	911.3	10
Zn	0.01	122.0	59.6	10
TDS	2879	59887.0	28223.0	2000
SO_4	1383	41809.0	17804.0	300
pH, pH units	6.4	2.3	3.8	6-9

The parameters are in mg/L unless stated otherwise.

* (Oryx Environmental and Jones & Wagener Consulting Engineers, 2003)

** (Steffen, 1989)

1.2 The High Density Sludge (HDS) process

Several techniques exist that can be used to remove heavy metals from acid mine drainage (Gazea et al., 1996). However, acid mine drainage in South Africa is commonly treated for heavy metals removal by the High Density Sludge (HDS) process. In this technique, ferrous iron is first oxidised before it is precipitated as mainly ferric iron and other metals (Pulles et al., 1996). The effective removal of metals in a stable form in the hydroxide precipitation process is primarily the result of the formation of co-precipitates with iron on the surface of the iron sludge. An example of the treatment of acid mine drainage by hydroxide precipitation is shown in Figure 1.1

Conventional hydroxide precipitation techniques produce a sludge which has poor dewaterability characteristics. The concentration of solids from the sedimentation processes rarely exceeds 4%. The cause of this poor settlement, clarification and reduced potential for thickening and filtration lies in the structure of the formed precipitate. The recycling of solids has been claimed to improve the solids concentration appreciably (Kostanbader and Haines, 970). The recycled sludge is mixed in a sludge reaction tank to which the alkali is added. The recycled sludge thus becomes alkalised prior to entering the neutralisation tank, forcing precipitation to occur on the surface of the existing recycled slurry particles. As the reaction is a growth of existing particles, gel formation, which is typical of a single pass system is excluded, the precipitates thus formed are denser; hence the name high density sludge process. The high density sludge process is claimed to be able to produce underflow sludge of concentrations between 15 and 35% solids which can then be gravity thickened to 45%.

As mentioned earlier, the treatment of acid mine drainage by this process requires the oxidation of ferrous iron before the conventional precipitation step. The mass transfer of the oxidising agent, air in this case, is an important factor in the formation of the sludge. The rate of oxidation of the ferrous iron has been found to be first order with respect to the concentration of dissolved oxygen (Deng, 1997); (Diz et al., 1999); (Barry et al., 1994). This means that the mass transfer of oxygen may be rate limiting and is thus an important design parameter for the reactor size and agitator. Ageing of the initially formed amorphous ferrihydrite results in the formation of the more stable goethite (Baltpurvins et al., 1996). Therefore the storage site for the sludge produced must allow for the possibility of longer term instability.

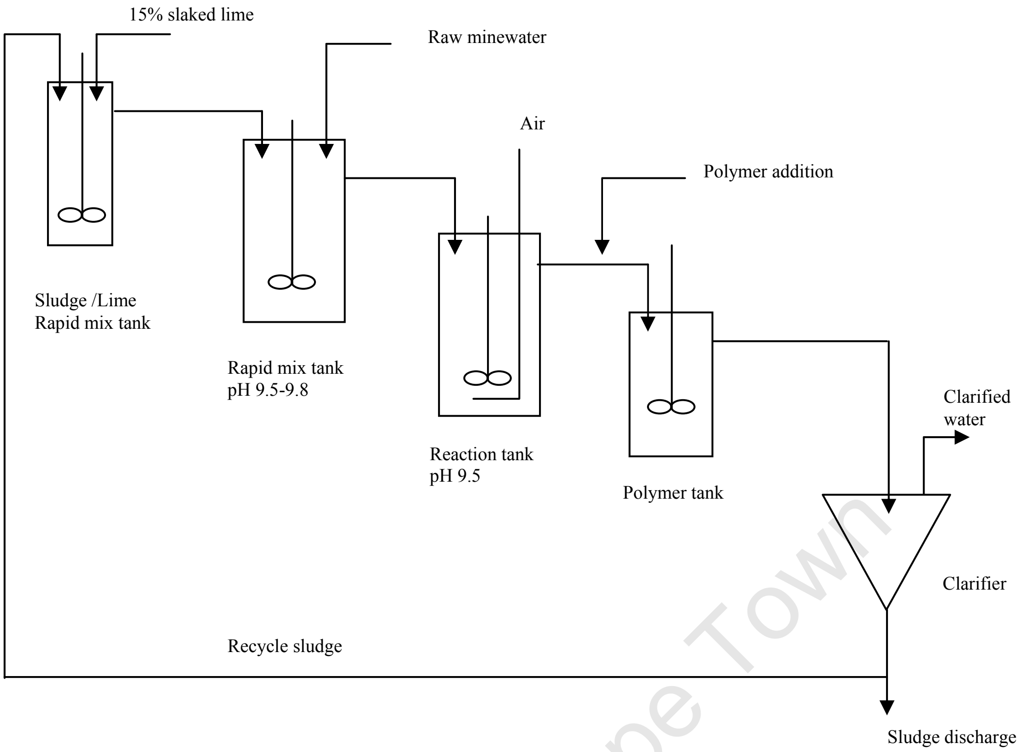

Figure 1.1 *High density sludge process (Cominco Engineering Services Limited, 1997)*

Although there are advantages that favour the use of the HDS process for the treatment of acid mine drainage, there are also challenges associated with this process. These problems include;

- The voluminous sludge produced needs a large land area for final disposal;
- The precipitation of metastable phases means there is a need for post precipitation stabilisation before final solids disposal. Again, the long term stability of these precipitates has also been questioned, especially with respect to their amphoteric solubility.
- The low solids density (15%) means a significant amount of water which could otherwise be recovered, is being wasted;
- The fine precipitates formed have poor dewaterability characteristics;
- The sludge formed is a complex mixture of iron phases which diminishes opportunities for recycle or reuse.

1.3 Chemistry of iron removal processes

1.3.1 Introduction

The chemistry of aqueous iron primarily involves the ferrous (Fe(II)) and ferric (Fe(III)) oxidation states and is of paramount importance in industrial and potable water supplies, wastewater treatment and acid mine drainage treatment. In the abstraction of groundwater for fresh water supplies, the significantly high concentrations of ferrous iron have to be reduced by first oxidising the ferrous iron and then precipitating ferric hydroxide. Not only is the oxidation of ferrous iron at the core of the treatment of acid mine drainage, it is also an important loop in the cyclical reactions that are responsible for the generation of acid mine drainage. It has also been established that the oxidation of ferrous iron is the rate limiting step in the passive and active treatment of mine waste waters (Kirby et al., 1998); (Gazea et al., 1996)

The oxidation of ferrous iron has also been found to be catalysed by some bacteria such as *Acidithiobacillus ferroxidans*. These bacteria are found in nature and have been found to increase the rate of ferrous oxidation significantly at low pH. Conversely the chemical oxidation rate of ferrous iron has been found to be very slow at low pH conditions (Stumm and Morgan, 1996).

Depending on the mixing, pH and other physico-chemical conditions, the chemical oxidation (also known as abiotic oxidation) of iron can proceed homogeneously or heterogeneously. Homogeneous oxidation is mostly encountered in natural water systems and laboratory experiments that are well mixed at low pH. At pH levels around 6.0 and above, heterogeneous oxidation is favoured due to the presence of the ferric solids that are instantaneously precipitated. Other factors such as the ionic strength (Sung and Morgan, 1980), (Millero, 1985) and the presence of other anions like SO_4^{2-} (Tamura et al., 1976a), (Sung and Morgan, 1980) have been found to have an effect of lowering the rate of ferrous iron oxidation.

1.3.2 Oxidation

The treatment of acid mine drainage by the HDS process as mentioned earlier in section 1.2 involves two chemical reaction steps: the oxidation of ferrous iron followed by the precipitation of ferric iron. The chemical nature of the product of acid mine drainage treatment as well as the plant throughput depends on the kinetics of ferrous iron oxidation. Thus, an understanding of the oxidation process is very important in the treatment of acid mine drainage by hydroxide precipitation. Many studies performed on the oxygenation of ferrous iron have shown that the rate of oxidation depends on a number of factors including, pH (or alternatively hydroxyl ions), temperature, reactor geometry and mixing effects (Maree et al., 1994); (Barry et al., 1994), (Deng, 1997); (Kirby et al., 1999) (Millero et al., 1987). Often, the researchers give different rate laws or only the rate of the oxidation reaction.

Previous studies

A number of studies have been performed on the oxidation of ferrous iron in both natural waters and in laboratory reactors. In acid solutions, the reaction proceeds slowly and shows no dependence on pH (Stumm and Lee, 1961).

For pH conditions higher than 5, Stumm and Lee (1961), proposed;

$$-\frac{d[\mathrm{Fe(II)}]}{dt} = k[\mathrm{Fe(II)}][\mathrm{OH^-}]^2 pO_2 \qquad (1.6)$$

Millero (1985), gave the rate law;

$$-\frac{d\ln[\mathrm{Fe(II)}]}{dt} = \frac{k_1\beta_1\alpha_{Fe}}{[H^+]} + \frac{k_2\beta_2\alpha_{Fe}}{[H^+]} \qquad (1.7)$$

Where, [ ] refers to species concentration, (M), k is the reaction rate constant, ($M^{-2}min^{-1}atm^{-1}$), p is partial pressure, (atm), β_1 and β_2 are hydrolysis constants for

$Fe(OH)^+$ and $Fe(OH)^0$ respectively and α is the fraction of free Fe(II), k_1 and k_2 are the pseudo first order rate constants, (min^{-1}) and t is the time (min).

The rate law as given by Millero, (1985), has the same form as that of Stumm and Lee (1961) where the rate constant is dependent on ionic strength and temperature. The change in the order of the reaction with respect to pH can be interpreted as the result of the speciation of iron and the different kinetic rates associated with each species (Barry et al., 1994). For a given pH, Stumm and Lee, (1961) also found that there was a ten-fold increase in the rate of oxidation for a 15°C temperature increase. Hustwit et al., (1992) proposed a rate law at near neutral pH conditions for acid mine drainage treatment that is independent of pH and ferrous iron concentrations as:

$$-\frac{d[Fe^{2+}]}{dt} = 7k_{o2}[O_2]_{sat} \tag{1.8}$$

Where, k_{o2} is the rate constant (min^{-1})

Other workers just quote the rates of oxidation without giving the rate laws (Wajon et al., 1985); (Carlson and Schwertmann, 1990); (Jonsson et al., 2005); (Jonsson et al., 2006). Yet other workers have reported the rate of oxidation to be dependent on other factors such as surface area of the alkalinity producing base (Maree et al., 1994), or the geometry of the reactor itself (Maree et al., 1999) or the presence of other chemical species (Sung and Morgan, 1980); (Tamura et al., 1976a); (Millero et al., 1987).

Another very important finding was that by Tamura et al., (1976b) who showed that the presence of amorphous ferric hydroxide solids catalysed the oxidation of ferrous iron. They found that, at constant pH and oxygen concentration, the rate was given by;

$$-\frac{d[Fe(II)]}{dt} = (k_1 + k_2[Fe(III)])[Fe(II)] \tag{1.9}$$

Where, k_1 is the homogeneous rate constant, (min^{-1}) and k_2 is the heterogeneous rate constant, ($M^{-1}min^{-1}$)

They also showed that:

$$k_2 = \frac{k_s[O_2]K}{[H^+]} \tag{1.10}$$

Where, k_s is the surface rate, ($M^{-1}min^{-1}$), K is the adsorption constant of ferrous iron on ferric hydroxide ($10^{-9.6}$mol mg^{-1}).

In the same study, Tamura et al (1976) found the values of k_1 and k_2 to be 7.5×10^{-2} min^{-1} and 133.6 M^{-1} min^{-1} respectively. At lower pH the oxide surface forms very slowly and consequently the adsorption of ferrous iron takes place slowly, thus autocatalysis is only significant at pH 7 or higher. In another study, Sung and Morgan, (1980), found that lepidocrocite had the same catalytic effect as amorphous ferric hydroxide. Sung and Morgan (1980) were also able to fit the rate law obtained by Tamura et al., (1976) to their experimental results. It was, however, found in the same study (Sung and Morgan, 1980) that goethite did not have the catalytic properties of amorphous ferric hydroxide and lepidocrocite. Although there was agreement between these independent studies (Sung and Morgan, 1980) and (Tamura et al., 1976b), it is difficult, within the operational pH ranges for the treatment of acid mine drainage, to study the intrinsic chemical kinetics of the oxidation of ferrous iron in homogeneous solutions. Kinetic investigations in such systems are not amenable to rigid chemical interpretation due to the overlapping of homogeneous and heterogeneous factors that exist at the phase boundaries.

1.3.3 The hydrolysis of iron in solution

The rates of oxidation and precipitation of iron phases from solution depend on the nature and concentrations of the ions in solution, the redox potential and the pH of the solution. In the treatment and removal of iron from mine waste water, the speciation of both ferrous iron (Fe^{2+}) and ferric iron (Fe^{3+}) is very important. Both iron cations form hexacoordinated aqua complexes in solution in which the hydroxylation of the cations can be visualised as polymerisation reactions upon deprotonation. This polymerisation proceeds through two possible condensation mechanisms. Olation involves the condensation of aquohydroxo complexes leading to the formation of hydroxo bridges (Jolivet et al., 2004), (Cornell et al., 1989); (Cornell and Schwertmann, 1996) and (Spiro et al., 1966). The second mechanism, which is the condensation polymerisation of oxohydroxo complexes, called oxolation involves an associative two step mechanism leading to the formation of oxo bridges and the elimination of a water molecule (Jolivet et al., 2004) and (Blesa and Matijevic, 1989).

The following sections illustrate how the speciation affects the precipitation and removal of iron from solution.

1.3.3.1 Hydrolysis of Fe^{2+}

The ferrous ion undergoes hydrolysis to form different hydroxyl complexes. The dominant hydroxyl complexes depend on the prevailing pH conditions. The possible complexes and the corresponding hydrolysis constants are shown in the equations below. The first three hydrolysis constants were obtained from Stumm and Morgan (1996) and the last from Blesa and Matijević (1989).

$Fe^{2+} + H_2O \leftrightarrow FeOH^{+} + H^{+}$ log $K_1 = -4.5$ (Stumm and Morgan, 1996)

$Fe^{2+} + 2H_2O \leftrightarrow Fe(OH)_2^{0} + 2H^{+}$ log $K_2 = -7.4$ (Stumm and Morgan, 1996)

$Fe^{2+} + 3H_2O \leftrightarrow Fe(OH)_3^- + 3H+$ log K_3 = -11.0 (Stumm and Morgan 1996)

$Fe^{2+} + 4H_2O \leftrightarrow Fe(OH)_4^{2-} + 4H^+$ log K_4 = -14.4 (Blesa and Matijevic 1989)

If the solubility product of ferrous hydroxide is expressed as:

$$[Fe^{2+}][OH^-]^2 : Ksp = 7.94^{-16} \text{ (Jackson, 1986)} \quad (1.11)$$

The total concentration of dissolved ferrous ion ($Fe^{2+}{}_T$) in solution at any pH is given by the sum of the concentration of the free Fe^{2+} and all the solubilised complexes of Fe^{2+} thus;

$$[Fe_T^{2+}] = [Fe^{2+}] + [Fe(OH)^+] + [Fe(OH)_2^0] + [Fe(OH)_3^-] + [Fe(OH)_4^{2-}] \quad (1.12)$$

By combining the complex formation equilibria and the solubility product, the concentration of the various ferrous species can be calculated at any given pH. Here Kw is defined as the ionic product of water at 25°C. Thus:

$$\log[Fe^{2+}] = \log Ksp - 2\log Kw - 2pH \quad (1.13)$$

$$\log[Fe(OH)^+] = \log Ksp - \log K_1 - \log Kw - pH \quad (1.14)$$

$$\log[Fe(OH)_2^0] = \log Ksp - \log K_2 \quad (1.15)$$

$$\log[Fe(OH)_3^-] = \log Ksp - \log K_3 + \log Kw + pH \quad (1.16)$$

$$\log[\mathrm{Fe(OH)}_4^{2-}] = \log \mathrm{Ksp} - \log \mathrm{K}_4 + 2\log \mathrm{Kw} + 2\mathrm{pH} \tag{1.17}$$

From the above equations the concentration of Fe^{2+} remaining in solution after hydrolysis can be calculated. It also has to be noted that complex formation is not a desirable phenomenon during the removal of metals from solution as it tends to reduce the amount of metal precipitated in solid form. Figure 1.2 is an illustration of the removal of iron as ferrous ion from solution. The figure was generated using the solubility and complex formation equilibria values form literature (Stumm and Morgan, 1996) and (Blesa and Matijevic, 1989). As can be seen from the figure, ferrous hydroxide is formed at high pH both as a crystalline hydroxide and amorphous hydrous oxide (Blesa and Matijevic, 1989). Both forms of the ferrous suspension are unstable and prone to oxidation when exposed to air.

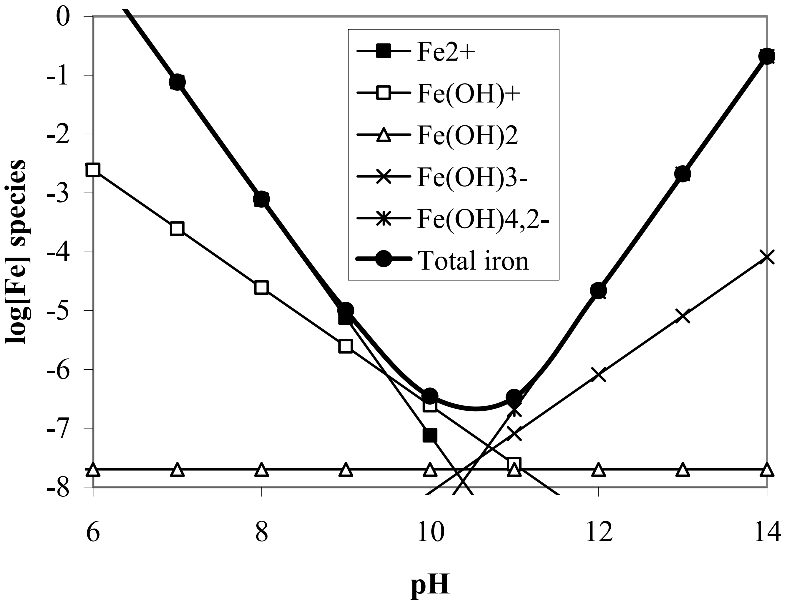

Figure 1.2 *Solubility/pH profile for* $Fe(OH)_2$ *at 25°C . Contributions from the various ferrous species are also indicated.* ***.*** *[Fe] is in M.*

1.3.3.2 Hydrolysis of Fe^{3+}

The consecutive deprotonation of hexa-aqua ferric complexes leads to the very fast formation of monomeric complexes in both acid and alkaline media (Blesa and Matijevic, 1989). These low molecular species determine the speciation of Fe^{3+} at any given pH. The equlibria governing the formation of these low nuclearity complexes are given in the following equations. The hydrolysis constants values were taken from Cornell and Schwertmann, (1996).

$Fe^{3+} + H_2O \leftrightarrow Fe(OH)^{2+} + H^+$ $\log K_1 = -2.19$

$Fe^{3+} + 2H_2O \leftrightarrow Fe(OH)_2^{+} + 2H^+$ $\log K_2 = -5.67$

$Fe^{3+} + 3H_2O \leftrightarrow Fe(OH)_3^{0} + 3H^+$ $\log K_3 = -12.0$

$Fe^{3+} + 4H_2O \leftrightarrow Fe(OH)_4^{-} + 4H^+$ $\log K4 = -21.6$

$2Fe^{3+} + 2H_2O \leftrightarrow Fe_2(OH)_2^{4+} + 2H^+$ $\log K5 = -2.95$

The low molecular weight species (complexes) formed through the reactions shown above polymerise to produce species of higher molecular weight and higher nuclearity referred to as cationic polymers (Cornell et al., 1989) as illustrated in equation 1.18

$$Fe_2(OH)_2^{4+} + FeOH^{2+} + H_2O \rightarrow Fe_3(OH)_4^{5+} + H^+ \qquad (1.18)$$

It has been argued that the molecular processes that occur during the formation of the low nuclearity species determine the morphology of the end products with various stoichiometric ratios developing which depend on the site at which the growth unit adds to the dimer (Cornell et al., 1989). This could be used to explain why different morphologies are obtained after addition of small quantities of different types of anions. The formation of the ferric oxide hydroxide, akaganeite, through the addition of trace amounts of chloride ions is a very good example (Cornell and Schwertmann, 1996). Further polymerisation of the monomers leads to the formation of red-brown colloidal cationic polymers which can be coagulated by addition of anions or base (Flynn, 1984). These colloidal dispersions have limiting diameters of 3-5nm (Van Der Woude and De Bruyn, 1983a). The final stages in the hydrolysis process involve aging of the amorphous colloidal polymers followed by transformation into more ordered and crystalline species (Dousma and de Bruyn, 1978; Spiro et al., 1966 and Flynn, 1984).

As in the case of Fe^{2+} hydrolysis, the total dissolved ferric iron ($Fe^{3+}{}_T$) at any pH is given by

$$[Fe_T^{3+}] = [Fe^{3+}] + [FeOH^{2+}] + [Fe(OH)_2^+] + [Fe(OH)_4^-] + [2Fe_2(OH)_2^{4+}] \qquad (1.19)$$

Again, as in the Fe^{2+} case, combining the complex formation equilibria with the solubility product of each of the ferric oxide/hydroxide, the concentration of any solubilised species can be expressed as a function of pH.

The solubility of iron oxide hydroxides can be represented as the dissociation of the hypothetical ferric hydroxide, $Fe(OH)_3$.

$Fe(OH)_3 \leftrightarrow Fe^{3+} + 3OH^-$

$$K_s = [Fe^{3+}]OH^-]^3 \qquad (1.20)$$

By taking logarithms on both sides of equation 1.20, the solubility becomes;

$$pK_s = pFe^{3+} + 3pOH^- \qquad (1.21)$$

The solubility products of the different types of ferric oxides/hydroxides are given in Table *1.2*

Table 1.2 *Solubility products of different iron mineral phases. Source; Schwertmann and Cornell (2000).*

Mineral Phase	**Solubility Product** as $pFe^{3+} + 3pOH^{-}$
Ferrihydrite	37-39.4
Haematite	42.2 – 43.3
Lepidocrocite	40.6 – 42.5
Goethite	43.3 - 44

The dependence of the removal of iron from solution upon the solubility products of the final precipitate is shown in Figure 1.3. The figure was obtained by using the solubility product values shown in Table 1.2 to calculate the concentration of iron remaining in solution. Two important facts can be inferred from Figure 1.3, first; it is thermodynamically feaseable to reduce iron in solution to below 0.1 ppm by precipitation as a hydroxide, second: maximum iron removal is achieved at pH 8.0 when iron is precipitated as goethite. From the thermodynamic representation in Figure 1.3, it is clear that strict control of the operational pH is very important in the effective removal of iron from wastewater streams.

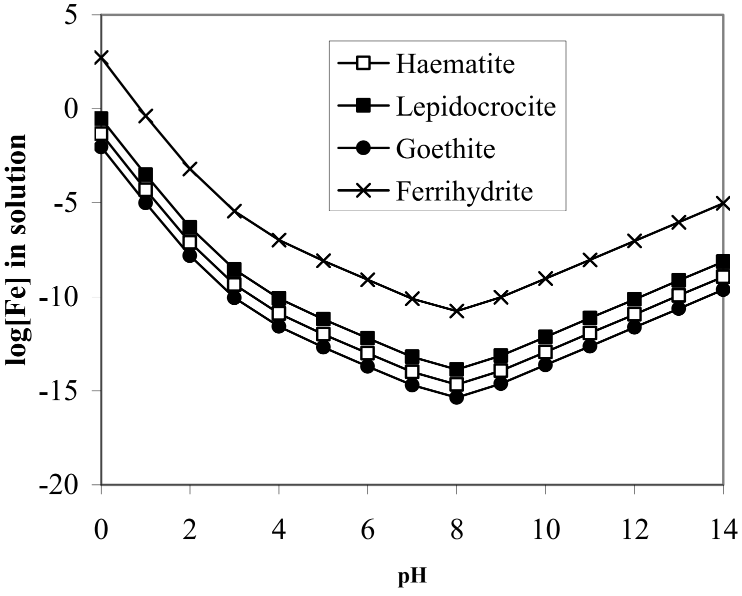

Figure 1.3 *Concentration of* Fe^{3+} *(M) remaining in solution after hydrolysis as a function of pH for different mineral phases of iron.*

1.3.4 Precipitation and transformation of iron phases

The final product of ferric iron precipitation (within a defined time frame) depends on the ageing and transformation reactions involving the red-brown cationic polymers. Whether the precipitate will be crystalline or not depends on the molar ratio of excess OH^- added per Fe^{3+}, *a.* When $0.5 < a > 1.0$, crystalline phases are formed. If *a* is greater 3.0, spontaneous precipitation of amorphous ferrihydrite occurs, otherwise when *a* is less than 3.0 a mixture of ferrihydrite and amorphous haematite is formed (Cornell et al., 1989). Neither the formula nor the structure of ferrihydrite has been fully established. The main reason for this is that the term ferrihydrite covers a range of poorly ordered compounds whose degree of ordering depends on the method of preparation and time of ageing (Gan et al., 2005), (Cornell et al., 1989). The phase transformation of the formed ferrihydrite depends mainly on the pH and the temperature. At pH 6.0 and below, and pH 8.0 and higher, where the solubility of ferrihydrite is high, it transforms into goethite by a dissolution reprecipitation mechanism. At neutral pH conditions, where the solubility of ferrihydrite is minimum, the transformation is by solid state internal rearrangement to give haematite (Jolivet et al., 2004; Blesa and Matijevic, 1989; Cornell et al., 1989 and Jambor and Dutrizac, 1998). The only crystalline phase that has been reported to form directly from solution without polymeric cation intervention is lepidocrocite and is usually in very small proportions (Cornell et al., 1989). The kinetics of ferrihydrite transformation and whether haematite or goethite will be formed depends on the pH and temperature. Cornell and Giovanoli found that, at high base concentrations, the transformation was slower and resulted in the formation of haematite while lower base concentration resulted in the formation of goethite at faster rates (Cornell et al., 1985).

The formation and transformation of ferric species in the presence of ferrous species follow different steps from the ones discussed so far. This is usually the case during the oxidation – precipitation of iron as in the HDS process where conditions that promote high oxidation rates prevail. In this case intermediate metastable green rusts are formed. These are layered iron (II) hydroxides where some of the Fe(II) is replaced by Fe(III). This extra positive charge is balanced by the incorporation of anionic species in the structure. The common anions are chloride (Green rust 1), sulphate (Green rust 2) and carbonate (Green rust 3) (Schwertmann and Fechter, 1994; Taylor et al., 1998). These species are formed in slightly acidic to alkaline conditions and at high Fe(II) concentrations.

The formation and transformation of these green rust species according to Blesa and Matijević, (1989), can be represented by the reaction scheme below.

$$Fe(OH)_2 \rightarrow \text{green rust} \rightarrow Fe_3O_4 \rightarrow \gamma\text{-}Fe_2O_3 \rightarrow \alpha\text{-}FeOOH \rightarrow \alpha\text{-}Fe_2O_3 \qquad (1.22)$$

It should be noted that this scheme represents the sequential steps and not the mechanistic pathway. Various studies have been performed to determine the mechanisms of transformation and the final products during the oxidation – precipitation of iron species. (Domingo et al., 1994) reported a dissolution/reprecipitation mechanism for the decomposition of the green rusts. In their study, Domingo et al, (1994) were able to form goethite and lepidocrocite under slightly acidic conditions and $[Fe^{2+}]/[(OH^{-})]$ ratio ≥ 0.5. Magnetite was formed at 90ºC in neutral or basic pH with $[Fe^{2+}]/[(OH^{-})]$ ratio around 5. Schwertmann and Fechter (1994), proposed a solid state transformation of green rust 1 to give lepidocrocite and occasional traces of goethite. They formed magnetite at low oxidation rates which transformed into lepidocrocite upon vigorous addition of oxygen. This finding is contradicted by that of Refait et al., (2003) who concluded that in solution, slow oxidation associated with dissolution and reprecipitation allows the formation of well ordered FeOOH phases such as goethite and lepidocrocite. In contrast, ferrihydrite, the most poorly ordered of the ferric oxides and hydroxides, is obtained if the oxidation process is so rapid that the dissolution of ferrihydrite and the subsequent recrystallisation of stable phases cannot occur. Lin et al., (1996) formed lepidocrocite and magnetite under slightly basic solution conditions. They proposed that magnetite was formed via green rust 2 and later transformed into lepidocrocite by a dissolution reprecipitation mechanism. Legrand et al., (2004) found that green rust 3 transformed into an ‘oxycarbonate’ green rust at the end of oxidation. This species was fairly stable and took days to transform into either goethite or haematite or remained unchanged depending on the ageing conditions. They proposed that the transformation of green rusts into stable oxyhydroxides took place either through the dissolution/oxidation/precipitation (DOP) mechanism or the solid state oxidation (SSO) mechanism. The DOP mechanism leads to the formation of lepidocrocite, goethite or ferrihydrite while the SSO mechanism leads to the formation of 'oxycarbonate' green rust 3 which slowly ages (several days) into goethite or haematite. They also concluded that fast oxidation rates favoured the SSO mechanism.

Ruby et al, (2003) and Schwertmann and Fechter (1994) proposed that the green rust itself was formed by the physisorption of Fe(II) and SO_4^{2-} ions onto the ferric hydroxide solid surface which later lead to incorporation by chemical reaction. The various possible precipitates of iron oxidation and precipitation are shown in Figure 1.4 below.

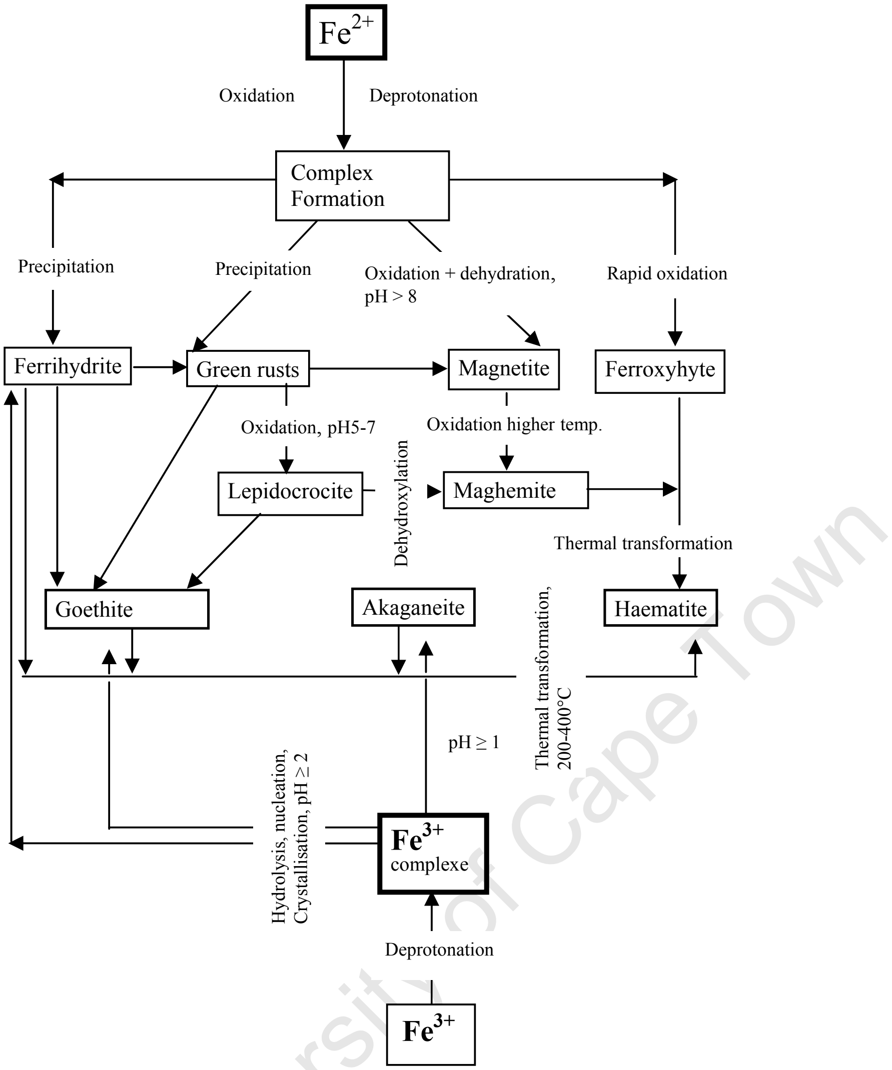

Figure 1.4 *Schematic representation of the formation and transformation of common iron oxides, together with approximate conditions where possible. Partly modified from Cornell and Schwertmann, (1996) and Jambor and Dutrizak (1998).*

In conclusion, it is clear from the studies performed so far that there is no consensus on the possible products of iron oxidation and precipitation, especially at higher pH where complex formation becomes very important. Schwertmann and Cornell (1996) point out that it is difficult to predict the product of iron oxidation and precipitation because of the various factors that influence such reactions. In summary, the many possibilities for the formation of iron phases are given in the schematic Figure 1.4.

1.4 Theory of precipitation kinetics

1.4.1 Introduction

The thermodynamic driving force for the precipitation process is given by the difference between the actual chemical potential of the solute in solution and that at equilibrium. For a system at constant temperature and constant pressure, this difference in chemical potential can be represented mathematically as:

$$\Delta\mu = \mu - \mu^* \tag{1.23}$$

Where; μ is the actual chemical potential (J), μ^* is the chemical potential at equilibrium and $\Delta\mu$ is the net thermodynamic driving force. For spontaneous precipitation to occur, the net chemical potential, $\Delta\mu$, must be greater than zero. The net chemical potential is also referred to as the supersaturation. In general, the expression for the chemical potential of a system in a solution is written as;

$$\mu = \mu_\circ + RT \ln a \tag{1.24}$$

Where, $\mu_\circ$ is the standard chemical potential of the crystallising product ($\mathrm{Jmol^{-1}}$) and a is the activity in solution ($\mathrm{mol\ m^{-3}}$). R is the universal gas constant, (8.314 $\mathrm{J\ mol^{-1}\ K^{-1}}$) and T is the absolute temperature, (°K). From this generalisation the expression for the supersaturation becomes;

$$\mu - \mu^* = RT \ln\left(\frac{a}{a^*}\right) \tag{1.25}$$

Where, a^* is the activity of the solute at equilibrium.

Usually, the ratio $\left(\frac{a}{a^*}\right)$, is defined as the supersaturation ratio, S, thus the equation becomes;

$$\Delta\mu = RT \ln S \tag{1.26}$$

For a compound which precipitates according to the general scheme,

$$xA + yB \longleftrightarrow AxBy, \tag{1.27}$$

Where, *x* and *y* are stoichiometric coefficients; the supersaturation ratio, *S,* is given by

$$S = \frac{a_A^x \times a_B^y}{a_{Aeq}^x \times a_{Beq}^y} = \frac{a_A^x \times a_B^y}{Ks} \tag{1.28}$$

Where, *eq* denotes equilibrium activity and *Ks* is the solubility product.

It is not possible to directly measure the species' activities in solution, and thus activity coefficients are used to convert the concentrations (which can be directly measured) into species activities using the equation below.

$$a_i = \gamma_i c_i \tag{1.29}$$

Where,

γ, *c* and *a* are the activity coefficient, concentration, (mol m^{-3}) and activity of species *i* respectively. The activity coefficient, γ_i, is calculated from the ionic strength of the solution according to the Debye Hückel theory of electrolytes.

It is common practice to use the concentration of species, *c*, instead of the activity, *a*. This is allowed for easily soluble compounds in which the actual solution activity coefficient is approximately the same as the activity coefficient at equilibrium. For sparingly soluble compounds the activity based supersaturation ratio should be used.

1.4.2 Nucleation

According to the classical theory of nucleation, nuclei are formed from a series of bimolecular collisions between solute molecules. Due to the presence of the thermodynamic force for precipitation, these collisions lead to the formation of clusters of solute molecules. Work is performed which is equivalent to the decrease in the Gibbs free energy for the creation of the cluster from the solution. The change in the Gibbs free energy, for the creation of a cluster of size n, can be expressed as;

$$\Delta G = -n\Delta\mu + A\gamma_s n^{2/3} \qquad (1.30)$$

Where, ΔG is the change in the Gibbs free energy, (J), γ_s is the interfacial surface energy (Jm^{-2}), n is the number of molecules and A is the cluster surface area (m^2).

The change in the free energy of formation with size of cluster n, passes through a maximum, ΔG^*, corresponding to a critical cluster size, n*. The cluster of size n* is referred to as the nucleus while the corresponding free energy is called the Gibbs free energy of nucleation. Above n*, clusters grow with each addition of a molecule while the free energy decreases. Clusters with size less than n* dissolve because their free energy is less negative than that corresponding to n*. The nucleus size, n* and the Gibbs free energy of nucleation, ΔG^*, are obtained by setting the condition that the first derivative of the free energy with respect to size is equal to zero.

1.4.2.1 Homogeneous Nucleation

The time independent nucleation rate J ($m^{-3}s^{-1}$) is defined as the frequency of appearance of supernuclei per unit volume. The rate of homogeneous nucleation can be expressed by an equation of the form;

$$J = zf^*C^* \qquad (1.31)$$

Where, z is the Zeldovich factor, f^*, the attachment frequency, (s^{-1}) and C^* the concentration of the nuclei (m^{-3}). To a first approximation, $z \approx 1/2$. For homogeneous nucleation, the concentration of nuclei is approximated by a Boltzmann type formula;

$$C^{*} = C_{\circ} Exp\left(\frac{-\Delta G^{*}}{kT}\right) \tag{1.32}$$

Where, C_0 is the concentration of nucleation sites, (m^{-3}) and k is the Boltzmann constant, ($k = 1.38 \cdot 10^{-23}$ J K^{-1}).

Thus the nucleation rate reduces to an Arrhenius type equation;

$$J = zf^{*} C_{\circ} Exp\left(\frac{-\Delta G^{*}}{kT}\right), \tag{1.33}$$

Substituting for -ΔG* according to the Gibbs Thompson equations (Sohnel and Garside, 1992) gives for the nucleation rate;

$$J = A_{\text{hom}} Exp\left(-\frac{16\pi\upsilon_{\circ}^{2}\gamma_{s}^{3}}{3(kT)^{3}\ln^{2} S}\right) \tag{1.34}$$

A_{hom} is the pre-exponential kinetic parameter (m^{-3}s^{-1}) and υ_o is the molecular volume, (m^3). The kinetic parameter can be estimated from the attachment frequency of the two possible mechanisms: volume-diffusion control and interface-transfer control.

1.4.2.2 Heterogeneous Nucleation

The formation of nuclei from homogeneous nucleation is a rare event. In most cases the formation of new crystals is catalysed by the presence of foreign particles even in thoroughly cleaned water that has been exposed to air. The catalytic effect of the foreign particles on nucleation is explained by their decreasing the Gibbs free energy of formation of the supernuclei. Thus in the presence of foreign surfaces, nucleation would take place at supersaturation ratios lower than those required for homogeneous nucleation. In heterogeneous nucleation, three different interfaces are formed and their interaction results in an effective interfacial energy term, γ_{eff} (J m^{-2}). Thus the Gibbs free energy of nucleation would be expressed as;

$$\Delta G^{*} = \frac{16\pi\upsilon_{\circ}^{2}\gamma_{eff}^{3}}{3(kT)^{2}\ln^{2} S} \tag{1.35}$$

Since the concentration of nucleation sites in heterogeneous nucleation is less than the molecular volume, the pre-exponential kinetic parameter for heterogeneous nucleation is smaller than that for homogeneous nucleation. However, it has to be noted that it is difficult to distinguish homogeneous nucleation from heterogeneous nucleation and in practice the two mechanisms occur together.

1.4.3 Crystal Growth

Crystal growth is the process of size enlargement of crystals by the deposition of growth units which can be molecules, ions, monomers, clusters etc. The overall growth rate, G, or R (ms^{-1}) can be expressed as;

$$\frac{1}{A}\frac{dm}{dt} = \frac{\rho k_v}{k_a L^2}\frac{dL^3}{dt} = 3\frac{\rho k_v}{k_a}\frac{dL}{dt} = 3\frac{k_v}{k_a}\rho G = 6\frac{k_v}{k_a}\rho R \tag{1.36}$$

Where m is the mass of a crystal, (kg), L is the volumetric diameter of a crystal (m), A is the surface area of crystal (m^2), k_a is the area shape factor and k_v is the volume shape factor, and ρ is the crystal density (kgm^{-3}).

The growth of crystals is divided into two steps that can be assumed to take place in order (Mersmann et al., 2001a):

i) Volume diffusion of growth units from the bulk solution towards the crystal surface through the diffusion boundary layer.

ii) Integration of the growth unit into the crystal surface layer.

These reaction steps are summarised in Figure 1.5

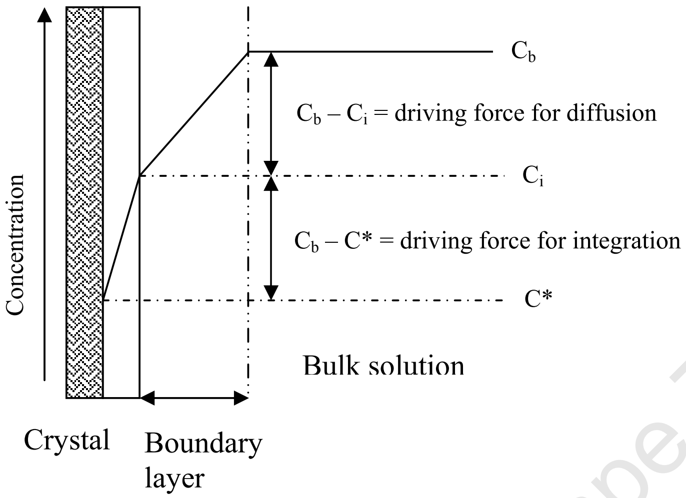

Figure 1.5 *Concentration profiles during crystal growth (Mersmann, 2001a)*

Here, C_b is the bulk concentration (mol m^{-3}), C_i is the concentration at the interface (mol m^{-3}) and C^* is the concentration at the crystal surface (mol m^{-3})

For crystal growth that is rate limited by diffusion; $C_b - C_i >> C_i - C^*$. The overall growth rate can then be expressed as;

$$G = k_d(C_b - C_i) \tag{1.37}$$

Where, k_d is the diffusion mass transfer coefficient (m s^{-1}).

On the other hand, if $C_i - C^* >> C_b - C_i$, the crystal growth process is dominated by the integration reaction. In which case the growth rate will be given by;

$$G = k_r(C_i - C^*) \tag{1.38}$$

Where, k_r is the reaction rate constant for surface integration (m^3 mol^{-1} s^{-1}).

For surface integration, different integration models exist which all depend on the supersaturation ratio, *S*. Firstly for smooth surfaces, growth units attach to kinks along the growth steps. The steps can be generated by either a two dimensional nucleation mechanism (also called the birth and spread mechanism) in which nuclei form growth layers on the crystal surface, or by spiral growth where a step source is a screw dislocation. Secondly, rough growth happens when growth units from the bulk impinge on a growth position that is available on a crystal surface. When the growth unit arrives at the surface it is immediately integrated into the crystal surface. For rough growth, faces tend to be rounded (Roelands, 2005). Rough growth is also a function of the supersaturation ratio.

1.4.4 Aggregation

The formation of agglomerates from primary particles in suspension is proceeds through a series of steps which can be represented in the following order;

i) Formation of the primary particles from nucleation and growth

ii) Transport and collision of the primary particles which can be due to Brownian motion, shear forces, difference in inertial forces and differences in particle settling velocities.

iii) Interaction of the particles through attractive and repulsive electrostatic forces and external forces like shear stress.

iv) Disruption of the 'aggregates'

v) Cementation and consolidation of the aggregates

Thus different types of aggregation can exist within a precipitating system; perikinetic aggregation where collisions are induced by Brownian motion, orthokinetic aggregation where collisions are induced by shear stress and inertial aggregation where collisions are due to differences in settling and inertial velocities. In all cases the rate of aggregation has been found to be a function of the square of the number of particles in the system (Mersmann et al., 2001b). For perikinetic aggregation the collision rate is given by;

$$r_{ij} = \beta_{coll} N_i N_j \tag{1.39}$$

$$\beta_{coll} = f\left(\bar{\varepsilon}, L_i, L_j\right) \tag{1.40}$$

Where r is the collision rate (s^{-1}), β_{coll} is the collision frequency function, N_i is the number of particles, L_i is the size of the particles (m), $\bar{\varepsilon}$ is the local energy dissipation rate ($m^2\ s^{-3}$). The overall aggregation rate shows second order dependence on particles concentration;

$$\frac{dm_0}{dt} = \frac{1}{2}\beta_{aggl} m_0^2 \tag{1.41}$$

Where m_o is the particle concentration (m^{-3}) and β_{aggl} is the aggregation rate constant ($m^3\ s^{-1}$).

The aggregation rate constant is a function of the collision frequency, β_{coll} and the agglomeration efficiency factor, ψ, which takes account of the presence of the disruptive hydrodynamic shear forces.

$$\beta_{aggl} = \psi\left(\bar{\varepsilon}, S\right)\beta_{coll}\left(\bar{\varepsilon}, L_i, L_j\right) \tag{1.42}$$

Where, S is the supersaturation.

1.4.5 Deducing Precipitation Mechanisms

A technique that is often used to make inferences about particle formation processes during precipitation is based on the moment transformation of the number density function *n(L)*, which is obtained by integrating the same with respect to the size of the particles, L. The *j^th^* moment is given by Randolph and Larson (1988) as;

$$m_j = \int_0^\infty L^i n(L) dL, \tag{1.43}$$

The symbols L, $n(L)$ and m_j represent the size of the particles (m), the number density function of the particles of size L and the j^{th} moment respectively. From the integration of the aforementioned term, the moments obtained are; Zeroth moment, m_o, (m^{-3}), first moment, m_1 (m/m^3), second moment, m_2, (m^2/m^3) third moment, m_3 (m^3/m^{-3}) which are proportional to total number of particles, total length of particles, total surface area of particles and total volume of particles respectively. The resultant moment equations for batch precipitation are given by the following equations.

$$\frac{d(Vm_\circ)}{dt} = B_\circ \cdot V \tag{1.44}$$

Where, B_0 is the rate of appearance of nuclei, (m^{-3} s^{-1}) and V is the reaction volume (m^3)

$$\frac{d(Vm_2)}{dt} = 2 \cdot G \cdot m_1 \cdot V \tag{1.45}$$

$$\frac{d(Vm_1)}{dt} = G \cdot m_\circ \cdot V \tag{1.46}$$

$$\frac{d(Vm_3)}{dt} = 3 \cdot G \cdot m_2 \cdot V \tag{1.47}$$

A plot of the various moments against time can then be used to deduce the active precipitation mechanisms. This technique has been successfully used by Ntuli and Lewis (2006), Andreassen and Hounslow (2004) and Randolph and Larson, (1988). Figure 1.6 is an illustration of how the moment transforms are used to deduce dominant precipitation mechanisms.

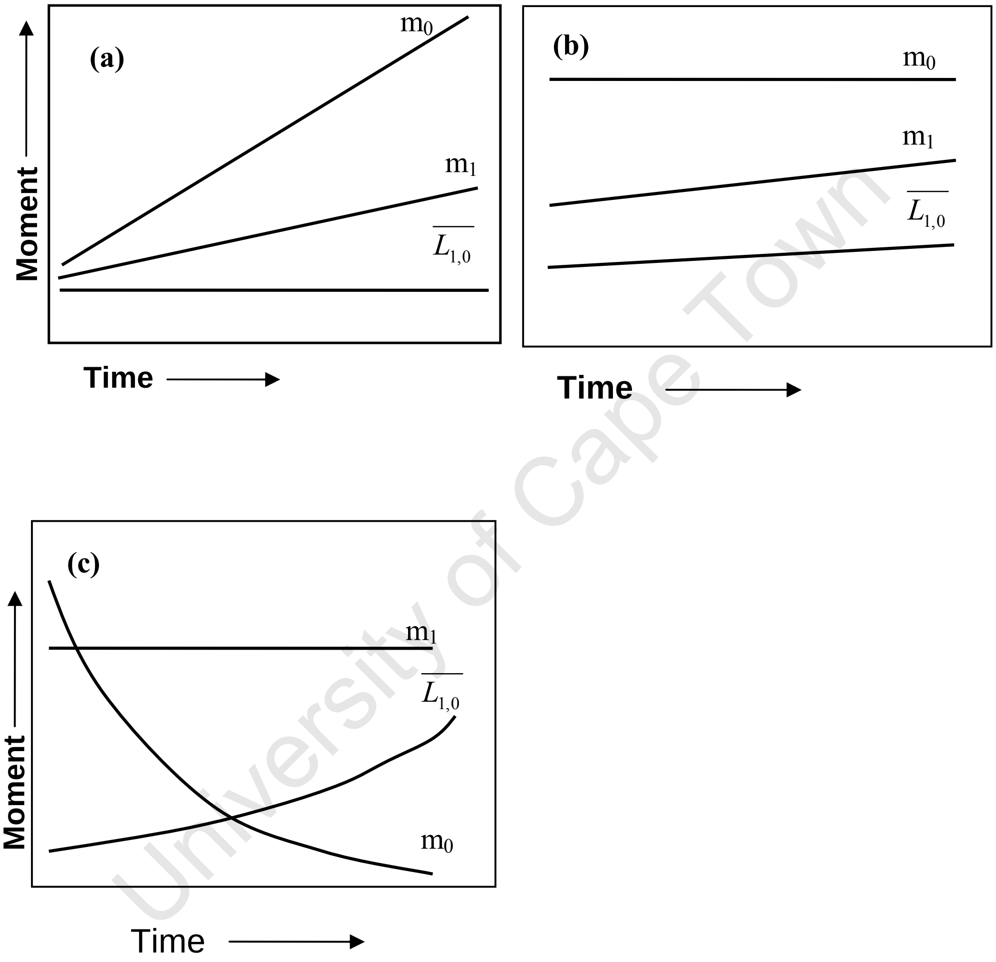

Figure 1.6 *Simplified illustration of the evolution of moment transforms for various precipitation processes; process (a) is nucleation dominated, process (b) is growth dominated and process (c) is aggregation dominated.* $\overline{L_{1,0}}$ *is the population based average size of the particles. It has to be noted however, that, in practice these processes often occur simultaneously and therefore the graphs may not be as straight forward as shown here.*

1.4.6 Seeding during precipitation processes

Precipitation processes are characterised by fast kinetics due to low solubility. The primary particles are formed by primary nucleation at high supersaturation levels. The resulting particles are usually very small, in the order of 1 μm (Heffels and Kind, 1999). Controlled growth of bigger size crystals can be achieved by either dilution or introduction of seed crystals. The surface area of the seed material should be large enough to consume the supersaturation, thereby suppressing homogeneous nucleation. In the following sections, pertinent issues pertaining to the seeded precipitation of iron are discussed.

1.4.6.1 Crystal lattice compatibility

This is a criterion that can be used to predict whether a given substrate is suitable for the overgrowth of another crystal lattice or not. The lattice misfit is defined as:

$$\delta = \frac{\Delta\alpha}{\alpha} \tag{1.48}$$

Where α is the lattice parameter of the stress free crystal and Δα is the difference in lattice parameters between substrate and growing crystal. According to the Royer – Friedel rule (Lioliou et al., 2007) a lattice misfit of 10-20% between the substrate and the overgrowth phase is considered adequate for the deposition of the precipitating component. Table 1.3 shows the α parameters for different types of iron oxide hydroxides. Included also is the α parameter for quartz. It should be noted that lattice misfit compatibility is a sufficient but not necessary condition for the deposition of the crystals on the substrate.

Table 1.3 *Crystallographic data for iron oxide hydroxides and quartz (Schwertmann and Cornell, 2000)*

Iron phase	**α**	**β**	**γ**
Ferrihydrite	0.508		0.940
Haematite	0.503		1.375
Goethite	0.996	0.302	0.461
Lepidocrocite	1.252	0.387	0.307
Schwertmannite	1.066		0.604
Maghemite	0.834		
Magnetite	0.839		
Feroxyhite	0.293		
Akaganeite	1.060	0.304	1.0513
Quartz	0.491	0.541	

Calculation of lattice misfit compatibilities gives the δ values as indicated in Table 1.4. The feasible combinations are shown in bold face. These misfit valuations were only used to formulate initial expectations.

Table 1.4 *Lattice misfit δ, for various combinations of iron phases and quartz*

Deposit/Seed	**Haematite**	**Goethite**	**Ferrihydrite**	**Quartz**
Haematite	-	49%	1%	3%
Maghemite	65%	**16%**	64%	70%
Ferrihydrite	1%	49%	-	3%
Lepidocrocite	148%	26%	146%	155%
Magnetite	66%	**16%**	65%	71%
Goethite	97%	-	96%	103%

Thus from the data shown in Table 1.4, the lattice misfit value calculations suggest that the epitaxial monolayer overgrowth of iron phases is possible for maghemite on goethite seed and magnetite on goethite seed only.

1.4.6.2 Mass of seed to be added

'No-one can predict what amount of seeds should be added into a crystallizer to produce a product of desired size, or to stabilise crystallisation. No methodology has been proposed. Seeding seems to be treated as an art' (Kubota et al., 2001).

In spite of the above statement, attempts have been made to convert seeding during crystallisation into a science. Below are some expressions that have been used to estimate the mass of seed that should be added to the crystalliser.

$$M_s = \frac{YL_0^3}{\left(L_p^3 - L_0^3\right)} \qquad \text{(Mullin, 2001)} \qquad (1.49)$$

Where M_s is the mass of seeds to be added (kg), L_0 is the mean size of seeds (m), L_p is the mean size of the product crystals (m) and Y is the theoretical yield (kg). The deficiency of this equation is that it can not be used in systems where the final product is not known or controlled. For example, in the high density sludge process where the objective is to precipitate iron oxide hydroxide particles that are as big as possible and there is no upper limit on the final product size, this expression cannot be used. Equation 1.49 is based on the assumption that all crystallisation takes place on the added seeds only. A slight variation of equation 1.49 expresses the final product mass as a function of the seed and product sizes as shown in equation 1.50.

$$M_s = M_p * \left[\frac{L_0}{L_p}\right]^3 \qquad \text{(Heffels and Kind, 1999)} \qquad (1.50)$$

M_p is the mass of the final product (kg) and L_p is the size of the final product (m). The shortcoming of equation 1.50 is that it assumes an ideal system where there is no nucleation and no crystal breakage. Due to the presence of nucleation and breakage, the final size of the product crystals is lower that that predicted from this calculation.

In such cases, the seed mass is determined from experience (the art!). In practice 0.1 to 0.3 times the final product size and 0.1 to 3% of the final mass of the seeds are good approximations (Heffels and Kind, 1999). The last expression that can be used to predict the amount of seed material to be added to a seeded precipitation system is shown in equation 1.51.

$$\frac{L_p}{L_0} = \left[\frac{1 + C_s}{C_s}\right]^{\frac{1}{3}} \tag{1.51}$$

C_s is the ratio of the amount of seed added to the theoretical yield calculated from solubility data. This expression also assumes no nucleation, no agglomeration, no breakage and no change in crystal shape (Doki et al., 2001); (Kubota et al., 2001). Doki et al., (2001) worked with C_s values of 0.0021 and 0.0715. In the same work (Doki et al., 2001) described a parameter, C_s^*, a seed concentration below which a bi-modally distributed product will be obtained and above which a mono-modal particle size distribution was obtained. Kubota et al., (2001) worked with seed concentrations of 0.003, 0.051 and 0.33. These workers also reached the same conclusion as Doki et al., (2001) concerning the critical seed mass, C_s^*.

1.4.6.3 The Art

For a number of workers, the amount of seed to be added seems to be derived from experience or trial and error. Adam (2004) used a seeded reactor to reduce gypsum scaling during sulphuric acid neutralisation from which the benefits of seeding were realised at concentrations of 5 g/L, 10 g/L, 25 g/L, and 40 g/L . However when the seed concentration was increased to 100 g/L and 500 g/L, benefits of seeding were not realisable.

1.4.6.4 Seed size

Seed crystals of very small size are not recommended because it is difficult to obtain small particles with a narrow size distribution. The other problem is that the solubility of small particles increases with decreasing size due to Oswald ripening. It is reported that many small crystals grow more slowly than large ones and small crystals of the same size exhibit a distribution in growth rate. However, the advantage of using small seed sizes is that they provide larger surface areas and enhance the precipitation process.

1.4.6.5 Seeds preparation

The simplest technique is to use the product of the previous batch as seed material. Milling may be required if the batch did not produce seeds of the desired size. Milled seeds need to be sieved and washed to remove adhering fine particles that may cause initial breeding. Milling, although simple and convenient, produces non uniformity of shape of the seeds which could affect the final shape and morphology of the product. Milling also introduces lattice defects which may result in internal stress which causes growth dispersion.

1.5 Hypotheses and objectives of the present study

1.5.1 Hypotheses

1) The rate of oxidation of ferrous iron is controlled by the operating pH. Increasing the pH results in an increase in the rate of oxidation.
2) The rate of oxidation determines the mechanisms of formation and rates of transformation of the iron species. Under slightly acidic to alkaline conditions, the phase transformations should follow the sequence;

Fe(II) → Green rusts → lepidocrocite → haematite.

This sequence of transformations can be 'short circuited' by the use of appropriate seeding resulting in the direct formation of the simple precipitate instead of the complex iron sludge which is obtained in industrial operations.

3) The rate of oxidation affects the particle processes as it determines the supersaturation with respect to the Fe^{3+} precipitates. High oxidation rates promote high supersaturation and the formation of small particles of amorphous phases.
4) The use of specific seed material will promote the formation of bigger particles of the targeted phases regardless of the prevailing pH conditions.

1.5.2 Objectives

1) To characterise the iron species that are formed during the oxidation-precipitation of iron.
2) To gain more understanding and make inferences about the mechanism of formation and transformation of iron species and the effect of seeding on the formation and transformation processes during the oxidation and precipitation of iron at high pH conditions.
3) To gain more understanding and make inferences about the active particle formation processes occurring during the oxidation and precipitation of iron under seeded and unseeded conditions at high pH.

References

Adams, J. F. (2004) Gypsum scale formation and control during continuous sulphuric acid neutralization. PhD Thesis, University of Toronto. Toronto.

Baltpurvins, K. A., Burns, R. C., Lawrence, G. A. (1996), Heavy metals in wastewater: Modelling the hydroxide precipitation of copper(II) from wastewater using lime as the preipitant, *Waste Management*, vol. 16, pp. 717 - 725.

Barry, R. C., Schnoor, J. L., Sulzberger, B., Sigg, L. and Stumm, W. (1994), Iron oxidation Kinetics in an acidic Alpine lake, *Water Research*, vol. 28, pp. 323-333.

Blesa, M. A. and Matijevic, E. (1989), Phase transformations of iron oxides, oxohydroxides, and hydrous oxides in aqueous media, *Advances in Colloid and Interface Science*, vol. 29, pp. 173-221.

Carlson, L. and Schwertmann, U. (1990), The effect of CO2 and oxidation rate on the formation of goethite versus lepidocrocite from an Fe(II) system at pH 6 and 7, *Clay Minerals*, vol. 25, pp. 65-71.

Cominco Engineering Services Limited;Water Treatment Technology (1997), Pilot scale testing of the high density sludge process, Britannia mine, Acid Mine Drainage Treatment, Vancouver, B.C. Canada.

Cornell, R. M. and Schwertmann, U. (1996), The Iron Oxides; Structure, Properties, Reactions and Uses, VCH, Weinheim.

Cornell, R. M., Giovanoli, R., Schneider, W. (1989), Review of the hydrolysis of iron(III) and the crystallisation of amorphous iron(III) hydroxide hydrate, *Journal of Chemical Technology and Biotechnology*, vol. 46, pp. 115-134.

Deng, Y. (1997), Formation of iron(III) hydroxides from homogeneous solutions, *Water Research*, vol. 31, pp. 1347 - 1354.

Diz, R. H., Novak, T. J. (1999), Modelling biooxidation of iron in packed-bed reactor, *Journal of Environmental Engineering*, pp. 109-116.

Doki, N., Kubota, N., Sato, A., Yokota, M. (2001), Effect of cooling mode on product crystal size in seeded batch crystallisation of potassium alum, *Chemical Engineering Journal*, vol. 81, pp. 313-316.

Domingo, C., Clemente-Rodriguez, R., Blesa, M. (1994), Morphological properties of alpha-FeOOH, gamma-FeOOH and Fe3O4 obtained by oxidation of aqueous Fe(II) solutions, *Journal of Colloid and Interface Science*, vol. 165, pp. 244 - 252.

Dousma, J. and de Bruyn, P. (1978), Hydrolysis-precipitation studies of iron solutions II. Aging Studies and the Model for Precipitation from Fe(III) Nitrate Solutions, *Journal of Colloid and Interface Science*, vol. 64, pp. 154 - 170.

Flynn, C. M. J. (1984), Hydrolysis of inorganic iron(III) salts, *Chemical Reviews*, vol. 84, pp. 31 - 41.

Gan, W. Y., Selomulya, C., Tapsell, G., Amal, R. (2005), Densification of iron(III) sludge in neutralisation, *International Journal of Mineral Processing*, vol. 76, pp. 149-162.

Gazea, B., Adam K.; Kontopoulos, Kontopoulos, A. (1996), A review of the passive systems for the treatment of acid mine drainage, *Minerals Engineering*, vol. 9, pp. 23 - 42.

Heffels, S. K. and Kind, M. (1999). Seeding technology: An underestimated critical success factor for crystallisation.14th International Symposium on Industrial Crystallisation.University of Cambridge. IChemE.

Hustwit, C. C., Ackman, T. E. and Erickson P. M., (1992), Role of Oxygen Transfer in Acid Mine Drainage Treatment, US Bureau of Mines Report of Investigations 9405.

Jackson, E. (1986), Hydrometallurgical extraction and reclamation, Ellis Horwood Limited, New York.

Jambor, L. and Dutrizac, J. E. (1998), Occurrence and constitution of natural and synthetic ferrihydrite, a widespread iron oxyhydroxide, *Chemical Reviews*, vol. 98, pp. 2549 - 2585.

Jolivet, J., Chaneac, C., Tronc, E. (2004), Iron oxide chemistry. From molecular clusters to extended solid networks, *Chemical Communications*, pp. 481 - 487.

Jonsson, J., Jonsson, J., Lovgren, L. (2006), Precipitation of secondary Fe(III) minerals from acid mine drainage, *Applied Geochemistry*, vol. 21, pp. 437-445.

Jonsson, J., Persson, P., Sjoberg, S. and Lovgren, L. (2005), Schwertmannite precipitated from acid mine drainage: phase transformation, sulphate release and surface properties, *Applied Geochemistry*, vol. 20, pp. 179-191.

Kirby, C. S., Elder Brady, J. A. (1998), Field determination of Fe2+ oxidation rates in acid mine drainage using a continuously-stirred tank reactor, *Applied Geochemistry*, vol. 13, pp. 509 - 520.

Kirby, C. S., Thomas, H. M., Southam, G. D. R. (1999), Relative contributions of abiotic and biological factors in Fe(II) oxidation in mine drainage, *Applied Geochemistry*, vol. 14, pp. 511 - 530.

Kostanbader, P. D. and Haines, G. F. (September 1970), High density sludge treats acid mine drainage, *Coal Age*, pp. 90 - 97.

Kubota, N., Doki, N., Yokota, M., Sato, A. (2001), Seeding policy in batch cooling crystallisation, *Powder Technology*, vol. 121, pp. 31-38.

Legrand, L., Mazerolles, L. and Chausse, A. (2004), The Oxidation of Carbonate Green Rust into Ferric Phases: Solid-State Reaction or Transformation via Solution, *Geochimica et Cosmochimica Acta*, vol. 68, pp. 3497 - 3507.

Lin, R., Spicer, R. L., Tungate, F. L., Davis, B. H. (1996), A study of the oxidation of ferrous hydroxide in slightly basic solution to produce gamma-FeOOH, *Colloids and Surfaces A: Physicochemical and Engineering Aspects*, vol. 113, pp. 79 - 96.

Lioliou, M. G., Paraskeva, C. A., Koutsoukos, P. G., Payatakes, A. C. (2007), Heterogeneous nucleation and growth of calcium carbonate on calcite and quartz, *Journal of Colloid and Interface Science*, vol. 308, pp. 421-428.

Maree, J. P., Strydom, W. F., de Beer, M. (1999), Integrated iron(II) oxidation and limestone neutralisation of acid mine water, *Water Science and Technology*, Maree, J. P., du Plessis, P. (1994), Neutralisation of acid mine water with calcium carbonate, *Water Science and Technology*, vol. 29, pp. 285-296.

Mersmann, A., Braun, B. (2001b), Agglomeration, in A. Mersmann Ed., Crystallization Technology Handbook. 2nd Edition: Marcel Dekker, USA.

Mersmann, A., Heyer, C., Eble, A. (2001a), Crystal Growth, in A. Mersmann Ed., Crystallization Technology Handbook. 2nd Edition: Marcel Dekker, USA.

Millero, F. J. (1985), The effect of ionic interactions on the oxidation of metals in natural waters, *Geochimica et Cosmochimica Acta*, vol. 49, pp. 547 - 553.

Millero, F. J., Sotolongo, S., Izaguire, M. (1987), The oxidation kinetics of Fe(II) in seawater, *Geochimica et Cosmochimica Acta*, vol. 51, pp. 793 - 801.

Mullin, J. W. (2001), Crystallisation, 4th Edition: Butterworth-Heinemann, London.

Oryx Environmental and Jones & Wagener Consulting Engineers (2003), The Grootvlei Proprietary Mines Limited Project to reduce and treat the volumes of water pumped from underground, Braamfontein, Oryx Environmental.

Pulles, W., Heath, R., Howard, M. (1996), A Manual to Assess and Manage the Impact of Gold Mining Operations on the Surface Water Environment, Pretoria.

Refait, P., Benali, O., Abdelmoula, M., Genin, J. M. R. (2003), Formation of 'ferric green rust' and/or ferrihydrite by fast oxidation of iron(II- III) hydroxychloride green rust, *Corrosion Science*, vol. 45, pp. 2435 - 2449.

Roelands, C. P. M. (2005), Polymorphism in precipitation processes. PhD Thesis, Technical University of Delft.

Ruby, C., Gehin, A., Abdelmoula, M., Genin, J. M. R., Jolivet, J. P. (2003), Coprecipitation of Fe(II) and Fe(III) cations in sulphated aqueous medium and formation of hydroxysulphate green rust, *Solid State Sciences*, vol. 5, pp. 1055 - 1062.

Schwertmann, U. and Cornell, R. M. (2000), Iron Oxides in the Laboratory, Preparation and Characterization, 2nd Edition, Wiley-VCH, Weinheim.

Schwertmann, U. and Fechter, H. (1994), The formation of green rust and its transformation to lepidocrocite, *Clay Minerals*, vol. 29, pp. 87 - 92.

Sohnel, O. and Garside, J. (1992), Precipitation Basic principles and industrial applications, Butterworth-Heinemann, Oxford.

Spiro, T. G., Allerton, S. E., Renner, J., Terzis, A., Bils, R., Saltman, P. (1966), The hydrolytic polymerization of iron(III), *Journal of American Chemical Society*, vol. 88, pp. 2721 - 2726.

Steffen, R. &. K. (1989), Research on the contribution of mine dumps to the mineral pollution load in the Vaal Barrage, WRC report No 136/1/89, Pretoria, South Africa.

Stumm, W. and Lee, G. F. (1961), Oxygenation of ferrous iron, *Industrial and Engineering Chemistry*, vol. 53, pp. 143 - 146.

Stumm, W. and Morgan, J. J. (1996), Aquatic Chemistry, Chemical Equilibria and rates in natural waters, 3rd Edition: John-Wiley & Sons, Canada.

Sung, W. and Morgan, J. J. (1980), Kinetics and product of ferrous iron oxidation in aqueous systems, *Environmental Science and Technology*, vol. 14, pp. 561 - 568.

Tamura, H., Goto, K., Nagayama, M. (1976a), Effect of anions on the oxygenation of ferrous ion in neutral solutions, *Journal of Inorganic and Nuclear Chemistry*, vol. 38, pp. 113 - 117.

Tamura, H., Goto, K., Nagayama, M. (1976b), The effect of ferric hydroxide on the oxygenation of ferrous ions in neutral solutions, *Corrosion Science*, vol. 16, pp. 197 - 207.

Taylor, R. M., Robins, R. G. (1998). Treatment of Berkeley Pitlake water using the green precipitate process.Proceedings of the Conference on Hazardous Waste Research.

Van Der Woude, J. H. A. and De Bruyn, P. L. (1983a), Formation of Colloidal Dispersions from Supersaturated Iron(III) Nitrate Solutions. I. Precipitation of Amorphous Iron Hydroxide, *Colloids and Surfaces*, vol. 8, pp. 55- 78.

Wajon, J. E., Ho, G. E., Murphy, P. J. (1985), Rate of precipitation of ferrous iron and formation of mixed iron-calcium carbonates by naturally occurring carbonate materials, *Water Research*, vol. 19, pp. 831-837.

Chapter 2 : Experimental methods and materials

2.1 General experimental set up

All the experiments were carried out in a 4 litre batch reactor as shown in Figure 2.1. The reactor had 4 equally spaced baffles and a central draft tube in order to maximise mixing. The agitator was fitted with a Rushton turbine and a speed of 350 rpm was used for all the experimental runs. The top of the reactor was covered by a lid with ports for electrodes to measure pH, dissolved oxygen concentration, and another port for sample collection.

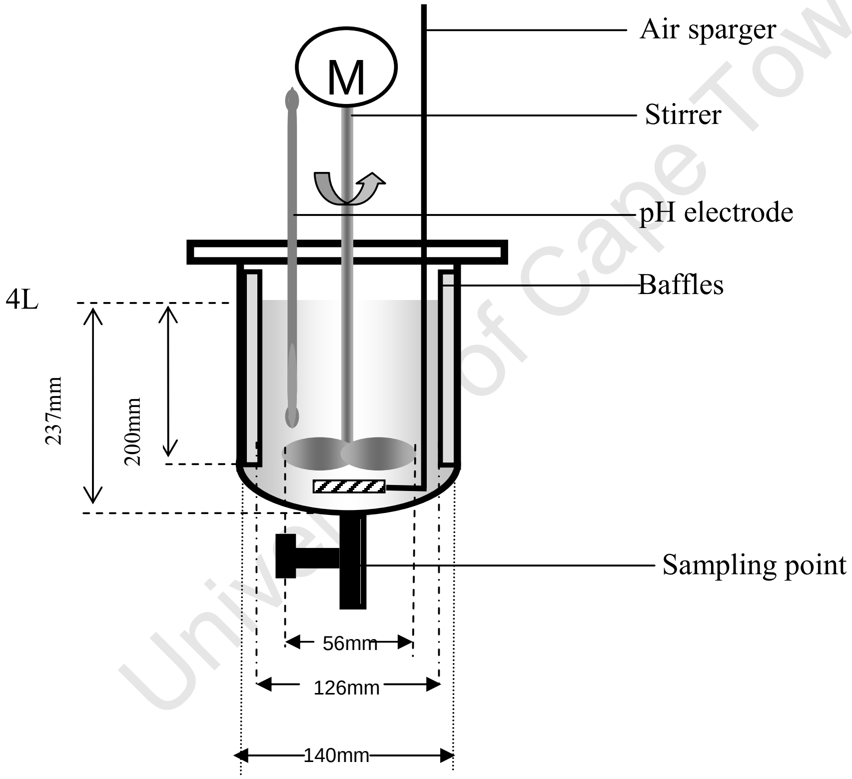

Figure 2.1 *Experimental setup*

The reactor was first filled with 4 litres of deionised water which was then deoxygenated using nitrogen. The pH was adjusted to the preset level by means of a custom made pH control system using a Hitech Micro Systems controller and Hanna MA911 pH electrode by injecting either 0.1 M H_2SO_4 or 0.1 M NaOH. The pH controller was calibrated against a commercial Hanna 211 meter coupled to a Hanna

MA911 electrode using commercial pH buffer solutions. The accuracy of the pH stat was 0.1 pH units. Oxygen was introduced into the reactor as air at a flow rate of 2ml/min. The air was dispersed into the reactor by meanns of a custom made stainless steel sparger. Dissolved oxygen concentration was monitored by a YSI 5739 electrode coupled to a Hitech Micro Systems controller. Iron at a concentration of 200 mg/L was then added as $FeSO_4.7H_2O$. The air supply was then opened up to a flow rate in excess of the stoichiometric oxygen requirements. Samples were collected from the reactor and analysed according to the specific objectives of each of the experiments that were carried out.

2.2 General sampling procedure and sample analyses

Samples were collected at predetermined time intervals from the bottom of the reactor and immediately quenched with H_2SO_4 to pH 3.0 and deoxygenated using nitrogen to stop oxidation. One part of the sample was filtered through 0.45 µm filter paper. The filtrate was analysed for dissolved iron ($Fe^{2+}$and Total Fe) using a Merck Spectroquant® NOVA 60. The procedure for iron analysis was based on the 1-10 phenanthroline method (APHA, 1998). The concentration of Fe^{3+} was found by difference. A detailed description of the analytical procedure for iron is given in Appendix 1.1. In cases where it was necessary to analyse the solids, the other part of the sample was washed several times with deionised water to remove excess ions and then freeze dried for 48 hours. The resulting solids were analysed for particle size distribution using a Zetasizer Nano ZS series, or a Malvern Mastersizer S. Phases in the precipitate were identified using X-ray powder diffraction techniques using a front loading preparation method and then analysed using a PANalytical X'Pert Pro powder diffractometer with X'Celerator detector and variable divergence and receiving slits with Fe filtered Co-Kα radiation. The phases were identified using X'Pert Highscore plus software. The relative phase quantities (weight %) were estimated using the Autoquan programme which is based on the Rietveld refinement method. The amorphous content of the samples was determined by standard addition of 15% silica. Diffuse Reflectance Infrared Fourier Transform (DRIFT) spectra were obtained with a

FTIR Perkin Elmer 2000 spectrometer using a KBr beam splitter and a DTGS detector.

For all the experiments, a portion of the solids was digested in order to determine the quantity of iron in the solids for purposes of computing a material balance on iron. All the experimental runs were carried out at room temperature and repeated several times for reproducibility. There was 23% variability in the results obtained, which is compatible with 20% variability found by other workers (Sung and Morgan, 1980).

2.3 Experimental procedure for the characterisation and mechanisms of formation of iron precipitates

The experiments were carried out at pH 6.0, 8.0, 9.0 and 10.0. The BET specific surface area was measured with a Tristar instrument supplied by Micromeretics. Degassing was performed at 90°C for 24 hours before measurement could be performed using N_2 adsorption. The zeta potential was measured using a ZetaSizer Nano ZS series. H_2SO_4, (0.01 M) and NaOH (0.01 M) were used for pH titration during the zeta potential measurements.

The method of moment transformation of the number density function n(L) which is obtained by integrating the same with respect to the size of the particles L, was used to make inferences on the particle formation processes. This method is described in more detail in Section 1.4.5.

2.4 Experimental procedure for the oxidation and precipitation of iron in the presence of seed material

Natural haematite and goethite seeds were prepared from rock specimens with a purity of 80% and 100% respectively. The X-ray powder diffraction spectra of the natural goethite and haematite are shown in Figure 2.2 and Figure 2.3 respectively.

The X-ray powder diffraction reference patterns for goethite and haematite, together with reference spectra of all the other iron phases encountered in this work are shown in Appendix 4.

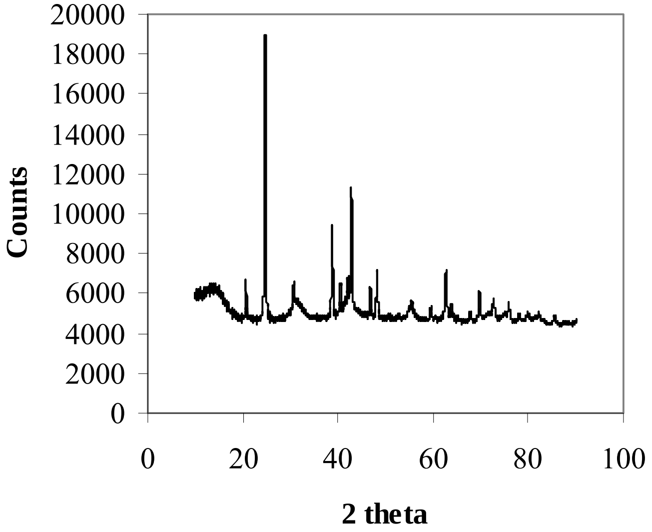

Figure 2.2 *X-ray powder diffraction spectra of natural goethite used as seed material. (Appendix 4, Figure 3)*

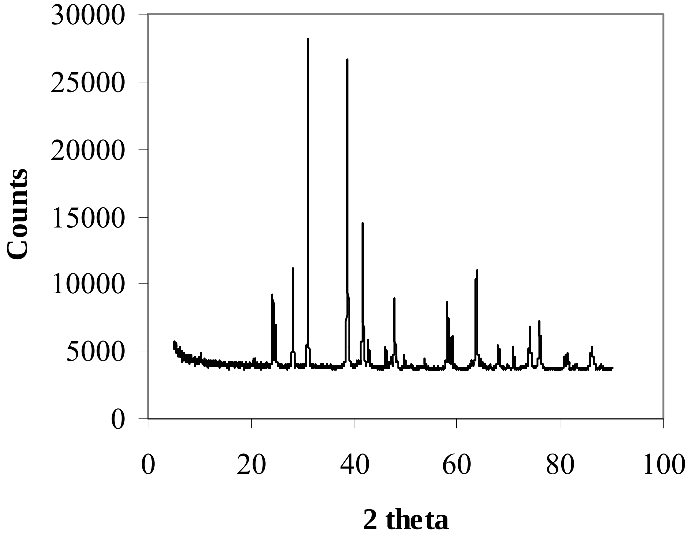

Figure 2.3 *X-ray powder diffraction pattern of natural haematite used as seed material. (Appendix 4, Figure 4)*

The minerals were first pulverised and then wet screened to sizes ranging from 25 µm to 53 µm. Next, the same samples were micronised for 10 – 15 minutes in an ethanol medium and dried at 30°C for 24 hours. The resultant material was then wet screened in an ultrasonic bath to between 1 µm and 5 µm using nylon mesh cloth (supplied by Merco Industries, South Africa). The ultrasonification was stopped when the discard was clear. The recycle solids seed material was obtained from a single pass iron oxidation and precipitation experiment carried at set pH conditions.

The reactor set up was as described in sections 2.1 and 2.2. The experimental conditions were as detailed in Table 2.1. The table was used for each of the seed materials used, that is, Recycled solids, haematite and goethite.

Table 2.1 *Experimental conditions for the seeded oxidation and precipitation of iron*

Seed concentration, C_s	**pH 6.0**	**pH 8.0**	**pH 9.0**	**pH 10.0**
0.1	x	x	x	x
0.5	x	x	x	x
1.0	x	x	x	x

After the reactor had been set up as described in section 2.1, seed material, either goethite or haematite or single pass product at concentrations as shown in Table 2.1 was added to the reactor. Iron at a concentration of 200 mg/L was then added as $FeSO_4.7H_2O$. The solution was titrated with sodium hydroxide, while at the same time being bubbled with nitrogen until a set pH was reached. The air supply was then opened and allowed to flow up to the end of the reaction. Samples were collected from the reactor as earlier described in section 2.2.

References

APHA. AWWA. WEF., (1998), Standard Methods for the Examination of Water and Wastewater, 20th Edition, APHA, AWWA, WEF, Washington.

Sung, W. and Morgan, J. J. (1980), Kinetics and product of ferrous iron oxidation in aqueous systems, *Environmental Science and Technology*, vol. 14, pp. 561 - 568.

Chapter 3 : Oxidation of Fe^{2+}

3.1 Introduction

The works cited in section 1.3.1 demonstrate the difficulty in the modelling of the oxidation of ferrous iron, especially in acid mine waters. This difficulty arises due to the variability in the concentration and speciation of iron and other chemical species in mine waters, oxidising agents employed, temperature conditions, solution pH, reactor geometry, mixing and other factors such as the size of gas bubbles in the case where oxygen is used as the oxidising agent. In fact there is not yet consensus on how to model the kinetics of ferrous iron oxidation (Kirby et al., 1998). The work presented here was aimed at evaluating the effect of ferrous iron concentration and pH only on the rate of iron oxidation under the experimental conditions described here. The experimental methods and materials were as described in sections 2.1 to 2.3

3.2 Experimental methods and materials

The experimental set up, the sampling procedure and sample analysis were performed as described in sections 2.1 and 2.2.

3.3 Results and discussion

The oxidation reaction rate law was first assumed to be of the form;

$$\frac{d\left[Fe^{2+}\right]}{dt} = k\left[Fe^{2+}\right]^m \left[O_2\right]\left[OH^-\right]^n \tag{3.1}$$

If the concentration of dissolved oxygen and the pH are kept constant, the oxidation rate becomes a function of [Fe^{2+}] only. Assuming a first order reaction, a plot of the logarithm of the ferrous iron concentration with time is shown in Figure 3.1. From this plot it can be seen that the order of the oxidation reaction is first order with respect to [Fe^{2+}] for all the pH levels considered relevant to the high density sludge process. This is in agreement with the findings of other workers (Stumm and Lee, 1961), (Tamura et al., 1976a) (Tamura et al., 1976b).

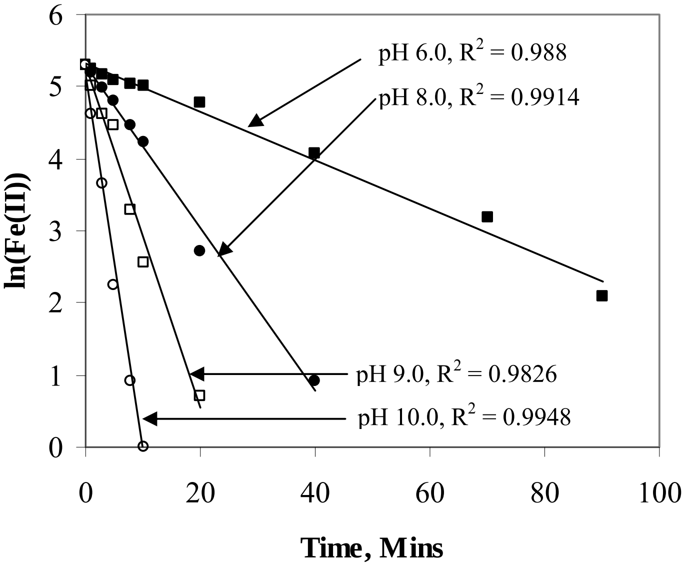

Figure 3.1 *Change in ln[Fe^{2+}] with time*

The gradient of each of the plots in Figure 3.1 gives the value of the reaction rate, which, if plottted against the pH, could be used to evaluate the value of n, the order with respect to [OH^-]. Such a plot is shown in Figure 3.2. The plot shows that the order of the reaction with respect to [OH^-] is ≈ 0.70. This order indicates that the rate of oxidation more than trebles for every unit change in the pH of the sytem. This is in disagreement with the findings of Tamura et al, (1976a), and Stumm and Lee, (1961). Even the model of Tamura et al, (1976b) and Sung and Morgan (1980) (equation 1.9) which takes into account the catalytic effect of ferric hydroxides could not fit the experimental results obtained here. This disagreement could be due to a number of factors. Firstly, in the instance where homogeneous oxidation is assumed, the presence of ferric hydroxides that were formed especially at higher pH could have meant that both homogeneous and heterogeneous oxidation were responsible for ferrous iron depletion from solution.

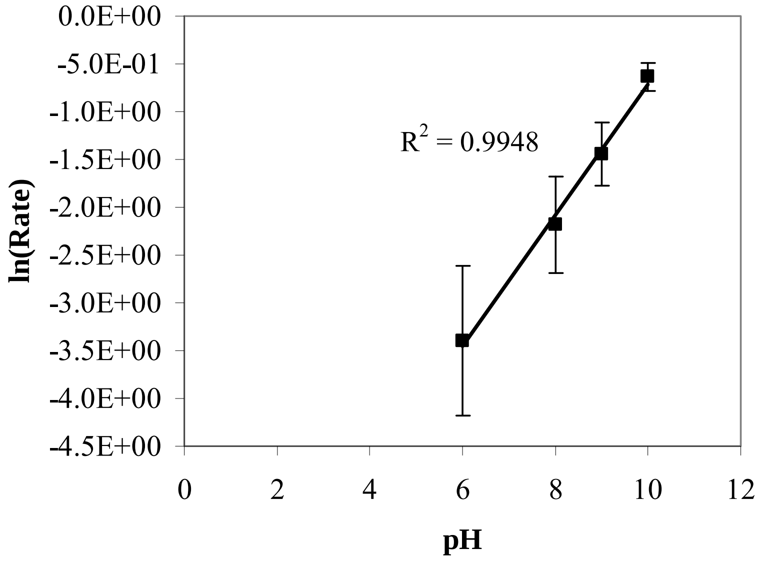

Figure 3.2 *Change of the reaction rate constant with pH during the oxidation of ferrous iron*

The increased complexity of iron speciation at higher pH could also have resulted in a different oxidation mechanism from that upon which equation 1.6 is based. This, could also be another reason for the observed disagreement. The other reason for the deviation from cited models could be due to the nature of the iron hydroxides formed. In the experiments performed here, green rusts were clearly formed during the earlier stages of the oxidation. It could be that green rusts and the predecessor stable oxides do not have the same effect on the oxidation of ferrous iron as does ferric hydroxide. An analysis of the precipitates formed here also showed them to be a complex mixture of iron oxide hydroxides. Also, it was found, using the model rate equation 2.1, that the value of k was 1.7×10^{15} $M^{-1}atm^{-1}Min^{-1}$ at pH 6.0. This is comparable to the values found by Stumm and Lee (1961), Tamura et al, (1976a) and Sung and Morgan (1980) although the conditions used here were slightly different. When the same model was applied to the other pH conditions, the reaction rate constant was found to decrease with pH, contrary to the findings shown in Figure 3.1. However when the value of n = 0.70 was applied to the same data, the value of the reaction rate constant was found to increase with pH in agreement with Figure 3.1. These comparisons indicate that the rate of oxidation ceases to have second order dependence on pH at levels higher than 6.0. It may also be true that the first order dependence of the oxidation rate on the concentration of ferrous iron is also violated at higher pH levels as reported by Wajon et al, (1985).

3.4 Conclusion

The measurement of the oxidation rate of ferrous iron is complex due to its dependence on several factors such as the pH, type of oxidising agent, mixing, reactor geometry and nature of alkalinity providing species. The increased complexity of the speciation of both ferrous and ferric iron with pH also means that the simple speciation models upon which most kinetic models are built fail to hold at higher pH levels. This could be one of the reasons why some workers (Wajon et al., 1985) have reported oxidation rate laws which do not show first order dependence on [Fe^{2+}] compared to other workers (Deng, 1997); (Barry et al., 1994) and (Tamura et al., 1976b). The formation of different types of iron oxide hydroxides under slightly different conditions also means that the oxidation kinetics will be different to the varying degrees to which these precipitates catalyse the oxidation of ferrous iron. The work presented here confirms the observation by (Kirby et al., 1998) that there is not yet consensus on how to model the kinetics of ferrous iron oxidation especially under conditions of acid mine drainage treatment.

References

Barry, R. C., Schnoor, J. L., Sulzberger, B., Sigg, L. and Stumm, W. (1994), Iron oxidation Kinetics in an acidic Alpine lake, *Water Research*, vol. 28, pp. 323-333.

Deng, Y. (1997), Formation of iron(III) hydroxides from homogeneous solutions, *Water Research*, vol. 31, pp. 1347 - 1354.

Kirby, C. S., Elder Brady, J. A. (1998), Field determination of Fe2+ oxidation rates in acid mine drainage using a continuously-stirred tank reactor, *Applied Geochemistry*, vol. 13, pp. 509 - 520.

Stumm, W. and Lee, G. F. (1961), Oxygenation of ferrous iron, *Industrial and Engineering Chemistry*, vol. 53, pp. 143 - 146.

Tamura, H., Goto, K., Nagayama, M. (1976a), The effect of ferric hydroxide on the oxygenation of ferrous ions in neutral solutions, *Corrosion Science*, vol. 16, pp. 197 - 207.

Tamura, H., Goto, K., Nagayama, M. (1976b), Effect of anions on the oxygenation of ferrous ion in neutral solutions, *Journal of Inorganic and Nuclear Chemistry*, vol. 38, pp. 113 - 117.

Wajon, J. E., Ho, G. E., Murphy, P. J. (1985), Rate of precipitation of ferrous iron and formation of mixed iron-calcium carbonates by naturally occurring carbonate materials, *Water Research*, vol. 19, pp. 831-837.

Chapter 4: Hydrolysis of iron in solution

4.1 Introduction

The hydrolysis of both ferrous and ferric iron is accompanied by a corresponding release of protons. From the stoichiometry of the hydroxylation reactions of the two iron cations, (equations 1.12 and 1.19), the extent of hydrolysis can be measured by considering the change in the pH of a given system. If the initial and final pH conditions of the system are known, then this change in the pH can be used to calculate the quantity of protons released through hydrolysis. The same can be used to make an inference about the extent of hydrolysis. In the same way, in systems where Fe^{2+} is the starting material, and the initial and final pH levels are known, the quantity of released protons can be used as a measure of the rate of ferrous iron oxidation. The extension of this technique to measure the rate of oxidation can only be correct if the hydrolysis is not kinetically hindered, that is, if the hydrolysis is instantaneous. The following experiments were performed in order to test if the hydrolysis of iron could be kinetically hindered as reported by Dousma and de Bruyn (1978). Secondly, if the hydrolysis is not kinetically hindered, can it be used to measure the rate of oxidation of ferrous iron?

4.2 Experimental methods and materials

The experiments were carried out in three parts, A, B and C. The conditions of each set of experiments are given in Table 4.1.

Table 4.1 *Experimental plan on the hydrolysis of iron*

Experiment No	**Details**
A	Oxidation of $FeSO_4$ was carried out as described in 2.1 but without pH control. Analyses were performed for Fe^{2+}, Fe^{3+} and pH.
B	Pre-weighed and mechanically mixed proportions of Fe^{3+} as $FeCl_3.6H_2O$ and Fe^{2+} as $FeSO_4.7H_2O$ (to give total Fe concentration of 200 mg/L) were transferred into a 500 ml beaker filled with deionised water. The solution was stirred for 30 seconds while nitrogen was bubbled through the solution. After the 30 seconds the solution pH was recorded. The mixing proportions were taken to represent the extent of oxidation, (%). $FeCl_3$ was used in these experiments because we could not obtain ferric sulphate of analytical grade.
C	OLI Stream Analyser 2.0 (2000) software was used to perform point calculations after mixing of predetermined proportions of Fe^{2+} and Fe^{3+} as $FeSO_4.7H_2O$ and $FeCl_3.6H_2O$. The mixing proportions represented extents of Fe^{2+} oxidation whilst pH corresponded to the hydrolysis of both Fe^{2+} and Fe^{3+} ions.

4.3 Results and discussion

The results for Part A are shown in Figure 4.1. The pH versus time curve shows that there is an initial sharp drop in the pH of the system without a corresponding sharp increase in the oxidation. This is because the initial drop in pH was mainly due to hydrolysis of ferrous iron and not of ferric iron. The appearance of a slight plateau at 25 hours indicates that the oxidation process probably proceeds through a two step process. The existence of this plateau is more visible on the % oxidation versus time curve. The first stage of the reaction could be the possible precipitation of ferrous hydroxide ($Fe(OH)_2$) and formation of green rusts. Lin et al., (1996) also observed a plateau during the oxidation of ferrous iron without pH control.

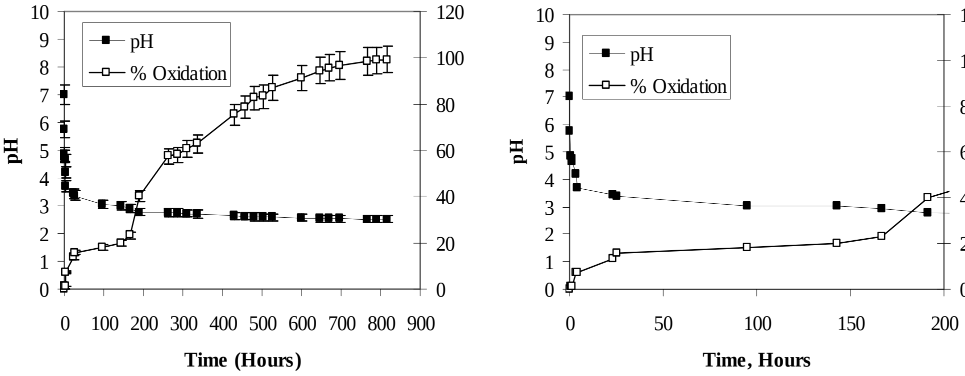

Figure 4.1 *Change in the pH and extent of oxidation with time. The plot on the right is a magnification of the x-axis in order to show the drop in pH for the first 200 hours of the reaction.*

The decrease in the pH due to actual oxidation (Part A experiment) was compared to the decrease that was predicted using OLI StreamAnalyser 2.0 and the pH found from experiment B. The comparison is shown in Figure 4.2. From the plot, it is clear that the change in pH predicted using OLI Stream Analyser 2.0 software (Part C) and that obtained from mechanical mixtures of Fe^{2+} and Fe^{3+} (Part B) is similar. However the pH drop found from Part A is different from Parts B and C especially during the early stages of the oxidation process.

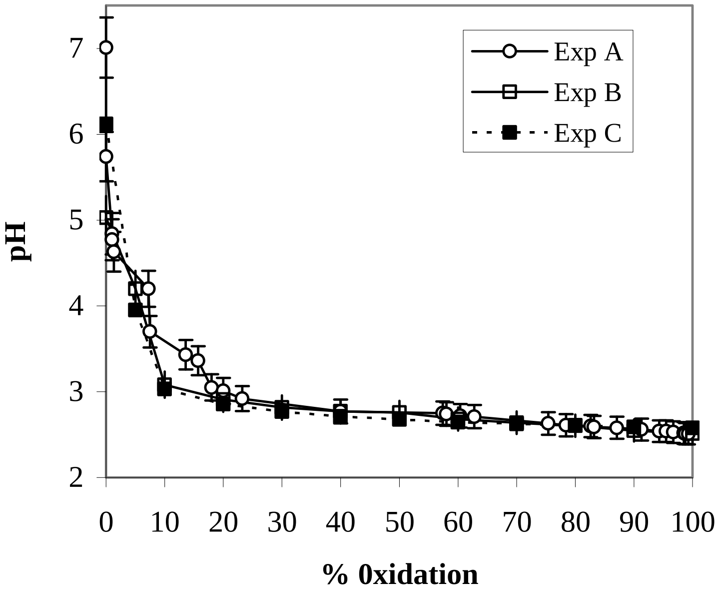

Figure 4.2 *Change in pH versus % oxidation for experiments A, B and C.*

This disagreement is probably due to the speciation of both ferrous and ferric iron and the initial precipitation of ferrous hydroxide and green rusts. These results indicate that, in the absence of oxidation, it is easy to predict the hydrolysis of ferrous and ferric iron. In the presence of oxidation, the hydrolysis is made complex by the formation of metastable species like green rusts and ferric hydroxide.

4.4 Conclusion

From the results obtained here it is can be concluded that the hydrolysis of ferric iron (alternatively the change in the pH) can not be used as a measure of the rate of oxidation of ferrous iron due to the complex nature of the speciation of both ferrous and ferric iron at high pH. Thus the best way to measure the rate of oxidation of ferrous iron is by measuring the concentration of ferrous iron in both solution and solid. Secondly the hydrolysis of both ferrous and ferric iron is instantaneous, that is, the hydrolysis is not kinetically hindered. However, when the ferric iron is derived from the oxidation of ferrous iron, the rate of oxidation then controls the rate of ferric hydrolysis.

References

Dousma, J. and de Bruyn, P. (1978), Hydrolysis-precipitation studies of iron solutions II. Aging Studies and the Model for Precipitation from Fe(III) Nitrate Solutions, *Journal of Colloid and Interface Science*, vol. 64, pp. 154 - 170.

Lin, R., Spicer, R. L., Tungate, F. L., Davis, B. H. (1996), A study of the oxidation of ferrous hydroxide in slightly basic solution to produce gamma-FeOOH, *Colloids and Surfaces A: Physicochemical and Engineering Aspects*, vol. 113, pp. 79 - 96.

Chapter 5 : Characterisation and mechanisms of formation of iron precipitates

5.1 Characterisation of the precipitates

5.1.1 Introduction

The treatment of acid mine drainage by hydroxide precipitation as indicated earlier involves two stages; oxidation of ferrous iron and precipitation of ferric oxide hydroxides as detailed in Section 1.2. The removal of metals and iron depends on the effectiveness of the oxidation and the precipitation stages of the process. The introduction of a solids recycle stream improves the removal and the density of the sludge formed (Kostanbader and Haines, September 1970), (Bosman, 1974). The plant throughput also depends on the two sub-processes. Operating at high pH ensures higher throughputs since the rate of oxidation increases one hundred fold for every unit increase in the pH (equation 2.3). The same reaction has been found to increase by about ten fold for every 15°C increase in temperature (Stumm and Lee, 1961) due to the dependence of ionic product of water and hydroxyl ion concentration on temperature. The composition and physico-chemical nature of the precipitates formed depend on a number of factors such as pH, presence of other anions, ionic strength and mixing. Figure 1.4 illustrates the many different types of products of iron precipitation. It is clear from the illustration that it is difficult to form a single type of iron precipitate under any given set of reaction conditions. In spite of the widespread use of this technique for acid mine drainage treatment, the disposal of metal laden sludge from acid mine drainage treated this way still experiences problems of low solids density, long term instability and the need for a large land area for disposal.

In view of the aforementioned problems, the aims of the present study were;

- To develop a deeper understanding of the particle formation mechanisms involved during the oxidation and precipitation of iron as obtained under conditions of the high density sludge process. The study focused on two areas; first: an investigation into the effect of pH on the rate of oxidation of ferrous iron, which indirectly generates the supersaturation needed for solids formation and secondly; an investigation into the precipitation of ferric ions in slightly acidic to alkaline aqueous systems and the characterisation of the precipitates so formed.

- To deduce the active process mechanisms involved in the formation and transformation of the precipitates.

The hydrolysis of both ferrous and ferric iron has been covered in Sections 1.3.2.1 and 1.3.2.3. The formation of particular iron phases depends on the rate of oxidation, which controls the level of supersaturation, and prevailing pH conditions (Cornell and Schwertmann, 1996). However, Van der Woude and De Bruyn (Van Der Woude and De Bruyn, 1983b) and Pavlides (Pavlides, 1995), found that the iron particles precipitated at low pH (2.5 - 4.5) had a limited size, independent of the iron concentration and pH. Deprotonation of these positively charged polymeric species (also referred to as colloids) by addition of a base leads to coagulation (Cornell et al., 1989). It is expected therefore that, in the work presented here, (pH 6.0-10.0), larger particles will be formed compared to the 3 – 5 nm ones formed by Van der Woude and De Bruyn (Van Der Woude and De Bruyn, 1983a) and Pavlides (Pavlides, 1995) due to base induced coagulation of the precursor polynuclear species.

Because of the very low solubility of most of the iron phases, very high supersaturation levels are encountered in iron precipitation processes. This leads to the high nucleation rates and the formation of fine particles. Although ferrihydrite is thermodynamically less stable, it has been found to be kinetically favoured relative to the more stable phases at pH 6.0 or lower (Jambor and Dutrizac, 1998). The mechanism of precipitation of ferrihydrite from homogeneous solutions at these low pHs has been found to start with formation of nuclei which are growth limited to about 3-5nm (Van Der Woude and De Bruyn, 1983a). These nanosized particles may then aggregate to form particles larger in size (Schwertmann and Cornell, 2000). All the studies cited here were done at low pH of 2.5 -5.0. The objective of the study presented here was to characterise the iron precipitates and also investigate the particle process mechanisms in the formation of iron precipitates at conditions of higher pH (6.0 - 10.0) and high iron concentrations, as encountered in the treatment of acid mine drainage by the HDS process.

5.1.2 Experimental method and techniques

The methods and materials used here were as described in sections 2.1, 2.2 and 2.3.

5.1.3 Results and Discussion

5.1.3.1 Oxidation of Fe^{2+}

The plot of the Fe^{2+} concentration remaining in solution as a function of time for pH 6.0, 8.0, 9.0 and 10.0 is shown in Figure 5.1 . The plots indicate that the rate of oxidation increases with increase in pH as would be expected according to the rate laws given by Stum and Lee (Stumm and Lee, 1961). The average rates of oxidation were found to be 2.1 mg(Fe^{2+})/L/min, 4.9 mg(Fe^{2+})/L/min, 9.8 mg(Fe^{2+})/L/min and 19.9 mg(Fe^{2+})/L/min at pH 6.0, 8.0, 9.0 and 10.0 respectively. For the pH 6.0 case, the average rate of oxidation obtained was more than 0.044 mg(Fe^{2+})/L/min which would be predicted from literature-based calculations (Stumm and Lee, 1961). A comparison of the measured oxidation rates and the literature-based oxidation rates is shown in Table 5.1. The reason for the higher than expected rate was due to the catalytic effect of ferrihydrite solids in the pH range 6.0-7.0 as found by Tamura et al., (1976a) and Sung and Morgan (1980).

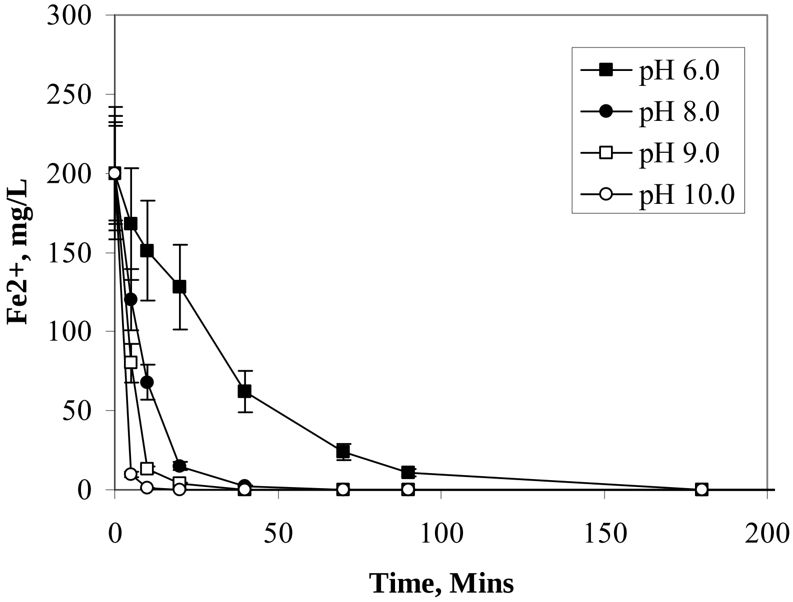

Figure 5.1 *Fe^{2+} remaining in solution as a function of time*

Table 5.1 *Comparison of measured oxidation rates and literature based oxidation rates*

pH	**Measured rate, mg/L/min**	**Literature rate, mg/L/min**
6.0	2.1	0.044
8.0	4.9	440
9.0	9.8	44000
10.0	24.7	4400000

The oxidation rates found in this work for pHs 8.0, 9.0 and 10.0 are significantly lower compared to the rates that would be predicted from literature-based calculations (Stumm and Lee, 1961). This reduced rate could be due to the increased complexity of iron speciation at higher pH (Blesa and Matijevic, 1989). It is also known that SO_4^{2-} (which is a dominating ion in this case) reduces the rate of Fe^{2+} oxidation (Sung and Morgan, 1980; Tamura et al., 1976b). It is also very likely that at higher ferrous iron concentration and higher pH, the rate law given by Stumm and Lee (1961) may not hold, due to the increased complexity of iron speciation. The rapid initial drop in Fe^{2+} concentration for all cases could have been due to direct aqueous oxidation while the slower rates towards the end of the reaction could have been due to transformation reactions involving Fe^{2+}/Fe^{3+} metastable complexies and/or Fe^{2+} adsorbed on the ferrihydrite surface. Also the green rusts formed here may not have the same catalytic effect as ferric hydroxides. As indicated in Section 2.1.3.3, the dependence of the rate of oxidation on pH was found to be ≈ 0.7 at pH higher than 6.0.

5.1.3.2 Particle Size Distribution

a) Solids formed after 5 minutes of reaction

The particle number distribution, N, ($\#/m^3$) of the particles formed after 5 minutes of reaction is shown in Figure 5.2. At pH 6.0 and 9.0, bimodal distributions were obtained while unimodal distributions were obtained at pH 8.0 and 10.0. The peaks were at 1280 nm and 4800 nm at pH 6.0, and 459nm and 531nm at pH 8.0 and 10.0 respectively. The distribution at pH 9.0 showed the formation of smaller particles with peaks at 190 nm and 712 nm. The total number of particles increased with higher pH due to the increase in the amount of precipitate formed in the same time interval. The wide span of the distribution in all cases supports the theory of initial formation of monomer species which condense into larger polymeric species by an aggregative mechanism (Flynn, 1984); (Dousma and de Bruyn, 1978). The open structure of the particles indicated that the solids were made up of mainly amorphous ferrihydrite while traces of green rusts and lepidocrocite were picked up by X-ray powder diffraction analysis. The decrease in the size of the particles at higher pH was due to the increased oxidation rate, which resulted in high primary nucleation rates and inhibited growth of the particles. These conditions of high oxidation rate (Figure 5.1) support high supersaturation levels, resulting in the formation of thermodynamically less stable but kinetically favoured ferrihydrite and green rusts (Jambor and Dutrizac, 1998; Dousma and de Bruyn, 1978). It is because of the high oxidation rates that the number of particles formed also increased significantly at pH 9.0 compared to pH 6.0.

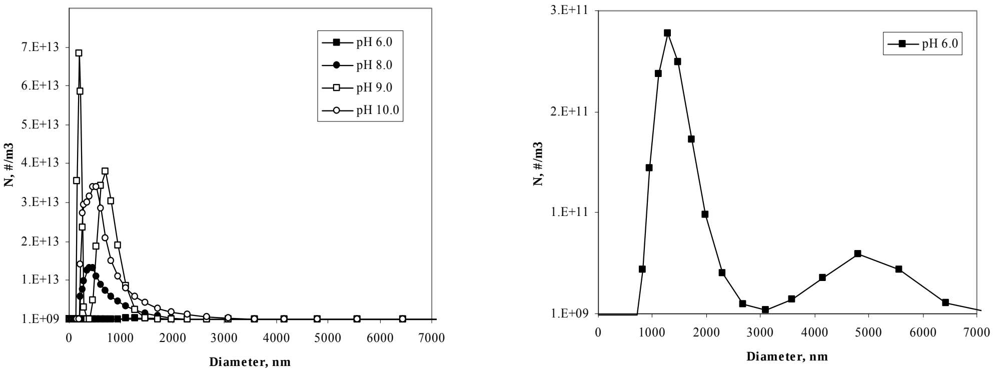

Figure 5.2 *Particle size distribution after 5 minutes of reaction. The graph on the right is a y-axis magnification of the graph on the left in order to show the distribution at pH 6.0.*

In all cases the size of the particles obtained was larger than the limiting colloid size reported by Van der Woude and De Bruyn (983b) of 3-5 nm. This could have been due to the high pH (more basic) which induced deprotonation of the polynuclear species and led to coagulative aggregation. However, at higher pH, it would seem that the rate of deprotonation was lower than the rate of nucleation; hence smaller particles were formed although there was more base compared to pH 6.0. The bimodal distribution obtained is typical of mixed phase systems, supporting the view that different iron phases were formed during the initial stages of the reaction.

b) Solids formed after 10 minutes of reaction

The particle number distributions for solids formed after 10 minutes of reaction are shown in Figure 5.3. The precipitate that had formed after 10 minutes at pH 6.0 showed high polydispersity with modal peaks at 396 nm, 1720 nm and 4800 nm. The number density distribution of the particles formed at pH 9.0 had a modal peak of 396 nm while that for pH 10.0 was 1280 nm.

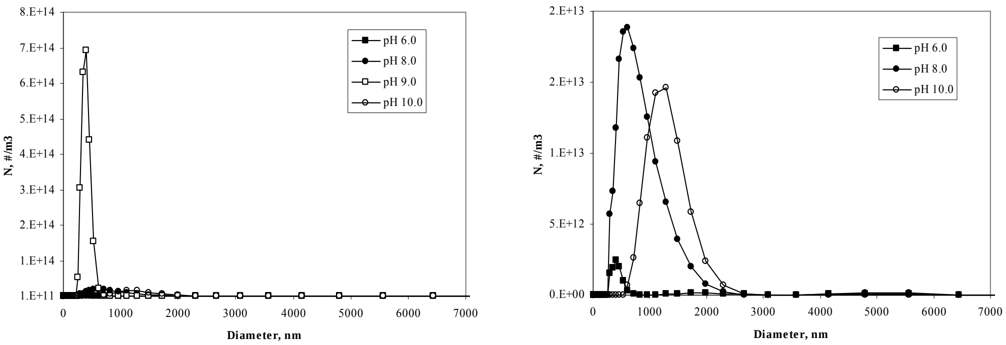

Figure 5.3 *Particle size distribution after 10 minutes of reaction. The graph on the right is a y-axis magnification of the graph on the left in order to show the distribution at pH 6.0.*

The distribution at pH 8.0 also showed a bimodal distribution with major peak at 615 nm, while the peak at 4800 nm was two orders of magnitude smaller and therefore not visible from Figure 5.3. The higher proportion of smaller particles at 10 minutes compared to 5 minutes implied that nucleation was faster than aggregation for the pH 6.0, 8.0 and pH 9.0 cases. The disappearance of the peak which was at 712 nm after 5 minutes in the pH 9.0 case was probably due to solution mediated transformation of the precipitates. The particles are much bigger for pH 10.0 because the oxidation at this stage was more than 90% complete. The change (at 10 minutes) in the particle size distribution compared to the one at 5 minutes could also be due to the formation of green rusts and transformation of polymeric ferrihydrite phases. Visual and X-ray powder diffraction analysis showed that green rust complexes were formed at this stage except for the pH 10.0 case.

c) Solids formed after 40 minutes of reaction

The particle number distributions are shown in Figure 5.4. The particle size distribution of the solids formed at this stage of the reaction showed narrower monomodal distributions at pH 6.0, 8.0 and 10.0.

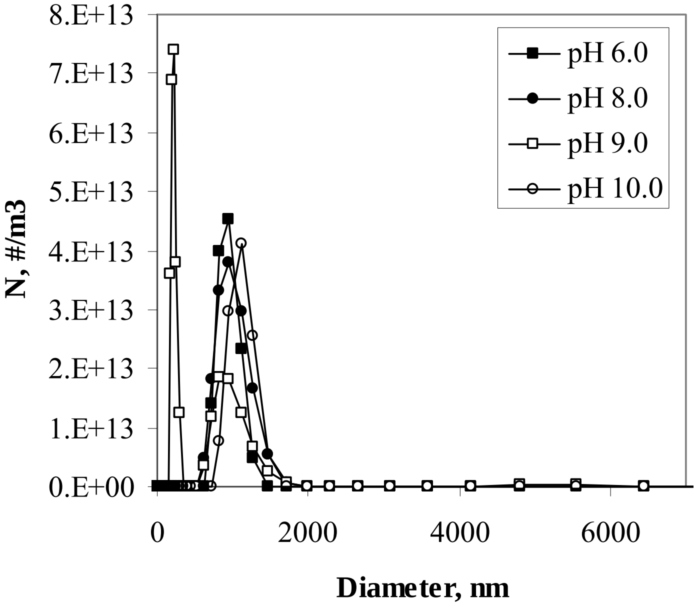

Figure 5.4 *Particle size distribution after 40 minutes of reaction*

The modal peaks were 955 nm, 955 nm and 1110 nm respectively. Two peaks (122 nm and 459 nm) were obtained at pH 9.0. These two peaks were probably a result of the continued solution-mediated transformation of most likely amorphous species into more crystalline and therefore more compact precipitates. The disappearance of the larger particles previously obtained at pH 6.0 and 8.0 was probably a result of solution-mediated transformation of the green rusts as air continued to be bubbled through the reactor. X-ray powder diffraction analysis confirmed the absence of green rusts in all precipitates at this stage of the reaction. This disappearance of the bigger particles cannot be attributed to dissolution because the concentration of dissolved iron continued to decrease during the course of the reaction. The decrease in the size of the particles for the pH 10.0 case was clearly due to the transformation of ferrihydrite into goethite (Lewis and Schwertmann, 1980). From this it can be concluded that the transformation of less stable species into more crystalline phases takes place in all cases but with the onset of the same coming earlier at pH 10.0 than at any other pH. From a wastewater treatment operation point of view this could mean that it is more beneficial (disregarding the increased mean particle size) to oxidise iron at pH 10.0 as this results in a more stable precipitate compared to oxidation at lower pH.

d) Solids formed after 90 minutes of reaction

The particle size distribution for the precipitate formed after 90 minutes of reaction is shown in Figure 5.5. The number distribution of the particles was monomodal with peak height at 1110 nm, 1280 and 712 nm for pH 6.0 8.0 and 9.0 respectively. The larger particle size at pH 8.0 was due to Van der Waals induced coagulation since the point of zero charge for most iron oxide hydroxides is around pH 7.0-8.0 (Jolivet et al., 2004).

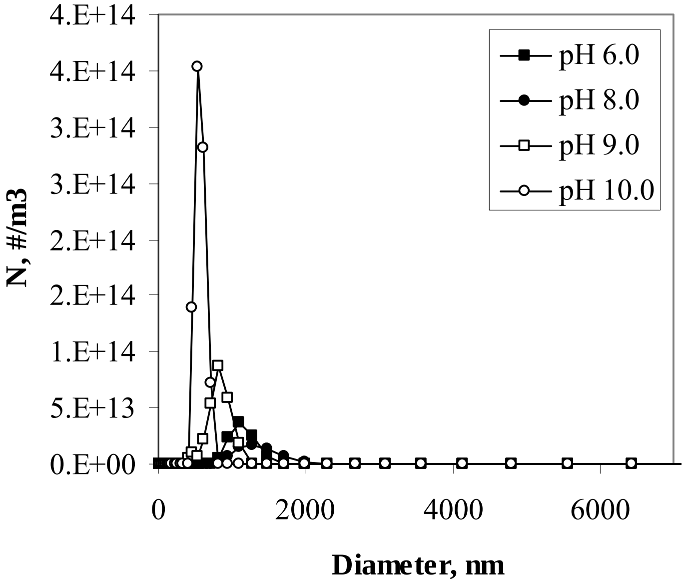

Figure 5.5 *Particle size distribution after 90 minutes of reaction*

The disappearance of the smaller size particles compared to the previous distributions and the increase in the modal size showed that the active size enlargement mechanism was aggregation for these particular pH cases. At pH 10, the modal size was 531 nm. The significantly smaller size was due to the dissolution of ferrihydrite to form the more stable goethite (Lewis and Schwertmann, 1980). Thus this stage represents the onset of 'goethite nucleation'.

e) Solids formed after 180 minutes of reaction

The number distribution of the particle size was monomodal with a peak at 1110 nm, 1480, 712 nm and 955 nm (Figure 5.6) for pH 6.0, 8.0, 9.0 and 10.0 respectively. The increase in the modal size at pH 10.0 was due to the formation of goethite since X-ray powder analysis showed that the major component at this stage was goethite (to be discussed in section 5.2.2.2). Cornell and Giovanoli (1985) also reported that ferrihydrite can transform into goethite at high pH in less than 24 hours.

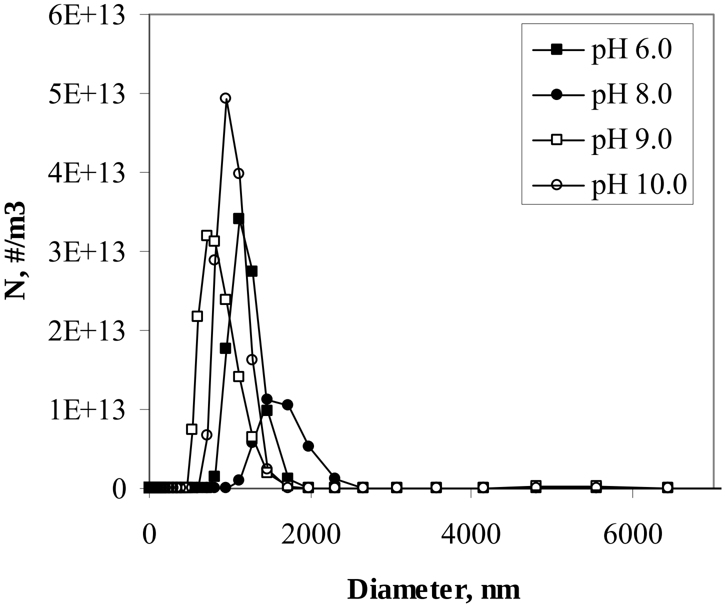

Figure 5.6 *Particle size distribution after 180 minutes of reaction*

f) Solids formed after 1440 minutes (24 hours) of reaction

The size distribution was narrower and monomodal with modal height at 1720 nm, 2300 nm, 1280 nm and 2670 for pH 6.0, 8.0, 9.0 and 10.0 respectively. In all cases there was a marked increase in the modal size of the particles accompanied by a corresponding decrease in the number of particles. The larger particle size obtained at pH 8.0 was due to Van der Waals induced aggregation since the point of zero charge of most iron oxide phases is around pH 7.0-8.0 (Jolivet et al., 2004). The decrease in the number of particles and increase in the modal size was probably due to aggregation and/or transformation amorphous ferrihydrite into goethite (Cornell and Giovanoli, 1985). The distribution is shown in Figure 5.7.

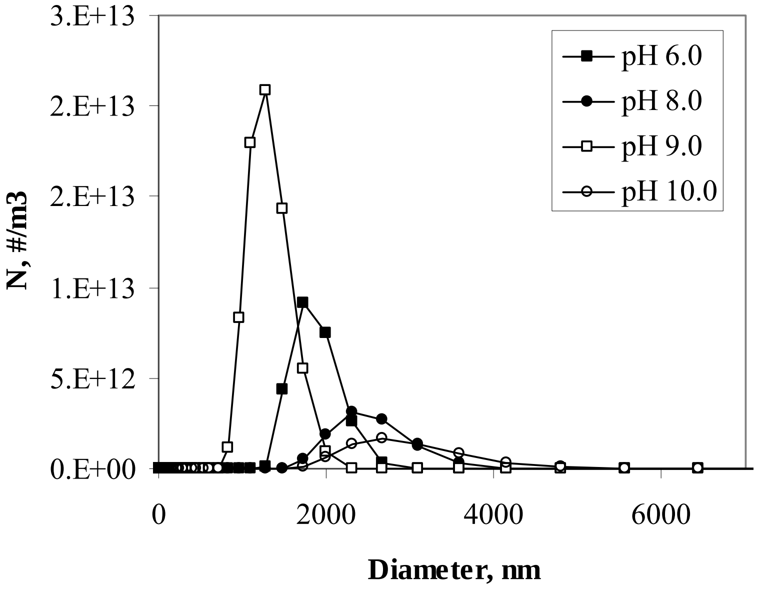

Figure 5.7 *Particle size distribution after 1440 minutes of reaction*

g) Polydispersity and Spread of the Particle Size Distribution

The span of the particle size distribution for each of the samples was estimated by calculating the relative standard deviation (RSD) of each distribution according to the equation;

$$\mathrm{RSD\%} = \frac{\mathrm{STDEV}}{(\bar{\mathrm{L}}_{1,0})} \times 100 \tag{5.1}$$

STDEV is the standard deviation of the distribution.

The variation of the RSD for each particle size distribution measurement is shown in Figure 5.8.

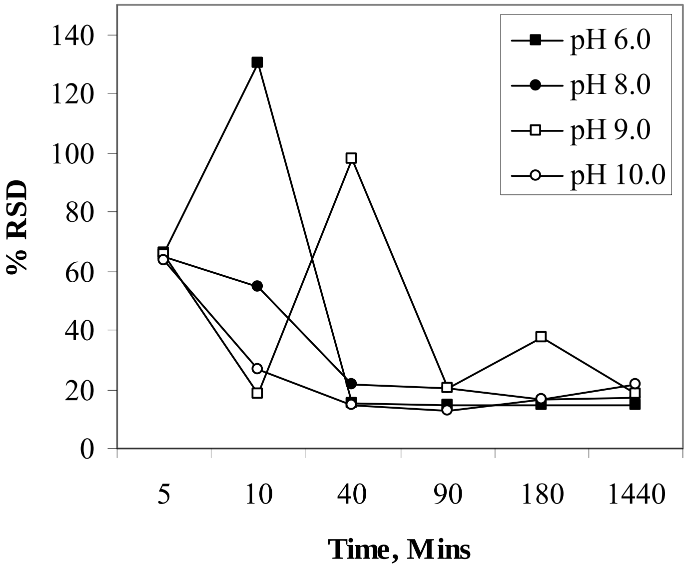

Figure 5.8 *Variation of RSD of the particle size distribution with time*

The plot indicates that the spread and the polydispersity of the particle size decreased with time for the pH 8.0 and 10.0 cases. The decrease in the RSD values for the pH 8.0 and 10.0 was probably due to increasing crystal order in the precipitates. The high initial RSD values for the pH 6.0 and 9.0 cases were due to the presence of the bimodal distribution at the initial stages of the process. As the bimodal distribution disappeared, the RSD values decreased and became more uniform. This trend could be due to the increasing order/crystallinity of the precipitated solids with time.

h) Evolution of number of particles (m_0) and mean size of particles, ($\overline{L_{1,0}}$)

The evolution of the zeroth moment (m_0) is shown in Figure 5.9. The increase in the total number of particles up to 40 minutes for cases pH 6.0, 8.0 and 9.0 was most likely due to nucleation. While breakage would have a similar effect on m_0, this is unlikely to be the cause of the observation since there was always a corresponding decrease in the amount of iron in solution which indicated consumption of supersaturation. The decrease in m_0 at pH 9.0 from 10 to 40 minutes was sharper than at pH 6.0 and pH 8.0. This indicated that the aggregation rates were higher at pH 9.0 than at pH 6.0 and 8.0 since aggregation is the only mechanism responsible for a decrease in the number of particles in this instance. From 90 minutes to 1440 minutes there was a continued decrease in m_0 for the four cases, this was probably due to Van der Waals forces or residual surface supersaturation induced aggregation. For the pH 10.0 case, after 5 minutes of reaction, the value of m_0 had already decreased, this is expected since at this stage the oxidation of ferrous iron was almost complete.

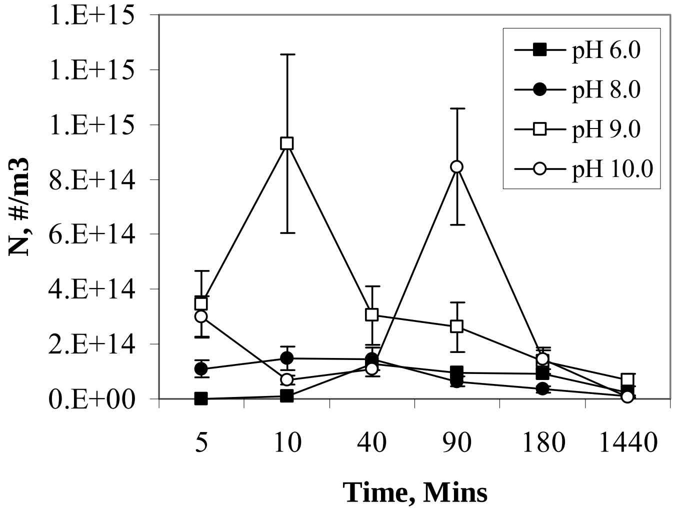

Figure 5.9 *Evolution of m_0 during the course of the reaction*

The change of the population based mean size ($\overline{L}_{1,0}$) of the particles as a function of time is shown in Figure 5.10. For cases pH 6.0 and 9.0, the initial decrease in $\overline{L}_{1,0}$ from 5 to 10 minutes was due to high rates of nucleation at the expense of growth and aggregation. From 10 minutes up to 90 minutes the mean particle size increased due to aggregation. This is supported by a corresponding decrease in m_0 for both cases. The near constant mean particle size between 90 and 180 minutes again showed that the system could have reached a state of dynamic equilibrium between particle breakage/or attrition and aggregation. For the pH 8.0 case, there was a gradual increase in the particle size up to the end of the reaction. This increase could only have been due to Van der Waals induced aggregation of the iron precipitates. A decrease in the population based average size for the pH 10.0 case from 5 minutes to 90 minutes was due to the transformation of ferrihydrite into goethite (Cornell et al., 1985). An increase in the average size from 90 minutes to 1440 was due to the aggregation and/or growth of goethite. In conclusion therefore, the formation of ferrihydrite particles at pH 6.0 to 9.0 is dominated by nucleation at the initial stages followed by limited growth. Aggregation dominates after the oxidation stage has been completed. At pH 10.0, the process is dominated by aggregation of ferrihydrite at the initial stages, followed by the dissolution/reprecipitation of goethite and finally by the aggregation of goethite.

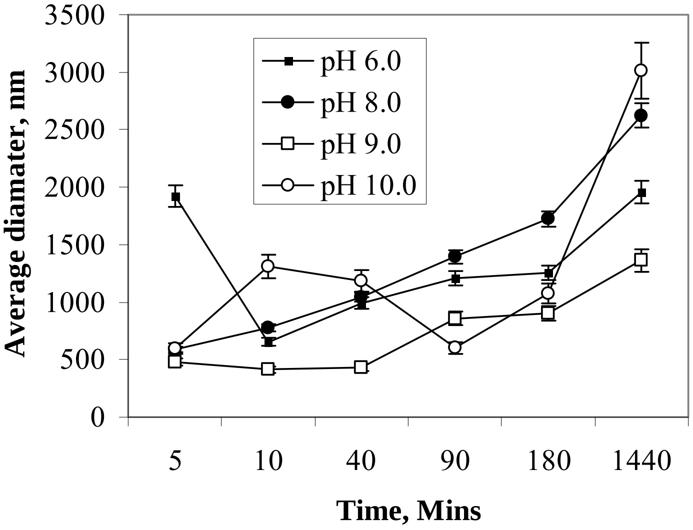

***Figure 5.10** Evolution of population based average size during the course of the reaction*

5.1.3.4 Particle settling rates and zeta potential

The settling rates were determined by measuring the height (cm) of the solids in a standard 1 L Imhoff cone. The observed particle size distributions were confirmed by settling rates and the zeta potential measurements shown in Figure 5.12. The results show that the settling rates at pH 9.0 were lower (corresponding to a smaller particle size) than those obtained at pH 8.0. This was unexpected. Visual observations indicated that the precipitates formed at pH other than 9.0 quickly coagulated to form flocs that settled faster.

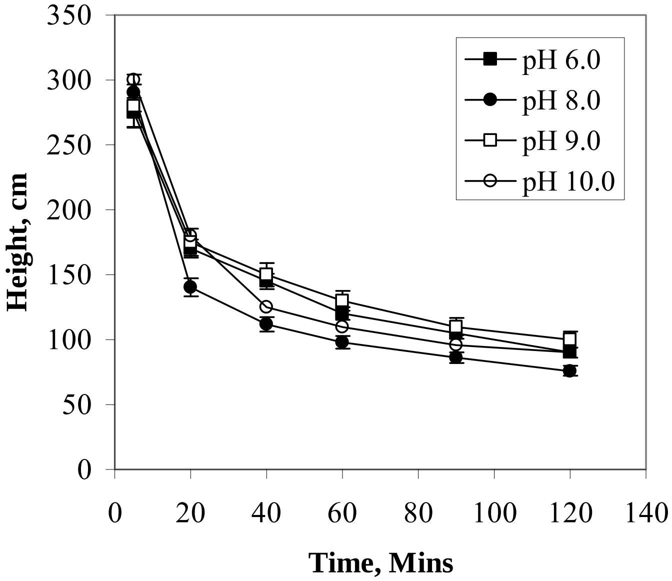

Figure 5.11 *Change in the solids height with time for the precipitates formed under the different pH conditions*

The explanation for the observed trends in settling rates was obtained from the zeta potential measurements (Figure 5.12) for the final precipitate sample collected after 1440 minutes.

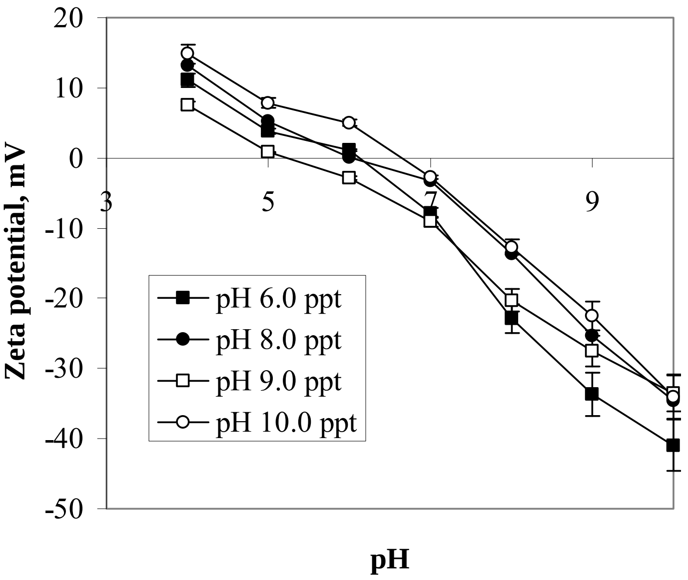

Figure 5.12 *Variation of the zeta potential with pH for the different precipitates.*

Figure 5.12 indicates that the precipitates formed at pH 6.0 and 8.0 had approximately the same point of zero charge of about pH 6. The precipitate formed at pH 10.0 had the highest point of zero charge of about 7. Everything else being equal this would make this particular solid material the fastest settling precipitate. This was not the case due to the smaller size of the particles. The point of zero charge for the precipitate produced under pH 9.0 conditions was about 5. This very low point of zero charge meant that the precipitate formed under pH 9.0 conditions was the most stable at the conditions of the measurement of the settling rates. From these zeta potential measurements, it can also be concluded that precipitates formed at 9.0 form the most stable dispersion and are therefore less amenable to coagulation and flocculation, resulting in the smaller particle size distributions as observed. Since the zeta potential for all the precipitates formed here was negative at pH 7.0, it can be concluded that the precipitates carry a net negative charge. This negative charge could be due to adsorbed SO_4^{2-} and/ or OH^- ions. Jönsson, (2003), who also found that SO_4^{2-} ions were always adsorbed on the surface of iron precipitates formed from acid mine drainage treatment.

The solids densities (m/v) were 0.87%, 0.92%, 0.85 and 0.90% for pH 6.0, 8.0, 9.0 and 10.0 respectively. The differences in the solids densities appear not to have a significant effect on the settling rates; this implies that it is more favourable to operate these processes at higher pH and thereby benefit from the kinetic advantages, since the same settling rates are achieved as at lower pH.

5.1.3.4 Morphology of the precipitates

The Scanning Electron Microscope (SEM) pictures for the final precipitate under the different reaction conditions showed that the particles were fluffy flocs or coagulates (Figure 5.13). The loose structural appearance also supports the view that the particles were not proper 'aggregates' formed from supersaturation induced processes, rather flocs formed from Van der Waals-induced electrostatic forces. Closer inspection of the pictures also indicate that the precipitates consisted of least two or more different types of precipitates or phases except for the pH 10.0 case. This also means that the bimodal distribution of the particles sizes observed in section 5.1.3.2 probably corresponded to crystals of different phases rather than to aggregates of the same phase. From the open structures of the particles, it is not surprising that the particles had high BET specific surface areas. A comparison of the SEM pictures indicate that freeze drying (Figure 5.13) reduces the aggregation of the particles during drying as opposed to air drying which results in caked material from which it is difficult to infer morphological properties.

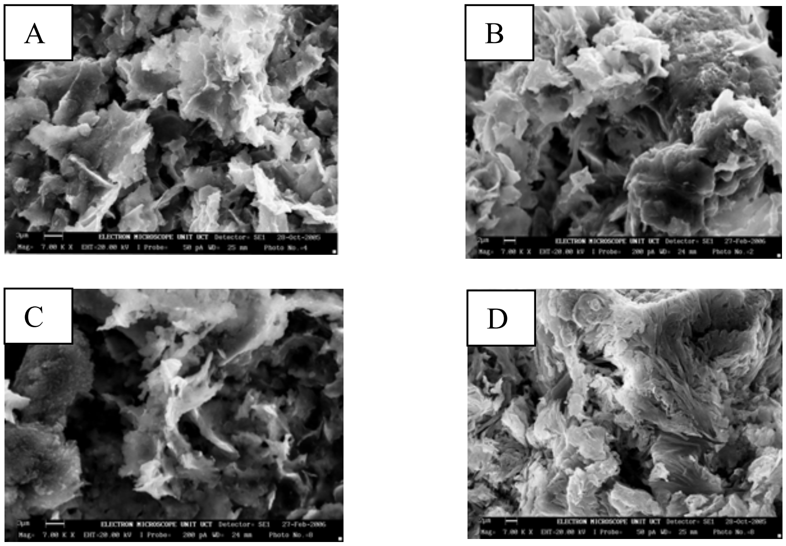

Figure 5.13 *SEM pictures of the freeze dried precipitates formed under the different pH conditions. A = precipitate formed under pH 6.0, B = pH 8.0, C = pH 9.0 and D = pH 10.0.*

5.1.3.5 Evolution of BET specific surface area

The change in the BET surface area with time is shown in Figure 5.14. The increase in the surface area from 5 to 40 minutes for the cases pH 8.0, pH 9.0 and 10.0, and up to 90 minutes for the pH 6.0 case could have been due to two factors. Firstly, the disappearance of the large particles which produced the second and third peaks in the particle size distribution could have resulted in an overall increase in the surface area of the particles. Secondly by considering Figure 5.1, it can be seen that in the corresponding time intervals for the pH 6.0, pH 8.0 and 9.0 cases, there was a corresponding consumption of supersaturation due to nucleation and a resultant increase in the proportion of smaller particles, this would have the same effect of increasing the BET surface area as in the first instance. The drop in the BET surface area after 40 minutes and 90 minutes for the pH 8.0, 9.0, and pH 6.0 cases respectively was most likely due to aggregation, resulting in the formation of ferrihydrite flocs. Indeed X-ray powder diffraction analyses at these time intervals showed the major component of the precipitates to be ferrihydrite. The traces of green rusts and lepidocrocite which were detected in the earlier stages could not be detected anymore. The decrease in BET surface area at the same point at pH 10.0 could not be explained. The next increase in the BET surface area for all cases could have been due to ageing which resulted in the formation of more crystalline phases. Ageing is accompanied by the release of adsorbed species like hydroxyl or sulphate ions (Jonsson, 2003) which allows for the penetration of nitrogen, thus resulting in higher surface areas.

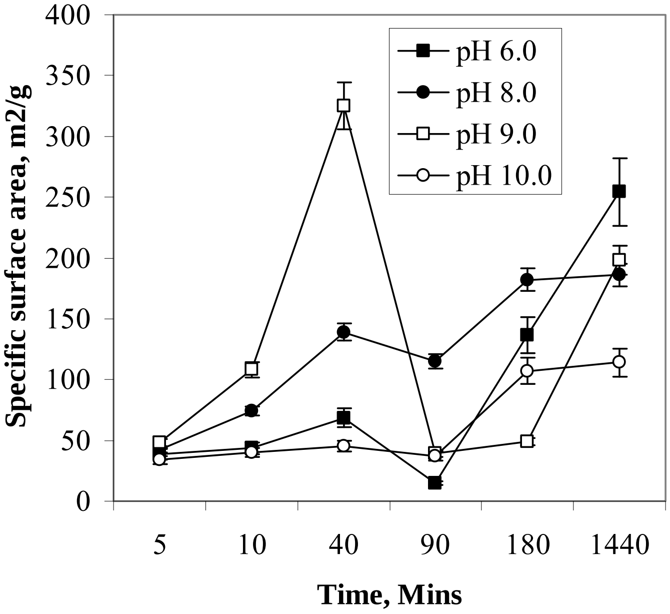

Figure 5.14 *Evolution of the BET specific surface area during the course of the reaction*

Also, sulphate is known to promote the aggregation of ferrihydrite particles and hinder the penetration of nitrogen (Claassen and Sanderbergh, 2006), which would result in lower BET surface areas. Measurement of the sulphate in solution showed that it was either adsorbed on the precipitate or incorporated in the precipitate or both during the early stages of the reaction. As the sulphate was released towards the end of the reaction, the disorder of the particles diminished, resulting in the formation of more crystalline species and hence higher BET specific surface areas (release of the sulphate allows penetration of more nitrogen and hence higher surface areas). During the earlier stages of the reaction the surface area of the particles formed at pH 9.0 was higher than at pH 6.0, in agreement with particle size measurement results. After the aggregation step, the BET surface area of the particles formed at pH 9.0 was lower than for the particles formed at pH 6.0. This could have been due to the presence of Fe^{2+} ions in the precipitate formed at pH 6.0 while the precipitate formed at pH 9.0 was predominantly Fe^{3+} at this stage. The Fe^{2+}/Fe^{3+} composition of the precipitates is shown in Figure 5.15.

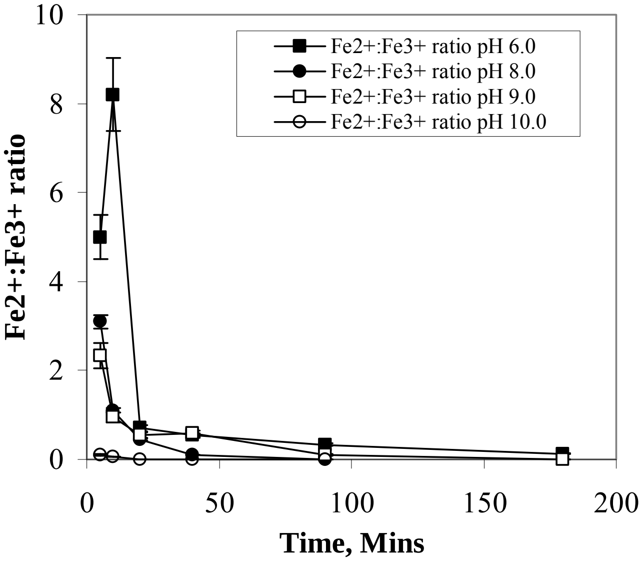

Figure 5.15 *Change in* $Fe^{2+}:Fe^{3+}$ *molar ratio of precipitates with time*

Another reason for this trend could be that the extent of aggregation is higher for the pH 9.0 case than for the pH 6.0 case, which resulted in lower BET surface areas. This can also be qualitatively inferred from Figure 5.8. The fact that there is an initial increase followed by a drop in the BET surface area in all cases and that the drop coincides with the disappearance of the bimodal distribution is very significant. The first significance is that the cycle of reactions that lead to the formation of the final product in the first three cases must be the same; the second is that, from a solid-liquid separation point of view, it should be technically better to effect solids liquid separation before the ferrous iron is completely oxidised in the three cases. The final BET specific surface area (≈200 m^2/g) found for the precipitates formed in the pH 6.0, 8.0 and 9.0 cases after 1440 minutes is typical of ferrihydrite. Schwertmann and Cornell, (2000) report surface areas for ferrihydrite precipitates in the range 200-300 m^2/g. The trend in the evolution of the BET specific surface area for both types of solids indicate that, regardless of the pH of operation, the sequence of reaction steps that lead to the formation of the final product could be the same for these cases except at pH 10.0. It is also important to mention that the individual specific surface areas have very little meaning since many different ranges have been reported for the same iron phases, for example, Jöhnsson (2003) reported surface areas of ferrihydrite of 42.9 m^2/g. More illustrations are found in Cornell and Schwertmann (Cornell and Schwertmann, 1996).

5.1.4 Conclusion

The rate of oxidation of Fe^{2+} in ferrous sulphate solutions for the pH 8.0, 9.0 and 10.0 cases is much slower than would be predicted from the rate equation given by Stumm and Lee (1961), Tamura et al., (1976b), Deng (1997) and Millero et al., (987). The reduction in the rate of oxidation was probably caused by a combination of the formation of solid complexes of Fe^{2+} (due to the high iron concentrations employed here unlike the cited works) (Jeon et al., 2003) and the high sulphate concentrations (Sung and Morgan, 1980; Tamura et al., 1976b). At pH 6.0, however, the experimental rate of oxidation was higher than that predicted from literature based calculations (2.1 mg(Fe^{2+})/l/min and 0.044 mg(Fe^{2+})/L/min respectively). This increased rate was due to the catalytic effect of the ferrihydrite solids (Sung and Morgan, 1980), (Tamura et al., 1976a). The initial fast decrease in Fe^{2+} in solution probably represents direct aqueous oxidation while the slower one represents the oxidation of complexed $Fe^{2+}$and Fe^{2+} adsorbed on ferrihydrite solids. This latter stage of the reaction represents the so-called instability of iron hydroxide sludge encountered in the treatment of acid mine drainage. To counter these transformation effects most operations employ a post precipitation stabilisation stage before final sludge disposal.

The characteristics of ferric particles formed from homogenous ferrous sulphate solutions are controlled by the rate of oxidation. High oxidation rates (achieved by raising the pH) produce high supersaturation levels, leading to high primary nucleation rates and the formation of small particles. However, there is competition between base-induced aggregation and nucleation. At pH 6.0, deprotonation dominates and the particles formed are bigger in size, whereas at higher pH, although there is more base available for deprotonating the cationic species, the high oxidation rates dominate, resulting in the formation of smaller particles. However, at pH 8.0, Van der Waals-induced aggregation dominates, resulting in the formation of bigger particles. At pH 10.0, these stages which take place during the initial stages of the formation of ferrihydrite could not be distinguished due to the more rapid kinetics experienced at this pH. The absence of hydroxyl ions necessary for deprotonation explains why Van der Woude and De Bruyn (1983b), Pavlides (1995) and Dousma and De Bruyn (1978) found a limiting 3-5nm size for the ferrihydrite particles compared to the several 100 nm obtained in this work. From the evolution of the zeroth moment, it can also be inferred that oxide hydroxide size enlargement is aggregation-dominated and growth limited. The aggregation is also enhanced around the point of zero charge of the precipitating iron species. Although the final particle sizes obtained in all cases are different, the solids formed have very similar settling characteristics. It seems logical therefore to operate HDS plants employing hydroxide oxidation and precipitation at higher than current pH values (although there is a cost trade-off for the higher pH) as this ensures higher throughput of sludge of the same settling character compared to lower volumes of sludge of the same settling characteristics that would be produced at current (lower) pH values. Operating at pH could also improve the iron conversion since, goethite, which is formed at pH 10.0 has the least solubility (Figure 1.3).

5.2 Mechanisms of formation of iron precipitates

5.2.1 Deducing the precipitate formation mechanisms

Assuming size independent growth and aggregation and absence of breakage, the molecular growth rate (G_0), aggregation kernel (β) and the aggregation rate (R_a) are given by equations 1.44 to 1.47. At constant volume, V, the same equations can be re-written as shown in equations 5.1, 5.2 and 5.3 respectively (Randolph and Larson, 1988).

$$G_0 = \frac{\Delta m_3}{3\Delta t \overline{\overline{m_2}}} \tag{5.1}$$

$$\beta = \frac{\Delta m_2}{\Delta t \left(\overline{m_1}\right)^2} - 2\frac{G_0}{\overline{\overline{m_1}}} \tag{5.2}$$

$$R_a = -\frac{\beta m_0^2}{2} \tag{5.3}$$

Where Δm_3 is the change in the third moment

Δm_2 is the change in the second moment

m_0 is the zeroth moment

$\overline{m_1}$ and $\overline{m_2}$ are mean first and second moments respectively

Δt is the time, (s)

These equations (5.1 to 5.3) were used to compute the respective process rates. The same experimental procedure and set up as described in sections 2.1 and 2.2 was used to obtain the results presented and discussed here.

5.2.2 Results and discussion

5.2.2.1 Evolution of precipitation kinetic processes

a) Evolution of the nucleation rate

The change in the average nucleation rate is shown in Figure 5.16. It must be noted that it was assumed here that there was no breakage and attrition, thus the nucleation rate was obtained by dividing m_0 by time. Only positive nucleation rates were considered in the discussions that follow. Negative values were taken to mean that nucleation process was less than aggregation process for that particular instance although it has to be noted that the same nucleation process could be significant. In all instances the nucleation rate was highest for the pH 9.0 case compared even to the pH 10.0 case. The high nucleation rates were probably due to the fact that pH 9.0 is much further away from the point of zero charge of these particles which was found to be around pH 5. This would mean sustained repulsion among the particles thus preventing them from coagulating or aggregating. The point of zero charge for the precipitates formed at pH 10.0 was found to be above 7.5. This means that these particles had a greater tendency to coagulate or aggregate compared to those formed at pH 9.0. This trend in the evolution of the nucleation rates is also in agreement with the particle size distribution results (Figures 5.2 -5.7).

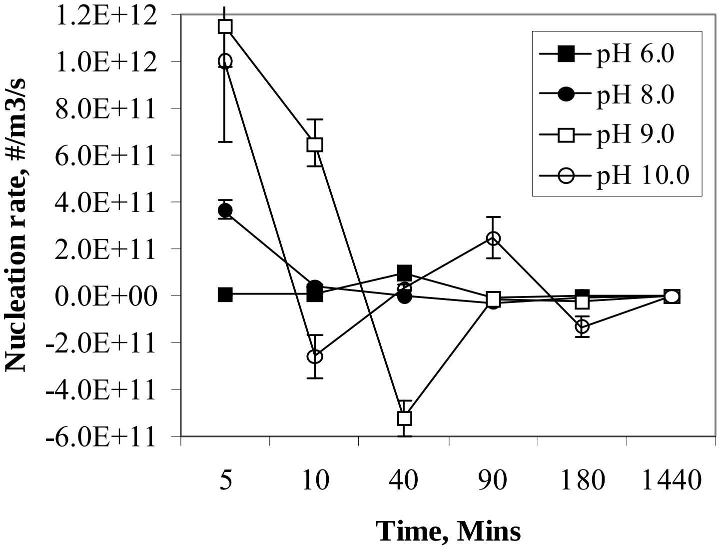

Figure 5.16 *Change in the nucleation rate with time*

Figure 5.16 also shows that the nucleation of the first primary particles takes place within the first 5 minutes of the reaction for the pH 8.0, 9.0 and 10.0 cases. This is also in agreement with high oxidation rates obtained which would result in high supersaturation levels and hence high nucleation rates. After 10 minutes, nucleation rate calculations at pH 10.0 gave negative values, implying that the rate of crystal birth by nucleation was already lower than death by aggregation or dissolution. The increase in the nucleation rate (for the pH 10.0 case) at 40 minutes and second drop after 90 minutes probably signals the onset of secondary processes like dissolution and reprecipitation of the more stable phases. The same trends can be observed for the other cases. This shows that, no matter what the operational pH, the cyclic secondary reactions or transformations involved in the oxidation and precipitation of iron are mechanistically the same. It can be deduced that the oxidation-precipitation of iron is nucleation dominated at the initial stages, with the nucleation decreasing and increasing with time in correspondence to transformation reactions that result in the formation of the more stable phases.

b) Evolution of the growth rate

The growth rates calculated for both cases covered the entire experimentation time. The results for the change in the growth rate are shown in Figure 5.17. Up to 90 minutes the growth rate at pH 6.0 was higher than all the other cases. This is expected since low supersaturation, (due to lower oxidation rates), which was experienced at low pH, promotes growth at the expense of nucleation. The higher growth rates at pH 9.0 compared to pH 8.0 were unexpected. This was probably due to the greater repulsive forces which suppressed aggregation, thus allowing growth to be the only kinetic process responsible for the consumption of the supersauration. The very low growth rates, of the order of 1×10^{-17} - 1×10^{-10} m/s, obtained show that the precipitation of iron from ferrous sulphate solutions is growth limited, more so at higher pH. Pavlides (1995) also concluded that the formation of ferric iron precipitates was growth limited. The gradual decrease in the growth rates with time was probably due to the exhaustion of supersaturation from the solution.

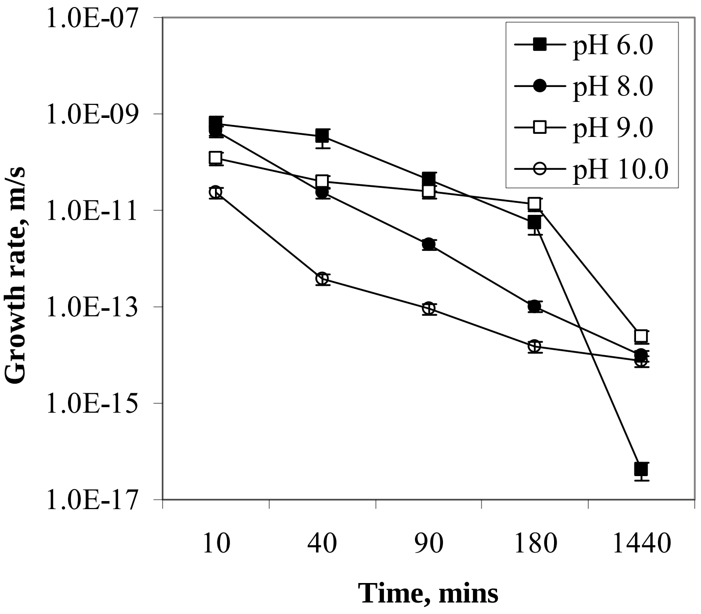

Figure 5.17 *Change in the molecular growth rate (G_0) with time*

c) Evolution of the aggregation rate

The change in the aggregation rates with time for both experimental cases is shown in Figure 5.18. The aggregation rates were all positive during the first 10 minutes of the process, this is evidence that at the initial stages the precipitation of iron was aggregation dominated. That the highest aggregation rates were obtained for the pH 10.0 case, (for the first 10 minutes) was due to the higher rates of oxidation which resulted in increased number of particles. This is because aggregation rate has second order dependence on the number of particles, m_0, as shown in equation 5.3. The negative values obtained after 40 minutes for all the other cases except pH 9.0, could indicate that aggregation was not the dominant particle enlargement mechanism, and probably coincided with the onset of transformation reactions. During the transformation of phases, it is possible that supersaturation may only be created on the surface of the precipitates and not in the bulk solution. This “surface supersaturation” may then induce aggregation of the forming phases. It can thus be suggested that the positive aggregation rates obtained after 90 minutes were probably due to surface supersaturation-induced aggregation accompanied by transformation. This surface supersaturation could not be detected by spectrophotometric determination because the Fe^{3+} ions are probably adsorbed on the surface of the existing solids. Again the trend (decrease-increase and decrease) is an unexpected result under classical precipitation kinetics because when m_0 decreases and $\overline{L_{1,0}}$ decreases, then the aggregation rate should also decrease.

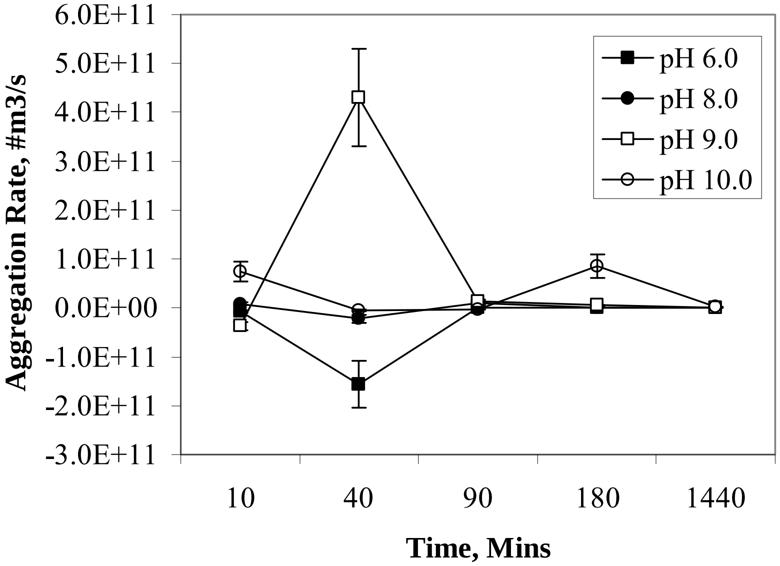

Figure 5.18 *Change in the aggregation rate (R_a) with time*

The decrease in m_0 and increase in $\overline{L_{1,0}}$ without an accompanying decrease in the aggregation rate can probably be explained in terms of solution transformation. In the earlier sections (5.1.3.2) it was shown that there was a disappearance of the bigger particles although the population based mean size continued to increase. This dissolution and re-precipitation of the iron species could be responsible for the increase in the aggregation rate without an accompanying decrease in m_0 and increase in $\overline{L_{1,0}}$.

These dissolution and reprecipitation processes can also be explained in terms of the evolution of Fe^{2+} and Fe^{3+} composition in the precipitate during the course of the reaction. This is shown in Figure 5.15. This ratio shows that although there was no detectable soluble iron (that is, detectable supersaturation) in solution, the presence of

Fe^{2+} in the precipitate means that this could provide surface supersaturation that could result in further nucleation or growth or aggregation or all of these processes. The other meaning of Figure 5.15 is that, although the particles formed at pH 6.0 are bigger and easier to dewater, they are less stable compared to those formed at higher pH. This could probably be the explanation for the anomalous trend obtained for the aggregation rates. The other implication, especially for wastewater treatment operations, is that it would be better to operate treatment plants at higher pH as this would ensure the formation of more stable precipitates at higher plant throughput that may not require post precipitation stabilisation.

5.2.2.2 Transformation of the precipitates

The data obtained from the characterisation of the iron precipitates can be used to make inferences about the transformation of the iron precipitates. Parameters such as the Fe^{2+}/Fe^{3+} ratio yield valuable information on the chemical nature and stability of the precipitates. In this section, the information obtained from the characterisation of the precipitates and some more evidence that will be presented here will be used to make inferences and conclusions about the transformation of the iron phases.

As mentioned earlier, (Section 1.3.4) the transformation of iron species under alkaline conditions involves the formation of green rusts. Thus, following the colour changes in the reaction suspension can yield important qualitative information regarding the possible process mechanisms. In this study, photographs of the suspension were taken at different time intervals during the course of the reaction for the four pH levels investigated. These photographs are shown in Figure 5.19.

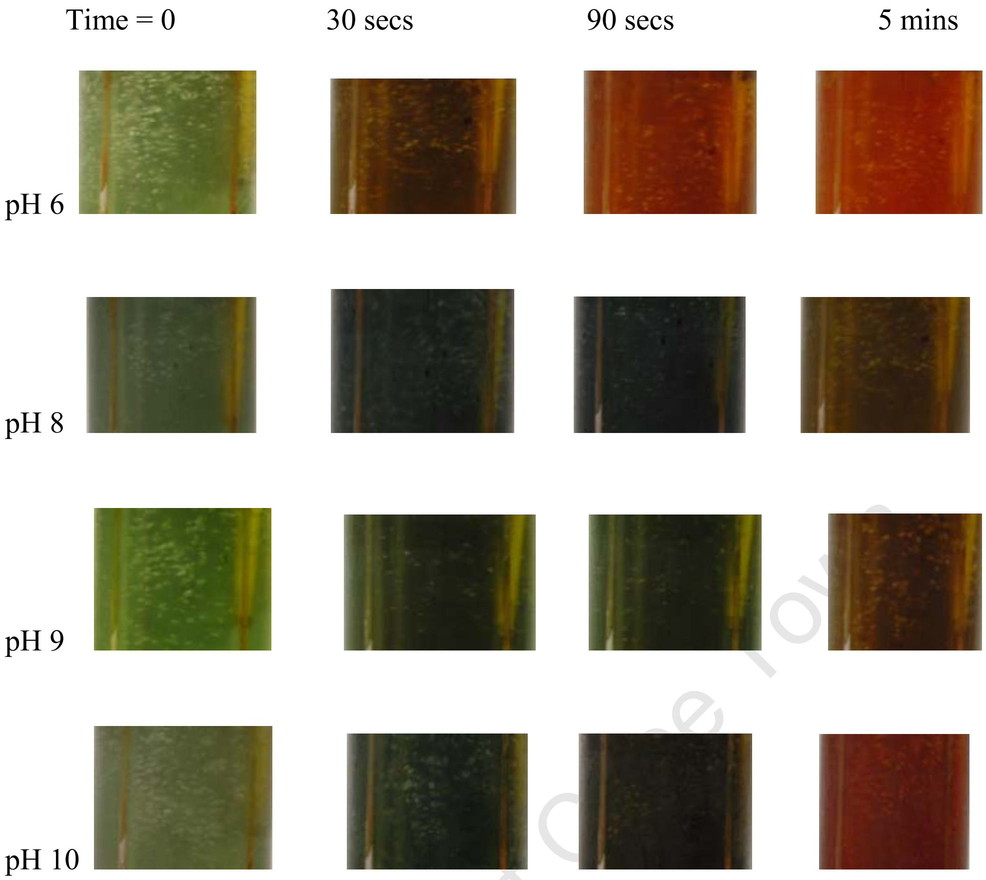

Figure 5.19 *Colour changes during the oxidation precipitation of iron. Photographs taken at time = 0 seconds, 30 seconds, 90 seconds and 5 minutes.*

From the photographs, it can be observed that green rusts were certainly formed in all the instances except for the pH 6.0 case. The pH 8.0 case showed the highest colour intensity, this is expected since the solubility of green rusts and ferrous hydroxide is around pH 8.0 (Jolivet et al., 2004). An analysis of soluble SO_4^{2-} also showed that, even before the onset of the oxidation reaction, some of the ferrous ions had already precipitated as ferrous hydroxide. This is shown in Figure 5.20. The ferrous hydroxide was also formed for the pH 9.0 and pH 10.0 cases.

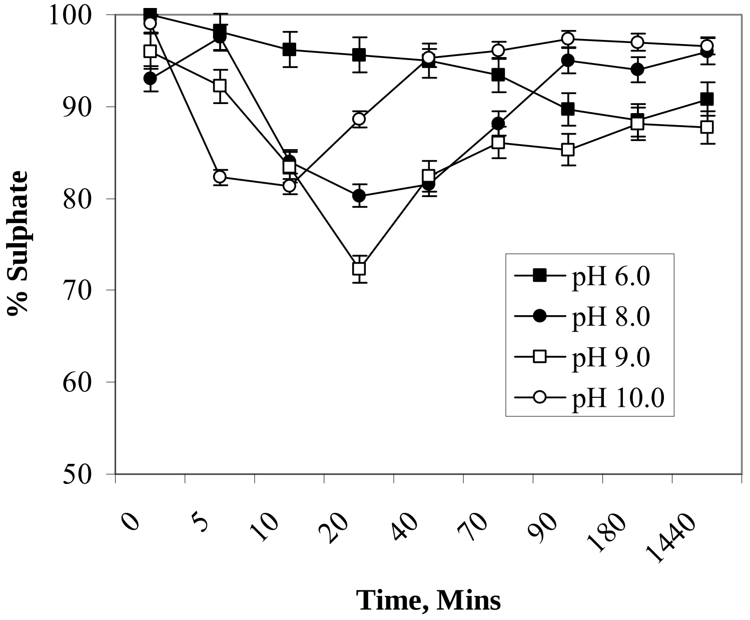

Figure 5.20 *Variation of soluble sulphate ion as a percentage of the sulphate added as* $FeSO_4$ *with time*

The formation of the solid ferrous hydroxide has significant implications on whether the oxidation of ferrous iron will be solid state oxidation (SSO) or dissolved state oxidation (DSO). From this result it can be concluded that the oxidation of ferrous iron was both solid state oxidation and DSO. Since the rate laws from literature (equations 1.6 and 1.9) do not take into account solid state oxidation, this could be one of the reasons for their failure to properly fit the experimental results presented here. The drop in the sulphate ion concentration for the pH 8.0, 9.0 and 10.0 cases was due to the formation of green rusts which incorporate the sulphate ion. The fact that at the end of the reaction, not all sulphate was recovered in solution for all the cases is an indication that green rust formation was not responsible for all the sulphate depletion. It is most likely that the remainder of the sulphate was adsorbed on the surfaces of the precipitate or that phases like schwertmannite were formed although they could not be detected by X-ray powder diffraction. Schwertmann and Fechter (1994) also found trends in soluble sulphate similar to the ones presented here and concluded that green rusts were precursors for the formation of lepidocrocite.

5.2.2.3 Evolution of the crystalline component

The evolution of the amorphous components in the solid precipitates can be used also to make inferences about the transformation reactions. The technique is based on the fact that ferrihydrite dissolves in acidified ammonium oxalate while the crystalline phases do not. The test was carried out as outlined in Appendix 1.2

The proportion of ferrihydrite was calculated using the equation;

$$\%\,\text{Ferrihydrite} = \frac{\text{Fe}_{\text{AAO}}}{\text{Fe}_{\text{Tot}}} \times 100$$

Where Fe_{AAO} represents the amount of iron soluble in acidified ammonium oxalate and Fe_{Tot} represents total iron found by digestion in concentrated HCl. The results of this test are shown in Figure 5.21.

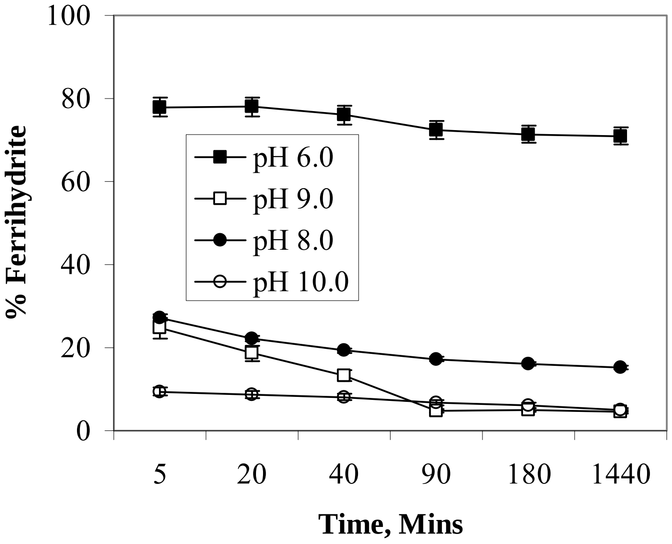

Figure 5.21 *Evolution of the ferrihydrite composition with time*

Figure 5.21 shows that at pH 6.0 the major component (70 %) of the precipitate was amorphous ferrihydrite. The DRIFT results showed that the crystalline part of this precipitate was lepidocrocite (Figure 5.22). The transformation of the precipitate at pH 6.0 thus consisted of the conversion of cationic polymers and probably some green rusts into ferrihydrite and lepidocrocite (constituting about 30% of the final product) respectively. These two transformation processes were responsible for the disappearance of the bigger particles from the particle size distributions shown earlier (Figures 5.2, 5.3 and 5.4). X-ray powder diffraction patterns obtained also confirmed the presence of lepidocrocite and ferrihydrite in the precipitate (Figure 5.23)

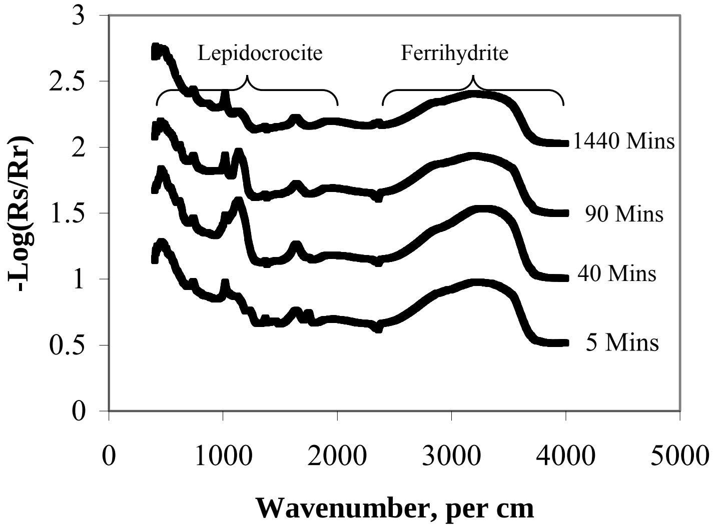

Figure 5.22 *DRIFT spectra of the precipitate formed under pH 6.0 conditions.*

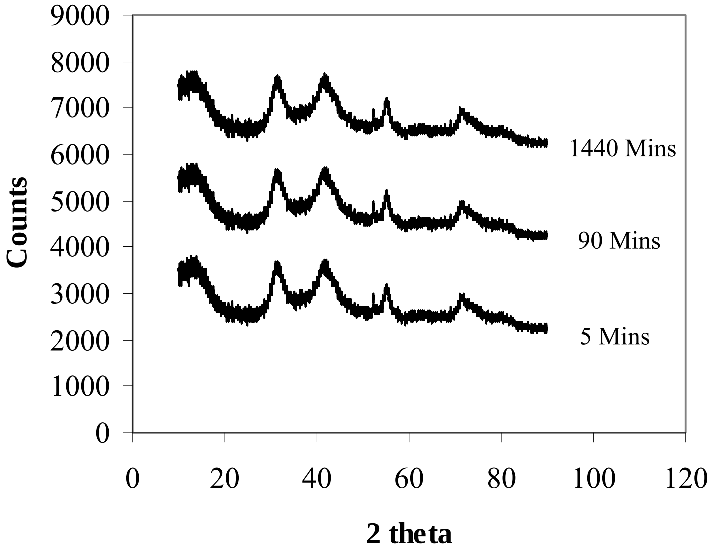

Figure 5.23 *X-ray powder diffraction spectra of the precipitate formed under pH 6.0 conditions. (Appendix 4, Figure 5)*

Considering the pH 8.0 and pH 9.0 cases, amorphous ferrihydrite constituted about 2% after 5 minutes and about 5% at the end of the reaction after 24 hours. From X-ray powder diffraction analyses, the crystalline component was made up of mainly lepidocrocite and traces of feroxyhyte (Figures 3.24 and Figure 3.25). The formation of feroxyhyte is an indication that the rate of oxidation was relatively high compared to the pH 6.0 case (Cornell and Schwertmann, 1996).

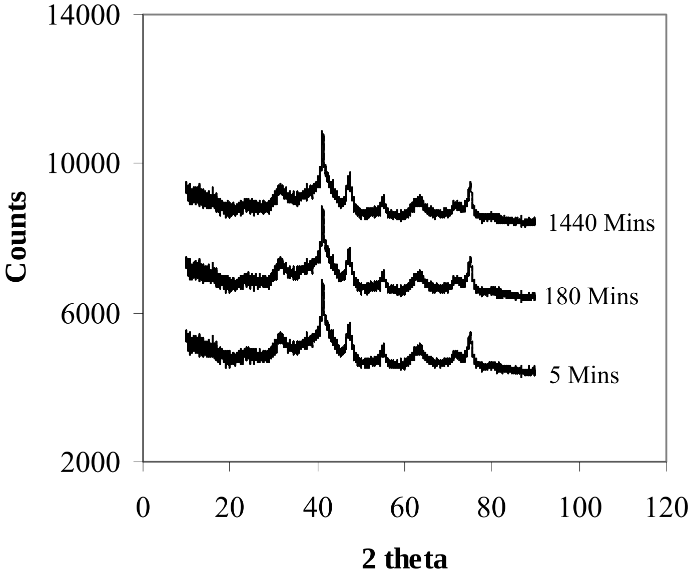

Figure 5.24 *X-ray powder diffraction pattern of the precipitate formed under pH 8.0 conditions. (Appendix 4, Figure 6)*

This means that the evolution of the particle size distribution was due to the transformation of polycationic monomers into feroxyhyte and of green rusts into lepidocrocite. However, the formation of feroxyhyte from green rusts cannot be ruled out. The XRD spectra for the pH 8.0 and 9.0 are shown in Figures 5.24 and 5.25 respectively. Interestingly the precipitate formed under pH 9.0 conditions was mainly ferrihydrite and lepidocrocite and appeared to have a greater proportion of amorphous or fine material as opposed to the pH 8.0 case. No traces of feroxyhyte were identified. The broad peaks in the spectra indicate that the precipitate had significant proportions of amorphous ferrihydrite or fine sized lepidocrocite.

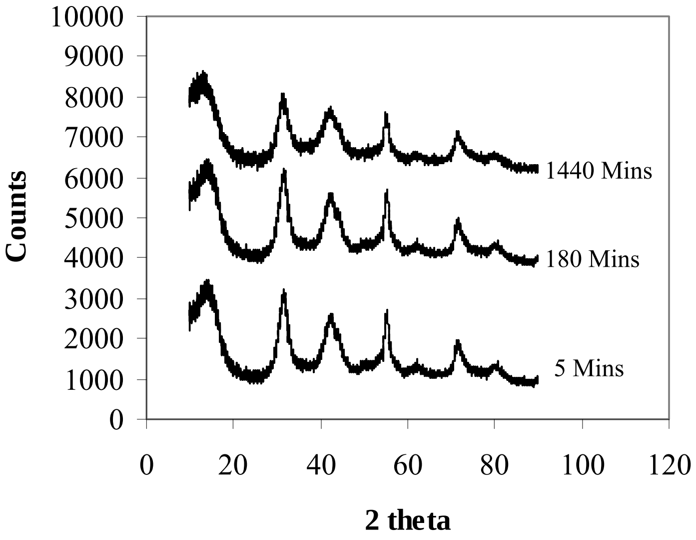

Figure 5.25 *X-ray powder diffraction spectra of the precipitate formed under pH 9.0 conditions. (Appendix 4, Figure 7)*

From the particle size distribution results (Figure 5.10), it is most likely that the broad peaks were due to the formation of small sized lepidocrocite particles. It is unlikely that the broad peaks were due to ferrihydrite since it is known that ferrihydrite has a high tendency to flocculate (Gan et al., 2005) thus forming bigger particles. The small particle size distribution could also have resulted in higher charge density around the particles which could explain the lower point of zero charge obtained for these particles.

The composition of the precipitate formed under pH 10.0 conditions was mainly crystalline material throughout the course of the reaction (Figure 5.21). X-ray powder diffraction analyses from Figure 5.26) showed that the crystalline component was mainly goethite but feroxyhyte was also present in significant proportions. The fact that the peaks were not very broad shows that there was very little amorphous material or ferrihydrite in this precipitate. Again the formation of feroxyhyte is indicative of very fast oxidation kinetics. The goethite was probably formed from the transformation of ferrihydrite since it is known that at high pH ferrihydrite will transform into goethite at relatively fast rates (Lewis and Schwertmann, 1980). This relatively fast transformation of ferrihydrite into goethite could be significant for wastewater treatment engineers. First it means that it will not be necessary to have a post precipitation stabilisation facility. Secondly operation at higher pH ensures faster kinetics and therefore higher plant throughputs.

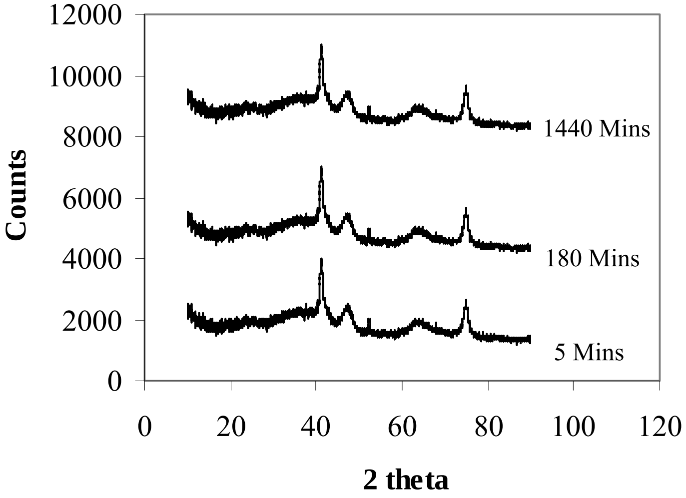

Figure 5.26 *X-ray powder diffraction pattern of the precipitate formed under pH 10.0 conditions. (Appendix 4, Figure 8)*

5.2.2 Conclusion

From results presented here, it is evident that the pH has a profound effect on the particle size distribution of the final precipitation product and the overall process kinetics and hence plant throughput, and the stability of the precipitates formed. High pH promotes high oxidation rates with resultant increased plant throughput and more stable precipitates but with significantly smaller particle size distributions.

The challenge for the wastewater treatment design engineer is two-fold; first whether to effect solids-liquid separation before oxidation is complete and get better solids-liquid separation at the expense of solids stability or allow for complete oxidation and get poorer removals but stable solids. The second scenario is to choose between fast or slow oxidation kinetics. High oxidation rates give a more stable precipitate in a shorter time period and hence higher treatment throughput. On the other hand, slow oxidation kinetics give bigger particles and better removals but less throughput and less stable precipitates. Obviously designers of such plants have the challenge of striking a balance among all these significantly intertwined parameters. In summary the oxidation precipitation of iron from ferrous solutions can be summarised as consisting of the following process steps:

Rapid initial homogeneous oxidation of Fe^{2+} at low pH and heterogeneous oxidation at higher pH followed by the instantaneous formation of primary particles (nucleation) from Fe^{3+} referred to as polynuclear cationic species (Blesa and Matijevic, 1989). These particles increase in size by a condensation mechanism resulting in the ejection of hydrogen ions (Jolivet et al., 2004). The rate of nucleation increases as the pH increases.

The particles formed associate with Fe^{2+} from solution through an adsorptive mechanism resulting in the formation of unstable green rusts at pH levels 8 and higher and ferrihydrite flocs with Fe^{2+} possibly adsorbed on them. These are the particles that were responsible for the higher modal sizes observed in the particle size distribution during the early stages of the reaction. Because of faster kinetics, precipitates formed at higher pH take shorter time periods to transform and completely oxidise the Fe^{2+}. This stage of the process is associated with limited growth of the particles and solution mediated transformation of the particles.

The last stage of the process is the aggregation of the particles. In this stage the mainly ferrihydrite particles consume the final traces of supersaturation by an aggregative mechanism (through the formation of inter-particle bridges) at pH 6.0 and through transformation into more crystalline phases at pH 8.0 to 10.0. The final aggregates formed at higher pH have a smaller size due to the initial high nucleation rates compared to the particles formed at lower pH.

Table 5.2 summarises the active kinetic processes and the effect of pH on these processes as well as on the final product.

***Table 5.2** Summary of the interactions and active processes in the oxidation precipitation of iron from ferrous sulphate solutions*

Kinetic process	**Lower pH (6.0)**	**Higher pH (8.0-10.0)**
Nucleation rate	Lower	Higher
Growth rate	Higher (but limited)	Lower (still limited)
Aggregation rate	High	High
Transformation	Slower	Faster
Stability	Lower	Higher
Particle size	Bigger	Smaller

The transformation processes can be further summarised as shown in the schematic Figure 5.27

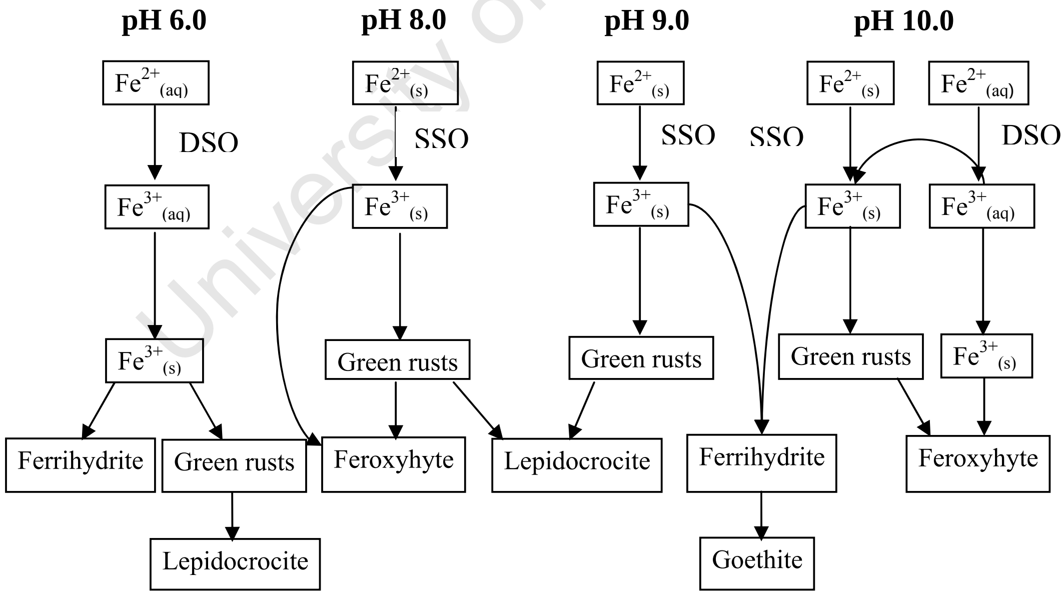

***Figure 5.27** Schematic diagram showing the transformation pathways during the oxidation precipitation of iron. DSO = dissolved state oxidation, SSO = solid state oxidation*

From the above scenarios, it can be concluded that the oxidation precipitation of iron involves complex reactions and transformations. This in turn results in complex precipitation process kinetics where it is difficult to isolate the competing nucleation, growth and aggregation processes. The transformation reactions further complicate these processes. In spite of these difficulties, it has been demonstrated here that, by using simple moment transforms and both qualitative and quantitative analytical techniques, inferences could be made about the mechanisms involved in the formation of iron precipitates from high concentration ferrous sulphate solutions at high pH. It has also been demonstrated that, by using various analytical techniques, valuable information can be obtained regarding the transformation and stability of various iron precipitates. The formation of crystalline precipitates at high pH is very significant, first, it is contrary to most studies (Kostanbader and Haines, September 1970), (Bosman, 1974), (Gan et al., 2005) which report that the product of the high density sludge process is amorphous ferrihydrite. Secondly, the formation of ferrihydrite is known to enhance the removal of other pollutants (organics and metals) by adsorption and co-precipitation; so if the ferrihydrite is not formed this could mean that the process may not be as effective with respect to the removal of other pollutants or that the crystalline precipitates formed here also have the same adsorption and co-precipitation properties as ferrihydrite. These results have profound impacts for the wastewater treatment operator in that optimum operational conditions will need a balance among the desired metal removals, throughput requirements, stability issues and dewaterability.

References

Blesa, M. A. and Matijevic, E. (1989), Phase transformations of iron oxides, oxohydroxides, and hydrous oxides in aqueous media, *Advances in Colloid and Interface Science*, vol. 29, pp. 173-221.

Bosman, D. J. (1974), The improved densification of sludge from neutralised acid mine drainage, *Journal of the South African Institute of Mining and Metallurgy*, pp. 340 - 348.

Claassen, J. O. and Sanderbergh, R. F. (2006), Particle growth parameters in the precipitation of metastable iron phases from zinc-rich solutions, *Hydrometallurgy*, vol. 84, pp. 165-174.

Cornell, R. M. and Schwertmann, U. (1996), The Iron Oxides; Structure, Properties, Reactions and Uses, VCH, Weinheim.

Cornell, R. M., Giovanoli, R. (1985), Effect of solution conditions on the proportion and morphology of goethite formed from ferrihydrite, *Clays and Clay Minerals*, vol. 33, pp. 424-432.

Cornell, R. M., Giovanoli, R., Schneider, W. (1989), Review of the hydrolysis of iron(III) and the crystallisation of amorphous iron(III) hydroxide hydrate, *Journal of Chemical Technology and Biotechnology*, vol. 46, pp. 115-134.

Deng, Y. (1997), Formation of iron(III) hydroxides from homogeneous solutions, *Water Research*, vol. 31, pp. 1347 - 1354.

Dousma, J. and de Bruyn, P. (1978), Hydrolysis-precipitation studies of iron solutions II. Aging Studies and the Model for Precipitation from Fe(III) Nitrate Solutions, *Journal of Colloid and Interface Science*, vol. 64, pp. 154 - 170.

Flynn, C. M. J. (1984), Hydrolysis of inorganic iron(III) salts, *Chemical Reviews*, vol. 84, pp. 31 - 41.

Gan, W. Y., Selomulya, C., Tapsell, G., Amal, R. (2005), Densification of iron(III) sludge in neutralisation, *International Journal of Mineral Processing*, vol. 76, pp. 149-162.

Jambor, L. and Dutrizac, J. E. (1998), Occurrence and constitution of natural and synthetic ferrihydrite, a widespread iron oxyhydroxide, *Chemical Reviews*, vol. 98, pp. 2549 - 2585.

Jeon, B. H., Dempsey, B. A., Burgos, W. D. (2003), Kinetics and mechanisms for reaction of Fe(II) with iron (III) oxides, *Environmental Science and Technology*, vol. 37, pp. 3309-3315.

Jolivet, J., Chaneac, C., Tronc, E. (2004), Iron oxide chemistry. From molecular clusters to extended solid networks, *Chemical Communications*, pp. 481 - 487.

Jonsson, J. (2003), Phase transformations and surface chemistry of secondary iron minerals formed from acid mine drainage. PhD Thesis, Umea University. Umea.

Kostanbader, P. D. and Haines, G. F. (September 1970), High density sludge treats acid mine drainage, *Coal Age*, pp. 90 - 97.

Lewis, D. G. and Schwertmann, U. (1980), The effect of [OH] on the goethite produced from ferrihydrite under alkaline conditions, *Journal of Colloid and Interface Science*, vol. 78, pp. 543-553.

Millero, F. J., Sotolongo, S., Izaguire, M. (1987), The oxidation kinetics of Fe(II) in seawater, *Geochimica et Cosmochimica Acta*, vol. 51, pp. 793 - 801.

Pavlides, A. G. (1995), The Precipitation of Iron Oxy-hydroxides from Ferrous Sulphate Solution. MSc Thesis, University of Witswatersrand. Johannesburg.

Schwertmann, U. and Cornell, R. M. (2000), Iron Oxides in the Laboratory, Preparation and Characterization, 2nd Edition, Wiley-VCH, Weinheim.

Schwertmann, U. and Fechter, H. (1994), The formation of green rust and its transformation to lepidocrocite, *Clay Minerals*, vol. 29, pp. 87 - 92.

Stumm, W. and Lee, G. F. (1961), Oxygenation of ferrous iron, *Industrial and Engineering Chemistry*, vol. 53, pp. 143 - 146.

Sung, W. and Morgan, J. J. (1980), Kinetics and product of ferrous iron oxidation in aqueous systems, *Environmental Science and Technology*, vol. 14, pp. 561 - 568.

Tamura, H., Goto, K., Nagayama, M. (1976a), The effect of ferric hydroxide on the oxygenation of ferrous ions in neutral solutions, *Corrosion Science*, vol. 16, pp. 197 - 207.

Tamura, H., Goto, K., Nagayama, M. (1976b), Effect of anions on the oxygenation of ferrous ion in neutral solutions, *Journal of Inorganic and Nuclear Chemistry*, vol. 38, pp. 113 - 117.

Van Der Woude, J. H. A. and De Bruyn, P. L. (1983a), Formation of Colloidal Dispersions from Supersaturated Iron(III) Nitrate Solutions. I. Precipitation of Amorphous Iron Hydroxide, *Colloids and Surfaces*, vol. 8, pp. 55- 78.

Van Der Woude, J. H. A. and De Bruyn, P. L. (1983b), Formation of Colloidal Dispersions from Supersaturated Iron(III) Nitrate Solutions. II. Kinetics of Growth at Elevated Temperatures, *Colloids and Surfaces*, vol. 8, pp. 79 - 92.

Chapter 6 : Oxidation and precipitation of iron in the presence of seed material

6.1 Introduction

The principles, chemistry and precipitation products of the oxidation and hydrolysis of iron have been explained in section 1.2. The problems associated with this process have also been highlighted in the same section. In view of the cited problems, this study was conducted based on the hypothesis that the seeding of a ferrous iron oxidation and precipitation process with a particular type of iron oxide will produce the same oxide. This would result in the formation of a more stable and simple precipitate of higher solids density. If this is found to be the case, then the problems associated with long term stability of the precipitates, poor dewaterability of the precipitates, and complexity could be understood better and possibly be resolved.

The advantage of seeding the overall process is that the seed material provides a large surface area that consumes the supersaturation, thereby suppressing primary nucleation. This results in enhanced formation and growth of bigger particles that have better dewaterability characteristics. Alternatively, even if fine particles are formed in the bulk solution, these may adhere on the surfaces of the seed material through electrostatic interactions resulting in a reduced proportion of the smaller particles. The general principles upon which seeded precipitation systems are built have been discussed in section 1.3.6.

6.2 Experimental methods and materials

The experimental procedure for this section was as described in sections 2.1, 2.2 and 2.4.

6.3 Results and discussion

The results and discussions pertaining to the oxidation and precipitation of iron in the presence of seed material are presented in two sections. The first part (section 6.3.1-6.5) deals with the effects of the different seed types on the oxidation rate, particle size distribution and effects on the composition of the precipitates. Throughout this part of the discussion, the concentration of the seed material, C_s invariant at $C_s = 1.0$. The results and discussions cover pH levels 6.0, 8.0, 9.0 and 10.0. The second part (sections 6.6.1 to 6.6.5) of the results and discussions covers the effects of seed concentration C_s on the rate of oxidation, particles size distribution, and composition of the precipitates at pH levels of 6.0, 8.0, 9.0 and 10.0.

6.3.1 pH 6.0; Effect of seed type; C_s = 1.0

6.3.1.1 Oxidation of Fe^{2+}

The rates of oxidation of iron in the presence of different seeding material are shown in Figure 6.1.

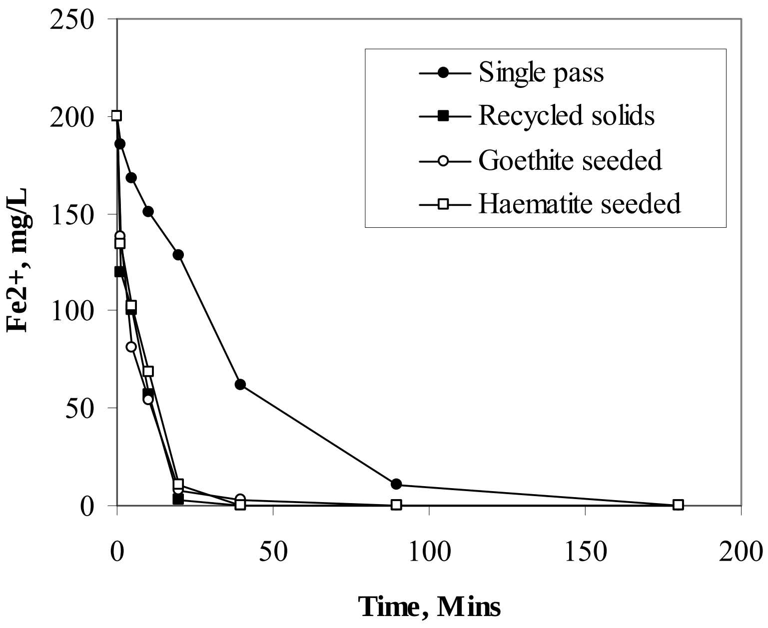

Figure 6.1 *Change in* Fe^{2+} *concentration in solution with time at pH 6.0*

All the materials considered showed a catalytic effect on the rate of oxidation of Fe^{2+}. The recycled solids had the highest average oxidation rate of 10.0 mg/L/min. The rates for the other cases were 2.1, 5.0, 5.0 mg/L/min for the single pass, goethite and haematite seeded systems respectively. From the results presented in Figure 6.1, the trends in oxidation rate are not different from one seed type to another. The reason for the higher oxidation rate in the recycled solids system was probably due to lattice compatibility between the freshly prepared recycle solids and the precipitating solids. The initial oxidation rates were found to be 80.0 mg/L/min, 66.0 mg/L/min and 62.0 mg/L/min for the recycled solids, haematite and goethite cases respectively. The initial oxidation rate for the single pass system was lowest at 15.0 mg/L/min. From these results it can be concluded that all the seed materials considered here had a catalytic effect on the oxidation of ferrous iron.

6.3.1.2 Characterisation of the precipitates

The analysis by X-ray powder diffraction of the final precipitate formed showed the presence of lepidocrocite, goethite, ferrihydrite and haematite (Figure 6.2). The reference spectra of all the phases encountered in this work are shown in Appendix 4. The X-ray powder diffraction patterns of the precipitates did not show any appreciable difference from the beginning of the experimental run up to the end (1440 minutes). This observation indicates that the stable phases were formed from probably a direct mechanism although seed enhanced transformation can not be ruled out.

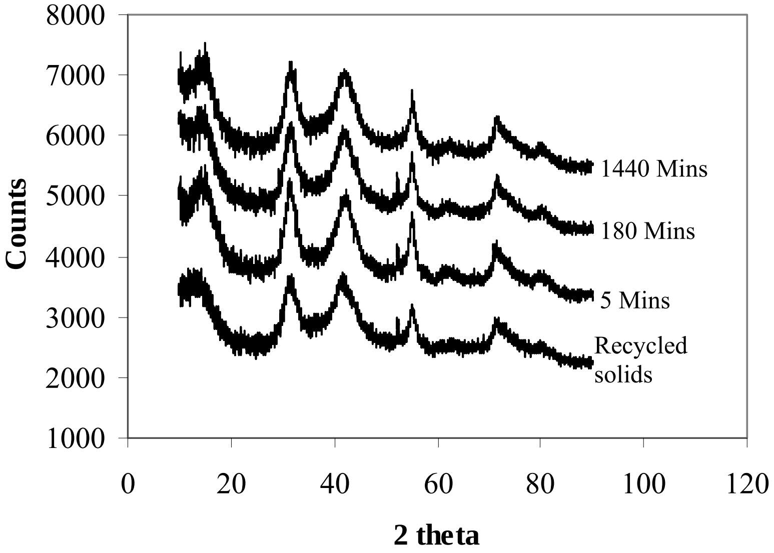

Figure 6.2 *X-ray powder diffraction spectra of the precipitate formed in recycled solids system at pH 6.0 including that of the recycled solids that were used as seed material. (Appendix 4, Figure 5)*

The broad peaks obtained in all the samples indicate either that the precipitate formed was composed of very fine particles or that there were significant proportions of amorphous material like ferrihydrite. Indeed the quantification analysis by X-ray diffraction showed about 14% of the precipitate was made up of amorphous ferrihydrite (Figure 6.3). This is an improvement when compared to the unseeded system where about 70% of the precipitate was amorphous ferrihydrite (Figure 5.21).

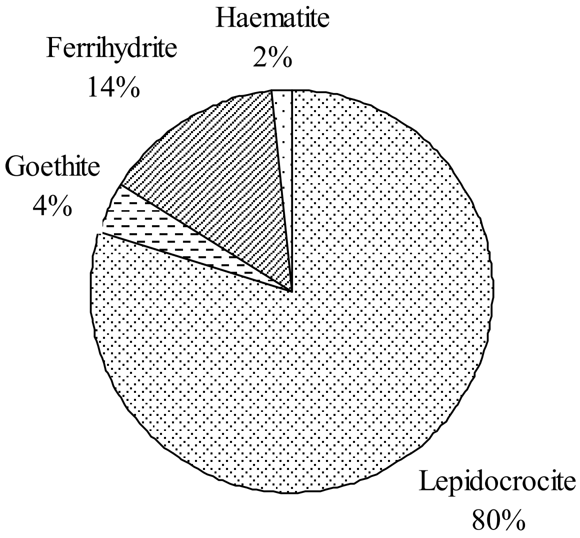

Figure 6.3 *Relative amounts of different types of phases formed during recycled solids seeded experimental system at pH 6.0.*

NOTE: *The uncertainties in all the X-ray powder diffraction quantitative results presented here and everywhere in this thesis were calculated to be about 2%. This was based on residuals given by the instrument. Duplicate tests could not be performed (for purposes of computing the uncertainties) due to the exorbitant costs involved in such an exercise.*

What can therefore be concluded from these findings is that seeding with recycled solids results in the formation of crystalline phases in greater proportions compared to unseeded systems.

The X-ray powder diffraction pattern obtained in the goethite seeded system is shown in Figure 6.4. The peaks obtained for this system are narrower; which means that the precipitation of amorphous ferrihydrite was suppressed resulting in the formation of more crystalline phases in higher proportions. The absence of observable differences in the patterns from the beginning of the experiment up to the end also means that the crystalline phases were formed through a direct precipitation mechanism or that the transformation of the less stable phases was so fast that it could not be detected within the time constraints of this study.

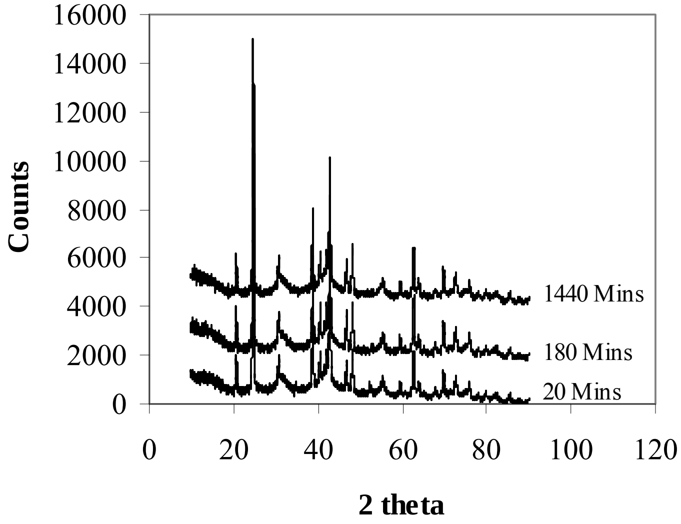

Figure 6.4 *X-ray powder diffraction spectra of the precipitate formed from the goethite seeded experimental system at pH 6.0 (Appendix 4, Figure 9)*

The quantitative analysis of the final precipitate showed it consisted mainly of goethite as shown in Figure 6.5. Compared to the results obtained for the unseeded system and recycled solids seeded system, goethite seeding suppresses the formation of the less stable phases lepidocrocite and ferrihydrite. It is interesting to note that goethite seeding suppressed the formation of lepidocrocite. This implies that it may not be necessary to allow for post precipitation stabilisation during the treatment of hydrometallurgical waste water by the high density sludge process (Cominco Engineering Services Limited, 1997). This has a consequent result of reduced capital and operational costs of hydrometallurgical waste water treatment plants.

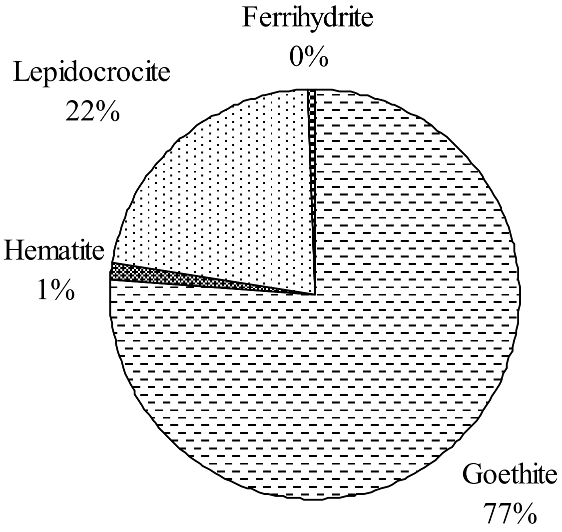

Figure 6.5 *Relative proportions of different types of phases formed during goethite seeded experimental system at pH 6.0*

The results obtained for the haematite seeded experiment are shown in Figure 6.6. The X-ray diffraction patterns are also narrow, indicating absence of amorphous material. Quantitative analysis indeed showed that ferrihydrite was not formed during the oxidation and precipitation of the ferrous iron solution. Goethite at 68% (Figure 6.7) was the major component in the final precipitate. The relative proportions of lepidocrocite and haematite were slightly higher compared to the system seeded with goethite.

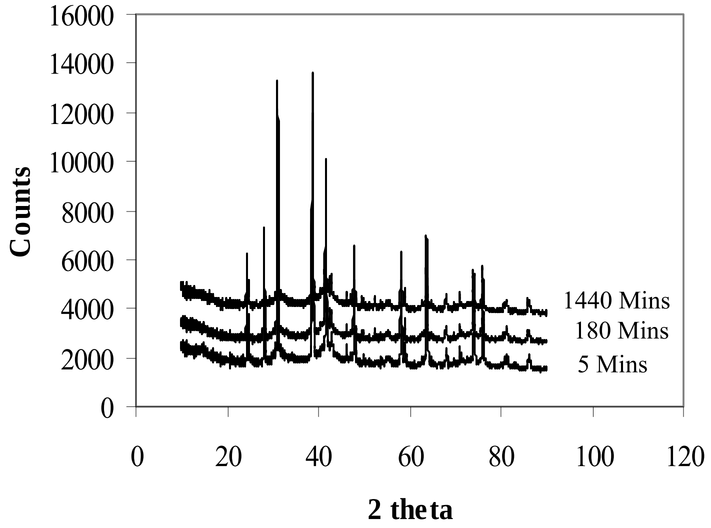

Figure 6.6 *X-ray powder diffraction spectra of the precipitate formed from the haematite seeded experimental system at pH 6.0 (Appendix 4, Figure 10)*

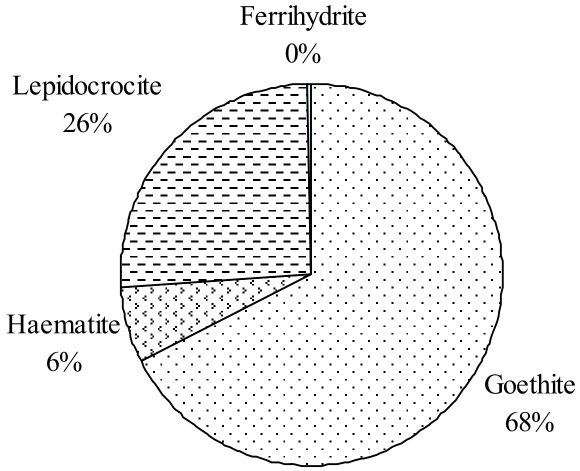

Figure 6.7 *Relative proportions of different types of phases formed during haematite seeded experimental system at pH 6.0*

In conclusion, the characterisation results indicate that, regardless of the type of seed used, the formation of amorphous ferrihydrite is suppressed. Goethite and haematite seeding both promote the precipitation of goethite while the use of (unseeded/single pass) recycled solids promote the precipitation of the less stable lepidocrocite.

6.3.1.3 Particle size distribution of the precipitates

The particle size distribution for system where the recycled solids from a single pass system were used as seed material is shown in Figure 6.8. The figure shows that, at the beginning of the oxidation reaction, there was a shift in the modal size to the left hand side when compared with the distribution for the seed material. This shows that there was nucleation of iron precipitates in the bulk solution up to about 20 minutes. Due to the increased oxidation rate at 5 minutes of the reaction, very small particles were formed which were below the instrument detection limit as shown by the 'cut' distribution for RS5 in Figure 6.8. After 20 minutes the modal size shifted to the right indicating the aggregation of the particles into bigger ones. The second shift to the left at 1440 minutes was probably due to transformation reactions involving the release of water molecules because of mechanical agitation (Gan et al., 2005) or ageing of the precipitate into a more crystalline form which would result in a decrease in the size of the particles. This was probably not a phase transformation since the composition of the precipitate was not changing with time as shown in Figure 6.2. It is also unlikely that the decrease in the modal size of the particles could be due to attrition since the particles formed in this case were very small compared to the eddy currents that would be formed from a stirrer speed of 350 rpm as suggested by Muhr (2006).

Considering the goethite and haematite seeded systems, the same trends in the particle size distributions as obtained in the recycled solids system were observed (Figure 6.9 and Figure 6.10).

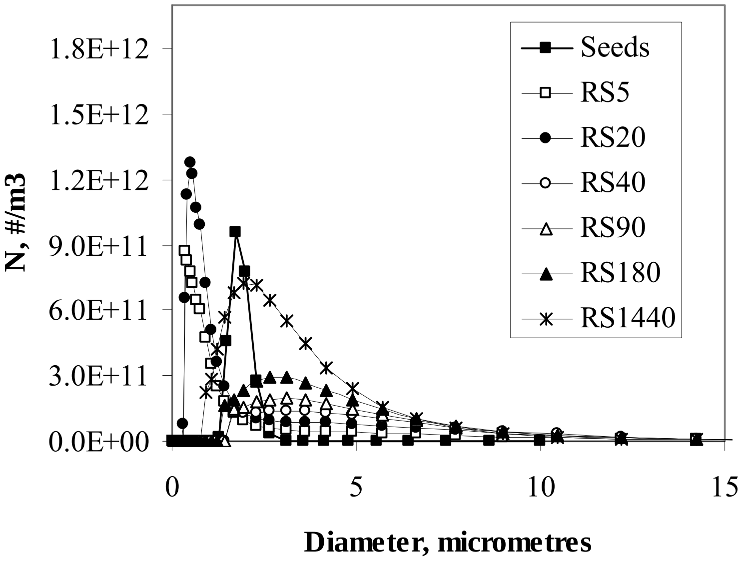

Figure 6.8 *Evolution of the particle size distribution in the recycled solids system at pH 6.0. RS5 = sample collected after 5 minutes of reaction,…….RS1440 = sample collected after 1440 minutes of reaction.*

It would appear that the cycle of reactions taking place in the three systems were probably the same. The only difference is that the ejection of water molecules from the precipitates due to mechanical agitation and ageing started at around 90 minutes in the goethite and haematite seeded systems whereas the probably presence of the mechanism was only appreciable after 1440 minutes in the case of the recycled solids seeded system.

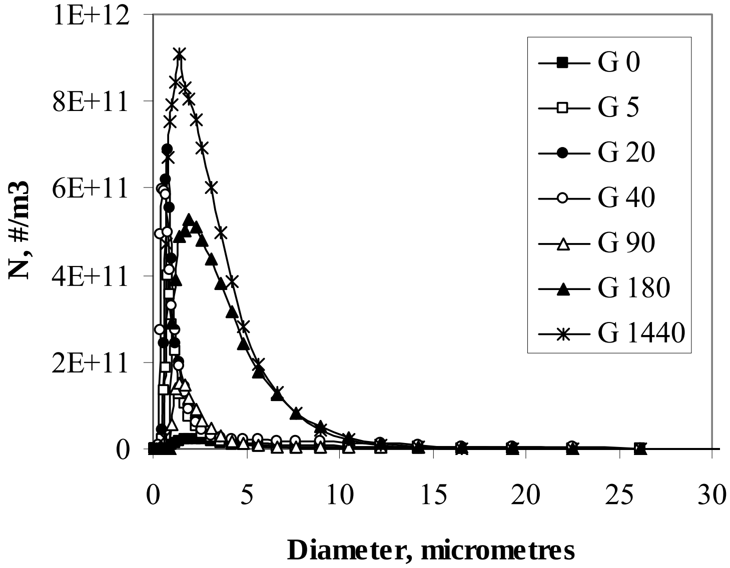

Figure 6.9 *Evolution of the particle size distribution in the goethite seeded system at pH 6.0. G0 = distribution of the seed material, G5 = distribution of the particles after 5 minutes of reaction, ……..G1440 = distribution after 1440 minutes of reaction.*

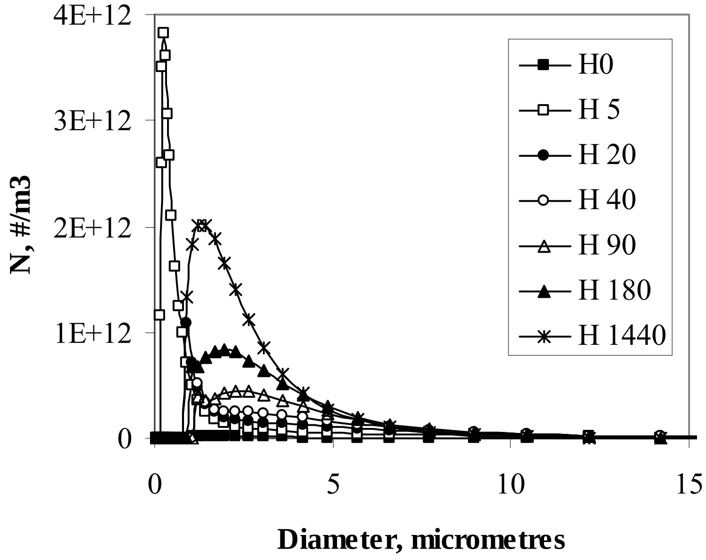

Figure 6.10 *Evolution of the particle size distribution in the haematite seeded system. H0 = distribution of the seed material, H5 = distribution after 5 minutes of reaction, …….H1440 = distribution after 1440 minutes of reaction.*

6.1.3.4 Evolution of the zeroth moment, m_0, and population based average size, $\overline{L_{1,0}}$, of the particle size distribution

The evolution of the total number of particles per unit volume, m_0, for the different seed types is shown in Figure 6.11. The number of particles at 5 minutes for the single pass system was much lower compared to the seeded systems; this was due to the lower oxidation rates (Figure 6.1) which meant that there was much less ferric iron available for solids formation. The increase in m_0 for the recycled solids system up to 20 minutes means that seeding did not total suppress the nucleation of ferric phases. After this, there was a decrease in m_0 due to aggregation and/or adherence of the smaller particles onto the seed material. The same trend that is, initial increase in m_0 followed by a decrease can be seen for the goethite and haematite seeded systems. The gradual increase in m_0 from 40 minutes onwards for the three seeded systems was probably due to mechanical release of water molecules and ageing as referred to earlier (section 6.3.2)

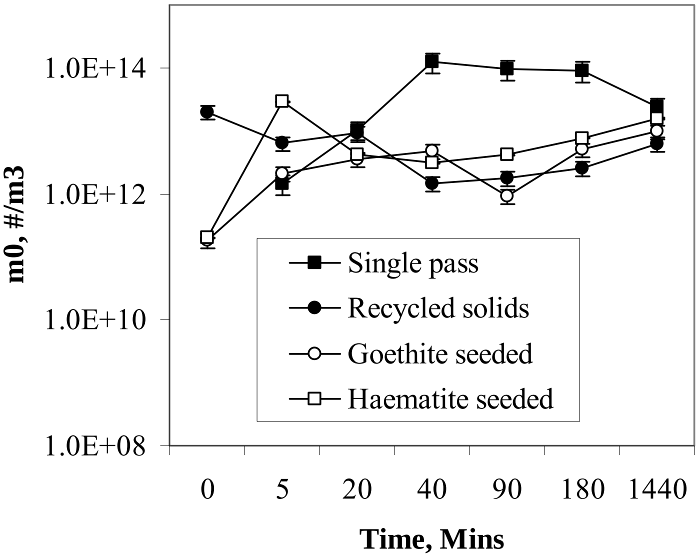

Figure 6.11 Evolution of the zeroth moment, m_0, for the different experimental regimes at pH 6.0

From Figure 6.11, it can be concluded that addition of seed material to the oxidation-precipitation of iron does not totally suppress nucleation in the bulk. The decrease in m0 in the seeded systems compared to the single pass system therefore could be due to direct surface precipitation of ferric species on the seed surface or coating of the fine particles nucleated from the bulk on the seed material by electrostatic deposition.

The corresponding change in the population based average size of the particles is shown in Figure 6.12

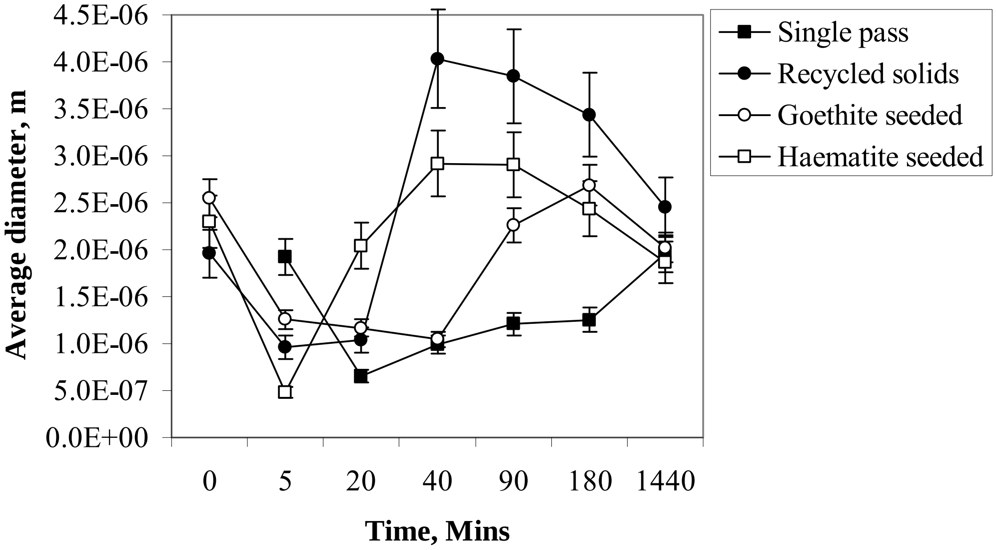

Figure 6.12 *Evolution of the population based average size,* $\overline{L_{1,0}}$ *, of the particles for the different experimental regimes at pH 6.0*

The initial decrease in the average size of the particles for all the seeded systems was due to nucleation of new precipitate in the bulk solution. This is further evidence that seeding did not totally suppress the formation of new nuclei. The aggregation of the particles started after 5, 20 and 40 minutes for the haematite, recycled solids and goethite seeded systems respectively. The decrease in the average size of the particles during the last stages of the reactions was probably due to mechanically induced ejection of water molecules or transformation of the precipitates into more crystalline structures. Jönsson et al., (2006), also reported that ageing of iron precipitates does not only result in phase transformation but also results in the formation of more crystalline order for the same phase. This is probably the transformation that was taking place in these systems. The increase in m_0 and the quantitative results (Figure 6.6 and Figure 6.7) is further evidence that primary nucleation in the bulk solution, especially for the goethite and haematite seeded systems, was the dominant particle formation mechanism. If the precipitates were formed by overgrowth on the seed surface, then there was no way in which the major precipitate constituents could be different from the seed material. It can therefore be concluded that the precipitate formation process involved two mechanisms; the direct formation of the precipitate on the seed material and nucleation in the bulk, which nuclei later adhered onto the seed material. The later mechanism appeared to be dominant in the goethite and haematite seeded systems while surface precipitation was probably dominant in the recycled solids seeded system. The slight differences in the final size of the particles for the seeded systems compare quite well with the settling rates (Figure 6.13) of the precipitates. The settling rates results show that seeding significantly improves the dewaterability characteristics of the precipitate and that this improvement is achieved regardless of the type of seed material used.

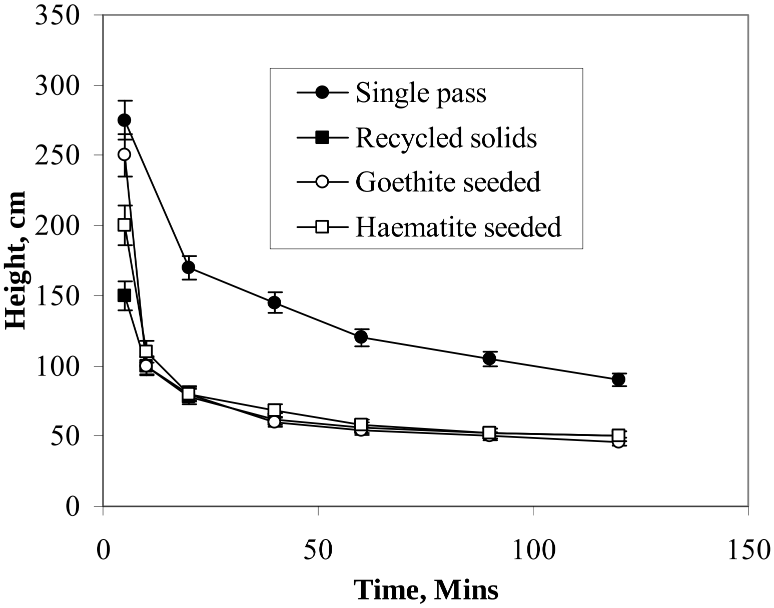

Figure 6.13 *Comparison of the settling rates of the precipitates formed under the different seeding systems at pH 6.0*

6.3.2 pH 8.0; Effect of seed type; C_s = 1.0

6.3.2.1 Oxidation of Fe^{2+}

The rates of oxidation of ferrous iron in the presence of the different seed materials at pH 8.0 are shown in Figure 6.14. All the seed types (like in the pH 6.0 case) had a catalytic effect on the rate of oxidation of ferrous iron when compared to the single pass system. The average oxidation rate for the single pass system was found to be 4.9 mg/L/min. Again the recycled solids showed the greatest catalytic effect with an average oxidation rate of 14.3 mg/L/min. The average oxidation rates for the goethite and haematite seeded systems were 8.6 mg/L/min and 7.9 mg/L/min respectively. The higher oxidation rates obtained in the recycled solids seeded system is probably due to the lattice and surface compatibility between the seed surface and the reaction intermediates which are probably formed in the catalytic transition state.

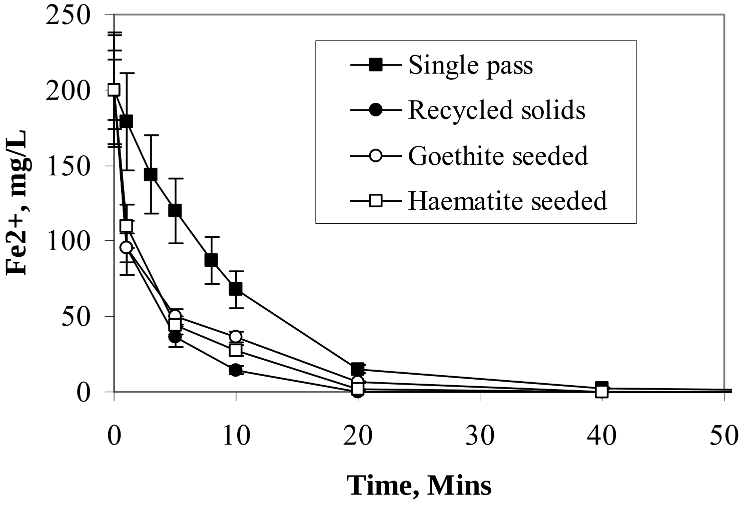

Figure 6.14 *Change in Fe^{2+} in solution with time at pH 8.0*

6.3.2.2 Characterisation of the precipitates

The X-ray powder diffraction pattern for the precipitate that was formed in the recycled solids system is shown in Figure 6.15. The narrower peaks obtained here indicate that the precipitates formed under pH 8.0 conditions were more crystalline than those formed in the pH 6.0 case (Figure 6.2). This is also in agreement with the results obtained from acidified ammonium oxalate extraction tests which showed that there was improved crystallinity in the particles from pH 6.0 to pH 8.0 (Figure 5.21). There were no observable differences in the spectra with time; this implies that the constituents of the precipitates were the same although there could be differences in relative proportions. The phases present in the precipitates were identified as goethite, 2%, feroxyhyte, 8%, haematite, 2% and lepidocrocite, 88% (Figure 6.16)

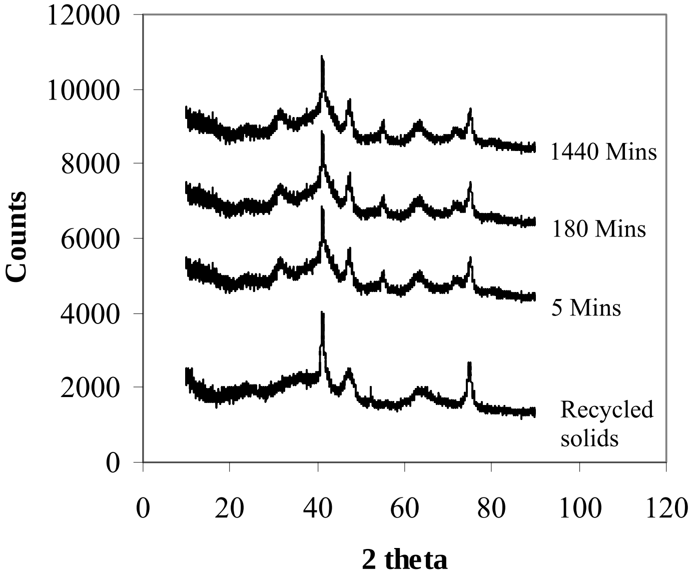

Figure 6.15 *X-ray diffraction spectra of the precipitate in the recycled solids experimental system at pH 8.0 including the spectra of the recycled solids that were used as seed material. (Appendix 4, Figure 6)*

These X-ray diffraction pattern indicates that there was little amorphous material in the precipitate. This is quite an improvement when compared with the recycled solids seed material which had about 20 % ferrihydrite content (Figure 5.21). It has to be noted however, that the ammonium oxalate extraction method tends to overestimate ferrihydrite content since fine particles of crystalline phases have been found to dissolve in the acidified ammonium oxalate solution (Weidler, 1997), (Cornell et al., 1985).

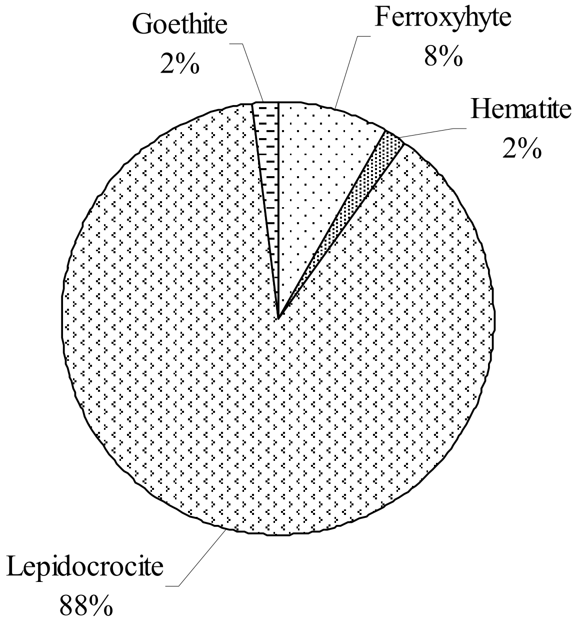

Figure 6.16 *Composition of the precipitate formed in the recycled solids experimental system at pH 8.0*

The X-ray pattern of the precipitate formed in the goethite seeded system also showed very narrow peaks indicating a higher degree of crystallinity (Figure 6.17)

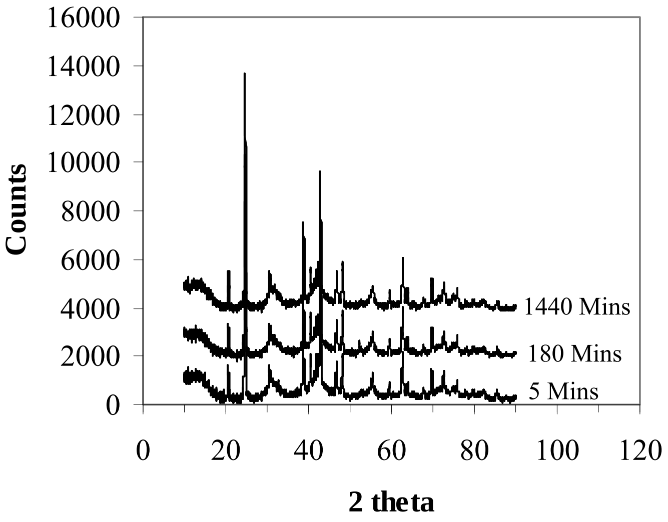

Figure 6.17 *X-ray powder diffraction pattern of the precipitate formed in the goethite seeded experimental system at pH 8.0 (Appendix 4, Figure 11)*

While lepidocrocite was still the phase in highest proportion, goethite seeding promoted the formation of goethite as its proportion increased to 16% (Figure 6.18) compared to the recycled solids system. Another difference was that no feroxyhyte was formed in the goethite system compared to the recycled solids system.

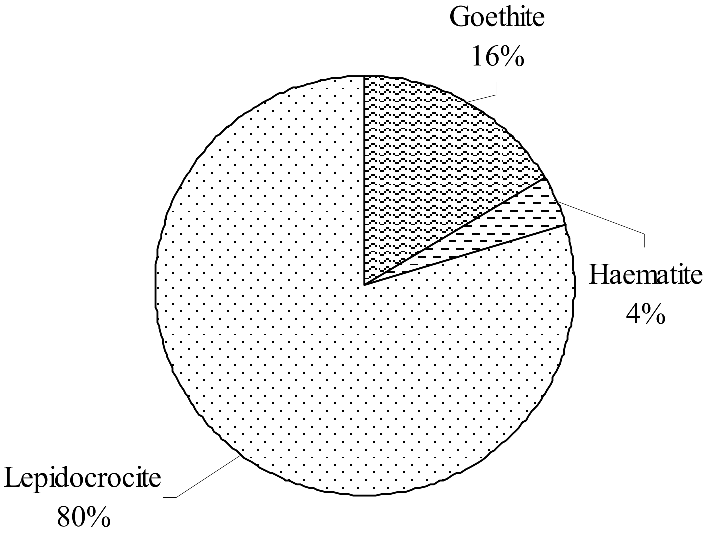

Figure 6.18 *Composition of the precipitate formed in the goethite seeded experimental system at pH 8.0*

The results of the haematite seeded system (Figure 6.19) showed that the precipitate was made up of 47% lepidocrocite, 43% goethite and 10% haematite (Figure 6.20). As in the goethite seeded system there was ferroxyhyte formed. It is interesting to note that haematite seeding tends to suppress the formation of lepidocrocite while promoting the precipitation of goethite. Compared to the recycled solids system the proportion of goethite increased from 2% to 43% while the proportion of lepidocrocite decreased from 88% to 47%. This result seems to suggest that haematite seeding promotes the formation of goethite as this same trend was observed for the pH 6.0 case.

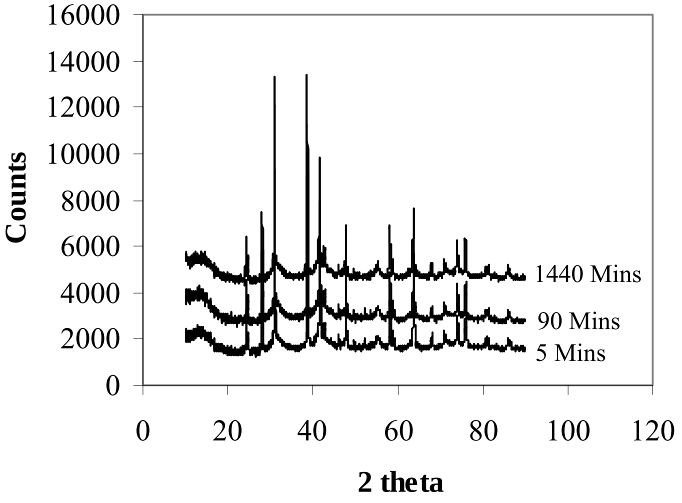

Figure 6.19 *X-ray powder diffraction spectra of the precipitate formed in the haematite seeded experimental system at pH 8.0 (Appendix 4, Figure 12)*

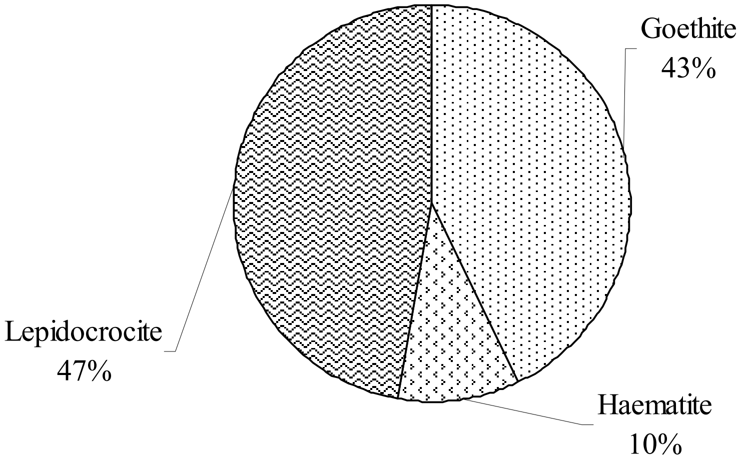

Figure 6.20 *Composition of the precipitate formed in the haematite seeded experimental system at pH 8.0*

6.3.2.3 Particle size distribution of the precipitates

The particle size distribution for the recycled solids seeded system is shown in Figure 6.21. The results indicate that during the early stages of the reaction (first 20 minutes) there was rapid nucleation of fine particles due to the rapid oxidation rates (refer to Figure 6.14). This is indicated on Figure 6.21 by a shift in the modal size of the particles to the left. The big right hand side tail obtained at 40 minutes means the particles were aggregating although there were still some smaller disaggregated particles which later aggregated after up to 180 minutes. The shift to the left in the distribution at 1440 minutes was probably due to mechanical agitation which induced ejection of water molecules from the solids (Gan et al, 2005) or was due to an increase in crystal order of the particles due to ageing.

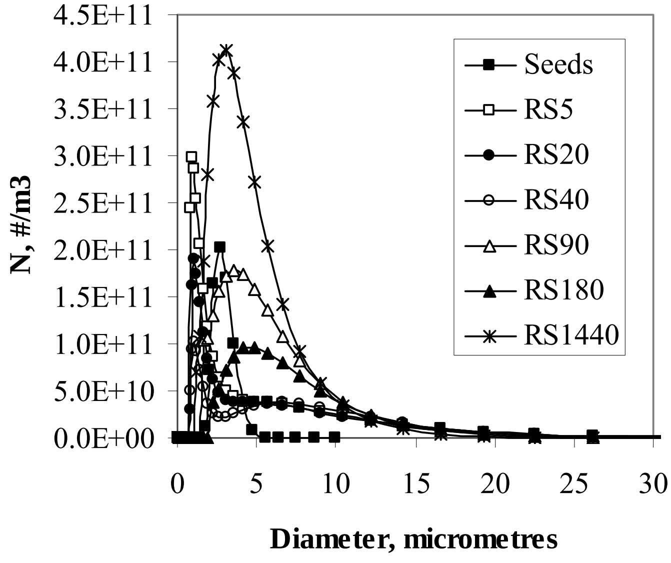

Figure 6.21 *Particle size distribution of the precipitate formed in the recycled solids seeded experimental system at pH 8.0. RS5 = sample collected after 5 minutes of reaction, …….RS1440 = sample collected after 1440 minutes of reaction.*

The particle size distribution for the goethite and haematite seeded systems showed the same trends and sequence of process stages as in the recycled solids seeded system.

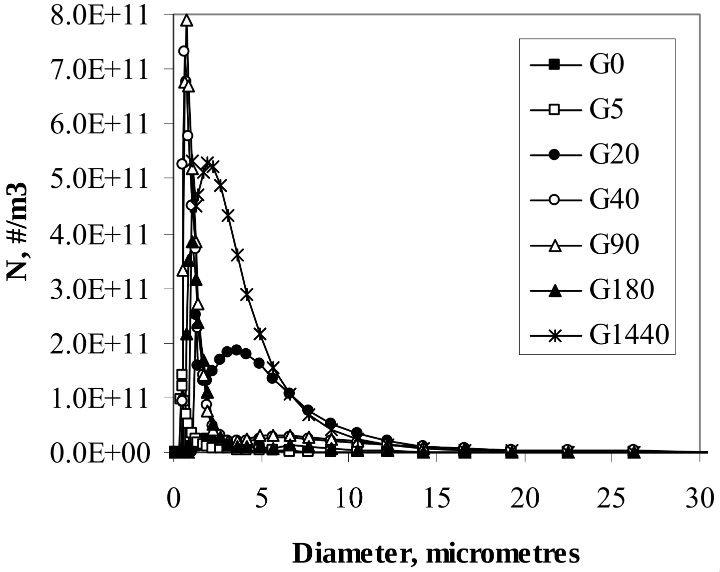

Figure 6.22 *Particle size distribution of the precipitate formed in the goethite seeded experimental system at pH 8.0. G0 = particle size distribution of the seed material, G5 = sample collected after 5 minutes of reaction, ……G1440 = sample collected after 1440 minutes of reaction.*

The particle size distribution for the goethite seeded system is shown in Figure 6.22 while that of the haematite seeded system is shown in Figure 6.23. The clear right hand side tail and the sharp mode at very small diameters for the goethite and haematite seeded systems was probably due to the mechanism of particle formation involved in the two systems. This observation probably means that the fine particles were consumed by adherence onto the seed material rather than by aggregating among themselves. This explanation would fit well with the observation that dominant mechanism in the particle formation process for the haematite and goethite seeded systems was nucleation in the bulk followed by coating of the precipitate on the seed material. Again the increase in the number of the particles in the two cases at 1440 minutes can be explained in terms of the removal of water molecules and ageing.

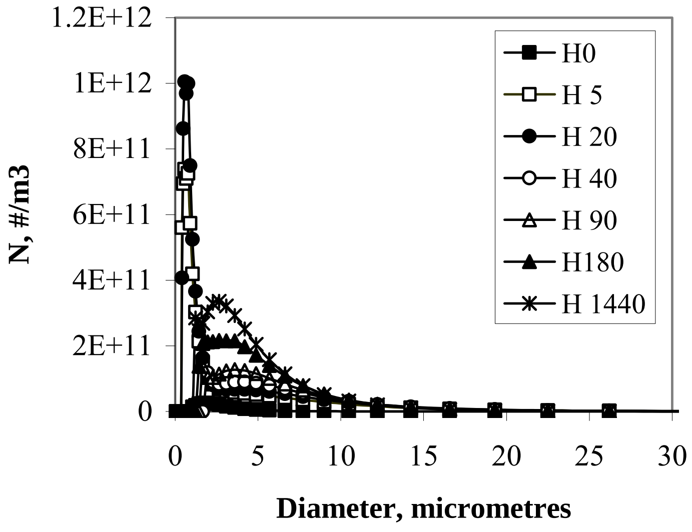

Figure 6.23 *Particle size distribution of the precipitate formed in the haematite seeded experimental system at pH 8.0. H0 = particle size distribution of the seed material, H5 = sample collected after 5 minutes of reaction, ……H1440 = sample collected after 1440 minutes of reaction.*

6.3.2.4 Evolution of the zeroth moment, m_0, and the average size, $\overline{L_{1,0}}$, of the particle size distribution

The changes in the m_0 and $\overline{L_{1,0}}$ of the particles with time are shown in Figure 6.24 and Figure 6.25. From Figure 6.24, it can be seen that seeding significantly suppressed nucleation as the total number of particles formed in the seeded systems was always lower than in the unseeded system. That the m_o increased during for each of the seeded systems during the initial stages is indication that seeding did not totally suppress nucleation of fine particles. From the results shown, recycled solids seeding produced the particles of biggest size. This was probably due to the fact that in this system there was true aggregation of the fine particles and also aggregation between the seed particles themselves, unlike the other systems where the process is coating dominated which would result in small changes in the particle size compared to aggregation.

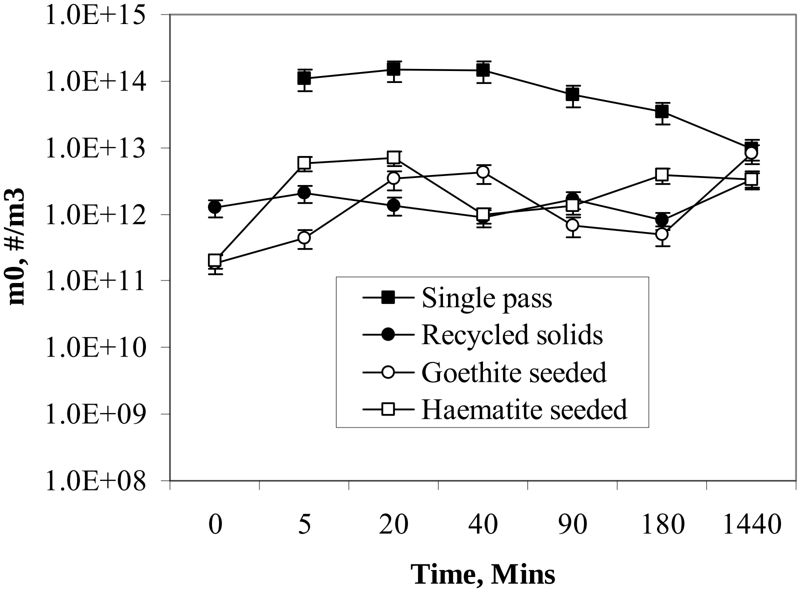

Figure 6.24 *Evolution of the zeroth moment, m_0, for the different seeding conditions at pH 8.0*

The decrease in the average size of the particles at 5 minutes in all the seeded systems supports the view that seeding did not totally suppress nucleation. The increase in the average size from 5 minutes up to 20 minutes, 40 minutes and 180 minutes for the goethite, haematite and recycled solids systems respectively was due to both aggregation and coating of fine particles on the seed material. The final decrease in the average particle size was due to ageing of the precipitate or the ejection of water molecules or both as earlier mentioned. Although the final sizes of the particles for the goethite, seeded system are smaller than the single pass system, this does not show in the settling rates data (Figure 6.26). This is probably due to the fact that in the goethite seeded system there is a higher proportion of the more dense lepidocrocite compared to the unseeded system. In all cases seeding has a significant and equal effect on the settling rates as shown in Figure 6.26

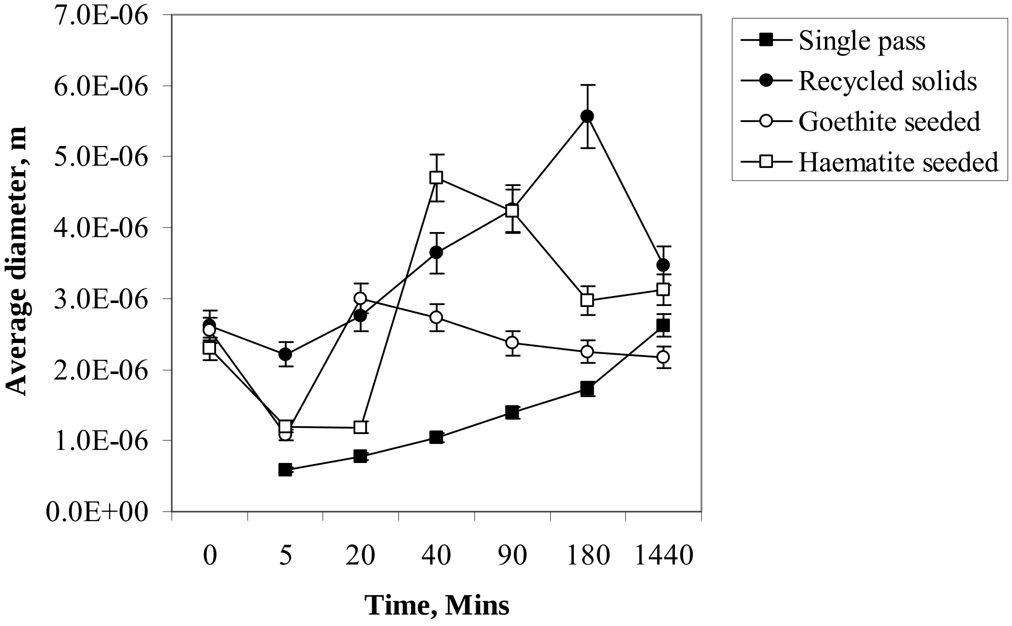

Figure 6.25 *Evolution of the population based average size of the particles for the different seeding conditions at pH 8.0*

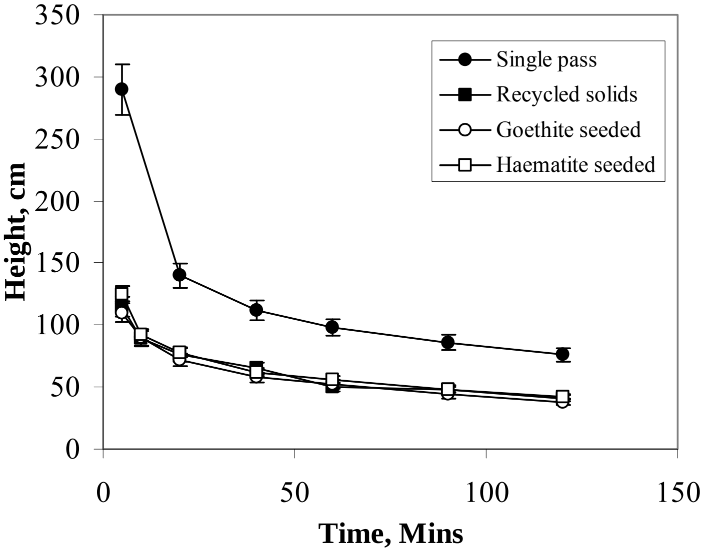

Figure 6.26 *Comparison of the settling rates of the final precipitates under different seeding conditions at pH 8.0*

6.3.3 pH 9.0; Effect of seed type; $C_s = 1.0$

6.3.3.1 Oxidation of Fe^{2+}

The rates of oxidation of iron in the presence of different seeding material are shown in Figure 6.27. All the materials considered showed a catalytic effect on the rate of oxidation of Fe^{2+}. The recycled solids seeds had the highest average rate of oxidation of 17.9 mg/L/min. The rates for the other cases were 9.8, 16.3 and 14.8 mg/L/min for the single pass, goethite seeded and haematite seeded systems respectively. The reason for the higher oxidation rate in the recycled solids was probably due to lattice and surface compatibility between the freshly prepared recycled solids and the precipitating solids.

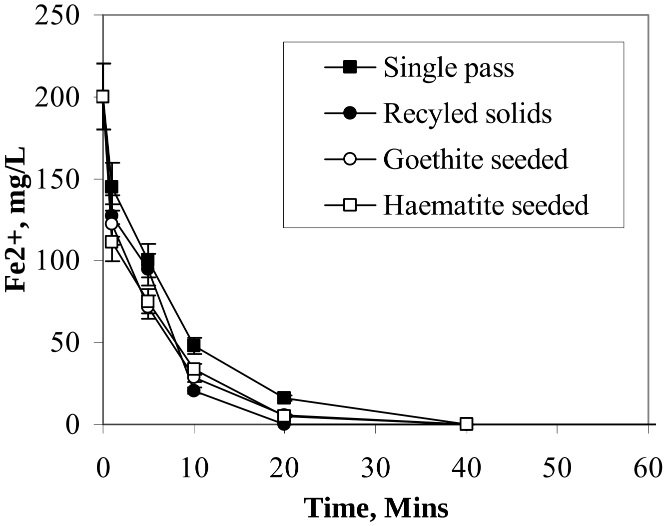

Figure 6.27 *Change in* Fe^{2+} *in solution with time at pH 9.0*

6.3.3.2 Characterisation of the precipitates

The X-ray powder diffraction spectra for the precipitate formed in the recycled solids system is shown in Figure 6.28.

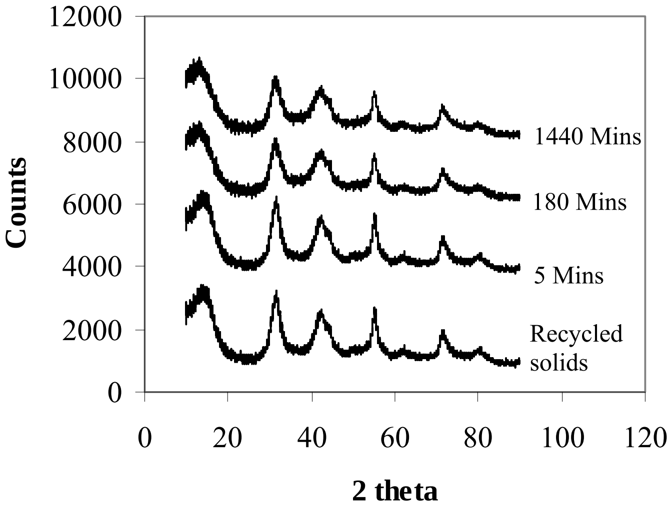

Figure 6.28 *X-ray powder diffraction pattern of the precipitate formed in the recycled solids experimental system at pH 9.0 (Appendix 4, Figure 7)*

The X-ray powder diffraction pattern obtained from the freshly precipitated sludge under recycled solids conditions showed it to be a mixture of different types of iron phases. An automatic search match showed the presence of lepidocrocite, schwertmannite, goethite, haematite, ferrihydrite and maghemite among other phases of iron. However, quantification analyses showed that only ferrihydrite, goethite, and lepidocrocite were in quantifiable proportions (Figure 6.29). Again the proportion of amorphous phases was much lower than what was predicted from the acidified ammonium oxalate extraction method (Figure 5.21). This was because the extraction method overestimates the proportion of ferrihydrite since fine particles of crystalline phases may dissolve in the ammonium oxalate solution (Cornell et al., 1985; Weidler, 1997).

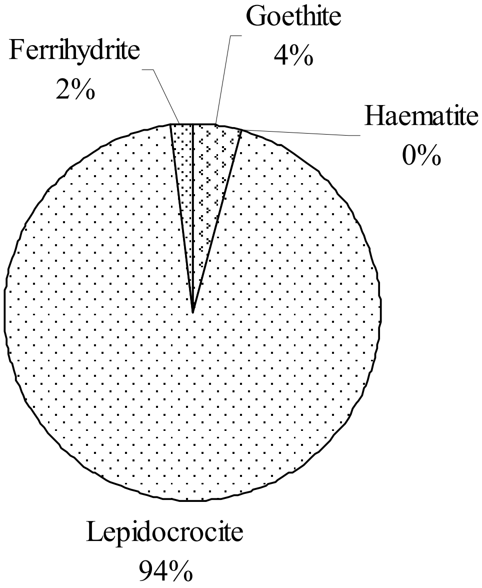

Figure 6.29 *Composition of the precipitate formed in the recycled solids experimental system at pH 9.0.*

The X-ray diffraction pattern obtained for the goethite seeded experiment is shown in Figure 6.30. The pattern showed the presence of mainly goethite and lepidocrocite. This result means that goethite seeding managed to reduce the number of precipitates formed. The proportions of the phases were found to be 81% lepidocrocite, 17% goethite and 2% magnetite (Figure 6.31). Again goethite seeding reduced the proportion of lepidocrocite from 94% to 81% while increasing that of goethite from 4% to 17%. Another probably significant effect is the formation of magnetite, which was never formed in any other system considered so far.

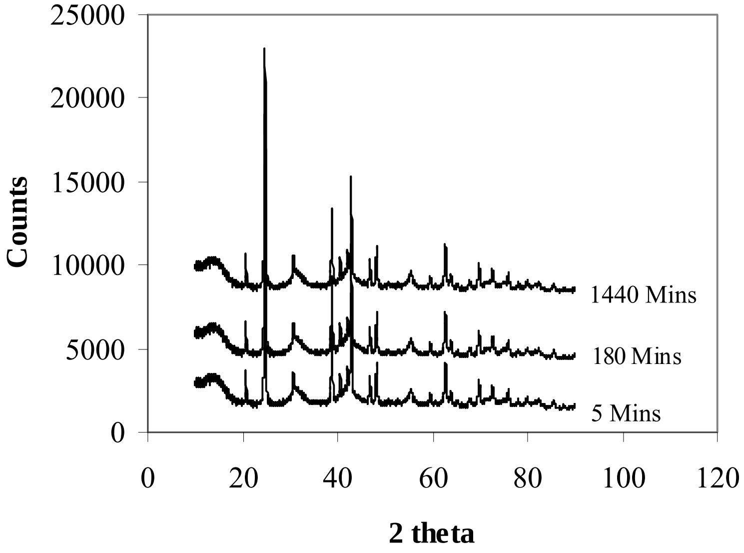

***Figure 6.30** X-ray powder diffraction spectra of the precipitate formed in the goethite seeded experimental system at pH 9.0 (Appendix 4, Figure 13)*

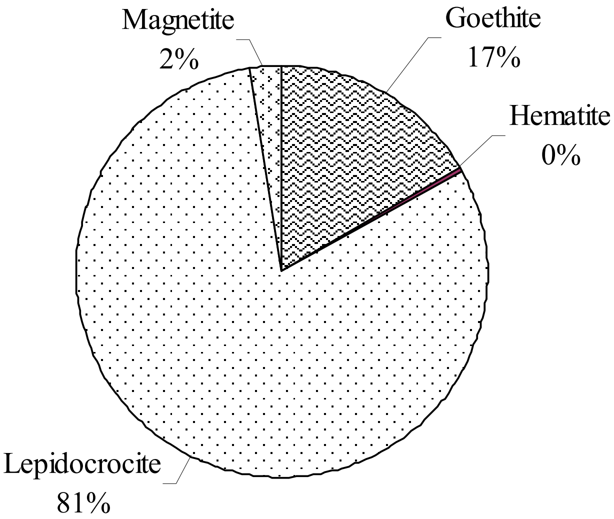

***Figure 6.31** Composition of the precipitate formed in the goethite seeded experimental system at pH 9.0*

In the case of the haematite seeded system, the analysis showed the presence of mainly goethite and haematite with traces of lepidocrocite and magnetite. The narrow peaks obtained showed that there was an improvement in the crystallinity of the precipitate compared to the recycled solids seeded system (Figure 6.32). The composition of the precipitate was 11% haematite, 85% goethite, 3% magnetite and 1% lepidocrocite (Figure 6.33). It is again interesting to note that haematite seeding promotes the formation of goethite at the expense of haematite and lepidocrocite. This observation is in contrast with the predictions based on lattice misfit as calculated in Table 1.3. The results from both haematite seeded and goethite seeded systems show that seeding induces the formation of the more thermodynamically stable phases (goethite at the expense of ferrihydrite and lepidocrocite for the haematite system and ferrihydrite for the goethite seeded system) at the expense of the kinetically favoured phases (less thermodynamically favoured phases).

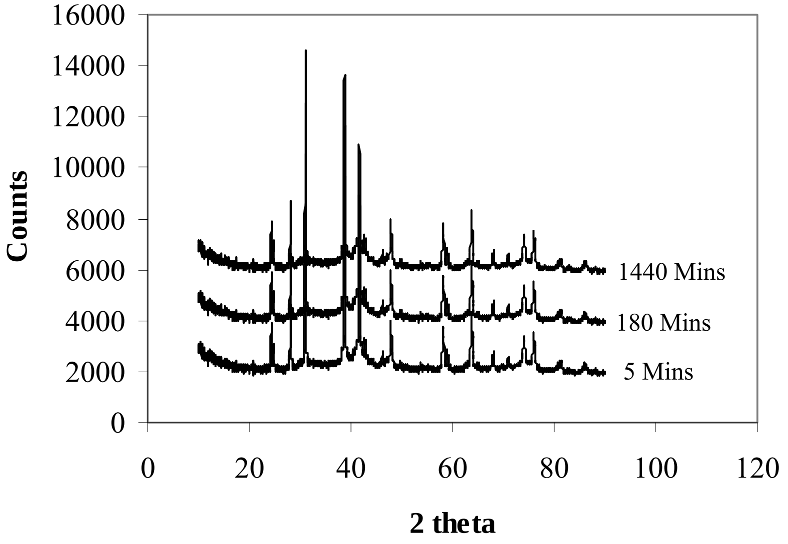

Figure 6.32 X-ray powder diffraction spectra of the precipitate formed in the haematite seeded experimental conditions at pH 9.0 (Appendix 4, Figure 14)

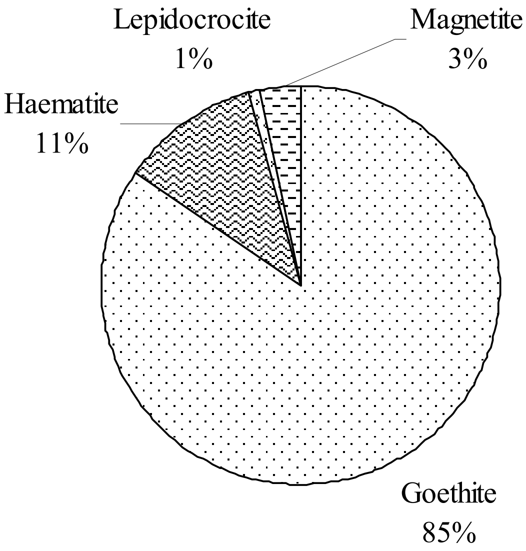

Figure 6.33 *Composition of the precipitate formed in the haematite seeded experimental system at pH 9.0*

The formation of the stable phases in the two cases can be due to either of two phenomena; The introduction of stable seed material directly caused the precipitation of the same material probably due to lattice compatibility between the ‘substrate’ and the precipitate and; the stable seed material, besides catalysing the oxidation reaction, also catalyses the transformation of the metastable phases into the more stable ones.

From the experiments carried out, it can not be concluded which of the two possible mechanisms cited above was dominant. However, it is most likely that the seed material catalyses the transformation of the metastable phases since the increased oxidation rates (due to solids catalysis) favour the formation of the less thermodynamically stable phases which are kinetically favoured under conditions of high oxidation rates. These same mechanisms can be extended to the other systems covered, that is, the pH 6.0 and pH 8.0 cases.

6.3.3.3 Particle size distribution of the precipitates

The particle size distribution for the recycled solids system is shown in Figure 6.34. In all the instances there is a shift of the modal size to the right, which is an indication of agglomeration or growth on seeds or both. This is in contrast to the trends observed for the pH 6.0 and pH 8.0 cases where there was an initial shift to the left indicating nucleation of new precipitates. This was probably due to the fact that, in the single pass systems, pH 9.0 had the finest particles compared to the other cases (refer to Figure 5.11). The very high number of particles corresponding with the modal size after 20 minutes is consistent with the end of the oxidation reaction. After this there is a decrease in the modal number of particles, which is an indication of agglomeration. The absence of a bimodal distribution is an indirect indication that there was little or no secondary nucleation (Kubota et al., 2001). The increase in the modal number of particles and the corresponding decrease in the modal size after 1440 minutes could be due to ageing of the precipitates.

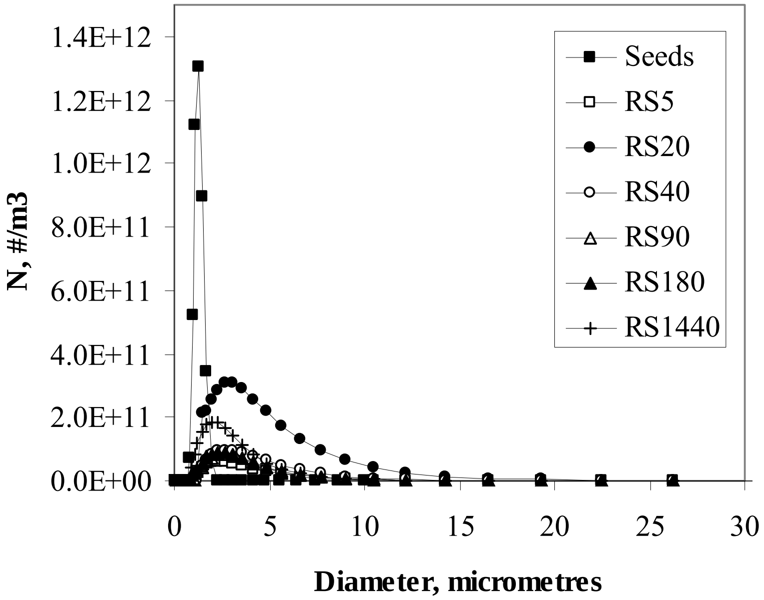

Figure 6.34 *Evolution of the particle size distribution during in the recycled solids system. RS5 = sample collected after 5 minutes of reaction,….. RS1440 = sample collected after 1440 minutes of reaction.*

The particle size analysis for the goethite seeded system showed a shift towards the left at 5 minutes, indicating the nucleation of precipitate in the bulk. The shift to the right at later stages indicates either agglomeration or growth or both (Figure 6.35). The absence of a bimodal distribution shows that the seed material provided enough surface area to suppress secondary nucleation. Again the increase in the mode at 1440 minutes could be due to ageing of the precipitates into more compact and crystalline phases or ejection of water molecules or both.

As in the previous two cases, the distribution for the haematite seeded system had a tail towards the right indicating aggregation or coating or both (Figure 6.36). The particle size distribution showed that primary nucleation was not very significant for this case as the most of the distributions are similar to the distribution of the seed material (Figure 6.36).

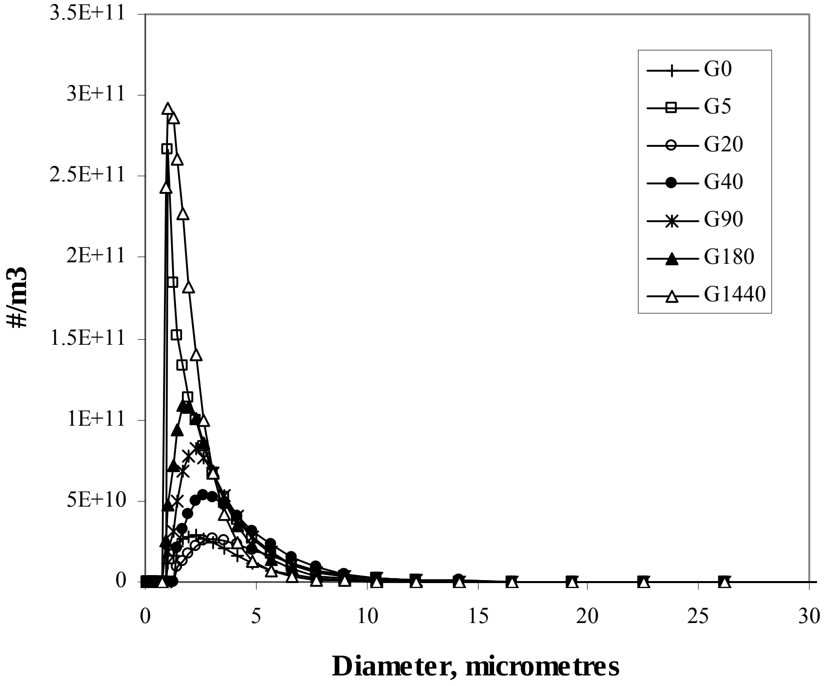

Figure 6.35 *Evolution of particle size distribution in a goethite seeded system at pH 9.0.*

This is unexpected when compared to the other systems, logically one would expect primary nucleation to also occur for the haematite seeded case. The very low numbers of new small particles showed that the precipitate was probably formed directly on the surface of the haematite seed and not in the bulk. This was probably due to pH 9.0 enhanced attractive electrostatic forces between the seed material and the freshly precipitated solids. The shift of the distribution towards the right was probably due to the particles formed in the bulk later adhering to the seed material or these small particles agglomerated among themselves or both. Again the increase in the modal number at 1440 minutes was probably due to ageing of the precipitates.

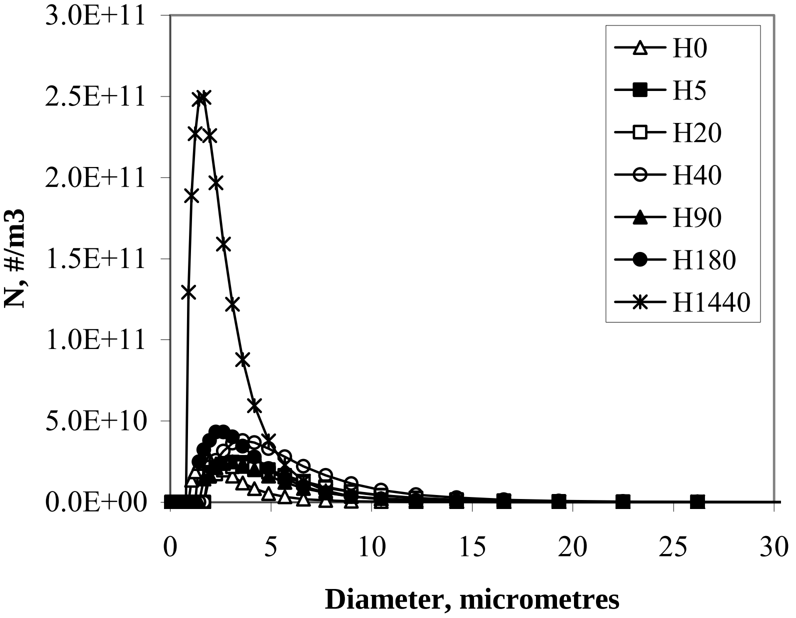

Figure 6.36 *Evolution of particle size distribution for the haematite seeded system at pH 9.0.*

6.3.3.4 Evolution of the zeroth moment, m_0, and the average particle size, $\overline{L_{1,0}}$, of the particle size distribution

The change in the total number of particles per unit volume for the pH 9.0 reaction conditions is shown in Figure 6.37. It is evident from the figure that seeding, regardless of the seed material, significantly reduces the nucleation rate, resulting in the formation of bigger particles. The single pass system resulted in a consistently higher number of particles throughout the course of the reaction. This was due to high primary nucleation rates. It can also be observed from Figure 6.37 that regardless of the type of seed used, the change in the zeroth moment is constant. This means that, irrespective of the type of the seed, all the seeds suppress nucleation equally. Another interesting feature for all the seeded systems was that, regardless of the type of seed material, the final number of particles was the same.

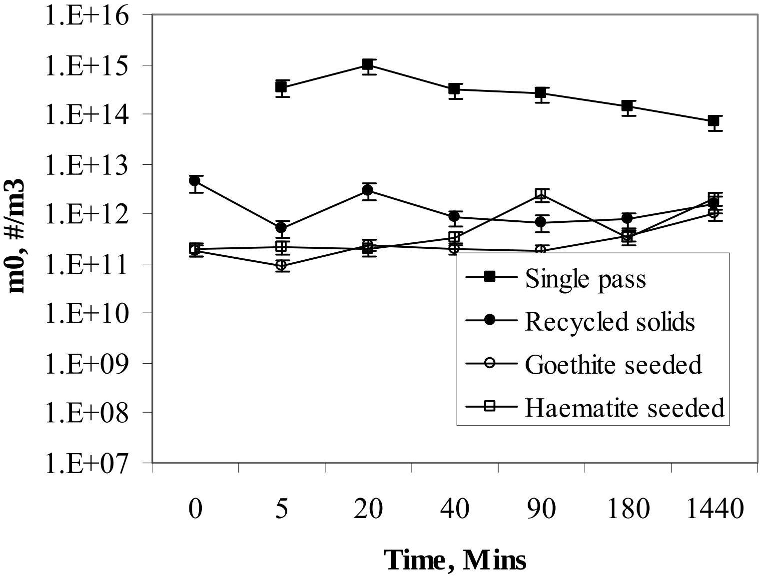

Figure 6.37 *Evolution of the zeroth moment, m_0, for the different seeding regimes at pH 9.0.*

The change in the average size of the particles is shown in Figure 6.38. There was a gradual increase in size for the single pass system, indicating that the active process was agglomeration since there was a corresponding decrease in the number of particles (Figure 6.37). For the haematite and recycled solids systems, there was an increase in the average size up to 40 minutes while for the goethite system the increase was up to 90 minutes. After these time intervals, there was a decrease in the size. This decrease could be due to transformations (the so called ageing) of the iron phases and/or polymorphs. It is also interesting to note that the final sizes of the particles, regardless of the seed type, are comparable. This agrees well with the precipitate settling rates obtained (Figure 6.39). Like in all the other cases considered so far, the type of seed seems to have the same effect regardless of the seed type.

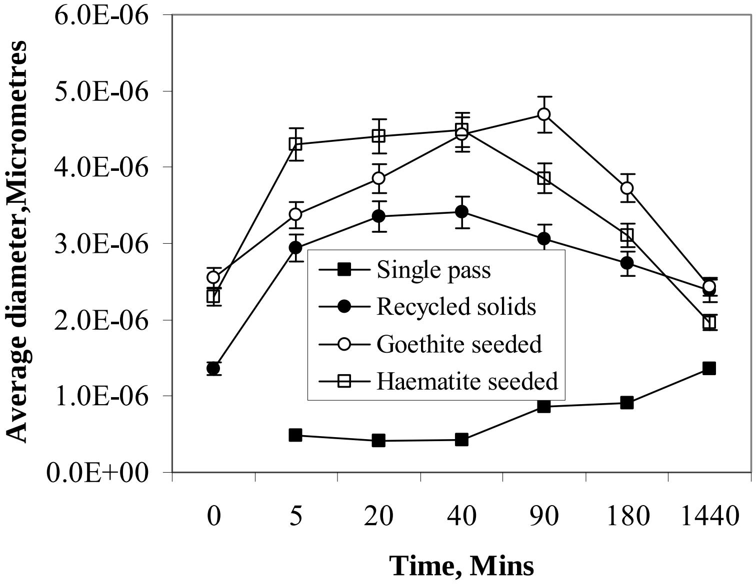

Figure 6.38 *Evolution of the population based average size,* $\overline{L_{1,0}}$ *, of the particles for the different seeding regimes at pH 9.0.*

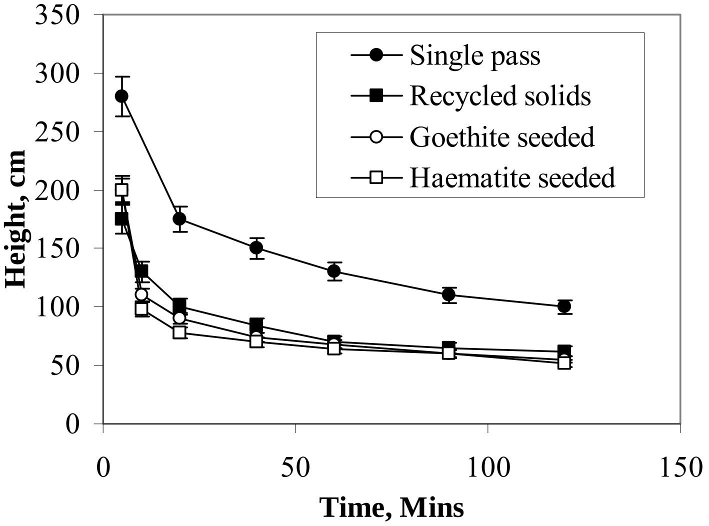

Figure 6.39 *Comparison of the settling rates of the final precipitates formed under the different seeding conditions at pH 9.0*

6.3.4 pH 10.0; Effect of seed type; C_s = 1.0

6.3.4.1 Oxidation of Fe^{2+}

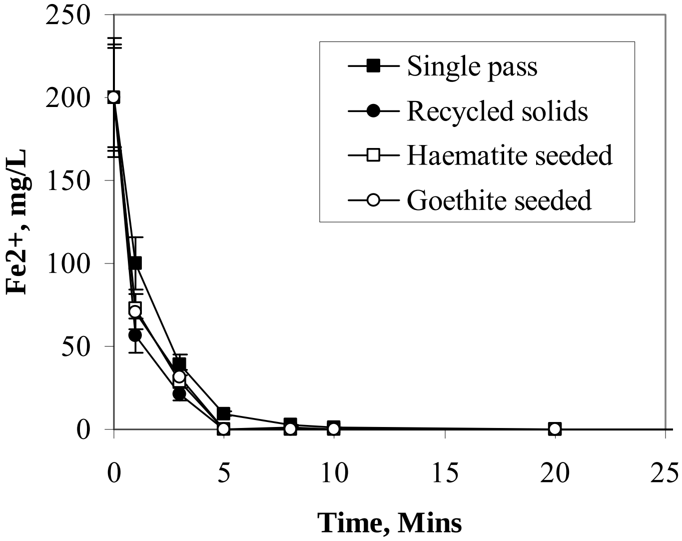

Figure 6.40 *Change in* Fe^{2+} *in solution with time at pH 10.0*

The change in the concentration of ferrous iron in solution at pH 10.0 is shown in Figure 6.40. The average oxidation rates were found to be 24.7 mg/L/min, 59.7 mg/L/min, 56.3 mg/L/min and 57.2 mg/L/min for the single pass, recycled solids, goethite and haematite seeded systems respectively. The rate of oxidation for the recycled solids seeded system was not significantly higher than other seeding systems when compared to the pH 6.0, pH 8.0 and pH 9.0 cases. This was probably due to the fact that at higher pH, the rate of oxidation depends more on the pH than on the presence/absence of solid catalysts.

6.3.4.2 Characterisation of the precipitates

The X-ray powder diffraction spectra for the precipitate formed in the recycled solids system is shown in Figure 6.41. The spectra had narrow peaks indicating that the crystallinity of the precipitate had increased compared to all the lower pH cases. The precipitate was made up of 94% goethite and 6% ferroxyhyte (Figure 6.42). This also indicates that at higher pH, less complex phase mixtures are precipitated. Interestingly, the more kinetically favoured lepidocrocite was not formed in this instance. This could mean that there was possibly direct formation of goethite or that the transformation of the less stable phases was very rapid.

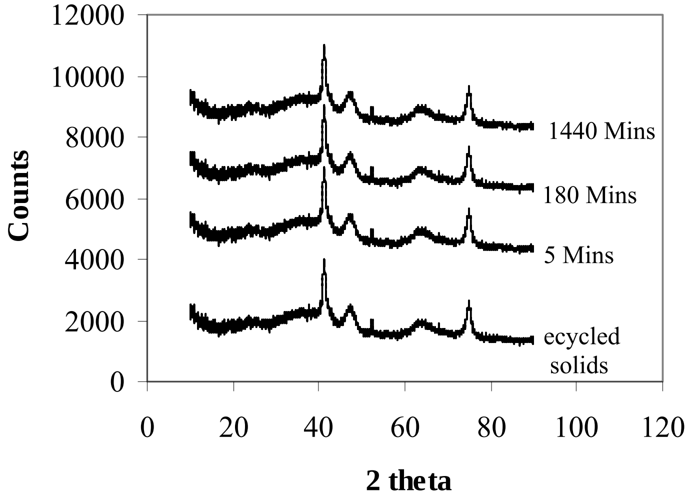

Figure 6.41 *X-ray powder diffraction pattern for the precipitate formed in the experiment seeded with recycled solids at pH 10.0 (Appendix 4, Figure 8)*

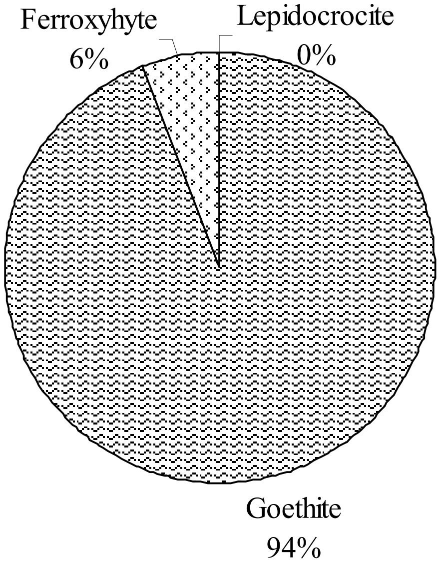

Figure 6.42 *Composition of the precipitate formed under recycled solids seeded experimental system at pH 10.0*

The X-ray diffraction pattern for the goethite seeded system is shown in Figure 6.43. The peaks obtained here were even narrower when compared to those for the recycled solids seeded system. This again indicates the absence of amorphous phases. The final product was found to consist of 95% goethite and 5% haematite (Figure 6.44). Again lepidocrocite was not formed in this instance. Thus the goethite seed slightly promoted the precipitation of goethite while suppressing the formation of feroxyhyte when compared to the recycled solids seeded system.

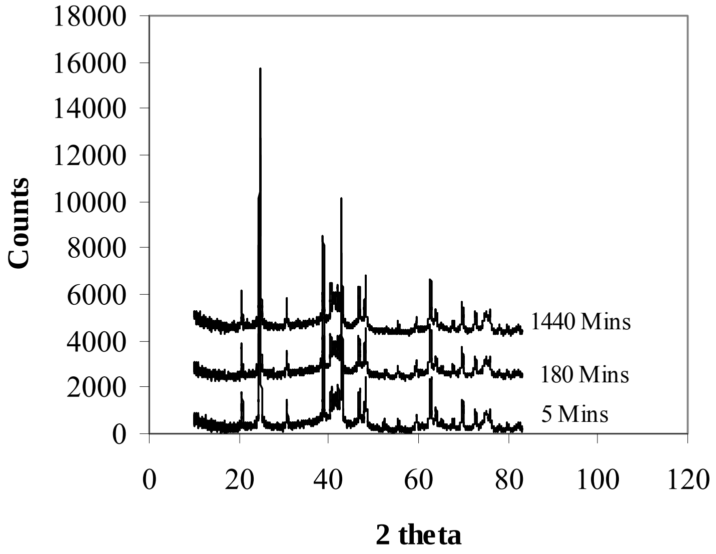

Figure 6.43 *X-ray powder diffraction spectra for the precipitate formed in the goethite seeded experimental system at pH 10.0 (Appendix 4, Figure 15)*

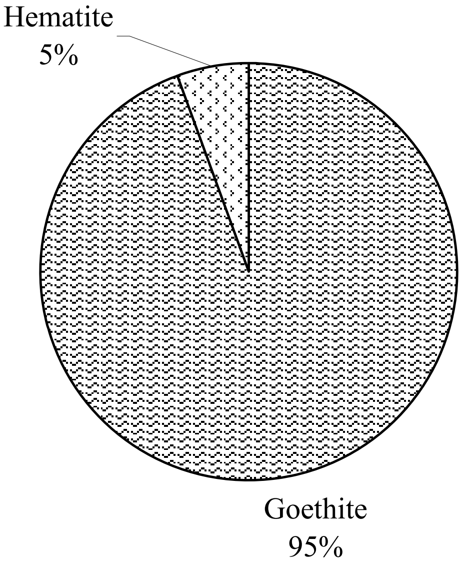

Figure 6.44 *Composition of the precipitate formed during goethite seeded experimental system at pH 10.0*

In the case of the haematite seeded system, the peaks were again narrow, showing the absence of amorphous phases (Figure 6.45). The composition of the precipitate was 97% goethite and 3% haematite (Figure 6.46). Again haematite seeding appeared to promote the precipitation of goethite. From these analyses, the precipitates were either formed from a seed mediated direct nucleation of the stable precipitate or seed catalysed transformation of the less stable phases into the more stable ones. Cornell et al., (1985), and Cornell et al., (1986), reported that less stable ferrihydrite can transform into goethite at high pH in less than 24 hours. It is most likely therefore that goethite was formed from the transformation of the less stable phases.

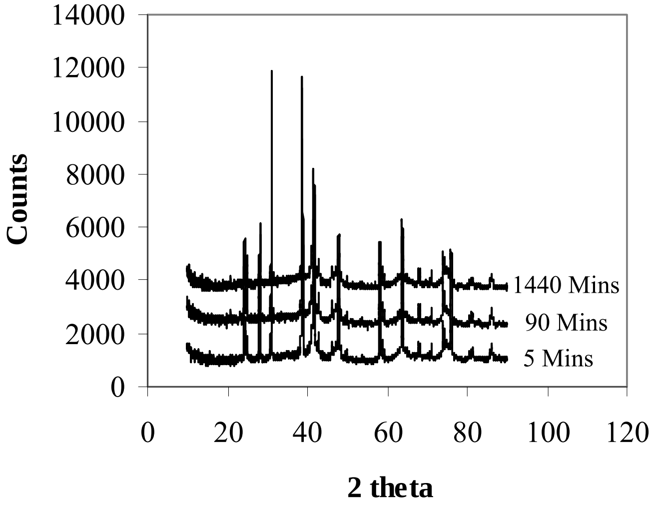

Figure 6.45 *X-ray powder diffraction spectra of the precipitate formed during haematite seeded experimental system at pH 10.0 (Appendix 4, Figure 16)*

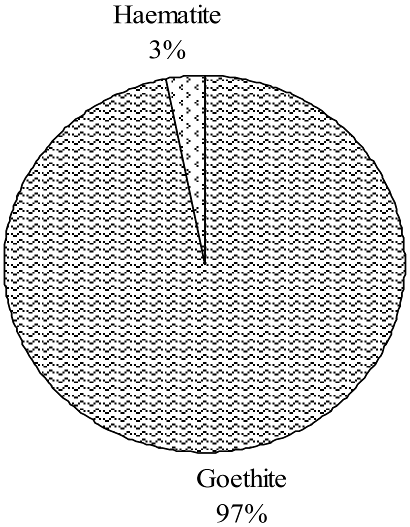

Figure 6.46 *Composition of the precipitate formed during haematite seeded experimental system at pH 10.0*

6.3.4.3 Particle size distribution of the precipitates

The particle size distribution for the recycled solids seeded system is shown in Figure 6.47. The shift in the modal size to the left from 5 up to 40 minutes indicates the nucleation of fresh precipitate in the bulk solution. The right hand side tails in the same distribution shows that aggregation or coating or both were also taking place at the same time. The increase in the number of particles from 180 minutes up to 1440 minutes was probably due to ageing of the precipitates or the release of water molecules due to mechanical agitation or both. It is most likely that in this case this was due to transformation since it has been reported that iron phases transform relatively faster at higher pH (Cornell et al., 1986).

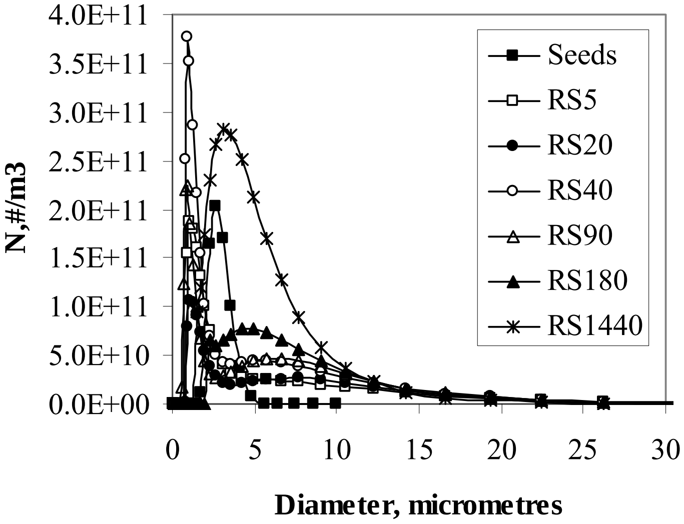

Figure 6.47 *Evolution of the particle size distribution in the recycled solids system. RS5 = sample collected after 5 minutes of reaction, ……RS1440 = sample collected after 1440 minutes of reaction*

For the goethite seeded system (Figure 6.48), there was a similar shift of the modal size to the left indicating nucleation of precipitate in the bulk solution. As in the recycled solids seeded system, the shift to the right of the modal size and the increase in the number of particles at the end can be explained in terms of aggregation and/or coating and ageing respectively.

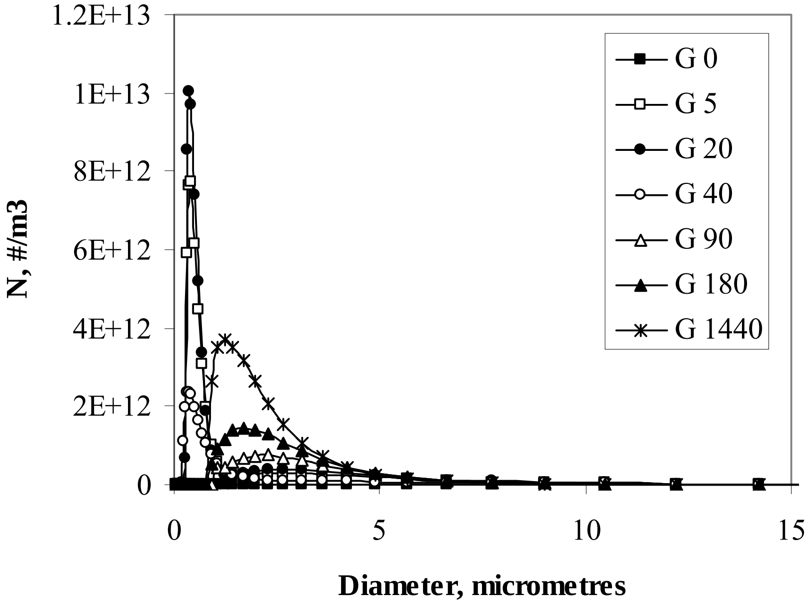

Figure 6.48 *Evolution of the particle size distribution in the goethite seeded system. G0 = particle size distribution of the seed, G5 = sample collected after 5 minutes of reaction, …….G1440 = sample collected after 1440 minutes of reaction.*

The behaviour of the haematite seeded system was different from that of either the goethite seeded or recycled solids seeded systems. The haematite seeded system showed little shift of the modal size to the left or to the right throughout the reaction (Figure 6.49). This probably means that the haematite system was dominated by precipitation on the surface of the seed and coating of the fine particles on the seed material than by nucleation the bulk. The final increase at the end of the reaction can again be attributed to ageing of the precipitates.

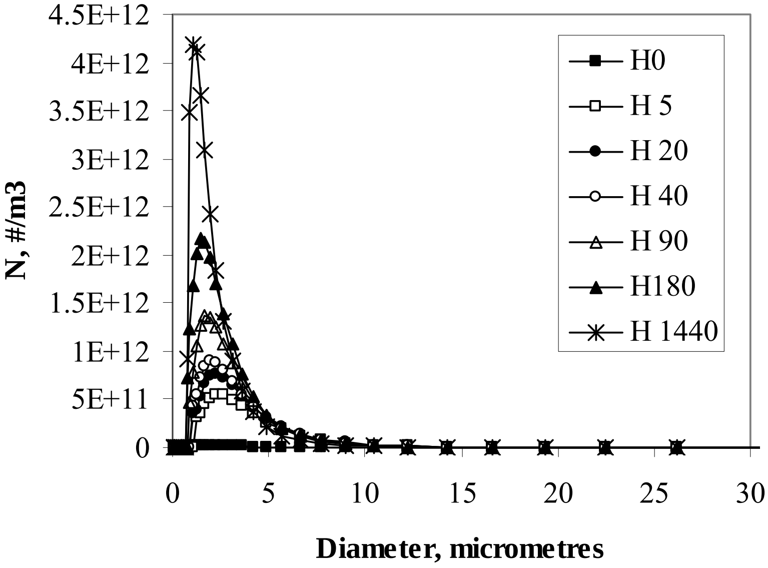

Figure 6.49 *Evolution of the particle size distribution in the haematite seeded system. H0 = seed material, H5 = sample collected after 5 minutes of reaction, …..H1440 = sample collected after 1440 minutes of reaction.*

6.3.4.4 Evolution of the zeroth moment, m_0 and the average size, $\overline{L_{1,0}}$, of the particle size distribution

The evolution of the m_0 is shown in Figure 6.50. The figure indicates that all the seed types considered here suppressed the nucleation of fresh precipitation in the bulk solution when compared to the single pass system. Since the recycled solids system had the lowest m_0, it can be deduced that this system suppressed nucleation the most or promoted the aggregation of the particles the most or both. From a particle size point of view, the recycled solids system had the most significant effect since it produced the largest particles (Figure 6.51). The goethite and haematite seeded systems had the highest m_0; this was probably due to the fact that the particle formation in these two cases was coating-dominated rather than aggregation-dominated.

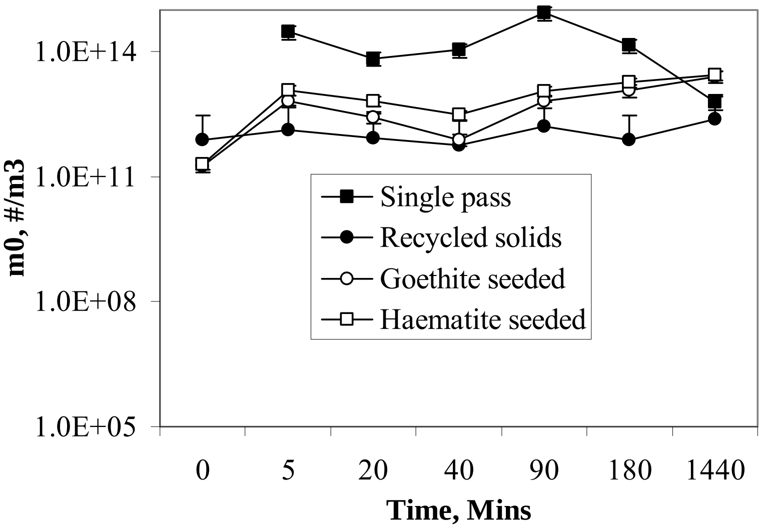

Figure 6.50 *Evolution of the zeroth moment,* m_0*, under the different seeding systems at pH 10.0*

The evolution of the $\overline{L_{1,0}}$ (Figure 6.51) also supported the mechanistic process stages suggested in the previous sections (4.3.4.2 to 4.3.4.3). It can therefore be concluded that, for all the systems considered here, the recycle reaction stages leading to the formation of the final precipitate after 1440 minutes are the same. The differences in the type and composition of the final product are most likely a response to kinetic factors. The final size of the particles formed for each particular instant is probably a function of both the kinetics of the process and the solution pH. As found out in Chapter 5, near neutral pH conditions tend to favour the formation of bigger particles through base-induced coagulation, while moving away from pH 7.0 in either direction supports colloid formation. It is interesting to note that although the final particle size for the goethite and haematite seeded systems are less than for the single pass system there is a significant improvement in settling rates in the seeded systems (Figure 6.52). The increased settling rates of the precipitates in the seeded systems is probably due to the increased density of the precipitates formed in these instances.

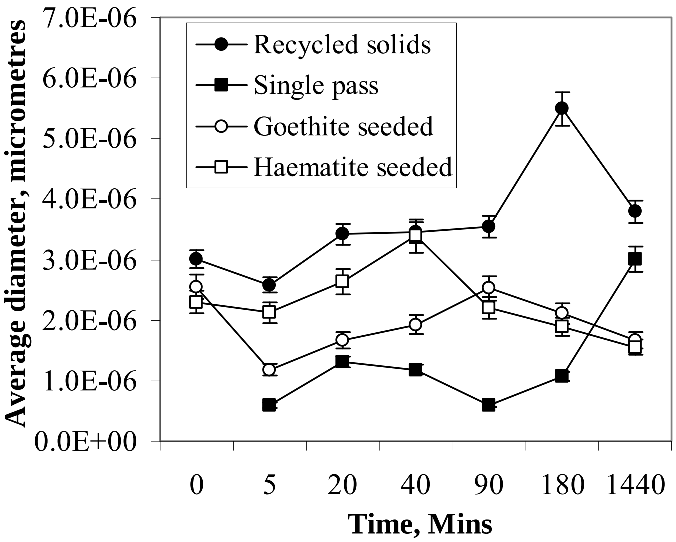

Figure 6.51 *Evolution of the population based average size of the precipitates formed under the different seeded system conditions at pH 10.0*

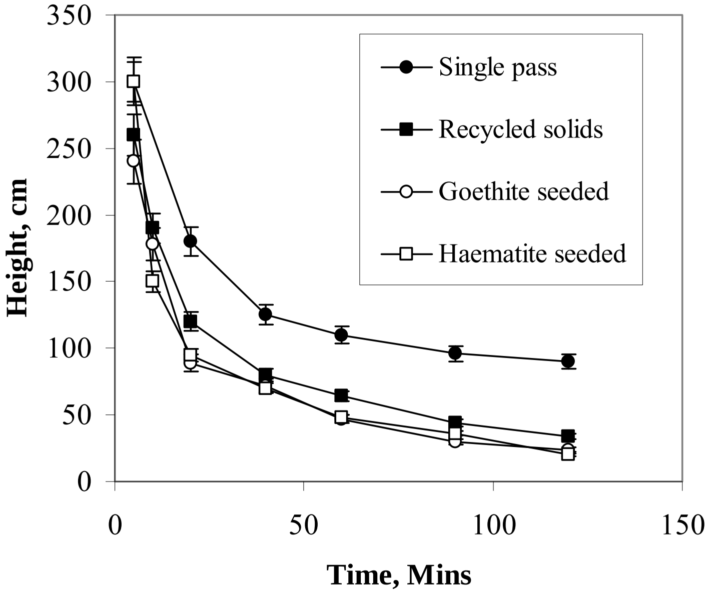

Figure 6.52 *Comparison of the settling rates of the final precipitates formed under the different seeding conditions at pH 10.0*

6.4 Active process mechanisms

The active mechanisms involved in the formation of the precipitates can be classified into those mechanisms that were responsible for particle formation in the recycled solids seeded system and those responsible in the goethite and haematite seeded systems. From the results presented here, the precipitates in the recycled solids were formed mostly through nucleation and aggregation among the fine particles while precipitates in the goethite and haematite seeded systems were formed from the nucleation in the bulk solution followed by coating of the fine particles on the seed material. The SEM pictures showing the coating process are given in Figure 6.53(a) while the schematic illustration of the process mechanisms is shown in Figure 6.53(b). The dominant process steps for the recycled solids seeded system are;

REACTION → **A** (nucleation) → **C**(aggregation) → **F**(ageing)

For the haematite and goethite seeded systems, the dominant process steps are;

REACTION → **A**(nucleation) + **B**(surface nucleation) → **D**(coating) + **E**(aggregation) → **F**(ageing)

(a)

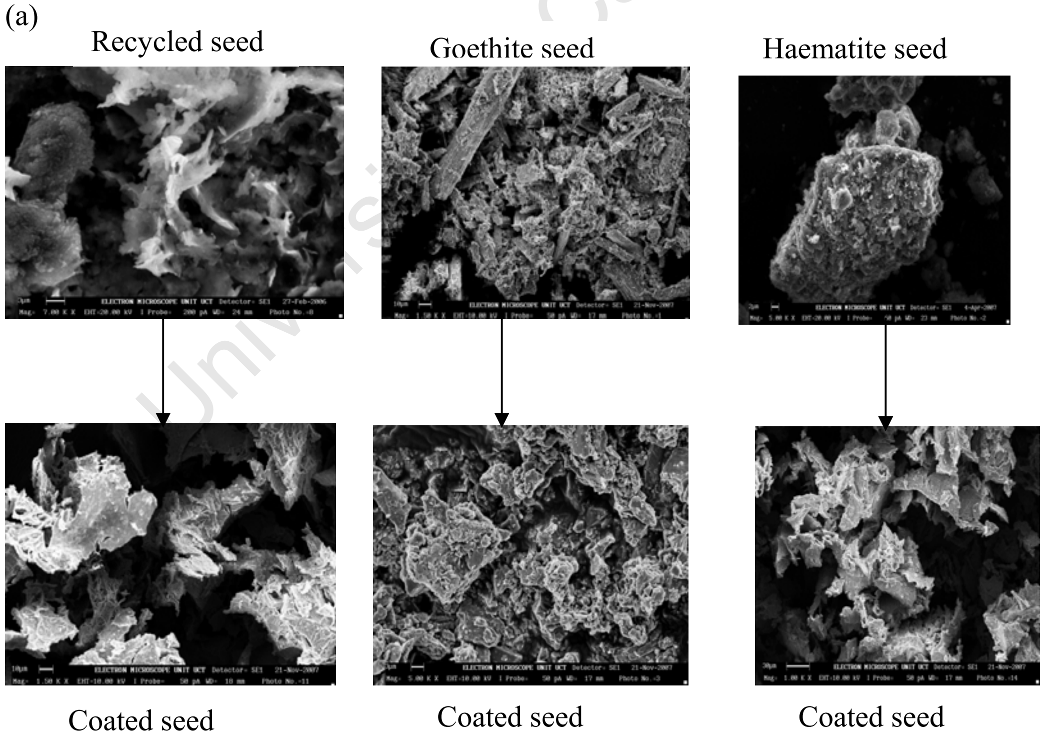

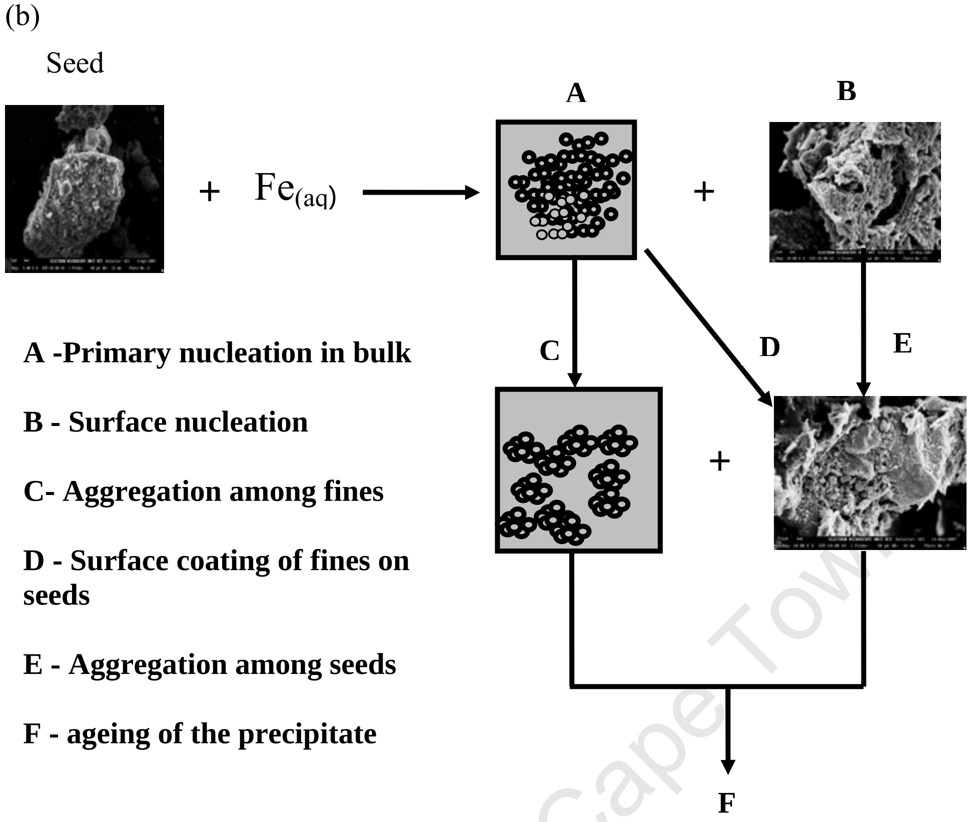

Figure 6.53 *Illustration of (a)coating of seeds (b) the mechanisms involved in the oxidation and precipitation process in the seeded systems.*

The surface coating process is probably due to electrostatic forces like Van der Waals forces since coating continued to occur after the depletion of supersaturation from solution. Scheidegger (1993) also found that different suspensions of iron oxides could coat on different types of substrate.

6.5 Conclusion

The addition of solid particles to ferrous solutions catalyses the oxidation of the ferrous iron. Recycled solids have a slightly greater catalytic effect on the rate of ferrous oxidation compared to haematite or goethite seeds when the rate of oxidation curves are used as basis of comparison. However when the overall average oxidation rates are used the differences become more significant as shown in Table 6.1 summarises the catalytic effect of each of the seed types at different pH conditions as investigated in this study. The catalytic factors are a ratio of the average rate of oxidation of the seeded system to that of the single pass system.

Table 6.1 *Catalytic factors for the different seed types at different pH conditions*

pH/seed type	**Single pass**	**Recycled solids**	**Goethite**	**Haematite**
pH 6.0	1	5	2	2
pH 8.0	1	3	2	2
pH 9.0	1	2	2	2
pH 10.0	1	2	2	2

The higher catalytic effect obtained for the recycled solids system at pH 6.0 are probably an indication that different iron phases catalyse the oxidation rate differently. It is suggested here that the higher oxidation rate obtained for the recycled solids system at pH 6.0 was due to the presence of ferrihydrite in the seed material. Sung and Morgan (1980) reported that ferrihydrite had a catalytic effect on the oxidation of ferrous iron while lepidocrocite did not show any catalytic effect. Although lepidocrocite showed catalytic effects in this study it can be concluded that ferrihydrite has a higher catalytic effect than lepidocrocite or haematite or goethite. Another interesting conclusion that can be made here is that, regardless of the pH and the seed type, seeding always doubled rate of oxidation except for the pH 6.0/recycled solids and the pH 8.0/recycled solids cases.

The oxidation-precipitation of iron in seeded systems proceeds through two mechanisms. The bulk of the precipitate is formed through primary nucleation in the bulk followed by ‘surface property (e.g. electrostatic properties) induced’ deposition of the precipitate onto the seed material for the haematite and goethite seeded systems. Although direct surface precipitation can not be ruled out, the high oxidation rates helped to ensure that the process was dominated by surface coating rather than surface precipitation. For the recycled solids seeded system, the process is dominated by nucleation followed by aggregation of the fine particles. As in the haematite and goethite seeded systems, surface precipitation and coating can not be ruled out. It can also be concluded that the use of stable seed material induces the formation of stable phases at the expense of the kinetically favoured metastable phases. The stable phases are formed either directly in the bulk solution, or, the seed material catalyses the transformation of the metastable phases into stable ones or both. In the haematite seeded systems, the formation of fine particles in the bulk followed by transformation and surface coating appear to be the dominant route since in all the instances considered in this study haematite seeding promoted the formation of goethite. The complexity of the precipitates formed for each case is diminished as the operating pH increases. This is due to faster transformation kinetics. The formation of stable, less complex sludge has some very attractive implications for the treatment of mining waste water, especially acid mine drainage. The formation of stable iron phases means that there is no more need for post precipitation stabilisation (Cominco Engineering Services Limited, 1997). This would result in higher plant throughput and reduced capital and operational costs. Also, the formation of such dense precipitates like goethite could result in lesser sludge volumes, higher solids density and better water recoveries. Overally, the formation of simple stable precipitates would open opportunities for material reuse and/or recycle which could add value to the whole waste water treatment process.

6.6 Effect of seed concentration on the oxidation and precipitation of iron

6.6.1 pH 6.0 case

6.6.1.1 Effect of C_s on oxidation rate

The effect of seed concentration C_s, on the rate of oxidation for the recycled solids, goethite seeded and haematite seeded systems are shown in Figure 6.54, Figure 6.55 and Figure 6.56 respectively.

From these figures, it can be observed that regardless of the concentration of the seed material used, the effect on the average rate of oxidation of iron was the same. However, the concentration of Fe^{2+} in solution at $C_s = 0.1$ was slightly higher than for

C_s = 1.0 and 0.5 for the recycled solids system and the goethite seeded systems. This difference is negligible since it was found to be below 20% whereas the reproducibility of the oxidation reactions was found to be 23% (Chapter 3).

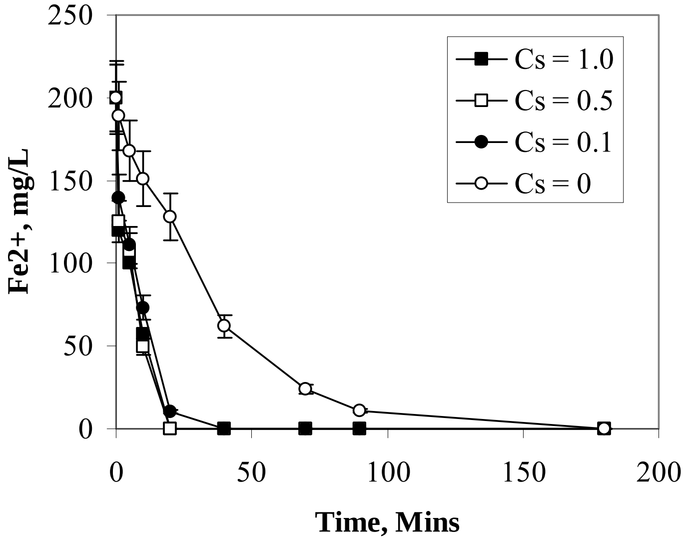

Figure 6.54 *Change in the Fe^{2+} concentration is solution in recycled solids seeded system at different C_s levels*

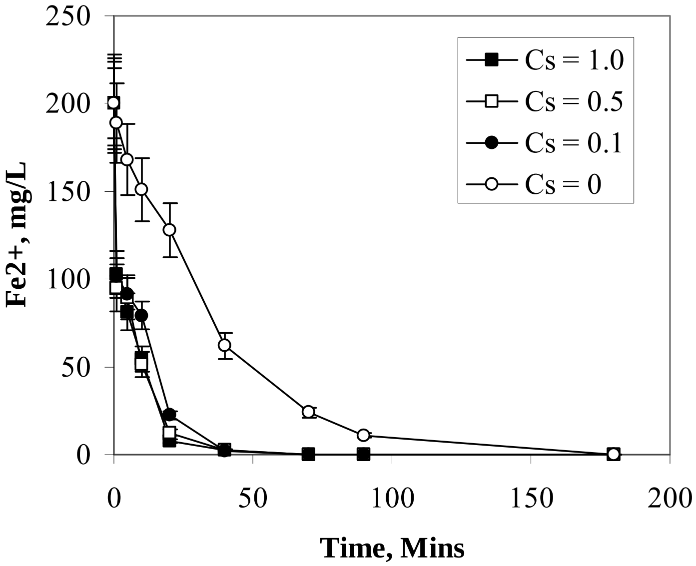

Figure 6.55 *Change in Fe^{2+} concentration in solution in goethite seeded system at different C_s levels*

Considering the haematite seeded system, the trend in Fe^{2+} in solution is slightly different (Figure 6.56). Seed concentration levels of 0.5 and 0.1 were found to have the same effect. The effect at these concentration significantly different from $C_s = 1.0$ case especially at 20 minutes where the difference in the concentration of iron was about 75%. This is quite high when compared to reproducibility of 23%. However it still has to be noted that the final average rate of oxidation was the same in all the cases.

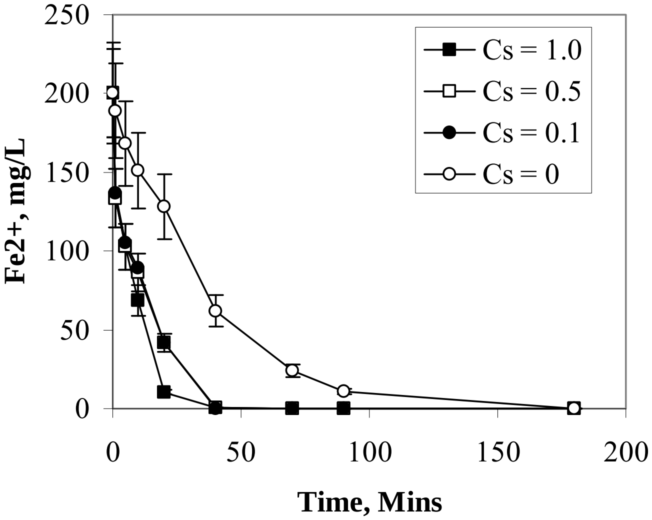

Figure 6.56 *Change in Fe^{2+} concentration in solution in the haematite seeded system at different C_s levels*

6.6.1.2 Effect of C_s on product size

The effect of seed concentration on the population-based average size of the particles is shown in Figure 6.57. L is the population based average size (m) and L_0 is the population-based average size (m) of the seed particles. The trends indicate that, at the beginning, the process is nucleation dominated followed by aggregation and or coating of the fine particles on the seed material. This is especially true for the $C_s = 1.0$ and 0.1 cases. The final stages of the process involve two processes; ageing and coating of the precipitates on the seed material resulting in smaller size particles. It is most likely that the decrease in size is due to coating of the aggregates on the seed material since, unlike aggregation, coating does not result in an appreciable increase in the size of the seed material. The high ratio found after 5 minutes for the

C_s = 0.5 case could not be explained. This was probably an outlier value. The change in the m_0 values (Figure 6.58) also support the trends observed in the L/L_0 ratio. That the largest particles were obtained at C_s = 0.5 is probably due to the fact that; at C_s = 1.0, the contribution to the final size of the seed material is more significant, thus the distribution tends towards that of the seed material while at C_s = 0.1, the contribution of the seed material is less significant and the distribution tends towards that of the single pass system which is that same as that of the seed material. At C_s = 0.5, the contributions of both the seed material and that of the formed particles are significant and hence the final particle size tends to be larger.

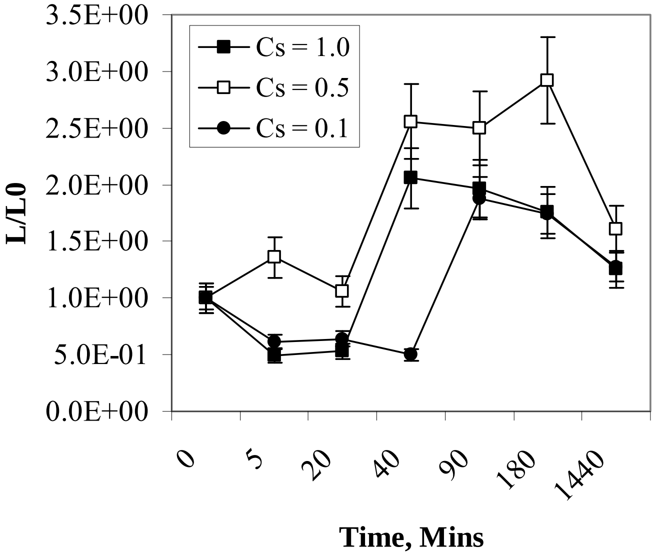

Figure 6.57 *Change in the L/L_0 as a function of time for the recycled solids system at pH 6.0*

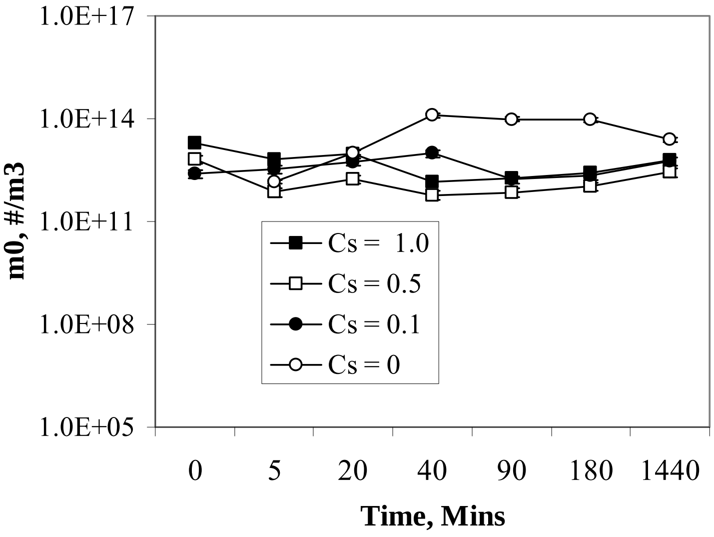

Figure 6.58 *Change in m_0 as a function of time for the recycled solids system at pH 6.0*

The results for the goethite seeded case are shown in Figure 6.59. The results indicate that goethite does not suppress nucleation to a greater extent when compared to recycled solids seeding. It also appears as if goethite seeding suppresses the formation of iron hydroxide flocs as the size of the particles at $C_s = 0.1$ are larger than at $C_s = 1.0$. From a size point of view it would be beneficial to use lower seed concentrations as this produces particles of bigger size. Again, as in the recycled solids seeded case, the change in m_0 as shown in Figure 6.60 supports the trends observed in Figure 6.59.

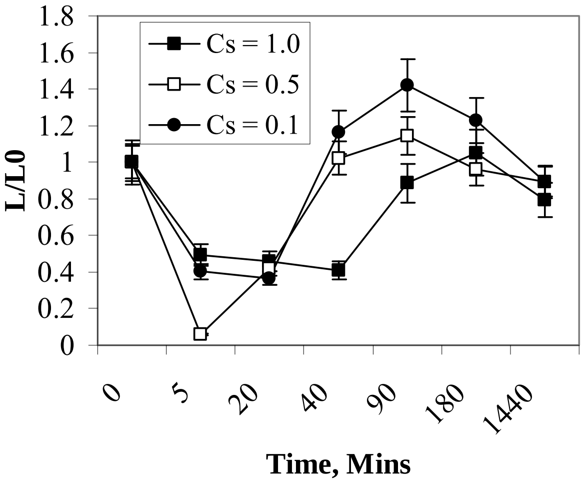

Figure 6.59 *Change in L/L_0 in the goethite seeded system as a function of time at pH 6.0*

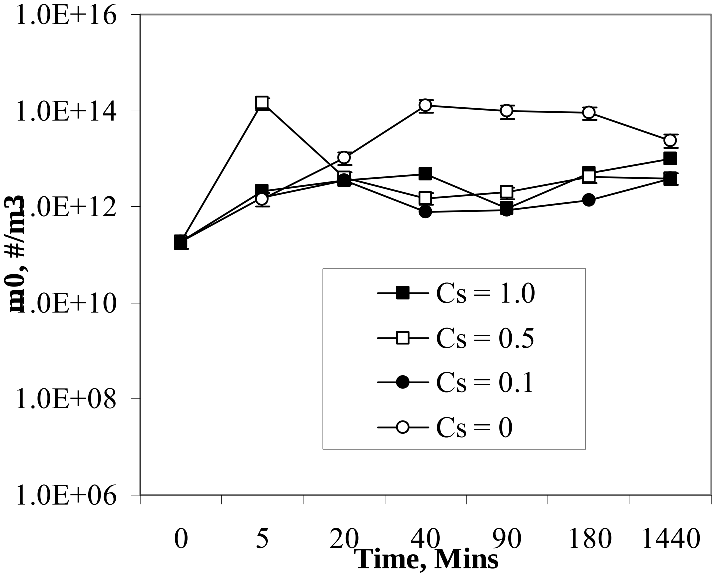

Figure 6.60 *Change in m_0 as a function of time for the goethite seeded system at pH 6.0*

The change in L/L_0 as function of time for the haematite seeded case is shown in Figure 6.61. As in the goethite seeded case, the lower seed concentration resulted in a larger particle size. This again means that high goethite and haematite seed concentrations suppress the persistence of hydroxide flocs by encouraging coating of the freshly precipitated solids on the seed material at the expense of aggregation of the same solid particles among themselves. This could also probably hasten the onset of ageing resulting in the formation of smaller particles.

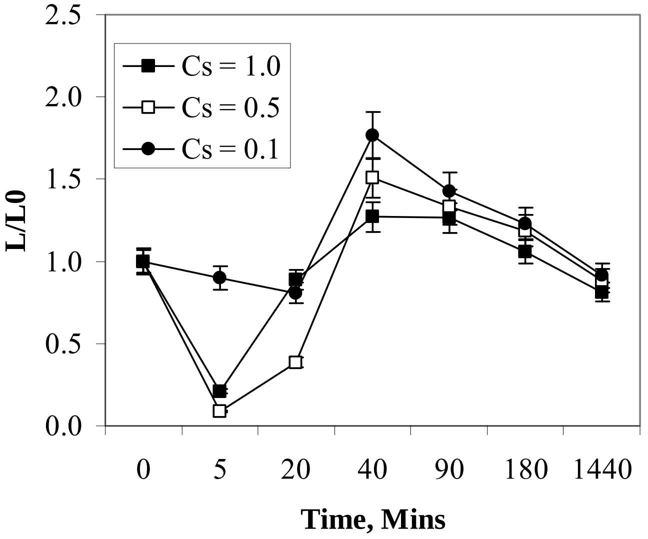

Figure 6.61 *Change in L/L_0 as a function of time for the haematite seeded system at pH 6.0*

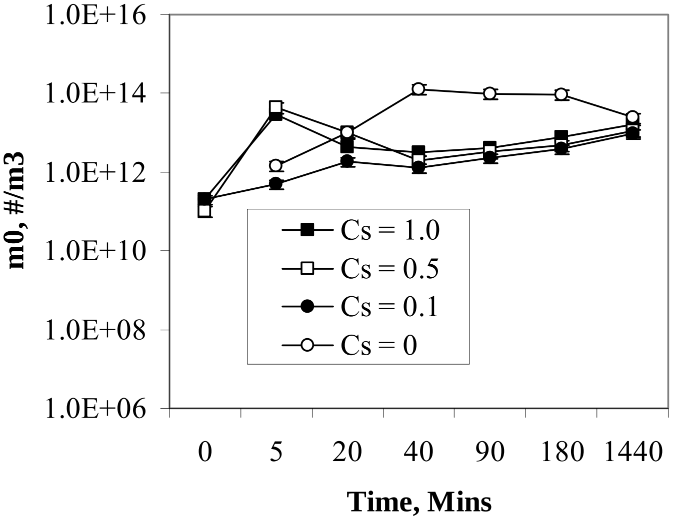

Figure 6.62 *Change in m_0 as a function of time for the haematite seeded system at pH 6.0*

From Figure 6.62, it can also be observed that, regardless of the seed concentration, the extent to which seeding suppresses nucleation is the same. This is also true for the goethite and the recycled solids seeded systems. The effect of the different seed types on the final product size is shown in Figure 6.63. The greatest seeding benefits would be obtained from recycled solids seeding compared to haematite or goethite seeding.

In fact both haematite and goethite seeding result in the formation of particles of the same size at all the three concentration levels considered here.

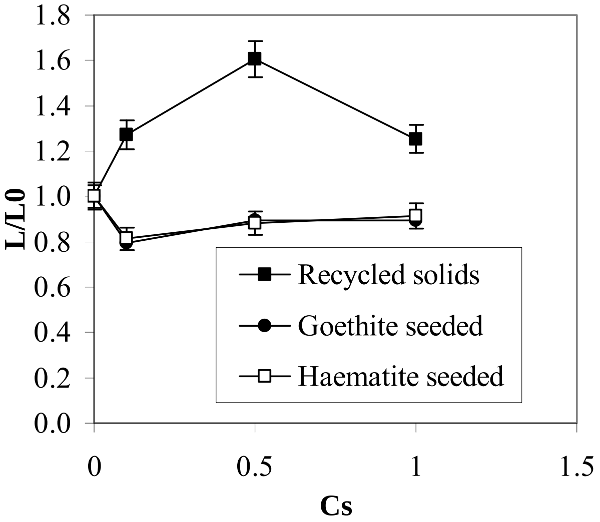

Figure 6.63 *Change in L/L_0 as function of seed concentration, C_s at pH 6.0*

By using equation 1.51, a theoretical average size of the seeded product Lp (m) can be calculated for known C_s and seed size L_0. If the ratios Lp/L_0 and L/L_0 are comparable, it can be concluded that the seeded system is dominated by the growth of the seed material (Doki et al., 2001), (Kubota et al., 2001). This criterion was used to make an inference about the mechanisms involved in seeded precipitation of iron. The results of such computations are shown in Table 6.2.

Table 6.2 *Comparison of theoretical and experimental average sizes of the precipitates formed under pH 6.0 conditions*

Seed material	**C_s = 1.0**	**C_s = 0.5**	**C_s = 0.1**
Recycled solids	L/L_0, **1.25** L_p/L_0, **1.25**	1.60 1.44	1.27 2.20
Goethite seeded	L/L_0, 0.79 L_p/L_0, 1.25	0.89 1.44	0.89 2.20
Haematite seeded	L/L_0, 0.81 L/L_0, 1.25	0.88 1.44	0.91 2.20

From Table 6.2, it can be seen that the two ratios are comparable only under C_s = 1.0 in the recycled solids seeded system. This means that this is the only instance when the process can be regarded as dominated by the growth of seed material. Indirectly, it also means that all other instances are dominated by nucleation, aggregation and coating of the freshly precipitated material onto the seed material.

In conclusion, the results presented here demonstrate firstly that; regardless of the seed concentration, the rate of oxidation of iron will be the same, secondly; the lower the seed concentration, the larger the final particle size of the product at least for the cases presented here. Lower seed concentrations result in greater proportions of the freshly formed precipitate, this precipitate has a higher tendency to aggregating rather than coating on the seed material thus forming larger particles compared to systems that have higher concentrations of the seed material. Thus, from a size point of view, it is more beneficial to effect the oxidation and precipitation of iron at lower seed concentrations since the kinetic gains are the same. Thirdly, seeding with single pass product produces product of the largest sizes, this is most likely due to the lattice compatibility between the seed material and the freshly precipitated solids.

6.6.1.3 Effect of C_s on the composition of the precipitate

The relative compositions of the precipitates formed under the different seeding regimes at pH 6.0 are shown in Table 6.3. The table shows that high C_s values of recycled solids suppress the formation of ferrihydrite while promoting the formation of the more stable lepidocrocite. The effect on the relative amounts of both goethite and haematite are not very significant.

Table 6.3 *Relative composition of the precipitates at pH 6.0*

Recycled solids seeded system			
Constituent	**C_s = 1.0**	**C_s = 0.5**	**C_s = 0.1**
Ferrihydrite, %	14	33	27
Feroxyhyte, %	-	-	-
Lepidocrocite,%	80	64	69
Goethite, %	4	3	4
Haematite, %	2	-	-
Goethite seeded system			
Ferrihydrite, %	-	-	-
Feroxyhyte, %	-	-	-
Lepidocrocite,%	22	28	48
Goethite, %	76	69	50
Haematite, %	1	3	1
Haematite seeded system			
Ferrihydrite, %	-	1	3
Feroxyhyte, %	-	-	-
Lepidocrocite,%	26	26	27
Goethite, %	68	66	63
Haematite, %	6	7	7

Considering the goethite seeded system, it can be observed that goethite seeds inhibit the formation of ferrihydrite and lepidocrocite while promoting the formation of goethite. At C_s = 1.0, 76 % of the precipitate was goethite while at C_s = 0.1, the proportion of goethite dropped to 50%. It can thus be concluded that the promotional effect of goethite seeding in this case decreases with a decrease in the concentration of the seed. The inhibitive effect of goethite seeding also decreases with decrease in the concentration of the seed material as can be seen in the lepidocrocite and ferrihydrite trends.

The effect of haematite seeding is more interesting. It is the only seed material which did not promote the precipitation of itself at all the concentration levels considered here. In all cases (as shown in Table 6.3), haematite seeding tended to promote the precipitation of goethite while suppressing the precipitation of lepidocrocite. Unlike goethite seeding, haematite seeding did not totally suppress the formation of ferrihydrite. It is therefore most likely that goethite is formed from the transformation of ferrihydrite rather than direct precipitation from solution. In this view it would be logical to suggest that haematite seeding probably catalyses the transformation of ferrihydrite rather than the direct precipitation of goethite. Another observation from this result is that, in the case of haematite seeding, the precipitate is formed by nucleation from solution rather than growth on the haematite seed. It can also be concluded that haematite seeding results in the formation of the most stable precipitates since goethite (which is more stable than lepidocrocite and ferrihydrite) is in the highest proportions.

6.6.2 pH 8.0 case

6.6.2.1 Effect of C_s on oxidation rate

The effect of C_s on the rate of oxidation of iron from solution is shown in Figure 6.64. The recycled solids used as seed material here catalysed the oxidation rate to the same extent regardless of the concentration. This means that from an operational point of view it would be more beneficial to use lower seed concentrations since the kinetic benefits will be the same as operating at high seed concentrations. Goethite and haematite seeding also showed the same trend in their effect on the oxidation rate. The results of the effect of seed concentration on the oxidation rate for the goethite and haematite seeded systems are shown in Figure 6.65 and Figure 6.66

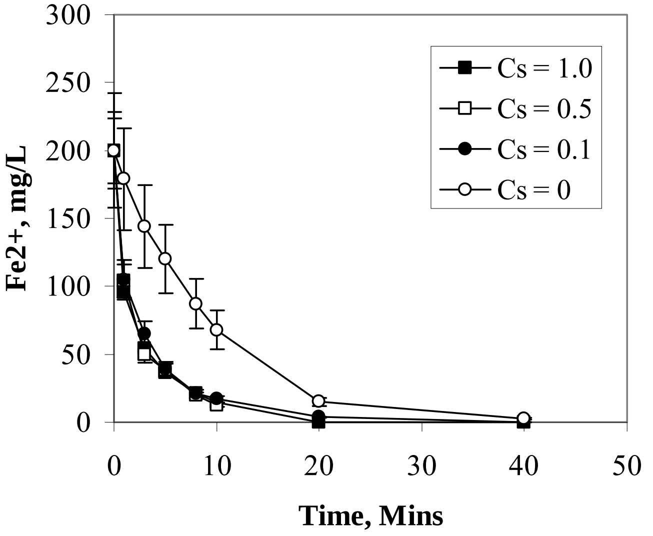

Figure 6.64 *Change in the* Fe^{2+} *concentration in solution as a function of time for the recycled solids system at pH 8.0*

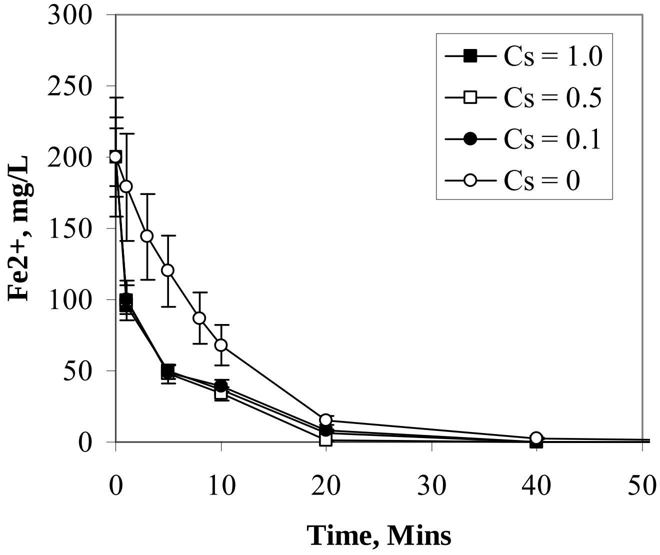

Figure 6.65 *Change in the concentration of* Fe^{2+} *as a function of time for the goethite seeded system at pH 8.0*

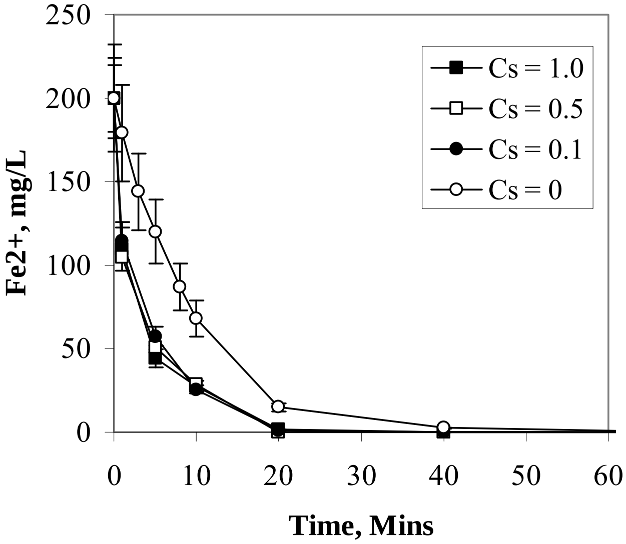

Figure 6.66 *Change in the concentration of* Fe^{2+} *in solution as a function of time for the haematite seeded system at pH 8.0*

6.6.2.2 Effect of C_s on the average size of the particles

The effect of seed concentration on the population-based average size of the particles in the recycled solids system is shown in Figure 6.67. The figure shows that, for C_s = 1.0 and 0.5, at 5 minutes the process is nucleation dominated. After this stage, the increase in the L/L_0 ratio indicates growth or aggregation or surface coating or all of these processes. However, if the evolution of m_0 is considered (Figure 6.68), it can be seen that there was a corresponding decrease in the number of particles, thus ruling out growth as a dominant process mechanism. After 90 minutes there was a decrease in the size of the particles corresponding to either the ageing of the particles, which is usually accompanied by the ejection of water molecules (Gan et al., 2005), or the onset of adherence of the aggregates onto the seed material. The same trend can be observed for the C_s = 0.1 case except that, at 5 minutes, the aggregation of the particles had already begun. This earlier onset of aggregation is probably due to the formation of more fresh precipitate species which have a higher tendency of aggregation than the ordered precipitates which are promoted by seeding. It is also most likely that the surface properties of the freshly prepared precipitates are different from those of aged precipitates, this could again affect the aggregation reactions of the precipitates. It can also be seen that regardless of the seed concentration, the presence of seeds inhibit primary nucleation to an equal extent (m_0 of the seeded systems was always lower than that of the single pass system or C_s = 0 case). Again seeding did not totally suppress nucleation as the m_0 of the systems increased with time to levels above that of the seed material.

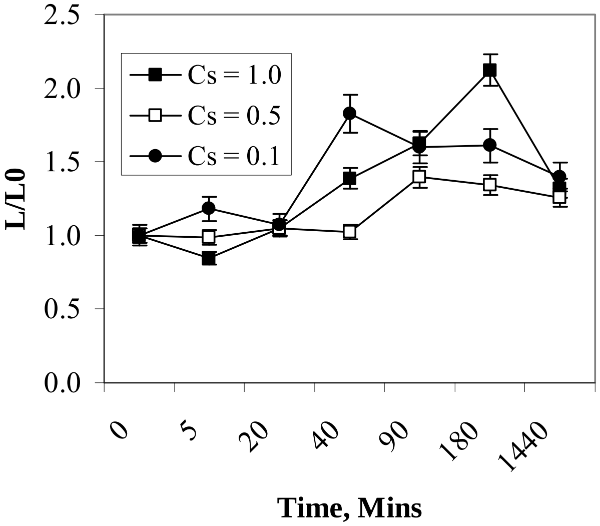

Figure 6.67 Change in L/L_0 as a function of time for the recycled solids seeded system at pH 8.0

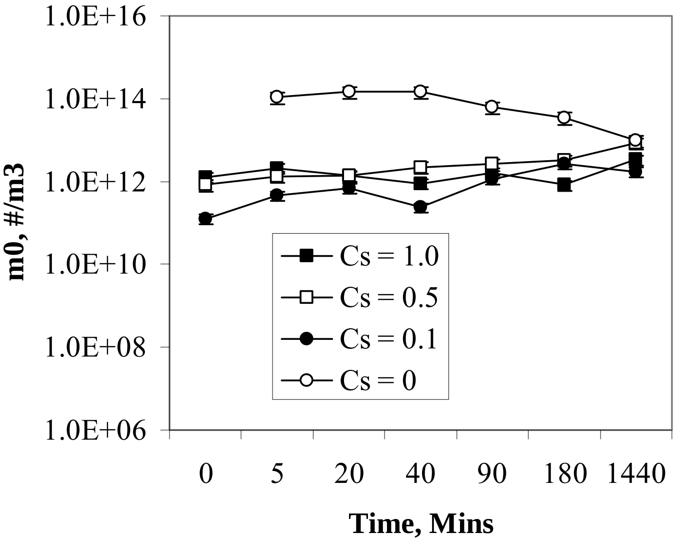

Figure 6.68 Change in m_0 as a function of time for the recycled solids system at pH 8.0

The goethite seeded system showed the same trend except that there was no evidence (Figure 6.69) of nucleation at the initial stages of the process. This was probably due to the fact that the solids formed here were dominated by fresh precipitate which has a higher tendency to aggregate than the natural goethite which was used as the seed material. The process stages were similar to those described for the recycled solids system. An interesting feature for the goethite seeded system is that, regardless of the seed concentration, the final size of the precipitate particles is almost the same. This means that the particle formation processes are not dominated by the influence of the seed material but most probably rather by pH conditions and oxidation rates. Like in the recycled solids case, seeding did not totally suppress nucleation (Figure 6.70)

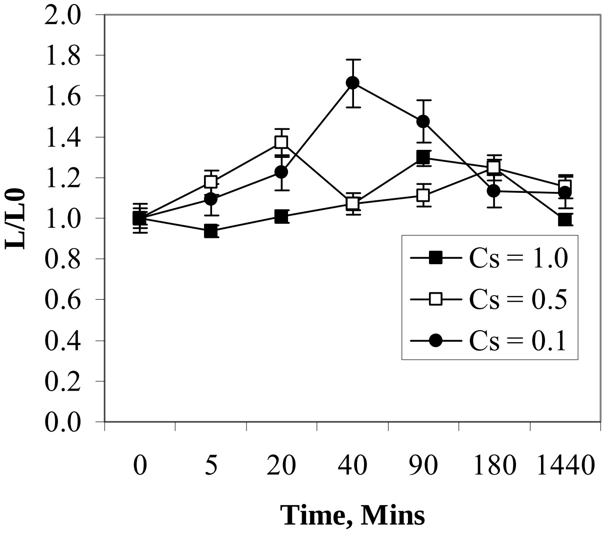

Figure 6.69 *Change in L/L_0 as a function of time for the goethite seeded system at pH 8.0*

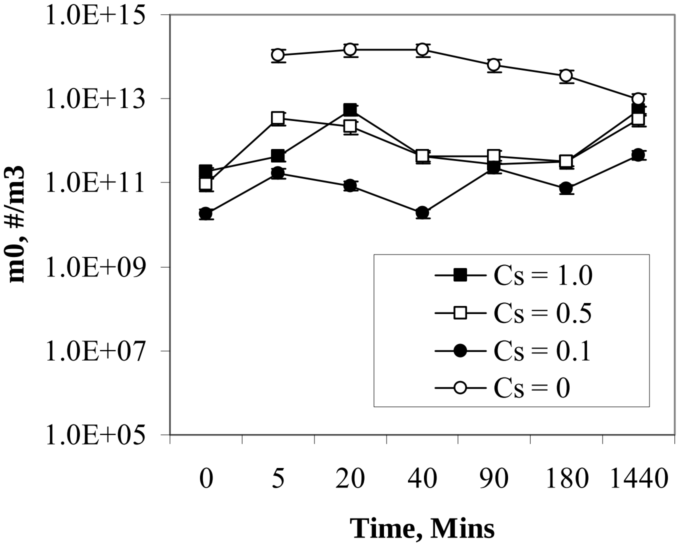

Figure 6.70 *Change in m_0 as a function of time for the goethite seeded system at pH 8.0*

Considering the haematite seeded system (Figure 6.71), the nucleation process was apparent at 5 minutes for all the seed concentration levels. The subsequent process stages are the same as those for the recycled solids and goethite systems. As in the other cases, seeding suppresses nucleation but not totally (Figure 6.72)

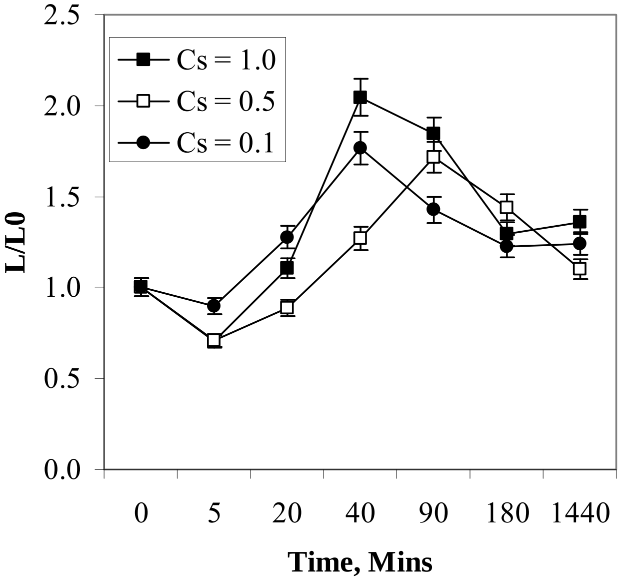

Figure 6.71 *Change in L/L_0 as a function of time for the haematite seeded system at pH 8.0*

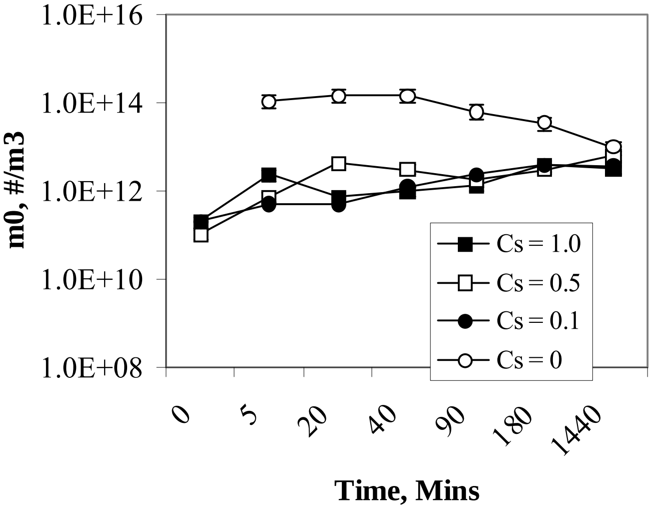

Figure 6.72 *Change in m_0 as a function of time for the haematite seeded system at pH 8.0*

The change in the population-based average size of the precipitates as a function of the seed concentration shows that, at C_s = 0.5 and 1.0 recycled solids systems produced bigger particles (Figure 6.73). At C_s = 0.1 haematite seeded and recycled solids seeded systems produce precipitates of identical population-based average sizes. In all cases, C_s = 0.1 produced the largest sized particles. This is probably due to the fact that the precipitate mass is dominated by freshly prepared solids which have a greater tendency to aggregate and flocculate resulting in the formation of bigger particles.

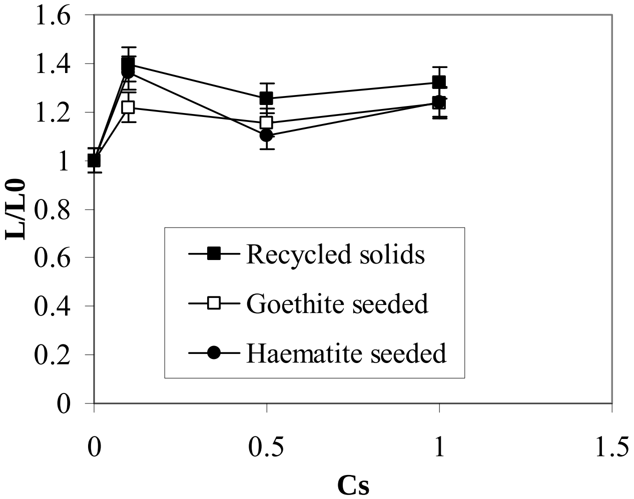

Figure 6.73 *Change in L/L_0 as a function of C_s for the different seed types at pH 8.0*

Comparison of the theoretical and measured size ratios is shown in Table 6.4. The results indicate that in all instances the particle formation processes did not involve the growth of the seed material. Again, since the experimental ratio L/L_0 was always less than the theoretical ratio L_p/L_0, it means that the final particle size was lower than theoretically expected sizes, which indirectly confirms the significance of coating of the seed material.

Table 6.4 *Comparison between theoretical and experimental particles sizes for the seeded systems at pH 8.0*

Seed material	**C_s = 1.0**	**C_s = 0.5**	**C_s = 0.1**
Recycled solids	L/L_0, 1.32	0.97	1.40
	L_p/L_0, 1.26	1.44	2.21
Goethite seeded	L/L_0, 0.99	1.16	1.13
	L_p/L_0, 1.26	1.44	2.20
Haematite seeded	L/L_0, 1.36	1.10	1.24
	L/L_0, 1.26	1.44	2.20

6.6.2.3 Effect of C_s on the composition of the precipitates

The relative composition of the precipitates formed under the recycled solids, goethite and haematite seeded systems are shown in Table 6.5. Seeding with recycled solids promoted the formation of lepidocrocite with its proportion increasing from 65% at C_s = 0.1 to 88% at C_s = 1.0. The formation of feroxyhyte was suppressed with increase in $C_{s,}$ decreasing from 32% at C_s = 0.1 down to 8% at C_s = 1.0. The changes in the proportion of goethite and haematite were invariant with changes in C_s.

Goethite seeding sustained the formation of lepidocrocite although there no systematic trends in lepidocrocite proportions. Compared to the recycled solids system there was a slight increase in the proportion of goethite formed. Another interesting observation is that, unlike the recycled solids system, feroxyhyte was not formed in the goethite seeded system. Since the dominant iron phase was lepidocrocite, it is most likely that the phase formation and transformation processes were still governed by pH and oxidation rate conditions rather than the presence of the seed material. Interestingly, as in the pH 6.0 case, haematite seeding promoted the formation of goethite at the expense of itself. The proportion of goethite increased from 28% at $C_s = 0.1$ to 43% at $C_s = 1.0$ while that of lepidocrocite decreased from 70% at $C_s = 0.1$ to 47% at $C_s = 0.1$. This result is also in contrast to the prediction based on lattice misfit compatibility as calculated in Table 1.4. The most stable iron phase in highest proportions formed under pH 8.0 conditions is lepidocrocite. This is contrary to the pH 6.0 case were the most abundant and most stable phase was goethite. If the two pH cases are compared, it would be better to effect the seeded precipitation of iron at pH 6.0 since this is the condition which would guarantee the formation of the most stable precipitate.

Table 6.5 *Relative composition of the precipitates at pH 8.0*

Recycled solids seeded system			
Constituent	**C_s = 1.0**	**C_s = 0.5**	**C_s = 0.1**
Ferrihydrite, %	-	-	-
Feroxyhyte, %	8	25	32
Lepidocrocite,%	88	71	65
Goethite, %	2	3	3
Haematite, %	2	2	-
Goethite seeded system			
Ferrihydrite, %	-	-	-
Feroxyhyte, %	-	-	-
Lepidocrocite,%	80	85	86
Goethite, %	16	10	9
Haematite, %	4	5	5
Haematite seeded system			
Ferrihydrite, %	-	-	-
Feroxyhyte, %	-	-	-
Lepidocrocite,%	47	57	70
Goethite, %	43	33	28
Haematite, %	10	9	3

6.6.3 pH 9.0 case

6.6.3.1 Effect of C_s on the oxidation rate

The effects of seeding on the oxidation rate of iron from solution at pH 9.0 for the recycled solids, goethite and haematite seeded systems are shown in Figure 6.74, Figure 6.75 and Figure 6.76 respectively. The explanations for the observed trends have been given in earlier sections (6.6.1.1 and 6.6.2.1) and therefore will not be repeated here.

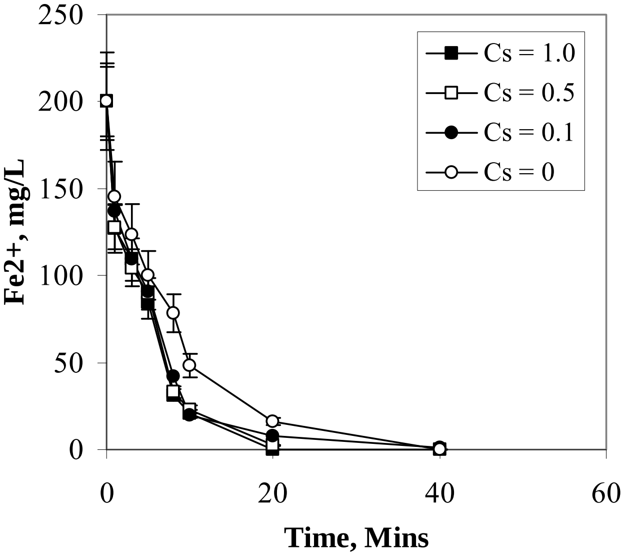

Figure 6.74 *Change in the concentration of* Fe^{2+} *in solution with time for the recycled solids seeded system at pH 9.0*

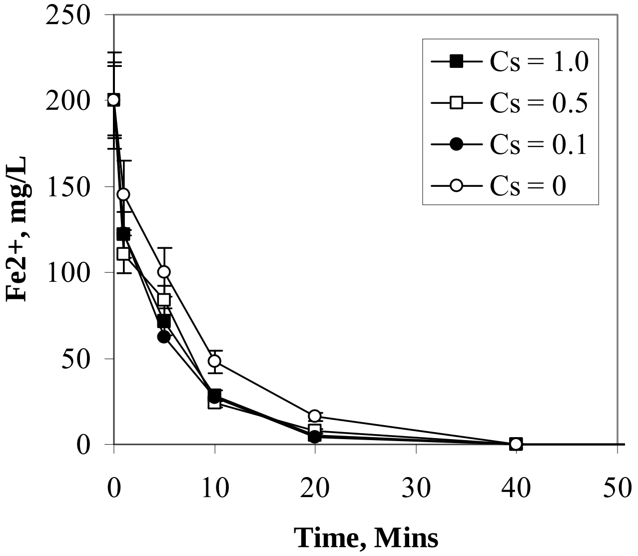

Figure 6.75 *Change in the concentration of* Fe^{2+} *in solution with time for the goethite seeded system at pH 9.0*

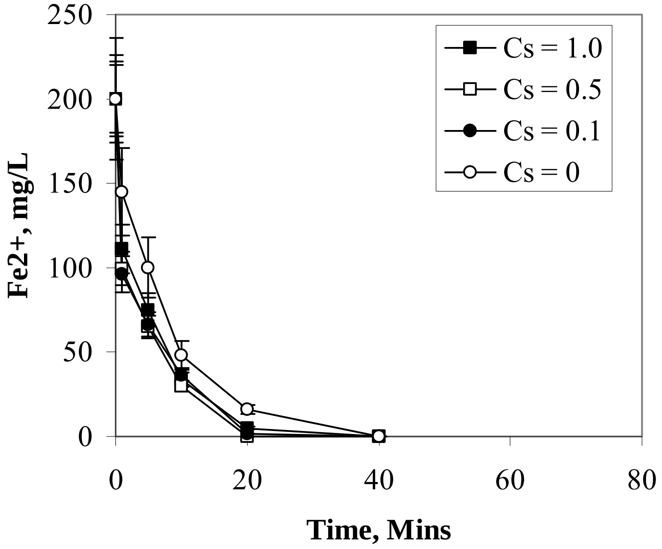

Figure 6.76 *Change in the concentration of* Fe^{2+} *in solution with time for the haematite seeded system at pH 9.0*

6.6.3.2 Effect of C_s on the average size of the particles

The effect of Cs on the population-based average size of the particles for the recycled solids system is shown in Figure 6.77. For the case C_s = 1.0, the process was dominated by aggregation or coating or both from 5 minutes up to 20 minutes. It is most likely that the nucleation process occurred much earlier than 5 minutes due to the high oxidation rates. From 20 minutes onwards the decrease in the size was probably due to ageing and coating of the smaller particles on the seed material. During coating, unlike during aggregation, it is possible to form particles of even smaller size than the aggregates. It is thus postulated again here that seed coating resulting from iron hydroxide flocs/aggregates results in the formation of seed material that is still smaller than the flocs themselves.

Figure 6.77 also shows that the largest particles were obtained for $C_s = 0.1$ and 0.5. This again is most likely due to the higher proportion of freshly prepared solids that have a greater tendency to aggregate than to coat on the seed surface. The evolution of m_0 (Figure 6.78) also shows the same trend and as in the other cases considered so far, confirm that seeding suppresses nucleation (although not totally).

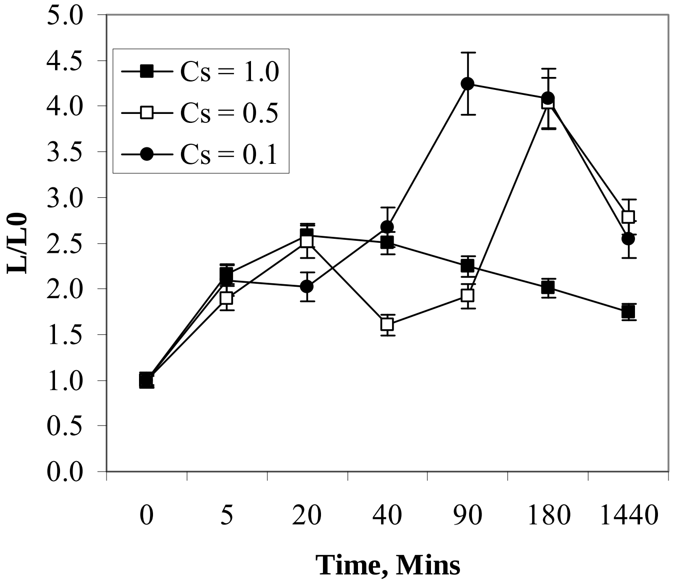

Figure 6.77 *Change in L/L_0 with time in the recycled solids seeded system at pH 9.0*

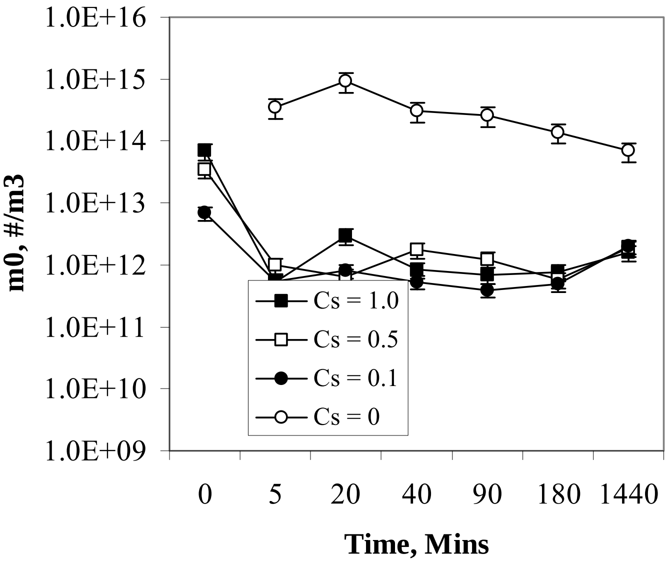

Figure 6.78 *Change in m_0 with time in the recycled solids seeded system at pH 9.0*

Considering the goethite seeded system, the same trends as those for the recycled solids system were obtained except for Cs = 0.5 (Figure 6.79 and Figure 6.80). The same explanations for the trends as given for the recycled solids system are again considered sufficient. The behaviour of the system Cs = 0.5 in the goethite seeded (Figure 6.79) could not be explained.

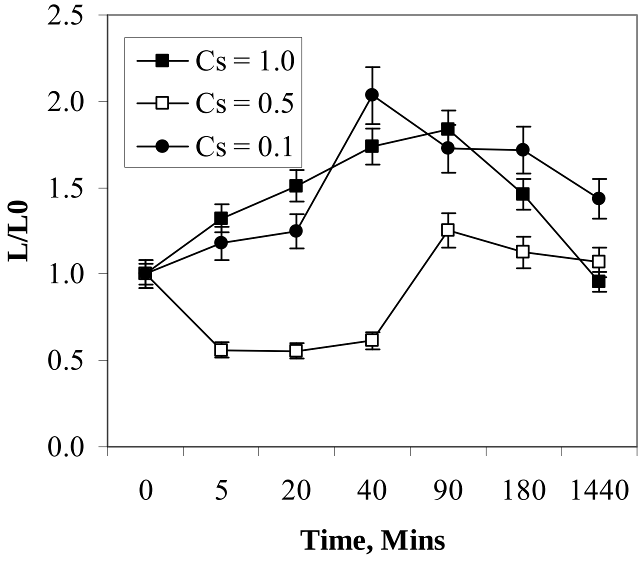

Figure 6.79 *Change in L/L_0 with time for the goethite seeded system at pH 9.0*

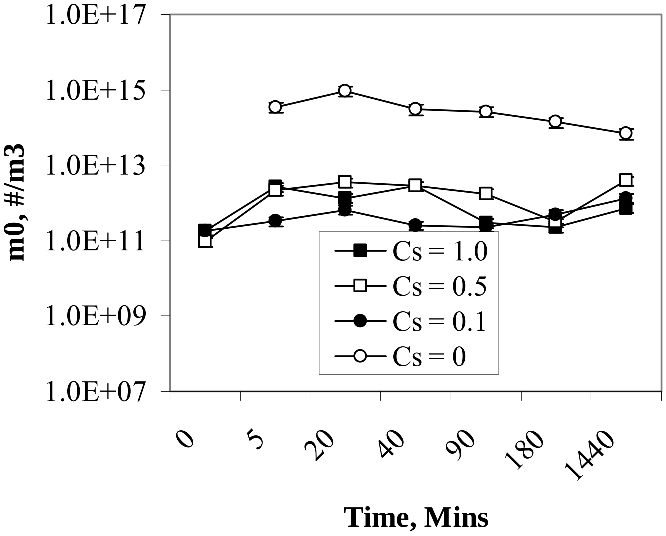

Figure 6.80 *Change in* m_0 *in the goethite seeded system at pH 9.0*

The change in the ratio L/L_0 for the haematite seeded experiments is shown in Figure 6.81. From 5 minutes up to 40 minutes (for $C_s = 1.0$) and 90 minutes (for $C_s = 0.5$ and 0.1) the process was dominated by aggregation. As in the recycled solids case, the biggest particles were obtained for Cs = 0.1 and 0.5 due to the dominance of the freshly precipitated solids which have higher tendency to aggregate compared to the aged or natural seed materials. Again the decrease in the size of the particles at the last stages of the process was due to ageing and coating of the previously formed aggregates on the seed surfaces. As in other cases, seeding managed to reduce the levels of primary nucleation (although not totally) thus growth and surface precipitation (section 6.4) cannot be completely ruled out.

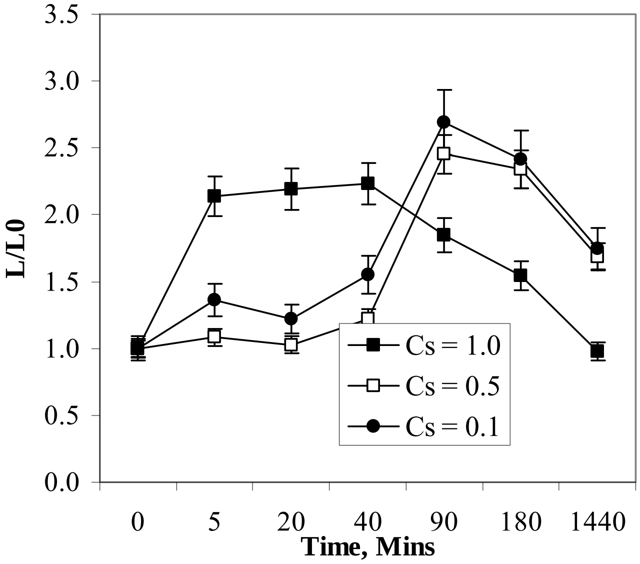

Figure 6.81 *Change in L/L_0 with time for the haematite seeded system at pH 9.0*

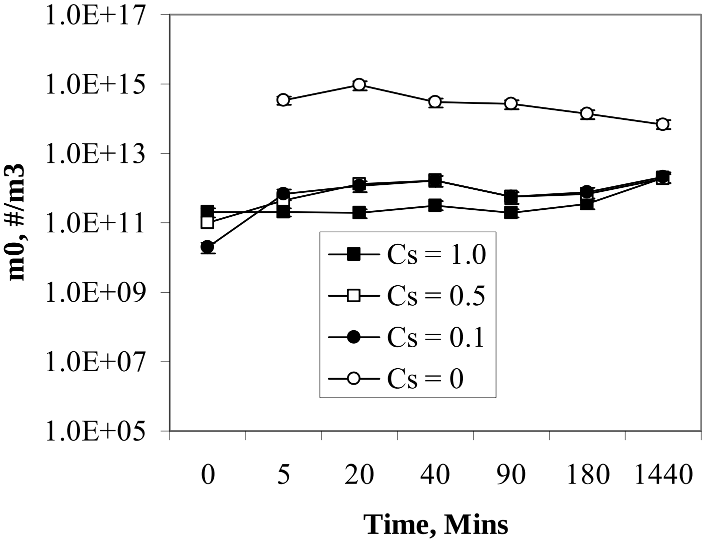

Figure 6.82 *Change in m_0 with time in the haematite seeded system at pH 9.0*

A comparison of the effect of seed type and seed concentration on the ratio L/L_0 for the seeded systems at pH 9.0 is shown in Figure 6.83. The figure shows that, as in the pH 6.0 and pH 8.0 cases, recycled solids seeding always resulted in the formation of the largest particles. Haematite seeding produced the second largest particle sizes at all the C_s levels considered. It is also very interesting to note that C_s = 1.0 always produced the smallest size particles. This is because aged precipitates are more ordered and have less bound water molecules.

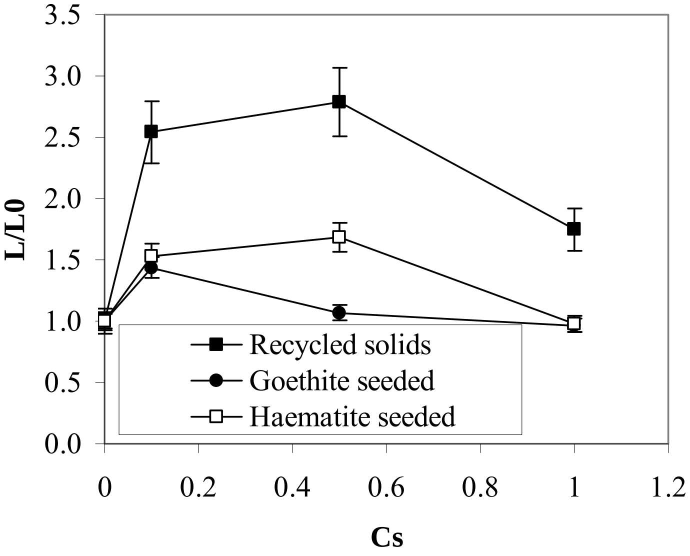

Figure 6.83 *Change in L/L_0 with C_s for the different types of seeds at pH 9.0*

Comparison of the theoretical and experimental seed sizes is shown in Table *6.6*. The table shows that as in the pH 8.0 case, growth of the seed material was not a dominant process in all the instances. An interesting observation however, is that for the recycled solids seeded systems, the experimentally determined size of the particles was higher than the theoretically calculated size. This most likely means that the particle formation processes were aggregation dominated for the recycled solids cases. In all other cases, however, the process seemed to have been dominated by coating of the freshly precipitated solids on the seed material.

Table 6.6 *Comparison of the theoretical and experimental average particle sizes of the particles formed under pH 9.0*

Seed material		**C_s = 1.0**	**C_s = 0.5**	**C_s = 0.1**
Recycled solids	L/L_0,	1.75	2.78	2.54
	L_p/L_0,	1.26	1.44	2.21
Goethite seeded	L/L_0,	0.97	1.07	1.44
	L_p/L_0,	1.26	1.44	2.21
Haematite seeded	L/L_0,	0.98	1.69	1.75
	L/L_0,	1.26	1.44	2.21

6.6.3.3 Effect of C_s on the composition of the precipitates

The composition of the precipitates formed at pH 9.0 under the different seed types and seed concentrations are shown in Table 6.7. In the recycled solids case, regardless of the seed concentration, lepidocrocite was the dominant iron phase formed. The formation of 2% ferrihydrite at C_s = 1.0 cannot be considered to be significant, the same applies to the invariant proportion of haematite. Goethite seeding as in the earlier cases promoted the formation of itself while suppressing that of lepidocrocite. Thus at C_s = 0.1, 81% lepidocrocite was formed, while 71% lepidocrocite was formed at C_s = 1.0. Correspondingly, the proportion of goethite increased from 17% at C_s = 0.1 to 27% at C_s = 1.0.

As in the pH 6.0 and 8.0 cases, haematite seeding promoted the formation of goethite. Thus goethite proportion increased from 8% at C_s = 0.1, 36% at C_s = 0.5 and finally 85% at C_s = 1.0. The proportion of lepidocrocite decreased from 89%, 56% and finally to 1% respectively. There was a slight increase in the proportion of haematite from 3% at C_s = 0.1 to 11% at C_s = 1.0. From a precipitate stability point of view, therefore, it would appear that it is better to effect the precipitation of iron under haematite seeding as this promotes the formation of the more stable goethite phase.

Table 6.7 *Relative composition of the precipitates formed at pH 9.0*

Recycled solids seeded system			
Constituent	**C_s = 1.0**	**C_s = 0.5**	**C_s = 0.1**
Ferrihydrite, %	2	-	-
Magnetite, %	-	-	-
Lepidocrocite,%	94	96	96
Goethite, %	4	4	4
Haematite, %	-	-	-
Goethite seeded system			
Ferrihydrite, %	-	-	-
Magnetite, %	2	-	-
Lepidocrocite,%	71	73	81
Goethite, %	27	25	17
Haematite, %	-	2	2
Haematite seeded system			
Ferrihydrite, %	-	-	-
Magnetite, %	3	-	-
Lepidocrocite,%	1	56	89
Goethite, %	85	36	8
Haematite, %	11	7	3

6.6.4 pH 10.0 case

6.6.4.1 Effect of C_s on the rate of oxidation

The effect of seed concentration on the rate of oxidation for the experiments carried out at pH 10.0 are shown in Figure 6.84, Figure 6.85 and Figure 6.86 for the recycled solids, goethite and haematite seeded systems respectively. The results indicate that, unlike in the pH 9.0, 8.0 and 6.0 cases, there was little catalytic effect on the rate of oxidation due to the seed addition. This means that at high pH the impact of pH on the oxidation rate is much more significant than the catalytic effect of solids. It can thus be suggested that the rate of oxidation at high pH was independent of the presence of seed material in the system.

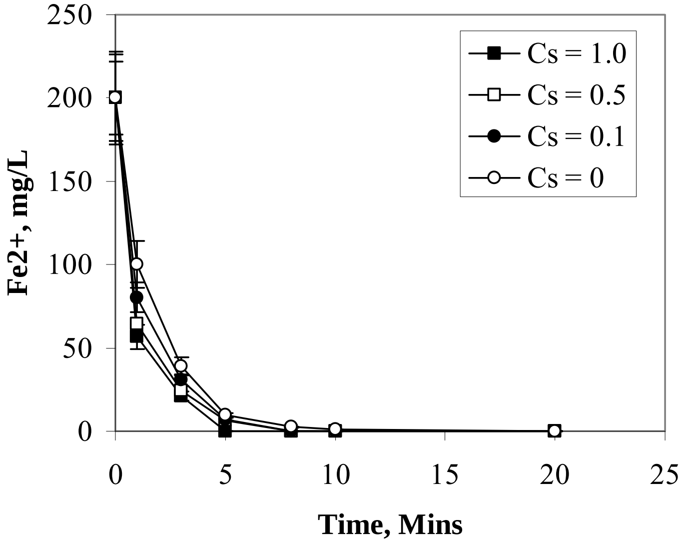

Figure 6.84 *Change in the concentration of* Fe^{2+} *in solution with time in the recycled solids system at pH 10.0*

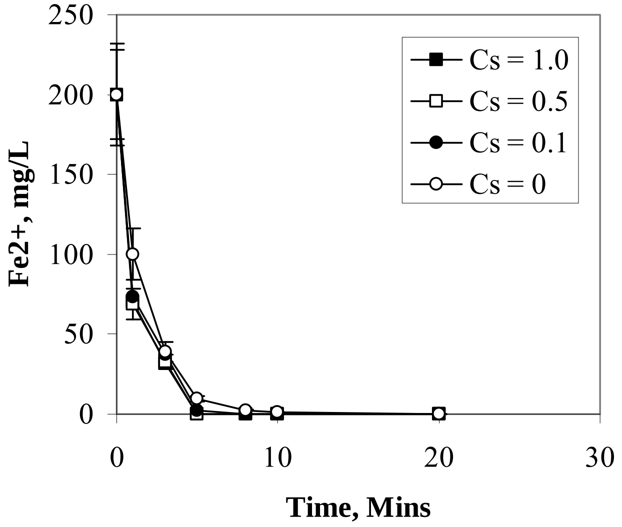

Figure 6.85 *Change in the concentration of* Fe^{2+} *in solution with time in the goethite seeded system at pH 10.0*

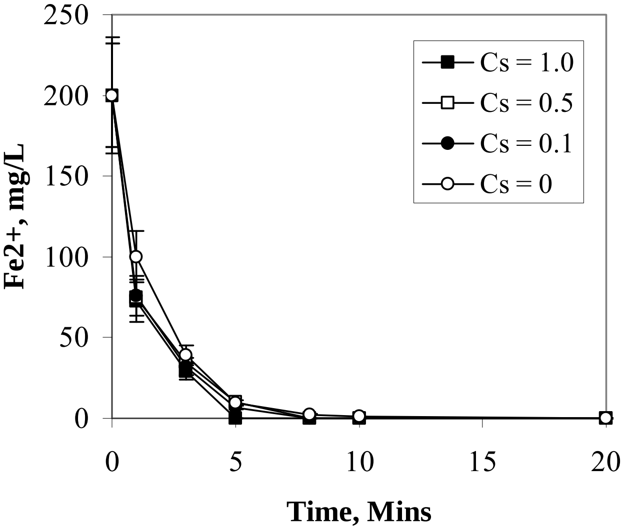

Figure 6.86 *Change in the concentration of* Fe^{2+} *in solution with time in the haematite seeded system at pH 10.0*

6.6.4.2 Effect of C_s on the average size of the particles

The effect of C_s on the population based average size of the particles in the recycled solids system is shown in Figure 6.87. In all the cases there was a general increase in the L/L_0 ratio, indicating aggregation of the particles, although coating can also not be ruled out.

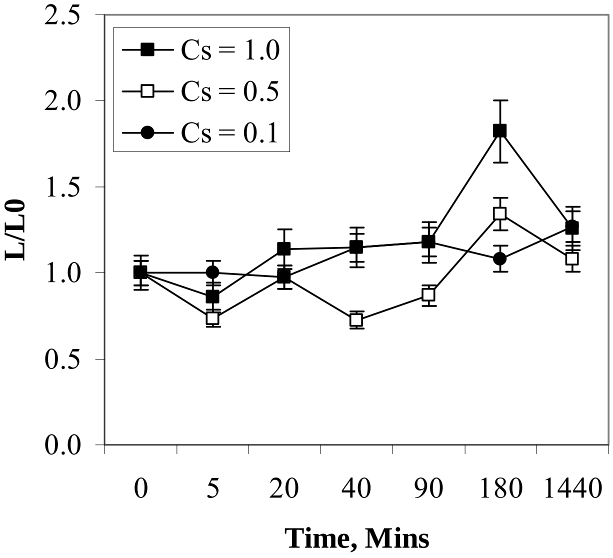

Figure 6.87 *Change in* L/L_0 *with time in the recycled solids system at pH 10.0*

From the figure, the biggest size particles were obtained for $C_s = 0.1$ and $C_s = 1.0$. This was probably due to the presence in higher proportions of freshly precipitated phases at $C_s = 0.1$ and the presence in more significant proportions of the aged precipitate for the $C_s = 1.0$ case. Another interesting feature in the pH 10.0 case is that, although the rate of oxidation was unchanged by the introduction of seed material, m_0 for the seeded systems was much lower, indicating that seeding suppressed nucleation (Figure 6.88).

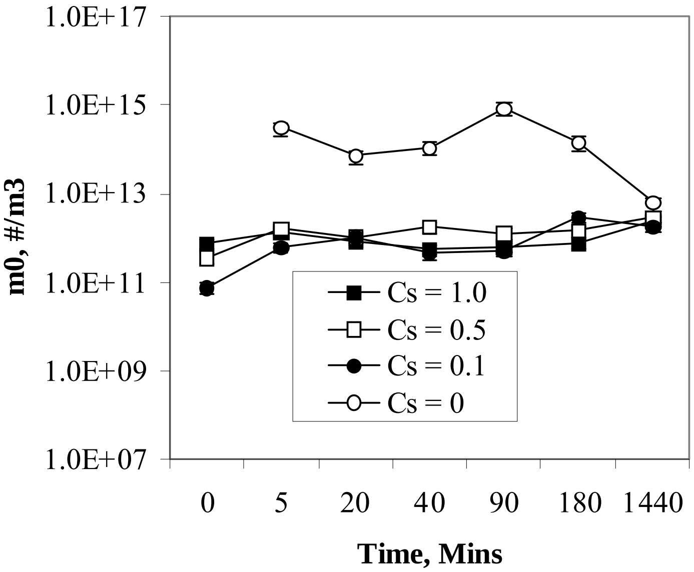

Figure 6.88 *Change in m_0 with time in the recycled solids system at pH 10.0*

For the goethite seeded system, initial nucleation of fresh precipitate is evident (Figure 6.89) at all the C_s levels considered. This could mean that although there are no major differences in the rates of oxidation between the goethite seeded system and the recycled solids seeded system, the processes leading to the formation of the final precipitate could be different. The delay in the onset of aggregation and/or coating in the case of the goethite seeded system could be due to the incompatibilities in the surface properties of the natural goethite and the freshly precipitated iron phases. It is again interesting to note that the largest particles were formed when C_s was 0.1, confirming the observations made in the earlier cases. It can thus be inferred that low seed concentrations promote aggregation of the freshly precipitated solids while high seed concentrations favour the adherence/coating of the freshly precipitated solids on the seed material, with the latter resulting in smaller sizes especially if it can be assumed that aggregation involves the collision and cementing together of two particles resulting in the doubling of the size (Zauner et al., 2000). As in all other cases, the evolution of m_0 (Figure 6.90) shows that the process was dominated by nucleation, aggregation, coating and ageing of the precipitates.

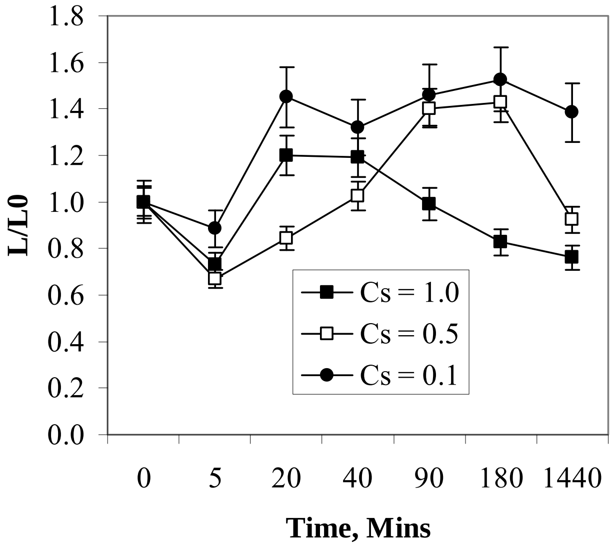

Figure 6.89 *Change in L/L_0 with time in the goethite seeded system at pH 10.0*

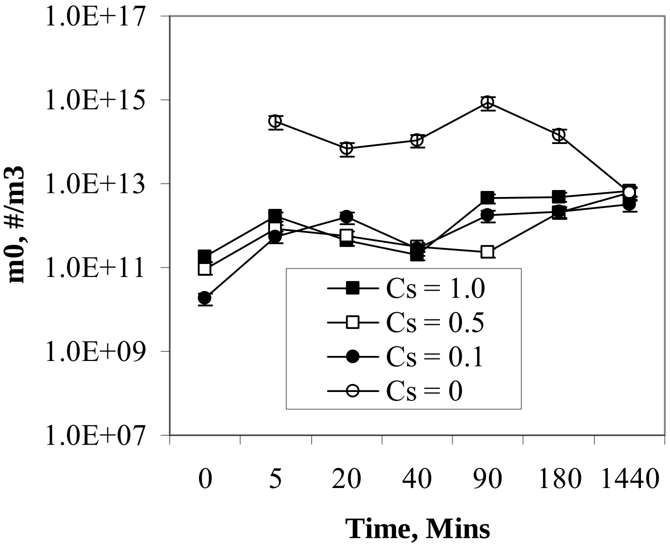

Figure 6.90 *Change in m_0 with time in the goethite seeded system at pH 10.0*

The evolution of L/L_0 for the haematite seeded system is shown in Figure 6.91. The explanation for the trends has been given in earlier sections. The differences in the onset of nucleation, aggregation and coating are a function of the surface characteristics of the seed material. It is again interesting to note that the biggest particles were obtained at the lowest seed concentration of $C_s = 0.1$. This again supports the earlier given hypothesis that high seed concentrations promote coating while low seed concentrations favour aggregation of the freshly formed solid precipitates. Although there was significant difference in the oxidation rate, seeding with haematite suppressed the primary nucleation of fresh precipitates Figure 6.92.

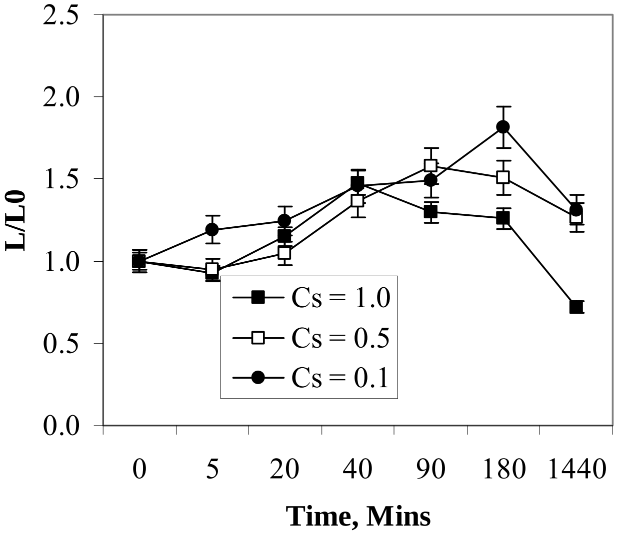

Figure 6.91 *Change in L/L_0 with time in the haematite seeded system at pH 10.0*

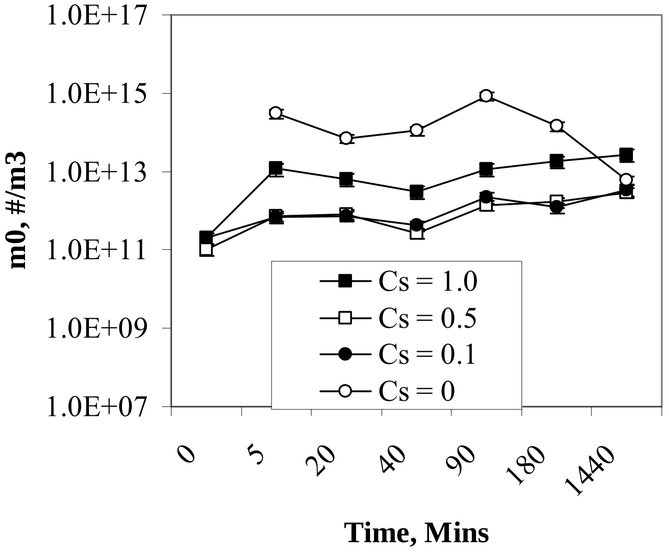

Figure 6.92 *Change in m_0 with time in the haematite seeded system at pH 10.0*

Comparison of the effect of the different types of seeds and seed concentration on the ratio L/L_0 (Figure 6.93) showed that like in other cases that recycled solids produced the largest size of particles. The close similarity in the size of the particles at $C_s = 0.1$ also confirms that, at low seed concentrations, aggregation of the freshly precipitated solids is the dominant process compared to coating. Likewise the smaller particle sizes obtained at high seed concentrations also confirm that high seed concentrations favour coating at the expense of aggregation.

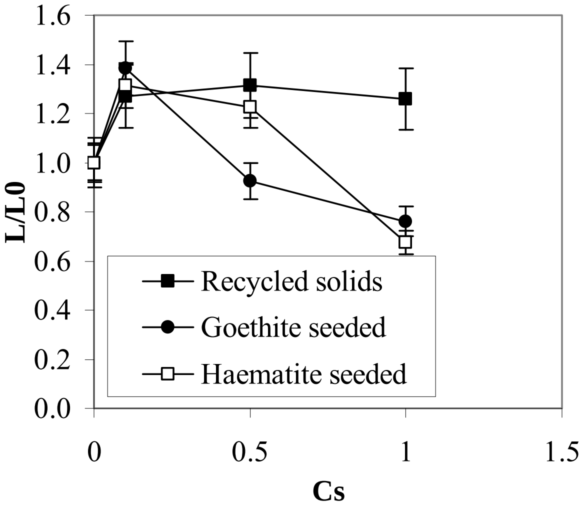

Figure 6.93 *Change in L/L_0 with C_s for the different seed types at pH 10.0*

The comparison between theoretically predicted sizes and the experimentally determined sizes of the particles are shown in Table 6.8. The results indicate that the particle formation process was dominated by growth of the seed material only at C_s = 1.0 in the recycled solids seeded system. In all the other cases the particle formation process was dominated by nucleation, aggregation and coating of the freshly precipitated solids on the seed material, since the theoretically determined sizes were always larger than the experimental ones. This observation is in agreement with the findings for all the other cases considered in this study. It can this be concluded that the seeded oxidation and precipitation of iron is dominated by nucleation, aggregation and adherence of the freshly precipitated solids onto the seed material rather than by growth of the seeds.

Table 6.8 *Comparison of the theoretical and experimental average size of the particles formed under pH 10.0 conditions*

Seed material	**C_s = 1.0**	**C_s = 0.5**	**C_s = 0.1**
Recycled solids	L/L_0, **1.26**	1.08	1.27
	L_p/L_0, **1.26**	1.44	2.21
Goethite seeded	L/L_0, 0.76	0.92	1.38
	L_p/L_0, 1.26	1.44	2.21
Haematite seeded	L/L_0, 0.68	1.27	1.31
	L/L_0, 1.26	1.44	2.21

6.6.4.3 Effect of C_s on the composition of the precipitates

The relative compositions of the precipitates formed under pH 10.0 are shown in Table 6.9. The interesting feature here is that, regardless of the seed type and seed concentration, the dominant iron phase is always goethite. It also interesting to note that, although the speciation of iron is complex at high pH (Blesa and Matijevic, 1989), the simplest iron precipitate consisting of mainly a single phase, was formed under high pH conditions. It is most likely that goethite was formed from the fast transformation of ferrihydrite (Cornell et al., 1985). It can also be concluded that at pH 10.0, the formation of the final stable precipitate is a function of the pH and not the seed concentration.

Table 6.9 *Relative composition of the precipitates formed at pH 10.0*

Recycled solids seeded system			
Constituent	**C_s = 1.0**	**C_s = 0.5**	**C_s = 0.1**
Ferrihydrite, %	-	-	-
Feroxyhyte, %	6	7	5
Lepidocrocite,%	-	-	1
Goethite, %	94	94	94
Haematite, %	-	-	-
Goethite seeded system			
Ferrihydrite, %	-	-	-
Feroxyhyte, %	-	-	-
Lepidocrocite,%	-	-	-
Goethite, %	95	96	98
Haematite, %	5	4	2
Haematite seeded system			
Ferrihydrite, %	-	-	-
Feroxyhyte, %	-	-	-
Lepidocrocite,%	-	-	-
Goethite, %	97	98	99
Haematite, %	3	2	1

6.6.5 Conclusion

The oxidation of ferrous iron is catalysed by the presence of different types of iron oxides as mentioned in section 6.5. For seeds concentrations C_s = 0.1 to C_s = 1.0, it was found that the catalytic effect did not depend on the concentration of the seeds added. However, it is expected that a threshold seed concentration exists where there would be a difference in the catalytic effect with change in seed concentration. Due to the scope and time constraints of the present study this could not be tested. The catalytic effect did not follow the model proposed by Tamura et al., (1976b). The lack of agreement could be twofold:

i) Different types of iron oxide hydroxides are likely to catalyse the oxidation reaction to different extents as shown in Table 6.1. Again as demonstrated here, various mixtures of oxide hydroxides were formed under the experimental conditions covered in this work, this could have resulted in varying degrees of catalysis for each of the systems considered. It has also been reported that iron oxides catalyse the oxidation reactions differently with some oxides showing no catalytic effect at all (Sung and Morgan, 1980).

ii) The kinetic model of Tamura et al., (1976b) is based on dissolved state oxidation of iron ($pH \leq 7.0$), which is not the case for pH 8.0 and above where the ferrous iron exists as solid ferrous hydroxide. As indicated earlier (Figure 5.27), at pH 8.0 and above solid state oxidation of iron dominates.

A second finding of the work presented here is that, as the seed concentration decreases, the population based average size of the product particles increases. This is due to the fact that at low seed concentration, the proportion of freshly precipitated solids which have a greater tendency to aggregate at the expense of coating is much higher. Secondly, if coating is assumed to be a filling of active surfaces, then, higher seed concentrations provide higher surface areas which promote higher levels of coating. Conversely, low seed concentrations provide smaller active surface areas which can be easily saturated, forcing the freshly precipitated solids to aggregate.

The evolution of the particle size in seeded iron systems is such that there is an initial increase in the size, reaching a maximum at some point and then dropping again. The increase in the size is due to the aggregation of the freshly precipitated particles as indicated in section 6.4. The decrease in the size of the particles is due to disappearance of the aggregates/flocs as they coat on the seed material and/or ageing (Gan et al., 2005). Using the size ratios L/L_0 and L_p/L_0, (Kubota et al., 2001; Doki et al., 2001), it was shown that the process was indeed not a growth of the seed except for the cases; $C_s = 1.0$, recycled solids seeds, pH 6.0 and $C_s = 1.0$, recycled solids seeds, pH 10.0. It was also found that recycled solids systems always produced particles of the largest average size. This was probably due to the presence in greater proportions of the freshly precipitated solids which have a higher tendency to aggregate and associate into loosely bound flocs. By considering the evolution of m_0, it can also be concluded that, regardless of the seed concentration, seeding suppressed nucleation to the same extent, at least for cases considered here.

The last conclusion that can be made here is that, regardless of the seed type or seed concentration, seeding always promoted the formation of a simpler and more stable precipitate mixture. The simplicity of the precipitates generally increased with increase in the seed concentration. At pH 10.0, however, the composition of the precipitate was independent of the seed type and concentration and only depended on the pH. Haematite seeding promoted the formation of goethite; goethite favoured itself, while recycled solids promoted the formation of lepidocrocite. In all cases, seeding was found to suppress the formation of ferrihydrite. At pH 10.0, goethite was always formed in highest proportions. It therefore follows from Figure 1.3 that haematite seeding and operation at pH 10.0 will achieve highest iron conversions since goethite has the least solubility.

Thus it has been demonstrated here that seeding of the oxidation and precipitation of iron improves the particle size distribution of the precipitate; forms a simpler and more stable precipitate mixture and improves plant throughput levels due to increased rates of oxidation especially at lower pH. These findings have significant potential impact on the practice of mining waste water treatment by the high density sludge process both in terms cost savings and operational efficiency.

References

Blesa, M. A. and Matijevic, E. (1989), Phase transformations of iron oxides, oxohydroxides, and hydrous oxides in aqueous media, *Advances in Colloid and Interface Science*, vol. 29, pp. 173-221.

Cominco Engineering Services Limited;Water Treatment Technology (1997), Pilot scale testing of the high density sludge process, Britannia mine, Acid Mine Drainage Treatment, Vancouver, B.C. Canada.

Cornell, R. M., Giovanoli, R. (1985), Effect of solution conditions on the proportion and morphology of goethite formed from ferrihydrite, *Clays and Clay Minerals*, vol. 33, pp. 424-432.

Cornell, R. M., Giovanoli, R. (1986), Factors that govern the formation of multi-domainic goethites, *Clays and Clay Minerals*, vol. 34, pp. 557-564.

Doki, N., Kubota, N., Sato, A., Yokota, M. (2001), Effect of cooling mode on product crystal size in seeded batch crystallisation of potassium alum, *Chemical Engineering Journal*, vol. 81, pp. 313-316.

Gan, W. Y., Selomulya, C., Tapsell, G., Amal, R. (2005), Densification of iron(III) sludge in neutralisation, *International Journal of Mineral Processing*, vol. 76, pp. 149-162.

Kubota, N., Doki, N., Yokota, M., Sato, A. (2001), Seeding policy in batch cooling crystallisation, *Powder Technology*, vol. 121, pp. 31-38.

Muhr, H. (2006), personal communication, ENSIC, CNRS, Nancy, France

Scheidegger, A., Borkovec, M. and Sticher, H. (1993), Coating of silica sand with goethite: preparation and analytical identification, *Geoderma*, vol. 58, pp. 43-65.

Sung, W. and Morgan, J. J. (1980), Kinetics and product of ferrous iron oxidation in aqueous systems, *Environmental Science and Technology*, vol. 14, pp. 561 - 568.

Weidler, P. G. (1997), BET sample pretreatment of synthetic ferrihydrite and its influence on the determination of surface area and porosity, *Journal of Porous Materials*, vol. 4, pp. 165-169.

Zauner, R., Jones, A. G. and, (2000), Determination of nucleation, growth, agglomeration and disruption kinetics from experimental precipitation data: the calcium oxalate system, *Chemical Engineering Science*, vol. 55, pp. 4219-4232.

Chapter 7: Conclusions and recommendations

7.1 Conclusions

From the results presented in this work, the following conclusions can be drawn on the oxidation and precipitation of iron in unseeded and seeded systems

- At pH 6.0, the rate of oxidation of iron shows second order dependence on the pH. As the pH increases, the speciation of iron in solution becomes more complex and the oxidation no longer follows second order dependence on pH. For the pH range considered in this work, the order of reaction with respect to pH was about 0.70. At pH 6.0 and 10.0, the oxidation proceeds via the DSO mechanism because the precursor ferrous iron exists as mainly soluble ferrous hydroxide while at pH 8.0 and 9.0, the oxidation proceeds via the SSO mechanism since the ferrous iron exits as solid ferrous hydroxide. Overally, the rate of oxidation increases as the pH increases as stated in the hypotheses.

- The physical and chemical characteristics of iron precipitates and the proportion of iron phases in the precipitate depend on the pH at which they were formed and also on the ageing time. Low pH leads to the formation of less stable phases like ferrihydrite while high pH (pH 10.0) leads to the formation of stable phases like goethite. This is in contrast to the hypothesis that high pH leads to the formation of the less stable and amorphous phases like ferrihydrite. At low pH, large particles are formed due to low supersaturation levels. As the pH increases, the supersaturation increases leading to the formation of smaller particles. However, at pH around 7.0, these fine particles aggregate extensively due to electrostatic interactions since the point of zero charge of iron oxides is around pH 7.0.

- The active process mechanisms in the formation of iron precipitates are; nucleation in the bulk solution, aggregation of nanosize polymers to about

3 µm diameters, transformation of metastable phases and finally ageing of the final precipitate product. The ageing process does not, however result in the formation of haematite as envisaged in the hypothesis but rather results in the formation of mainly lepidocrocite. Regardless of the operating pH, the formation of iron oxide precipitates is always growth limited.

- Seeding the oxidation and precipitation of iron process has the following effects:

  -Recycled solids, natural haematite and natural goethite all have a catalytic effect on the rate of oxidation of iron. For seed concentrations, C_s, between 1.0 and 0.1, the catalytic effect is independent of the concentration.

  -Seeding using recycled solids results in the formation of particles of larger size at all concentrations and all pH levels. Goethite and haematite seeding does not produce precipitates significantly larger in size except at pH 9.0.

  -Seeding promotes the formation of simpler and more stable precipitates. Haematite seeding promotes the formation of goethite while suppressing lepidocrocite and ferrihydrite which is contrary to the stated hypothesis concerning the formation of targeted stable phases. Goethite promotes the formation of itself while suppressing the formation of ferrihydrite and lepidocrocite. Recycled solids seeding promotes the formation of lepidocrocite. In all cases, the proportion of the favoured more stable phase increases with increase in seed concentration.

- The oxidation and precipitation of iron in the presence of seed material proceeds through the following stages; nucleation in the bulk, surface nucleation, aggregation and coating on seed surface and finally ageing.

The work presented here shows that the oxidation and precipitation of iron is a complex process. However, using various combinations of simple techniques, it has been demonstrated that useful information and insights that can help in the understanding of the process can be extracted. The information that has been presented on oxidation kinetics, the origin of chemical instability in the precipitates, the factors that govern the size of the particles and the effects of seeding of the oxidation process, all have important implications for waste water treatment processes. It follows therefore that the design and operation of waste water treatment plants employing the high density sludge process have to strike a balance between these variables; operating at high pH to achieve high through puts or medium to low pH to have larger particles with better dewaterability characteristics, and seeding with recycled solids to improve the particle size (without improving the chemical stability of the precipitates) and seeding with natural iron oxides to improve the iron conversions (since from Figure 1.3 goethite precipitation ensures the highest conversions), chemical stability and simplicity of the precipitates but without necessarily improving the particle sizes of the precipitates. Seeding the oxidation and precipitation process with natural products opens potential opportunities for material reuse and/or recycle and water savings through formation of products with higher solids densities.

7.2 Recommendations

In view of the results and constraints encountered in this work, the following recommendations are suggested.

- The oxidation of iron in this work was effected by sparging air at a constant flow rate. This resulted in relatively high rates of iron oxidation hence primary nucleation. In view of this it is recommended that an air-nitrogen mixture be used in further work in order observe the effect of oxygen partial pressure on the process mechanisms. This could possibly eliminate primary nucleation.

- Further studies are needed in order to characterise the surface properties of the various iron oxide hydroxides that are formed during the oxidation and precipitation of iron. Such studies would help to predict and understand the physical properties of iron sludge and the removal of other pollutants from waste water by adsorption and/ co-precipitation.

- More tests need to be carried out at lower seed concentrations in order to establish the critical seed concentration below which the desirable effects of seeding will not be realised any more. Further tests also have to be performed in which the product of seeded experiments is continuously recycled to see if the simplicity and stability of the precipitate will be sustained.

- The effects of other factors like pH and ionic strength on the coating of substrates have to be investigated as well in order to establish optima for adherence of freshly precipitated solids on the seed material.

- A classical approach to the study of iron precipitation is hampered by the absence of data on the stoichiometry of the polycationic species which are precursors to the precipitation process. A study to establish the stoichiometry of the polycationic species would provide valuable information that could be used to predict and control the precipitation of iron from solution.

Appendices

Appendix 1: Analytical procedures and methods

Appendix 1.1 Procedure for the determination of iron in samples

The method for the determination of iron was based on the following facts:

- The formation of orange red complexes when Fe^{2+} is mixed with 1-10 phenanthroline. Three molecules of 1-10 phenanthroline chelates with one Fe^{2+} ion.

- The reduction of Fe^{3+} by hydroxylamine according to the well known stoichiometry shown below

$$2NH_2OH + 4Fe^{3+} \rightarrow N_2O + 4Fe^{2+} + 4H^{+} + H_2O$$

By first reducing all the Fe^{3+} present in a sample, total iron can be determined by use of the 1-10 phenanthroline complexing agent. The amount of Fe^{3+} is found as the difference between total iron obtained after reduction with hydroxylamine and Fe^{2+} obtained without reduction.

Reagents and procedure

Standard Fe^{2+} stock solution (100ppm Fe^{2+})

Slowly add 20 ml of concentrated H_2SO_4 to 50 ml of distilled water and dissolve 497.629 mg of $FeSO_4.7H_2O$. Dilute to 1000 ml with distilled water and mix thoroughly. Standard solutions of lower concentration are obtained by dilution as indicated in Table 1.

1-10 phenanthroline indicator solution

Dissolve 2127.708 mg of 1-10 phenanthroline (as $C_{12}H_8N_2$.H2O) in about 100 ml of water. Dilute with more distilled water to 1000 ml mark. This gives a concentration of 1-10 phenanthroline in excess of the stoichiometric requirements.

Ammonium acetate buffer solution

Dissolve 250 g of ammonium acetate ($NH_4C_2H_3O_2$) in 150 ml of distilled water. Add 700 ml of concentrated glacial acetic acid.

Calibrating the instrument

Prepare standard samples for the calibration of the spectroquant according to Table 1. Read off the absorbance at wavelength 500 nm

Table 1

Standard (ppm Fe^{2+})	**Vol of stock (ml)**	**Vol of dist water (ml)**	**Vol of buffer (ml)**	**Vol of indicator (ml)**
1	0.01	0.99	2.00	2.00
10	0.10	0.90	2.00	2.00
20	0.20	0.80	2.00	2.00
30	0.30	0.70	2.00	2.00
40	0.40	0.60	2.00	2.00
50	0.50	0.50	2.00	2.00
60	0.60	0.40	2.00	2.00
70	0.70	0.30	2.00	2.00
80	0.80	0.20	2.00	2.00
90	0.90	0.10	2.00	2.00
100	1.00	0.00	2.00	2.00
Blank	0.00	1.00	2.00	2.00

The confidence interval was set at 95%. Figure 1 shows one such calibration curve.

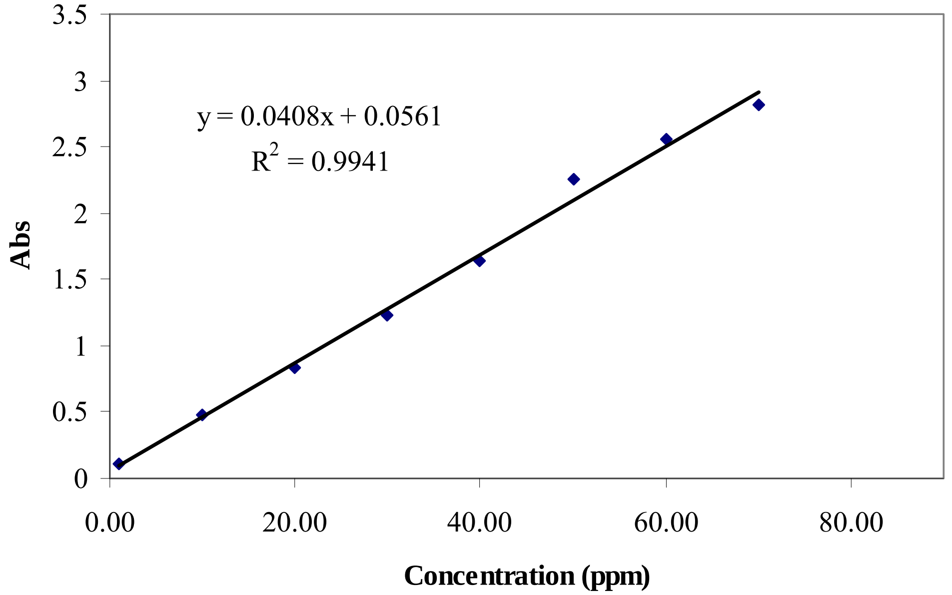

Figure 1 Calibration of the spectroquant NOVA60.

All the other calibrations performed gave R^2 correlations greater than 99%.

Deviation of measured values from true values

Comparison of the true mean and the measured mean was performed using the student's t-test. The number of repeats performed on the true and measured values was 10 and this gave 18 degrees of freedom. The critical t-value from the statistical tables was 1.7341. The comparisons were performed at three different concentrations. The results are shown in Table 2 below.

Table 2 Student's t-test results

True value	Measured value	t-critical at 95%	t-calculated	Conclusions
25.00±0.54	24.48±0.84	1.7341	1.6467	Accept the null hypothesis
30.00±0.54	29.52±0.93	1.7341	1.4115	Accept the null hypothesis
40.00±0.54	39.64±0.79	1.7341	1.1897	Accept the null hypothesis

Conclusion

The method developed for the analysis of dissolved iron is statistically accurate within 95% confidence.

Dissolved Fe^{2+}

Premix buffer solution and indicator solution in the prescribed test tubes according to the last two columns of Table 1. Pipette 1.00 ml of sample into the test tube and mix thoroughly. Allow to react for 3 minutes. Read off the concentration from the spectroquant.

Total iron

Add buffer and indicator solutions into test tube according to Table 1. Pipette 1.00 ml of sample into the test tube. Add one scoop of hydroxylamine and vortex for 2 minutes. Allow to stand for 5 minutes and then read off the concentration of iron from the spectroquant.

Dissolved Fe^{3+}

Concentration of Fe^{3+} is the difference between total iron and Fe^{2+} concentration.

Total Iron analysis in solids

Transfer 0.1 g of solids into conical pyrex flask.
Add about 15 ml of 9 M HCl
Heat the flask at 60-80°C until all the particles have dissolved
Transfer the contents of the flask to a 100 ml volumetric flask
Top up with reverse osmosis or distilled water to the mark
Leave the solution to cool to room temperature
Transfer 1 ml of sample to prescribed test tube and analyse for ferrous and total iron using the NOVA60 spectroquant

Appendix 1.2 Determination of the proportion of ferrihydrite in iron precipitates

Reagents preparation

0.2 M oxalic acid

Weigh 25.214 g of oxalic acid, $(COOH)_2.2H_2O$

Transfer the measured oxalic acid into a 1000 ml volumetric flask.

Dissolve the acid in about 200 ml of distilled water

When all the acid has dissolved, fill up to the mark with distilled water.

0.2 M ammonium oxalate

Weigh 28.422 g of ammonium oxalate $(COONH_4)_2.H_2O$

Transfer the measured oxalate into a 1000 ml volumetric flask

Dissolve the oxalate in about 200 ml of distilled water

When all the oxalate has dissolved, fill up to the mark with more distilled water.

Measurement procedure

Measure 0.0500 g of iron solids

Transfer the solids to a conical flask that is covered with aluminium foil to avoid sunlight

Add 100 ml of ammonium oxalate solution (buffered to pH 3 using oxalic acid) to the solids

Stir the contents for 2 hours

After 2 hours, filter the sample for iron analysis purposes.

Analyse the total iron in the filtrate (this represents amorphous iron) using the spectroquant.

Proportion of ferrihydrite/amorphous iron is give by the ratio

$$\frac{Fe_{AAO}}{Fe_T} \times 100\%$$

Where Fe_{AAO} is the ammonium oxalate soluble iron and Fe_T is the total iron in the solids before dissolution in ammonium oxalate. This amount of iron is found by doing a 9 M HCl digestion of the solids and then reading off the concentration on the spectroquant.

Appendix 2 Instrumental methods

Appendix 2.1 Surface area measurement

A Tristar surface and porosity analyser supplied by Micromeretics was used for the measurement of the BET specicific surface area. The samples were first degassed at 100°C for 24 hours before analyses began. More details on the operation of the instrument are given in the user manual.

Below is a sample result print out from the instrument.

```
                          Full Report Set

TriStar 3000  TriStar 3000  Unit 1      Serial # 1076   Anl Port #3     Page  1
V5.02         V5.02

         Sample: 000-824 Sample 6 (18/5)
        Operator: Helen
       Submitter: Hove
       File Name: C:\WIN3000\DATA\000-824.SMP

        Started: 2006/06/20         Analysis Adsorptive: N2
             12:15:53PM
       Completed: 2006/06/20              Analysis Bath: 77.35 K
             13:49:32PM
     Report Time: 2006/06/20              Sample Weight: 0.1423 g
             14:02:05PM
    Warm Freespace: 8.4786 cm³  MEASURED     Cold Freespace: 25.1506 cm³
   Equil. Interval: 5 secs             Low Pressure Dose: None
    Sample Density:   1.000 g/cm³          Automatic Degas: No

                          Analysis Log

  Relative       Pressure     Vol Adsorbed   Elapsed Time     Saturation
  Pressure        (mmHg)      (cm³/g STP)      (HR:MN)       Press.(mmHg)

                                  01:09       758.56683
 0.063399349      48.09264        53.1749        01:17
 0.076203665      57.80557        54.9246        01:20
 0.115844628      87.87589        59.8725        01:24
 0.155534723     117.98348         64.5779        01:28
```

```
   0.195099289      147.99585        69.2609        01:32


Full Report Set

 TriStar 3000  TriStar 3000  Unit 1        Serial # 1076    Anl Port #3       Page  3
 V5.02         V5.02

              Sample: 000-824 Sample 6 (18/5)
            Operator: Helen
           Submitter: Hove
           File Name: C:\WIN3000\DATA\000-824.SMP

             Started: 2006/06/20          Analysis Adsorptive: N2
                      12:15:53PM
           Completed: 2006/06/20               Analysis Bath: 77.35 K
                      13:49:32PM
         Report Time: 2006/06/20              Sample Weight: 0.1423 g
                      14:02:05PM
      Warm Freespace: 8.4786 cm³  MEASURED     Cold Freespace: 25.1506 cm³
     Equil. Interval: 5 secs              Low Pressure Dose: None
      Sample Density:   1.000 g/cm³           Automatic Degas: No

                          BET Surface Area Report

             BET Surface Area:        254.2432   ±    2.0134 m²/g
             Slope:                  0.016909 ±    0.000134
             Y-Intercept:              0.000213 ±    0.000018
             C:                    80.247750
             VM:                      58.403761    cm³/g STP
             Correlation Coefficient:    9.999052e-01

             Molecular Cross-section:    0.1620      nm²

          Relative                Vol                   1/
          Pressure               Adsorbed           [VA*(Po/P - 1)]
                              (cm³/g STP)

         0.063399349             53.1749                0.001273
         0.076203665             54.9246                0.001502
         0.115844628             59.8725                0.002188
         0.155534723             64.5779                0.002852
         0.195099289             69.2609                0.003500



                             Full Report Set

 TriStar 3000  TriStar 3000  Unit 1        Serial # 1076    Anl Port #3       Page  5
 V5.02         V5.02
```

Sample: 000-824 Sample 6 (18/5)
Operator: Helen
Submitter: Hove
File Name: C:\WIN3000\DATA\000-824.SMP

Started: 2006/06/20 12:15:53PM   Analysis Adsorptive: N2
Completed: 2006/06/20 13:49:32PM   Analysis Bath: 77.35 K
Report Time: 2006/06/20 14:02:05PM   Sample Weight: 0.1423 g
Warm Freespace: 8.4786 cm³ MEASURED   Cold Freespace: 25.1506 cm³
Equil. Interval: 5 secs   Low Pressure Dose: None
Sample Density: 1.000 g/cm³   Automatic Degas: No

Summary Report

Area

Single Point Surface Area at P/Po 0.19509929 : 242.6829 m²/g

BET Surface Area: 254.2432 m²/g

Appendix 2.2 Particle size distribution

Particle size distribution was measured using a Malvern Mastersizer-S instrument supplied by Malvern Instruments. The instrument gives the result as a volume distribution and this had to be converted into a number distribution on an excel spreadsheet. The conversion is illustrated below as well as the calculation of moments from the distribution.

Result: Analysis Table

ID: s5_14_12_7 Run No: 1 Measured: 12/14/07 10:08AM
File: HOVE Rec. No: 181 Analysed: 12/14/07 10:08AM
Path: C:\SIZERS\DATA\ Source: Analysed

Range: 300RF mm Beam: 2.40 mm Sampler: MS1 Obs': 12.6 %
Presentation: 3THD Analysis: Polydisperse Residual: 1.237 %
Modifications: None

Conc. = 0.0207 %Vol Density = 3.800 g/cm^3 S.S.A.= 0.1294 m^2/g
Distribution: Volume D[4, 3] = 28.51 um D[3, 2] = 12.20 um
D(v, 0.1) = 6.57 um D(v, 0.5) = 18.74 um D(v, 0.9) = 64.23 um
Span = 3.076E+00 Uniformity = 9.495E-01

Size (um)	Volume In %	Size (um)	Volume In %	Size (um)	Volume In %	Size (um)	Volume In %
0.05	0.00	0.58	0.06	6.63	3.67	76.32	2.08
0.06	0.00	0.67	0.09	7.72	4.61	88.91	1.69
0.07	0.00	0.78	0.11	9.00	5.52	103.58	1.35
0.08	0.00	0.91	0.13	10.48	6.29	120.67	1.01
0.09	0.00	1.06	0.15	12.21	6.85	140.58	0.67
0.11	0.00	1.24	0.17	14.22	7.13	163.77	0.33
0.13	0.00	1.44	0.19	16.57	7.12	190.80	0.00
0.15	0.00	1.68	0.21	19.31	6.87	222.28	0.00
0.17	0.00	1.95	0.25	22.49	6.41	258.95	0.00
0.20	0.00	2.28	0.33	26.20	5.82	301.68	0.00
0.23	0.00	2.65	0.46	30.53	5.16	351.46	0.00
0.27	0.00	3.09	0.67	35.56	4.49	409.45	0.00
0.31	0.01	3.60	0.99	41.43	3.91	477.01	0.00
0.36	0.02	4.19	1.44	48.27	3.40	555.71	0.00
0.42	0.03	4.88	2.04	56.23	2.95	647.41	0.00
0.49	0.04	5.69	2.79	65.51	2.51	754.23	0.00
0.58		6.63		76.32		878.67	

SIZES	Delta L,m	Lbar, m	*RESULT*	N
0.0582			0	
0.0679	9.7E-09	6.31E-08	0	0.00E+00
0.0791	1.12E-08	7.35E-08	0	0.00E+00
0.0921	1.3E-08	8.56E-08	0	0.00E+00
0.1073	1.52E-08	9.97E-08	0	0.00E+00
0.125	1.77E-08	1.16E-07	0	0.00E+00
0.1456	2.06E-08	1.35E-07	0	0.00E+00
0.1697	2.41E-08	1.58E-07	0	0.00E+00
0.1977	2.8E-08	1.84E-07	0	0.00E+00
0.2303	3.26E-08	2.14E-07	0	0.00E+00
0.2683	3.8E-08	2.49E-07	0	0.00E+00
0.3125	4.42E-08	2.9E-07	0	0.00E+00
0.3641	5.16E-08	3.38E-07	0.01319	8.71E+11
0.4242	6.01E-08	3.94E-07	0.01976	8.25E+11
0.4941	6.99E-08	4.59E-07	0.02945	7.78E+11
0.5757	8.16E-08	5.35E-07	0.04318	7.22E+11
0.6707	9.5E-08	6.23E-07	0.0613	6.48E+11
0.7813	1.11E-07	7.26E-07	0.09025	6.03E+11
0.9103	1.29E-07	8.46E-07	0.11234	4.75E+11
1.0604	1.5E-07	9.85E-07	0.13096	3.50E+11
1.2354	1.75E-07	1.15E-06	0.14968	2.53E+11
1.4393	2.04E-07	1.34E-06	0.1679	1.80E+11
1.6767	2.37E-07	1.56E-06	0.18803	1.27E+11
1.9534	2.77E-07	1.82E-06	0.21211	9.07E+10
2.2757	3.22E-07	2.11E-06	0.25467	6.89E+10
2.6512	3.76E-07	2.46E-06	0.32897	5.63E+10
3.0887	4.38E-07	2.87E-06	0.45864	4.96E+10
3.5983	5.1E-07	3.34E-06	0.66895	4.58E+10
4.192	5.94E-07	3.9E-06	0.98709	4.27E+10

4.8837	6.92E-07	4.54E-06	1.43751	3.93E+10
5.6895	8.06E-07	5.29E-06	2.03831	3.53E+10
6.6283	9.39E-07	6.16E-06	2.79047	3.06E+10
7.7219	1.09E-06	7.18E-06	3.66749	2.54E+10
8.996	1.27E-06	8.36E-06	4.60626	2.02E+10
10.4804	1.48E-06	9.74E-06	5.51671	1.53E+10
12.2096	1.73E-06	1.13E-05	6.29142	1.10E+10
14.2242	2.01E-06	1.32E-05	6.84621	7.58E+09
16.5712	2.35E-06	1.54E-05	7.12698	4.99E+09
19.3055	2.73E-06	1.79E-05	7.12425	3.16E+09
22.4909	3.19E-06	2.09E-05	6.86579	1.92E+09
26.2019	3.71E-06	2.43E-05	6.40566	1.14E+09
30.5252	4.32E-06	2.84E-05	5.81628	6.52E+08
35.5618	5.04E-06	3.3E-05	5.16215	3.66E+08
41.4295	5.87E-06	3.85E-05	4.48709	2.01E+08
48.2654	6.84E-06	4.48E-05	3.9071	1.11E+08
56.2292	7.96E-06	5.22E-05	3.40478	6.11E+07
65.507	9.28E-06	6.09E-05	2.94599	3.34E+07
76.3157	1.08E-05	7.09E-05	2.50686	1.80E+07
88.9077	**1.26E-05**	**8.26E-05**	**2.08396**	**9.45E+06**
103.5775	**1.47E-05**	**9.62E-05**	**1.6936**	**4.86E+06**
120.6678	1.71E-05	0.000112	1.35203	2.45E+06
140.578	1.99E-05	0.000131	1.01046	1.16E+06
163.7733	2.32E-05	0.000152	0.66889	4.85E+05
190.7959	2.7E-05	0.000177	0.32732	1.50E+05
222.2773	3.15E-05	0.000207	0	0.00E+00
258.953	3.67E-05	0.000241	0	0.00E+00
301.6802	4.27E-05	0.00028	0	0.00E+00
351.4575	4.98E-05	0.000327	0	0.00E+00
409.4479	5.8E-05	0.00038	0	0.00E+00
477.0068	6.76E-05	0.000443	0	0.00E+00
555.713	7.87E-05	0.000516	0	0.00E+00
647.4056	9.17E-05	0.000602	0	0.00E+00
754.2275	0.000107	0.000701	0	0.00E+00
878.675	0.000124	0.000816	0	0.00E+00
		m0		6.38E+12
		m1		6122349.033
		m2		20.90707888
		m3		0.000255769
		m4		7.31265E-09
		lbar1,0		9.59E-07

The excel formulae used to perform the conversion of the volume distribution to number distribution are shown below;

Delta L = (103.5775-88.9077)/1000000 = 1.47E-05

Lbar = 103. 5775 + (Delta L)/2

N = (Vol %/100) * V/(PI()/6*Lbar^3)

Where V is the volume of the solids and N is the number distribution.

m_0 = sum(N)

m1 = sum(lbar*N)

m2 = sum(lbar^2*N)

m3 = sum(lbar^3*N

m4 = sum(lbar^4*N)

m_0 is the zeroth moment............m_4 = fourth moment

Appendix 3 Reproducibility of experimental results

Appendix 3.1 Reproducibility of oxidation experiments

The reproducibility of the experimental results was tested by repeating randomly selected experiments. Results obtained for the oxidation reaction at pH 6.0 will be used as an illustration;

Table 3 Oxidation results obtained at pH 6.0

Time/min	Run 1, Fe2+	Run 2, Fe2+	Run 3,Fe2+	Run 4, Fe2+	Run 5, Fe2+	average	stdev	% stdev
0	250	250	250	250	250	250	0	0
5	228	222.5	220.5	212.5	219.8	220.66	5.58149	2.52945
10	123.5	110	113	108	117.4	114.38	6.20661	5.42631
20	74	68.5	55.5	62.5	77.9	67.68	8.94774	13.2207
40	25	25.5	19.5	21	26.7	23.54	3.11175	13.219
70	24.5	20	23.4	16.5	18.88	20.656	3.28492	15.903
90	1.15	0.5	0.8	1	0	0.69	0.45607	66.0971

Sum of % standard deviations 116.396

Average %standard deviation 19.3993

From these results the reproducibility was calculated as 19.40%. The average for all the randomly selected experiments was found to be ≈ 20 %

Appendix 3.2 Reproducibility of the particle size distribution

The particle size distribution determination was repeated three times for each of the samples collected. The results presented in this work are averages of the three measurements. It was found that the trends in particle size distribution were reproducible but not the actual numbers (m_0) of particles. The average % deviation in the number of particles was found in some instances to as high as 260%.

The result presented below is used to illustrate the reproducibility of the distribution. These are results for an experiments carried out at pH 6.0, and sample taken after 5 minutes of reaction.

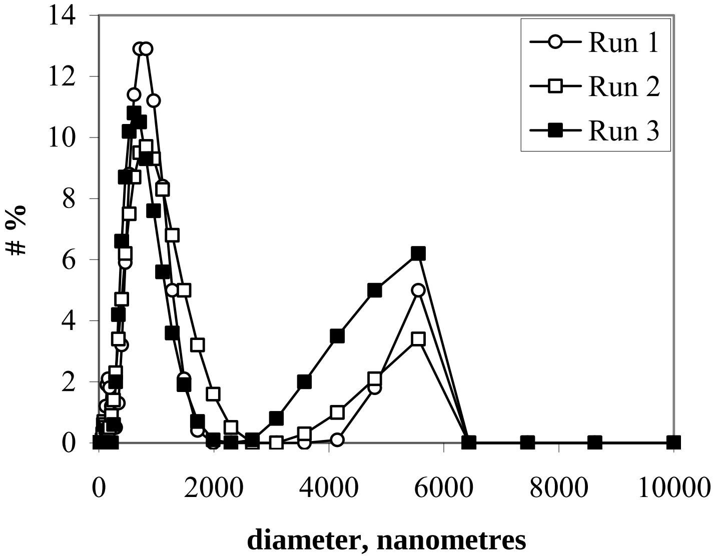

Figure 2 Reproducibility of the particle size distribution of the iron precipitates

Appendix 4 X-ray diffraction patterns of selected samples indicating reference patterns

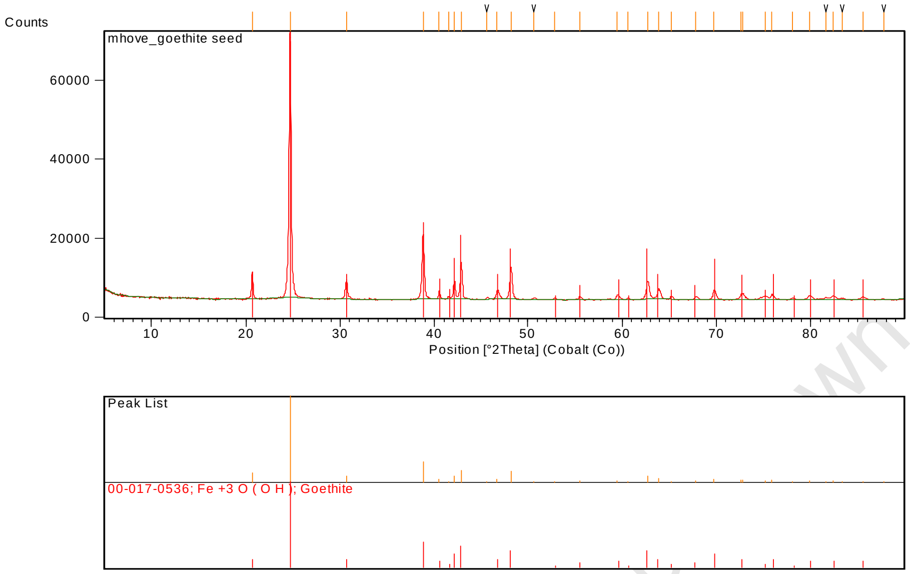

Figure 3 X-ray powder diffraction pattern of the goethite seed showing the reference pattern of goethite and haematite

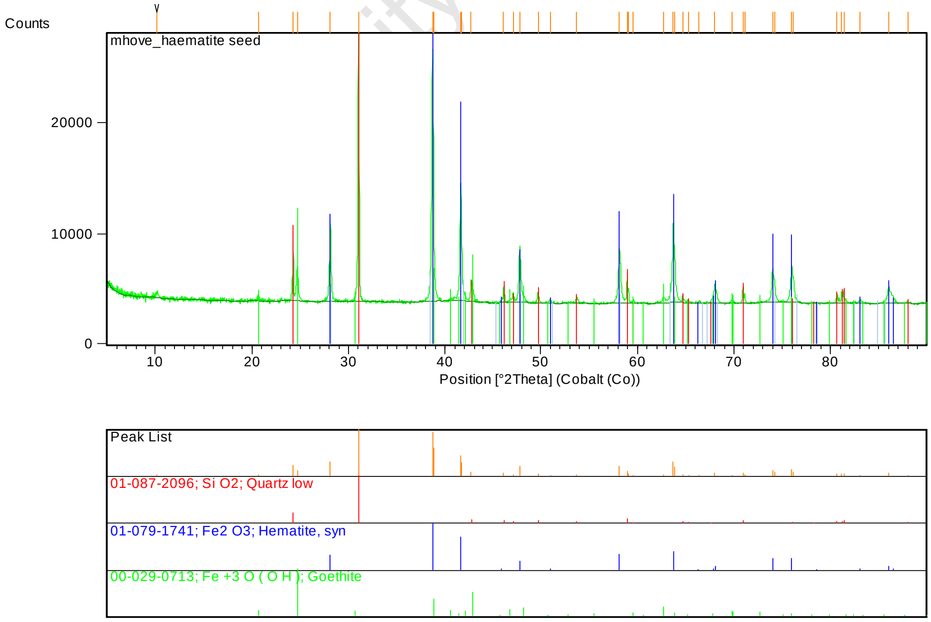

Figure 4 X-ray powder diffraction pattern of haematite seed showing reference pattern for goethite and haematite

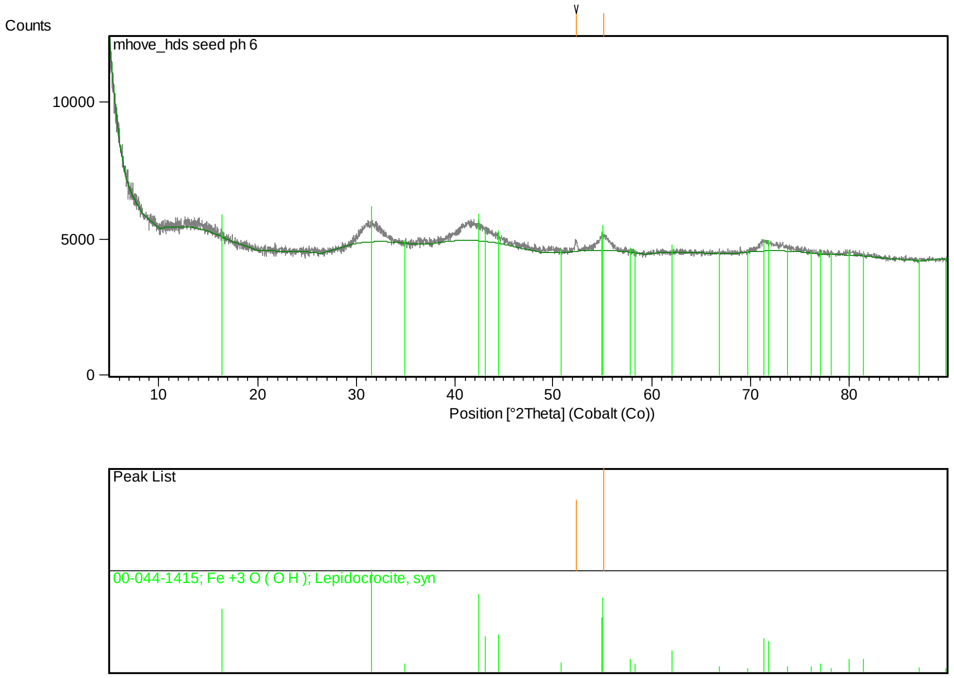

Figure 5 X-ray powder diffraction of the precipitate formed at pH 6.0 showing reference pattern for lepidocrocite. The hump around 2 theta = 15 is indicative of amorphous ferrihydrite.

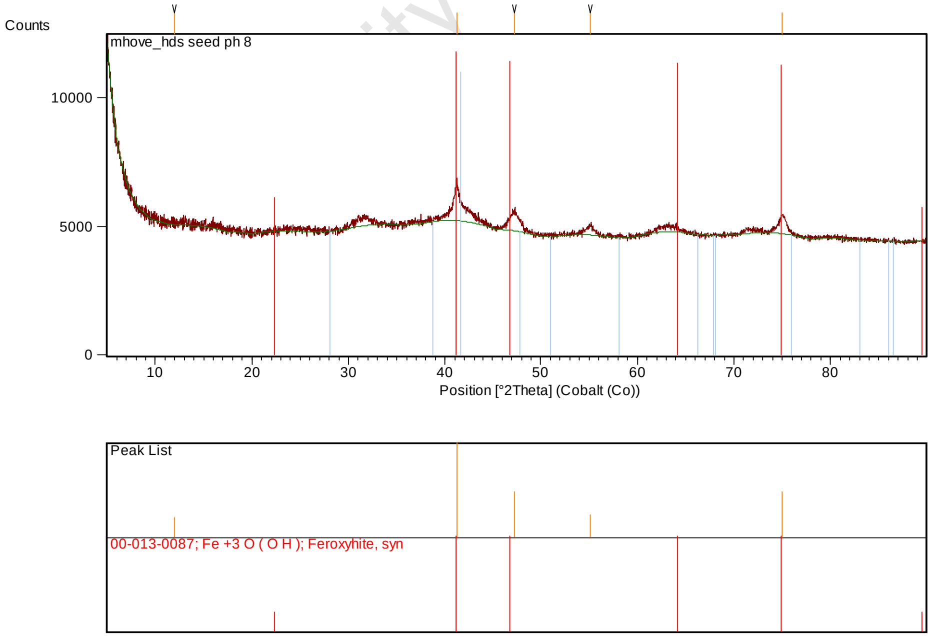

Figure 6 Typical X-ray powder diffraction pattern for the precipitate formed at pH 8.0 showing the reference pattern of feroxyhyte.

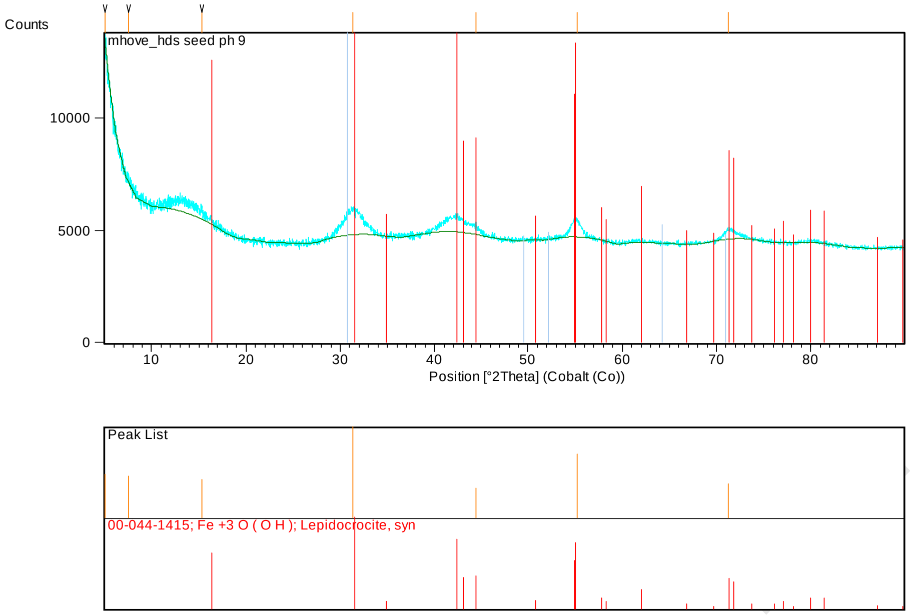

Figure 7 Typical X-ray powder diffraction pattern for precipitate formed at pH 9.0 showing the reference pattern of lepidocrocite.

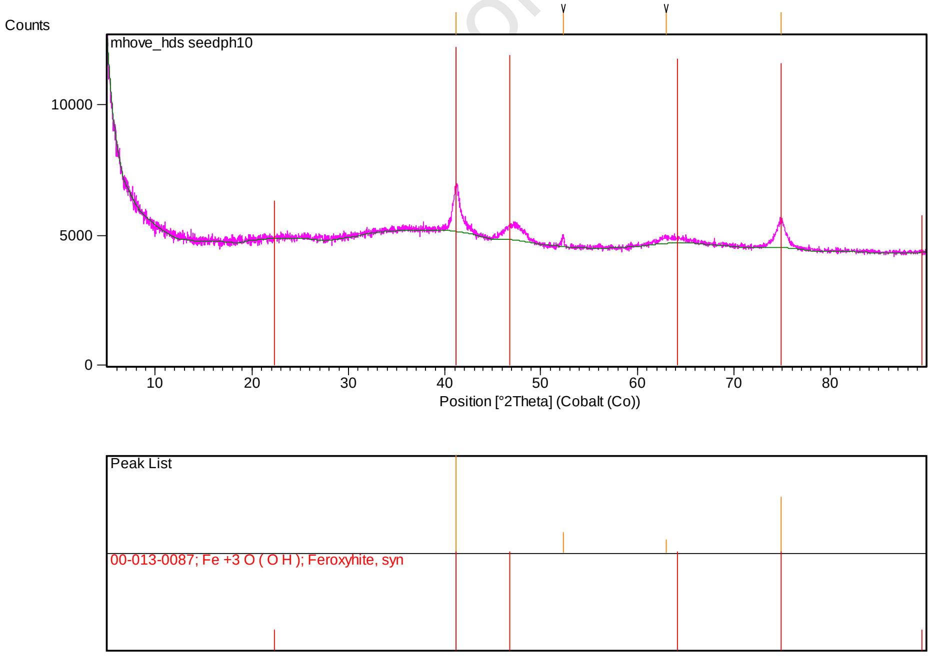

Figure 8 Typical X-ray powder diffraction pattern for precipitate formed at pH 10.0 showing the reference pattern for feroxyhyte.

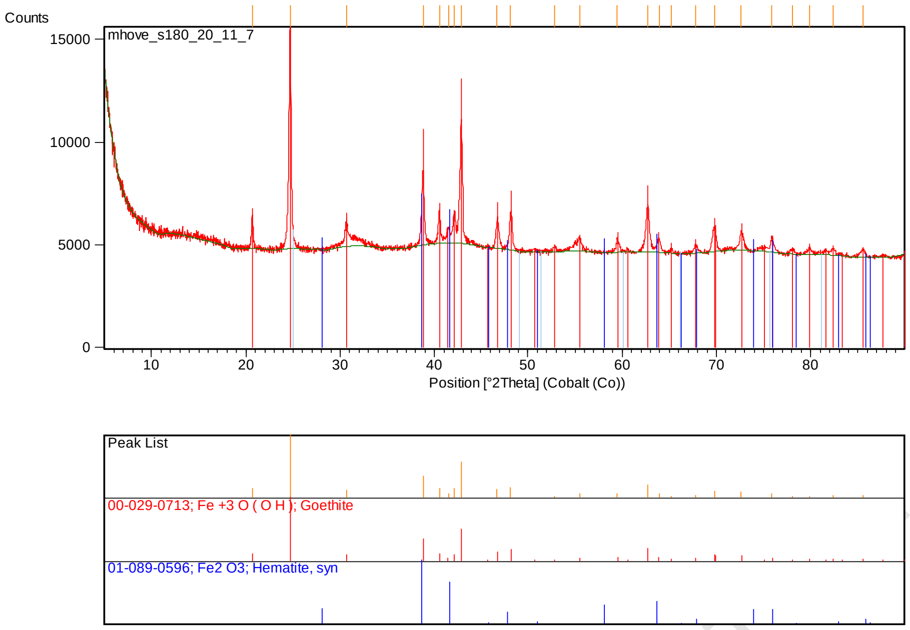

Figure 9 Typical X-ray powder diffraction pattern for the precipitate formed in the goethite seeded system at pH 6.0

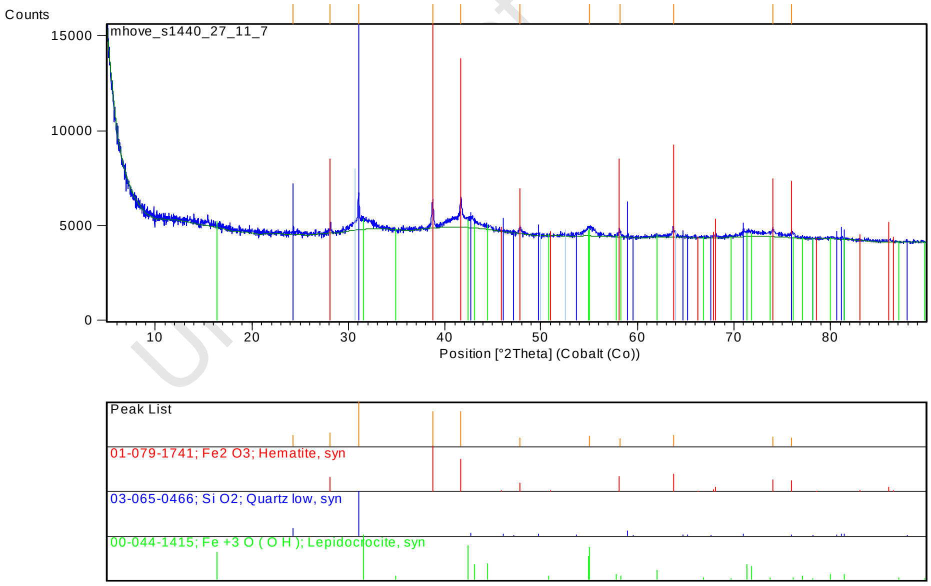

Figure 10 Typical X-ray powder diffraction of the precipitate formed in a haematite seeded system at pH 6.0

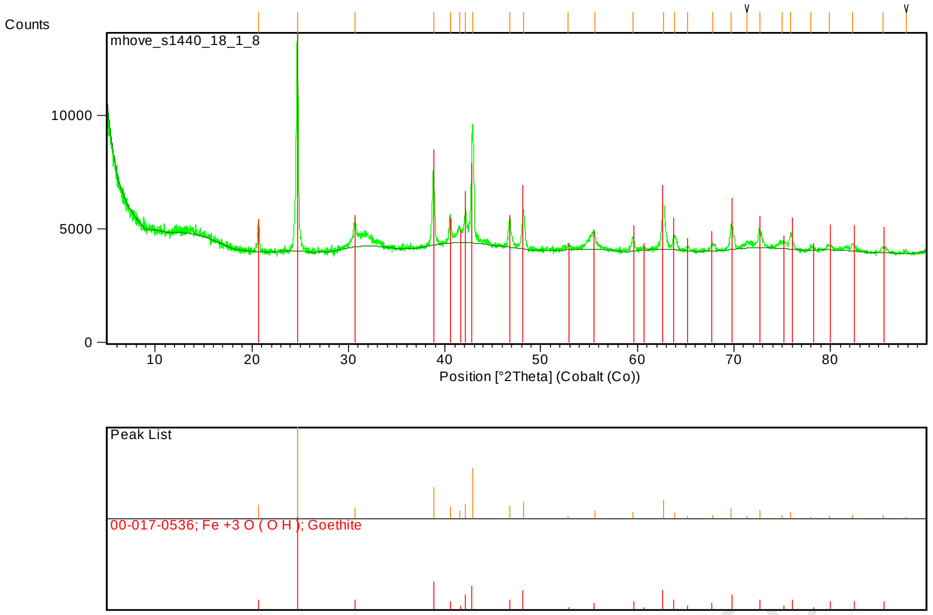

Figure 11 Typical X-ray powder diffraction pattern for the precipitate formed under goethite seeded conditions at pH 8.0

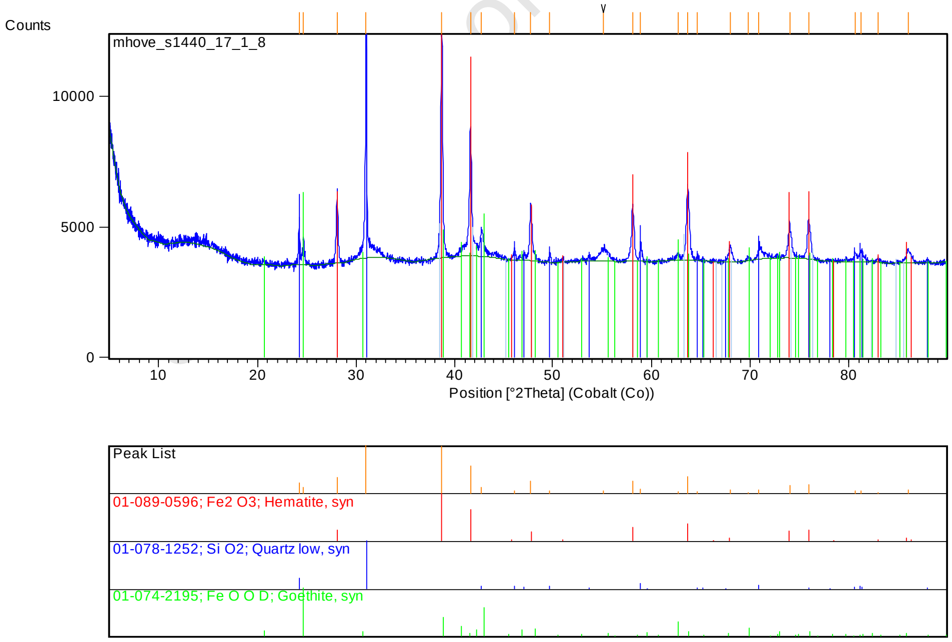

Figure 12 Typical X-ray powder diffraction pattern for the precipitate formed under haematite seeded conditions at pH 8.0

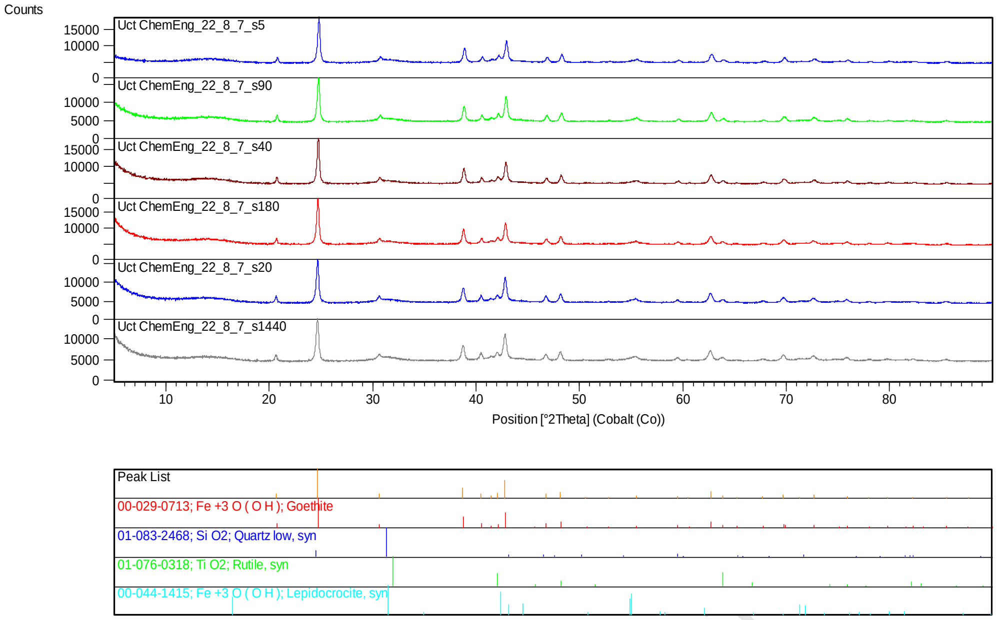

Figure 13 Typical X-ray diffraction patterns for precipitate formed under goethite seeded conditions at pH 9.0

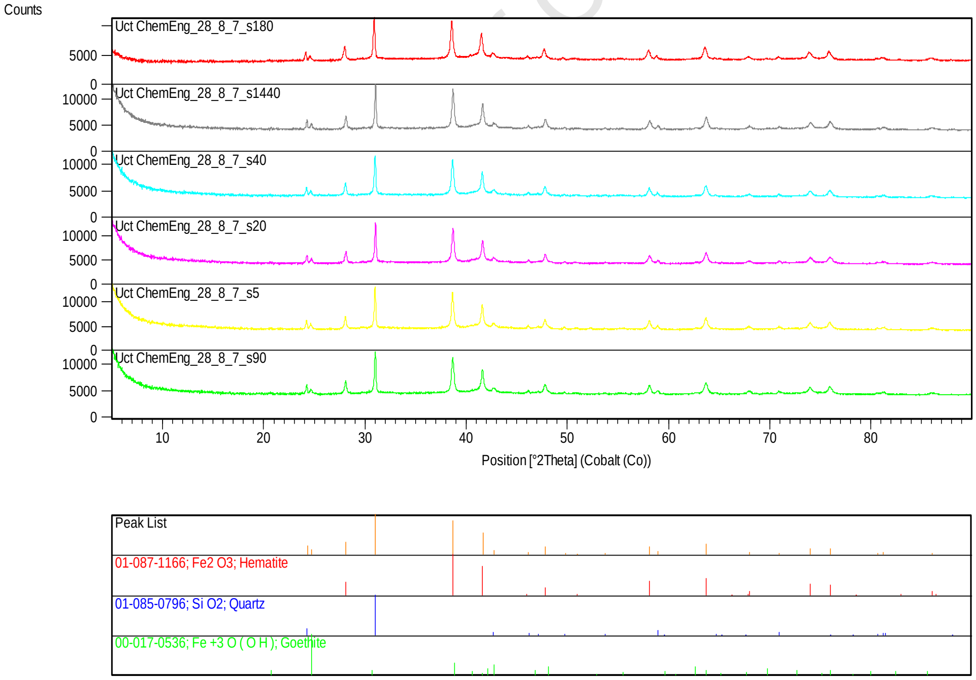

Figure 14 Typical X-ray diffraction patterns for precipitate formed under haematite seeded conditions at pH 9.0

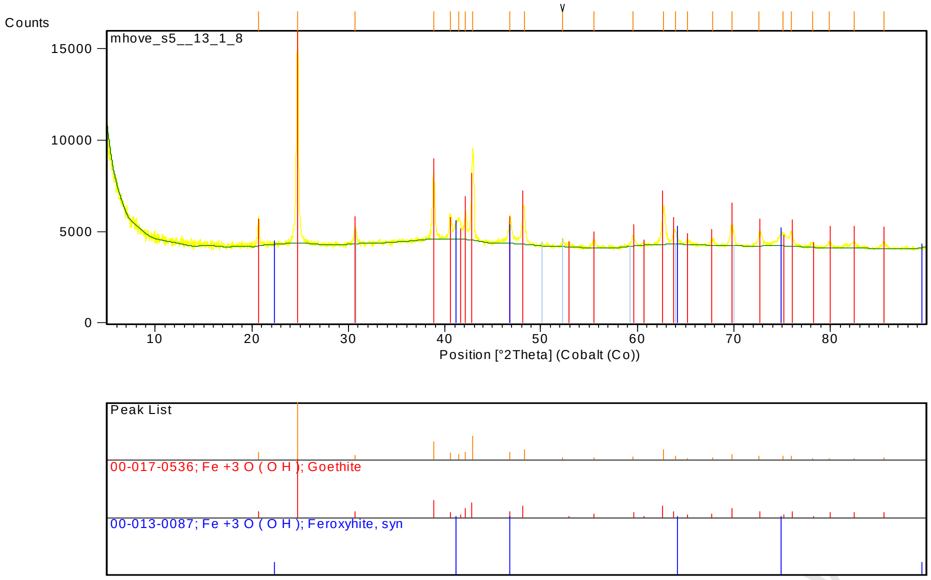

Figure 15 Typical X-ray diffraction pattern for the precipitate formed under goethite seeded conditions at pH 10.0

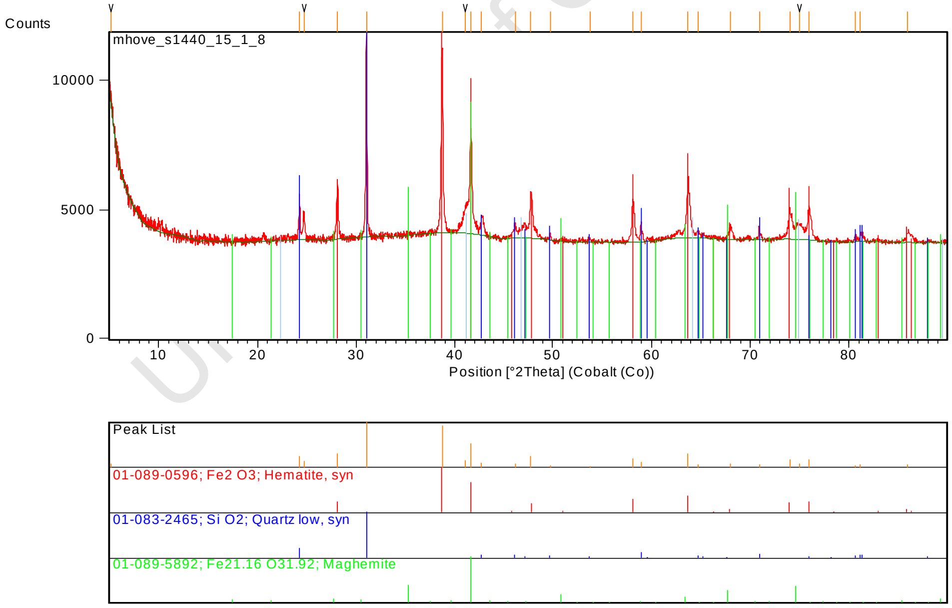

Figure 16 Typical X-ray diffraction pattern for the precipitate formed under haematite seeded conditions at pH 10.0

*